Description of the main research directions investigated by the institute

As stated above, FZU currently comprises of six scientific divisions. Below, we describe them and their structure in more detail:

Division of Elementary Particle Physics
Teams: 1 – Astroparticle Physics, 2 – Experimental Particle Physics, 3 – Particle Physics Theory and Cosmology

The experimental research program of the Division is mainly carried out within large international collaborations, which run their experiments in a few main research centres equipped with powerful accelerators or other large experimental facilities. The principal purpose of these experiments is to study the structure of matter at subnuclear scales and the properties of fundamental forces acting among its constituents. Particle physics is in many ways connected to various topics of modern astrophysics, such as the structure and evolution of the early universe, or the existence of extremely energetic cosmic rays. The Division consists of four departments.

The accelerator experimental program of the Division has been conducted within the Department of Experimental Particle Physics as well as the Department of Detector Development and Data Processing, which for the purpose of this evaluation together form Team 2. It is focused on the ATLAS experiment at the LHC collider at CERN and neutrino experiments NOvA and DUNE at Fermilab. The activity of this team covers a wide range of areas – physics analyses as well as design, development, and production of detector components, data acquisition, software development, and distributed computing used for detector simulation and data analysis within the GRID project. Experimental activities of the Division utilise the facilities and personnel of this team for semiconductor detectors.

The program of the Department of Particle Theory and Cosmology (Team 3) focuses on a range of topics from purely theoretical and formal subjects, from string theory to cosmology, to phenomenological aspects of real-world hadrons - strongly interacting particles. On the theoretical side, a dominant subject of interest includes string theory, conformal field theory, higher spin theory, and quantum gravity, which are often interrelated. Within cosmology, we try to understand the physical processes pertaining to the large-scale structure and evolution of the universe. Thanks to European and national funding new teams were established and the Central European Institute for Cosmology and fundamental physics (CEICO) was formed in 2016. This centre ties together string theory, cosmology, and astroparticle groups working on instrumentation for cosmological surveys, enabling appropriate synergies between the three.

The department of Astroparticle Physics (Team 1) participates in the Pierre Auger Observatory to study particles with energies several orders of magnitude higher than those found in terrestrial accelerators. The observatory measures cosmic ray showers in the atmosphere. The team is involved in the operation of fluorescence telescopes, data analysis related to the characteristics of hadronic interactions, and atmospheric monitoring, which is essential for an unbiased shower reconstruction. Since 2011 the Department has been active in the Cherenkov Telescope Array (CTA), a future generation observatory of high-energy gamma-rays. Other activities concern the Vera C. Rubin Observatory and measurement of the fluorescence yield in air.

Division of Condensed Matter Physics
Teams: 4 – Functional Metal Materials and Thin Films, 5 – Dielectrics, 6 – Magnetic Materials, 7 – Microscopic Theory of Advanced Materials

The division of Condensed Matter Physics is a dynamically evolving research unit dealing with the physical properties of modern materials. Research is currently organized in six research departments containing twelve research groups, seven central laboratories and two joint laboratories with universities. These six research departments are Functional Materials (Team 4), Dielectrics (Team 5), Magnetic Measurements and Materials (Team 6), Condensed Matter Theory (Team 7), Material Analysis, and Chemistry. The last two departments (Material Analysis and Chemistry) are not evaluated as they host central laboratories, which serve as support facilities for all FZU research teams.

Current research in the Division focuses on the theoretical and experimental investigation of properties of solids derived from their crystal and electronic structures, and in particularly mechanical, magnetic, dielectric, optical, chemical, electric and transport properties. Changes of properties derived from the phase transitions in solids (structural, magnetic, dielectric) are of particular interest. Research groups from the Division significantly contributed to the progress of knowledge in several research fields, such as spectroscopic studies of advanced ferroic materials, experimental and theoretical studies of shape memory alloys or thermodynamic analysis and modelling of segregation in metals. In these areas FZU belongs amongst world leading research centres.

Division researchers recently investigated multiferroic, piezoelectric and spintronic materials, liquid crystals, nanostructured metals and alloys, shape memory alloys and composites, magnetic Heusler compounds and nanodiamond coatings. Theoreticians focussed on ab-initio calculations and modelling of electronic properties of metals, semiconductors, and complex materials with enhanced electron correlation effects. Several research groups studied physical processes in solids taking place in response to external stimuli, other groups investigated interactions of solids with electromagnetic radiation. The aim is typically to discover and develop new tailor-made materials with specific properties and functions to be utilized in innovative engineering applications. The physics research in the Division has significant outreach, not only in the field of material science, but also other disciplines, for example medicine, robotics, transport or energy with enormous societal impact.

Overall, the research in the Division has been following modern trends in material physics over the years and, recently, it has gradually shifted toward the nanoscale. Additionally, it has become highly interdisciplinary and its results have been increasingly exploited in engineering applications. These trends have accelerated in the Evaluation period, for example, modifications of functional properties of superelastic NiTi wires, development of biodegradable metals for applications in medical devices, or development of technology for diamond anticorrosion coatings for nuclear fuel cladding.

The Division operates modern mechanical testing facilities for smart material research and dedicated laboratories for dielectric, infrared, Raman, terahertz and Mössbauer

spectroscopies. Researchers make advanced alloys by casting and powder metallurgy methods, grow large metallic single crystals and crystals for applications in optics, prepare organic liquid crystals and grow thin films and coatings by CVD (nanodiamond) and PVD (metal complexes) techniques.

Central laboratories operated by the Division (LEM, ROTAN, SLMS, GDOES and Chemistry) provide services to researchers not just from the Division, but from the whole of FZU as well as external users, partially in the framework of open access to large scale infrastructures. The central laboratories operate highly specialized experimental equipment for characterization of structure and physical properties of solids with high exploitation potential. Experimental equipment comprises of scanning and transmission electron microscopy, x-ray diffraction, spectroscopic and chromatographic evaluation of chemical composition, analytical chemistry, and measurement of magnetic and other physical properties of solids over a wide range of temperatures and magnetic fields. This equipment is maintained and operated by skilled and highly qualified continuously trained staff.

Organization of research in the Division is based on a balanced combination of work carried out in specialized laboratories of individual research groups with research accomplished through services provided by the central laboratories. This organization enables fair and regular access to a wide range of unique equipment and methods, whilst at the same time facilitating fast development of experimental facilities and implementation of novel sophisticated experimental methods in central laboratories. This new strategy helps the Division perform contemporary world-class competitive research.

Division of Solid State Physics
Teams: 8 - Spintronics and Nanoelectronics, 9 – Low-Dimensional Atomic and Molecular Structures, 10 – Thin Films and Nanostructures, 11 – Structural Analysis, 12 – Semiconductors, 13 – Magnetics and Superconductors, 14 – Optical Materials

Solid state physics is a field that has an immediate impact on the everyday functioning of human society and its economically sustainable growth. It enables understanding the principles that govern the behaviour and manifestations of matter and creating solids purposefully with defined properties necessary for the development of our technically advanced civilization. The Solid State Physics division deals with the complex study of solids, from general theoretical principles to the synthesis and experimental exploration of specific technological materials.

With its needs, modern society defines the main challenges related to solid state physics and material research. These needs and challenges include rapid and efficient work with data, data storage, advanced medical diagnostics and therapy, detection and analysis of environmental processes, and sustainable energy production and storage methods. The decisive factor for achieving these needs is finding ways of targeted preparation of nanomaterials, their characterization and their utility in devices. A prerequisite for success is full understanding of the related physical phenomena from macroscopic down to the atomic scales.

One of our most advanced topics is spintronics (Team 8), with the long-term goal of improving the performance of computers to a point that enables functionality of individual components at sub-nm spatial and sub-ps temporal scales, dissipation-less electronics, and the realization of artificial neural networks. Other important topics are molecular electronics, low dimensional molecular materials and their characterization at the atomic scale (Team 9), with a vision of the development of quantum technologies based on molecular systems and new methods of controlling their electronic properties using self-organized layers. In the field of thermoelectric phenomena research (Team 13), we aim at the construction of so-called spin-caloritronic components, which will open the way to master and extend current photodynamic and photothermal therapies. In the area of detection (Team 14), we focus on nanomorphologic, nanocomposite and hybrid scintillation and phosphor materials, combining several detection functions into one material, thereby exceeding the possibilities of current classical volume materials. Another important area is improvement of growth technologies of high-quality silicon and diamond layers and structures important for the development of optoelectronic elements, biosensors and actuators (Team 10), and preparation of semiconductor structures for novel devices (Team 12). Modern material research also implies the need to develop new analytical methods focused on structural analysis (Team 11) of matter at the nanocrystalline level, with the vision of application of electron diffraction tomography for characterization of unstable materials or identification of drug structures.

In 2019, the division of Solid State Physics was organized in six departments corresponding to teams 8, 10, 11, 12, 13, and 14. Team 9 became a new department within the division in Spring 2020. The diamond materials research groups running within teams 10 and 14 were merged into Department of Diamond and Associated Materials in Autumn 2020, resulting in eight thematically well-defined closely collaborating units.

Division of Optics
Teams: 15 – Classical and Quantum Optics, 16 – Low-Temperature Plasma, 17 – Optical and Biophysical Systems, 18 – Fabrication and Analysis of Functional Materials

This division covers a wide range of research topics, which include optics, material science and engineering, optical technology, and biophysics. It consists of one technical and four scientific departments.

The Joint Laboratory of Optics, considered as a department in FZU's organizational scheme (Team 15 - Classical and Quantum Optics), is active in the investigation of both Quantum and nonlinear optics, as well as modern optical technologies. In the area of quantum and nonlinear optics, the research topics are mainly related to the generation, transmission, detection, and quantum processing of information using the fields of photon pairs obtained by parametric down-conversion. The department has been steadily concerned with advanced approaches and applications focused on various areas of applied (and technical) optics and optoelectronics, which find numerous applications for large international collaborations in particle physics and astrophysics. The department has also developed advanced methods for synthesis of

surfaces and layers, as well as related optical measurement methods, which have been offered to both researchers and industry.

The research of low-temperature plasma deposition processes within the Department of Low-Temperature Plasma (Team 16) is focused on the research and development of new low-temperature plasma sources used for the deposition of advanced thin film structures. The team has developed hybrid deposition systems based on the combination of pulsed high-power magnetrons and pulsed hollow cathode plasma jets, which are used for the deposition of high-quality semiconductor thin films at low temperatures. The development of UHV deposition systems with “in situ” advanced monitoring of deposition processes and plasma diagnostics have enabled detailed research into the growth processes of the said thin film structures.

The Department of Optical and Biophysical systems (Team 17) is mainly focused on the research and development of optical materials and systems for microelectronic, optoelectronic and biomedical applications. Spectroscopic ellipsometry and other optical techniques are used for the study of nanostructures, surfaces, and thin films; detection of surface, bulk, and interface phase transitions; and study of dynamics of biological films and surfaces. The optical structures for this research are prepared by pulsed laser deposition techniques. Research in the field of biophysics is comprised along the following lines: advancing the current knowledge of interfacial biomolecular interactions in their native environments, development of novel functional biomaterials for various biomedical applications, and understanding how physical factors (e.g. non-thermal plasma, nanomaterials, mechanical forces and laser irradiation) influence the processes that drive cell behaviour and functionality.

Advanced characterization of materials is performed within the Department of Fabrication and Analysis of Functional Materials (Team 18), which is a part of the Centre of Analysis of Functional Materials (SAFMAT). This department uses sophisticated analytical instruments, NanoESCA and EPR, the combination of which is optimized for the non-destructive analysis of chemical compounds (Imaging ESCA/XPS), imaging ultraviolet photoemission spectroscopy (UPS), and Angular Resolution UPS (ARUPS). The EPR laboratory is equipped by a Bruker ELEXSYS E580 spectrometer, which is a first-class scientific device for the measurement of electron paramagnetic (spin) resonance in both modes – classic (CW) and pulsed (FT), in the common X-band as well as high-frequency Q-band.

Division of High-Power Systems
Teams: 19 – Laser Interactions and Chemical Physics, 20 – Development of Lasers and Advanced Technologies (HiLASE)

Our mission is to explore and develop the field of high-power photonics, to push the frontier of laser technology beyond its current limits, and to improve understanding of fundamental aspects of laser-matter interaction and high-energy-density physics. The key pillar of this Division is the HiLASE laser Centre. In this research & development infrastructure, we combine scientific excellence with application potential oriented to technological development and hi-tech applications of high-power lasers according to the specific needs of industrial and scientific spheres. The basic modes of using the HiLASE infrastructure are collaborative and contract research, academic research, optimisation of laser technologies and processes, external user projects under Open

Access, and training of next generation laser scientists in cooperation with universities. Together with the Institute of Plasma Physics CAS, we also jointly operate and further develop the PALS research Centre. In addition to laser physics, our experts are active in plasma physics and ionized environments, physics of high energy densities and extreme states of matter, high-energy chemistry, atomic, ion and molecular spectroscopy, laboratory astrophysics, planetology, astrobiology, biophysics, nanotechnology, nanophotonics, and plasmonics. Both laser centres HiLASE and PALS are full members of the international network Laserlab Europe.

ELI Beamlines Project Division.
Team: 21 – Laser Physics at ELI Beamlines

This division has a very specific role. Its main goal is to establish and operate the ELI Beamlines centre as an experimental facility, which is part of the European Extreme Light Infrastructure (ELI) project listed on the ESFRI (European Strategy Forum for Research Infrastructures) roadmap since 2006. In both scope and expected impact, the ELI Beamlines centre is the largest research initiative in the history of the Czech Republic. In terms of scientific scope the centre represents mutually complementary and interconnected activities. Therefore, it is presented as one, in Team 21 (ELI Beamlines).

Since 2007, FZU has acted as the coordinator of ELI related efforts in the Czech Republic and as a recipient of funding mainly based on European Structural and Investment Funds administrated by Ministry of Education, Youths and Sports through the Operational Programme “Research and Development for Innovations” and later “Research, Development, Education”.

The vision of ELI is to establish the first international laser infrastructure with world-unique parameters, which will be fully open for user-oriented research.

ELI Beamlines provides a facility to perform a large variety of scientific applications, both of basic and applied research, examining the interactions of light with matter using light beamlines with intensities so far not reached.

Thanks to the combination of four high-repetition and high-power laser systems of up to 10 PW output and projected intensities of over 10^{23} W/cm^2, users have the possibility of employing unique laser-driven X-ray, and particle beams (electron and ion sources), and a plasma physics research platform to study high-intensity electro-magnetic fields and their interaction with matter and vacuum. The research laboratories of the facility are based on different beamlines enabling pioneering research in many areas, such as material science, biomolecular and biology, chemistry including medical, astrophysics and other scientific applications.

ELI Beamlines also strives to serve as a platform for local and regional innovation initiatives, as well as for providing top-level training for new generations of researchers and engineers.

Research activity and characterisation of the main scientific results

Introductory note: As the team's mission is to guarantee the successful participation of the Institute in international astroparticle projects which are usually large collaborations, the team was not allowed to provide a selected list of main publications for the first stage of the evaluation. In this section we thus carefully describe the team's activities together with references to major papers to which we contributed. During the evaluation period the group also published several short-author-list papers in peer-reviewed impacted journals. The total number of papers in impacted journals during the evaluation period reached 69, out of which 25 have a short author list. The bibliography of these papers is provided centrally in the section "*Participation in large collaborations*". To demonstrate the role of the team and its activity, the peer-reviewed outputs are extended by an additional 18 selected proceedings, all with a short author list, written on behalf of the corresponding collaboration by our group member(s).

The team's activity is focused on five research topics:

- Ultrahigh energy cosmic rays – Pierre Auger Observatory (including activities of the team *Laboratory for astroparticle physics)*
- High energy photons from space – CTA, SWGO and other experiments
- Instruments for atmospheric calibration of astroparticle experiments
- Related astronomical research
- Sky Surveys – Vera C. Rubin Observatory (LSST) (including activities of the team *Laboratory for testing and development of optical sensors for astronomy*)

Ultrahigh energy cosmic rays – Pierre Auger Observatory

The highest energy cosmic rays coming to the Earth from the Universe have been one of the most intriguing puzzles of modern physics for more than 50 years. These cosmic particles have an energy above 10 million trillion (10^{19}) electron volts (eV). One would need to increase the beam power of the LHC, the world's largest particle accelerator, by a million times, to achieve energies as high as these remarkable cosmic rays. There is no scientific consensus on how or where cosmic rays with these ultra-high energies originate. Cosmic rays with energies above 10^{19} eV arrive on Earth at a rate of only one particle per square kilometre per year. The especially interesting cosmic rays, which have energies of over 10^{20} eV have an estimated arrival rate of just one per square kilometre per century. In order to record a large number of these events, the Pierre Auger Observatory (www.auger.org) [1] has created a detection area in western Argentina of the size of 3 000 km^2. With unprecedented collecting power and experimental controls, the Observatory gathers the data needed to solve several important questions, namely: Where do these particles come from? What are they (composition)? How are they accelerated (source mechanism)? Does their energy spectrum end?

The Pierre Auger Observatory, the largest cosmic-ray detector ever built, records the so-called cosmic ray showers, which develop in the atmosphere as a result of an interaction of a primary cosmic ray particle coming from space with the atomic nuclei of air molecules. The properties of these showers are studied using two detection techniques – an array of 1660 surface detection stations (water Cherenkov tanks) used to measure the lateral shower profile and the fluorescence telescopes used to measure the longitudinal shower development.

The Institute joined the international collaboration in its early days in 1999 and participated in the design and prototyping as well as the construction of the Observatory. The main hardware contribution of the Institute was the design and production of 15 out of 27 (13 m^2) segmented mirrors of the fluorescence detector (see Fig. 1 for one of the four fluorescence detector buildings). Scientific topics connected with the fluorescence detector have remained the main part of the team's interest for many years. A member of the department continued serving as the Fluorescence Detector Task Leader at the Observatory through the years 2015-2018, another three team members currently serve in leadership positions: as the task leaders of the mass composition analysis working package and the Monte Carlo (MC) simulation package and, recently also as the task co-leader of the fluorescence detector. The team is also involved in the recent upgrade of the Observatory, operation of the fluorescence telescopes, data analysis and atmospheric monitoring.

Figure 1 Coihueco - one of the four fluorescence detector buildings at the Pierre Auger Observatory.

Our researchers attempt to understand how the properties of hadronic interactions taking place during shower development influence the properties of the observed showers [2] particularly in the context of the observed excess of the hadronic signal in the data of the Pierre Auger Observatory [3]. Having in mind the inconsistencies between the predictions of hadronic interaction models and measured data they search for less model-dependent methods to disentangle the composition of cosmic rays [4, 5, 6, 7]. The main author responsible for the paper [4], who is the coordinator of the mass composition task, strengthened the department team in 2017 together with another experienced scientist working on the estimation of muon content in atmospheric showers. Regarding composition of cosmic rays, the members of the department also contribute to the activities of the joint working group of the Telescope Array experiment located in the northern hemisphere [8]. Another recent activity of the group is to investigate how cosmic particles propagate through the Universe to the Earth [9]. The team is also responsible for the massive production of Monte Carlo libraries of cosmic ray showers used by the whole Pierre Auger collaboration. The team together with CERN colleagues in the Institute initiated the usage of the grid computing for the Observatory simulations. The grid has since become a major part of the official simulation production. The so-called AUGER grid virtual organization (VO) is now supported by ca 20 computing centers all over the world with central servers of the organization in Prague. This VO AUGER has been the largest computing organization in terms of computing time in astroparticle physics already for several years.

Our group is also closely cooperating with Charles University on the low-energy extension (up to 2 orders in magnitude) of the measurement of the cosmic-ray energy spectrum using Cherenkov- dominated events instead of fluorescence-dominated events that are used for the standard analysis [10]. The team is also involved in other novel projects related to the detection of cosmic rays based on Resistive Plate Chambers [11] or simplified fluorescence telescopes [12].

The Pierre Auger Observatory is in fact indispensable to the whole field of ultra-high energy cosmic ray physics. However, as this scientific field rapidly evolves, the structure, size and complexity of the Observatory needs to be modified to answer the newly appearing questions in sufficient detail. This is the major motivation for the ongoing upgrade of the Observatory called AugerPrime. While the flux suppression above the energies ~$10^{19,6}$ eV was unambiguously established by the Observatory and some hints towards origin of cosmic ray sources were recently found [13,14], the questions of the cosmic ray composition at ultra-high energies, location of sources of these rare particles and the characteristics of hadronic interactions remain open and will be addressed by the upgraded Observatory. The AugerPrime upgrade includes installation of scintillator detectors above each surface detector station as well as replacement of the electronics with a faster and a more powerful system that provides channels for additional detectors, increased dynamic range and processing capability, higher sampling frequency, and improved timing, calibration and monitoring systems. The testing of the new electronics boards [15] is conducted in three stages: the production test performed at the manufacturer site, the climate tests including accelerated aging executed in our laboratory and finally the end-to-end tests performed before their deployment at the Observatory in Argentina. The team *Laboratory for astroparticle physics*, established to cater for the experimental needs of experiments, which are in the scope of interest of the Department of astroparticle physics, became responsible for climate tests and accelerated aging of all the produced electronics boards. During the period 2015-2019 the laboratory was equipped with several crucial instruments and the testing bench has been developed by the department personnel, see Fig. 2. The participation in the AugerPrime upgrade clearly became one of the key team activities.

High energy photons from space – CTA, SWGO and other experiments

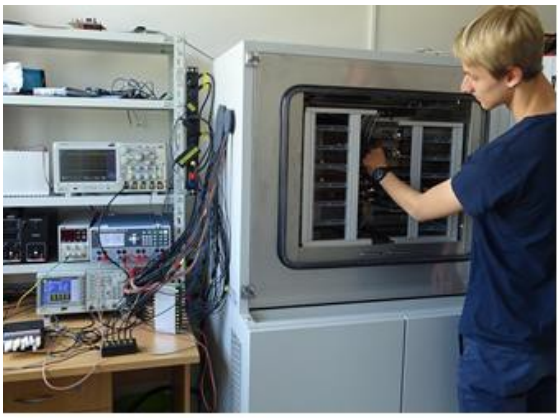

Figure 2 The experimental setup for climate tests of AugerPrime electronics boards in the Prague laboratory in June 2019.

Electromagnetic radiation at gamma-ray energies differs fundamentally from that detected at lower energies. Energies of gamma rays of the order of GeV to TeV cannot conceivably be generated by thermal emission from hot celestial objects. Instead, we find that high-energy gamma-rays probe a "non-thermal" universe and objects capable of the concentration of large amounts of energy onto a single quantum of radiation. Active Galactic Nuclei, Supernova remnants as well as, from as yet, unclassified sources produce the highest energy gammas reaching the Earth from the Universe. The Cherenkov Telescope Array (CTA - https://www.cta-observatory.org/) [16] will be the new generation observatory of (very) high-energy gamma-rays and as such it will enable the discovery of a large number of new astrophysical sources of gamma-rays and determination of their characteristics. This Observatory will be located at two places – on the La Palma island and at ESO, Chile and will consist of tens of Cherenkov telescopes of different sizes – Small Size, Middle Size and Large Size – detecting atmospheric showers induced by impinging gamma rays.

In the period 2015-2019 the Astroparticle Physics team was involved in two main CTA working packages – in the central calibration and in prototyping of Small Size Telescopes (SST). A member of the team was one of the leaders of the central calibration working group. The team was involved in atmospheric monitoring and observation scheduling. A novel method to determine the aerosol content of the atmosphere from wide-field stellar photometry (obtained by the FRAM telescopes) was developed and refined to a precision comparable with state-of-the-art methods in the field. It will serve as a tool to both characterize aerosol climatology at future sites of optical experiments (such as CTA) and to provide real-time data on atmospheric transparency during the operation of such experiments without producing any artificial light as in the case of laser-based methods. Three FRAM telescopes were constructed and shipped to both CTA sites. The first FRAM telescope was constructed in Chile in 2017, the second FRAM telescope was erected in 2018 at La Palma and the third FRAM telescope was installed in the autumn of 2019 again in Chile (see Fig. 3). The work was done in very close collaboration with Joint Laboratory of Optics in Olomouc which is responsible for another monitoring device, the All-sky Camera. More about the methods used to estimate atmospheric properties and outputs description is provided in part of the text about *Instruments for atmospheric calibration of astroparticle experiments.* Another study regarding the calibration of the telescopes was done jointly with the experts from Charles University and group task leaders [17].

Figure 3 The FRAM telescopes. Top left: the first CTA FRAM in Chile; top right: upgraded Auger FRAM in Argentina; bottom left: the second CTA FRAM on La Palma; bottom right: packing of the third CTA FRAM before its shipment to Chile.

Our team participated in the design, construction, operation and data analysis of the Swiss-Polish-Czech prototype of the SST-1M telescope. SST-1M was developed as a prototype of a Small-Sized Telescope for the CTA, designed for observations of the gamma-ray induced atmospheric showers for energies above 3 TeV. The SST-1M design is based on the Davies-Cotton concept with a 4-m multi-segment mirror dish composed of 18 hexagonal facets. The telescope is

equipped with an innovative camera which features a fully digital readout and trigger system, called DigiCam and adopts silicon photomultipliers (SiPMs) as light sensing technology. Most cameras being used nowadays in Cherenkov astronomy use Photo Multiplier Tubes, which have great sensitivity in the UV band, but suffer from shortened lifespan when exposed to background light. In contrast with PMTs, the novel SiPM-technology-based cameras can be operated without any aging under high night sky background (NSB) conditions. The first fully operational SST-1M prototype was installed in Krakow in 2017 (see Fig. 4) and it has been extensively tested since then [18]. The second prototype telescope is under construction. The prototype telescopes have the advantage that they can also be used outside the framework of CTA at another international gamma ray facility. Since CTA decided in favour of a different, dual mirror solution for SSTs, this turned out to be the case and the consortium is in the negotiation phase with several international observatories which are in principle interested in the opportunity to install two SST-1M prototypes at their sites.

In order to understand the data from the telescope prototype, to estimate its performance in Krakow conditions and to perform a high level analysis such as that of gamma/hadron separation or image reconstruction, a precise MC simulation of the telescope is necessary. The MC library was prepared by our team with the use of the high computational capacity of the Golias computer farm at the Institute. Our team, in close collaboration with the University of Geneva, JLO and Polish Academy of Sciences, was also responsible for the validation of the MC model. Various parameters of telescope optics, camera and electronics were measured in the lab and then validated and fine-tuned by comparison of MC results with real data [19]. For example, gain, camera electronics noise and dark count rate were determined by comparison of a raw distribution of signal measured in individual pixels with simulations. As a high level test of the validity of the MC model, distributions of image parametrization quantities for simulated cosmic ray background were compared with the real data and showed a good match.

Our team also participated in development of Digicampipe, which is a software for Cherenkov telescope data calibration and reduction up to image parametrization. We implemented features for single-telescope reconstruction, which are necessary for processing of the prototype observational data. To distinguish a shower image from a signal due to the Night Sky Background (NSB), a method of image cleaning has to be adopted during image processing. For the SST-1M data reduction, the ‘tailcut’ cleaning method was used and the parameters were optimized using our MC simulations of the prototype. The best parameters were found in order to reach optimal resolution without losing too many events.

Figure 4 Left: Prototype of SST-1M telescope with completed structure, Krakow, August 2016; Top right: Installation of the camera, August 2017; Middle right: Camera successfully installed, August 2017; Bottom right: one of the first cosmic ray showers detected by the SST-1M telescope.

For a single telescope, methods of machine learning were tested by our team members for the purposes of the reconstruction of energy, source position and the separation between gammas and protons based on shower image parameters [19]. The number of emitted Cherenkov photons is proportional to the energy of the primary gamma ray. Therefore, the energy of the primary photon can be reconstructed from the number of photons (or photo electrons) detected, and the distance of the shower core from the telescope, which is expressed by the impact parameter. In the case of multi- telescope detection, the impact parameter can be calculated from trivial geometry, which is not possible for mono reconstruction. In that case, however, the impact parameter for

distant showers can be derived from the timing of a shower image. For the energy reconstruction, we tested Random forest regressors, trained on simulated point-source gammas and found energy resolution of the method to be about 30%. Arrival direction of a shower and thus the position of the source in the camera FOV can be estimated from the shape of the shower image. For the reconstruction of the arrival direction of the shower, the members of our team first extensively tested several implementations of the so-called DISP method, but finally concluded that the machine learning approach using Random forest gives the best results. A similar approach was also used for gamma/hadron separation. As the event rate in the whole Field of View from background is about three orders of

magnitude higher than the rate from the strongest gamma ray source in the sky – the Crab nebula, gamma/hadron separation is a very important step in the data analysis. As a final step, differential sensitivity of the prototype was calculated and event rates for Crab gammas and CR background depending on chosen cuts were estimated [19]. Further analysis of the first scientific data taken by the telescope during 2017-2018 with the use of the methods implemented is still ongoing.

Another team activity, started only in 2019, is the participation in the Southern Wide-field-of-view Gamma Ray Observatory (SWGO - https://www.swgo.org/) which is an international initiative to design the future wide field gamma observatory in the southern hemisphere. While SWGO would be able to study the whole southern gamma ray sky permanently with worse spatial resolution, CTA will be able to trace the details of the selected sources with unprecedented sensitivity.

Instruments for atmospheric calibration of astroparticle experiments

Extensive air showers produce only very faint light (be it fluorescence or Cherenkov radiation) and are usually observed from distances of many kilometres. Naturally, knowledge of the attenuation of light on its path between the shower and the detector is important in the data analysis. Under normal conditions at the typical sites of optical astroparticle experiments, the main contribution to the attenuation comes from the molecular atmosphere through absorption and Rayleigh scattering. As the molecular component varies slowly in time and the necessary data can be obtained using meteorological tools, the main challenge is the determination of the contribution of aerosols, which, while typically smaller, is still significant and can vary quickly in time and space. Additionally, the presence of clouds needs to be monitored, sometimes with unusually high requirements for sensitivity to small and optically thin clouds. We commissioned the first version of the FRAM robotic telescope at the Pierre Auger Observatory in 2005 as a device to monitor the attenuation of light in the atmosphere using stars as reference sources. By 2015, the FRAM had already undergone several upgrades, as well as major changes in its scientific program, with the search for atmospheric showers with anomalous profiles clearly taking a priority. In this program, commonly referred to as “Shoot-the-Shower” (StS), the fluorescence detector of the Observatory sends a trigger when a shower with an unusual profile is detected and the FRAM takes a series of images along the apparent path of the shower to assess the presence or absence of clouds and other inhomogeneities that could have affected the profile. The potential detection of such showers (in absence of any atmospheric explanation) has profound implications for hadronic physics and mass composition of the primary beam [20,21].

The idea that stellar photometry with FRAM could also be used for precise determination of the aerosol contents of the atmosphere has been touted from the beginning, as this method has the advantage of being fully passive, unlike the more commonly used LIDARs that actively produce light which then interferes with the operation of the optical detectors. The passive character of FRAM measurement would allow for much larger temporal and spatial coverage than any active method. However, this measurement is notoriously difficult to perform with a precision better than 0.01 in the total vertical atmospheric optical depth (VAOD) as required by the needs of the astroparticle experiments (and commonly achieved by LIDARs) due to high demands on the calibration and stability of the detector, knowledge of the properties of the sources (stars) and possibly fast temporal changes of the measured quantity. The first promising results have been obtained using a novel method whereby a large number of stars at different apparent altitudes are measured in a short time span and the VAOD is obtained from the altitude dependence of the attenuation, independently of the absolute sensitivity of the detector. The method was developed using the data taken during the StS program but the data acquisition was quickly expanded to dedicated aerosol observations [22].

Since 2012 and during the whole evaluation period, we have been involved in the preparatory phase of the Cherenkov Telescope Array (CTA) project, first mainly in the site selection campaign through a collaboration with our colleagues from the Joint Laboratory of Optics [23]. We proposed the possibility to use a variant of the FRAM design for atmospheric monitoring at the CTA, first mainly for the detection of thin or small clouds [24], later – as the aerosol analysis surfaced – as a device to continuously monitor the aerosol contents in the field of view of the CTA telescopes [25]. We have developed a FRAM design tailored to the CTA use and eventually deployed three prototypes to the future CTA sites for testing and also for the preliminary characterization of the conditions at the sites in preparation for the data analysis from the CTA telescopes [26]. The future CTA sites are some of the best astronomical locations on the planet (as evidenced by the presence of some of the prime astronomical installations in close proximity) and the data obtained there allowed significant progress in the development of the analysis [27].

The most significant progress was obtained after the source of the spurious dependence of measured aerosols on the Moon phase was traced to a previously unknown non-linearity of the CCD detectors

used at small light fluxes and a laboratory method of calibration for this effect was developed [28]. Currently, a complex overview of the systematic effects of the method is ongoing, with the goal of achieving a reliable measurement of the VAOD with a total uncertainty smaller than 0.01 after a 5-minute series of exposures in various apparent altitudes. Such a method could eventually find various applications even outside the field of astroparticle physics.
In parallel to the prototype operations, the procedures to be applied during the future data taking with the CTA are being developed [29]. It is foreseen that the FRAM measurements, which only provide the integral VAOD between the ground and the edge of the atmosphere, will serve as a bridge between individual measurements of the LIDARs which can provide vertical profiles of aerosols, at the cost of interference with the CTA observations. If the FRAM data show a significant change in transparency, a LIDAR run can be triggered to investigate the vertical structure of the effect. In this way, the FRAMs will be an integral part of the CTA Observatory and thus a significant effort is being expended towards making them reliable through the 30 years of planned operations. In 2019 FRAM installations were recognized as so called CTA pathfinders, i.e. devices installed at the sites prior the installation of the main array with the aim to be accepted by the Observatory as an in-kind contribution of the Czech Republic.
Over time, we have expanded our involvement in atmospheric calibration beyond the original FRAM project. The Sun/Moon Photometer is a commercially available device with a similar concept to the FRAM, using the Sun and the Moon as reference sources instead of the stars. The daytime measurements using the Sun are considered to be a solid reference in aerosol climatology. Currently, one Photometer is installed on each of the future CTA sites and we are responsible for their operation and data processing. While the analysis of the daytime data is standardized, the behaviour of aerosols on a site may be vastly different during the day and the night. However, the state-of-the-art analysis of the Moon-based measurement quotes an error of 0.04, which is too large for use in aerosol climatology for the CTA purposes. We have thus developed new methods for data processing [30] and the resulting correlations between the Photometer and the FRAM measurements are several times better. This improved analysis has also clearly indicated that one of the Photometers was faulty. Another commercial device we are preparing for the use by the CTA is the Ceilometer, a portable infrared LIDAR for fast determination of the altitude of clouds detected by the All-sky Cameras.
Our growing involvement in the atmospheric calibration working group of the CTA means that we are also often tasked with coordination of the presentation of the various activities [31, 32].

Related astronomical research

In addition to atmospheric monitoring, the spare time of the FRAM telescopes is being used for the observation of carefully selected eclipsing binaries (EB), mostly those on eccentric orbits or with a third companion. In close cooperation with Astronomical Institute of the Czech Academy of Sciences and Charles University, our team members ensure scheduling and observation of selected targets, data processing [e.g. 33, 34] and eventually participate in analysis, modelling and interpretation of the data [e.g. 35, 36].
It is well known that a substantial fraction of all types of stars in the solar neighbourhood form binary or multiple stellar systems. The eclipsing binaries are important objects to study. In particular, multiple stellar systems are unique laboratories for astrophysics, because they can help us in solving the problem of their origin and subsequent evolution of higher order multiples.
Despite the huge effort of astrophysicists in the field of stellar multiplicity in recent years, some mysteries about multiple systems still remain. For instance, recent results of a thorough analysis of data from the Kepler mission have shown that there is a significant drop in population of triple systems with the period of a third component less than 200 days. A convincing theoretical explanation for this effect still remains to be proposed. In spite of the intense research, there are still only a few multiple systems with precisely determined orbits and physical parameters of all components, especially outside the Milky Way galaxy. A particularly interesting situation occurs when the inner binary in a compact triple system is eclipsing. This is because the stellar interaction, typically resulting in precession of orbital planes, may be observable as a variation of depth of the eclipses on a long timescale.
In the study [35] a member of our group presented a novel method to identify compact triples using publicly available photometric data from large surveys. The method was applied on archive photometric data from the OGLE database in order to identify the cases where the orbital plane EB evolves in accord with expectations from the interaction with a third star. Among more than 32000 light curves of eclipsing binaries in Large and Small Magellanic Clouds, 58 candidates of new compact triples were found, eight of them were thoroughly analysed and physical parameters of their inner binary systems were determined together with an estimation of basic characteristics of the third star in the system. The analysis also led to restrictions on the upper limit of the possible orbital period P2 of the third body. It

was shown that the studied sample of new compact triples is almost completely located within the area of the lack of these systems. Moreover, periods of some systems in the sample might be close to the limit of stability, which is not determined unambiguously. Thus further analysis of these new systems may provide important clues about stellar formation.

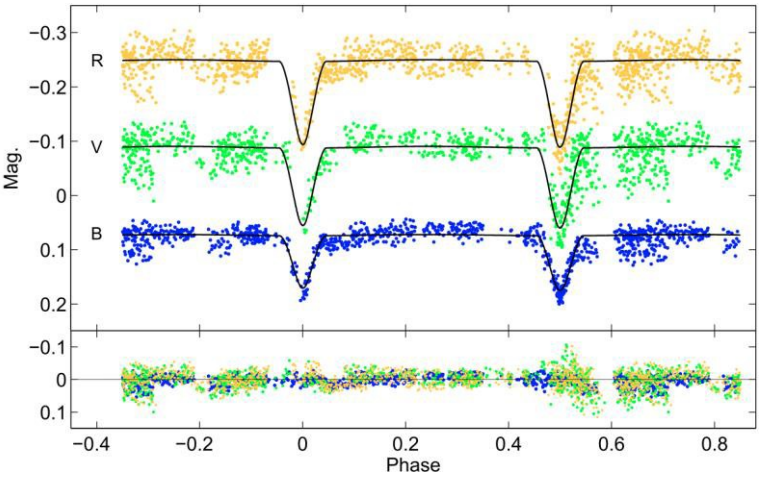

Figure 5 Light curve of eclipsing binary BR Ind as obtained by FRAM.

In the study [36], members of our group, in close cooperation with a different team at Charles University, focused on three close eclipsing binaries, suspected for presence of a third body in the system. In this case, the FRAM telescope located in Argentina was used for observation of the BR Ind eclipsing binary and a light curve in three photometric pass-bands was obtained (Fig. 5). Our team members also contributed by a complete analysis of the V773 Cas system. Light-curves together with radial velocity curves were analysed and modelled in order to determine physical parameters of the system. Our analysis confirmed the presence of a third body in the system and showed that this system has to be much closer to the Sun than previously expected.

Photometric data observed and reduced by members of our group with the use of the FRAM telescope was also used in the work [33], where 54 eclipsing binaries on eccentric orbits were studied. If a binary orbit is eccentric, apsidal motion occurs due to general relativity effects and also dynamical effects caused by the internal structure of the stars, which makes eccentric binaries very important objects for stellar astrophysics. The apsidal motion can be observed as timing variation of light curves minima. To observe such effect, however, relatively long time-base of measurements are needed. In the above mentioned study [33], archive observations were used in combination with those performed by the FRAM telescope and apsidal motion parameters of all the systems studied were determined.

Sky Surveys - Vera C. Rubin Observatory (LSST) (including activities of team *Laboratory for testing and development of optical sensors for astronomy*)

Observational projects in cosmology typically rely on gathering of huge amounts of data that are later statistically analysed, e.g. in order to determine gravitational microlensing statistics, to study baryonic acoustic oscillations or the statistics of type Ia supernovae. By far the largest and most ambitious ground-based sky survey project is currently the Vera C. Rubin Observatory – LSST (www.lsst.org). The telescope is currently under construction and should see first light in 2022. The LSST telescope will be equipped with the 8.4-meter primary mirror and the largest focal plane in the world that will be composed of 200 16-Megapixel CCD (CCD – Charge Coupled Devices) sensors. Since 2008, the Institute of Physics has been involved in the characterization and testing of these CCD chips for the LSST telescope camera and since 2012, the Institute of Physics is an affiliate member of the LSST Corporation, becoming the third non-U.S. member of this scientific collaboration. Our activities include working on both, the instrumentation and the sky objects detection. We investigated the “tree rings”, a phenomenon typically affecting the signal measured in the wavelengths range from 400 nm to 800 nm, while other surface features appear only on shorter wavelengths below 400 nm. The tree rings [37] are circular patterns due to the variation of the monocrystal silicon boule concentration induced by the manufacturing process (see Fig. 6). The parasitic electric field inside the sensor creates a non-uniform density of charges and can cause some displacement of generated photoelectrons and thus distortion of the observed astronomical sources. The longest wavelengths penetrate deeper into the silicon explaining the decreasing amplitude of the tree rings pattern with the wavelength. The resistivity varies with the radius of the tree rings, reaching 0.1 to 1.0% from the centre to the outer part of the wafer. Another study within the LSST looked at the shortest wavelengths, where another effect has been observed,

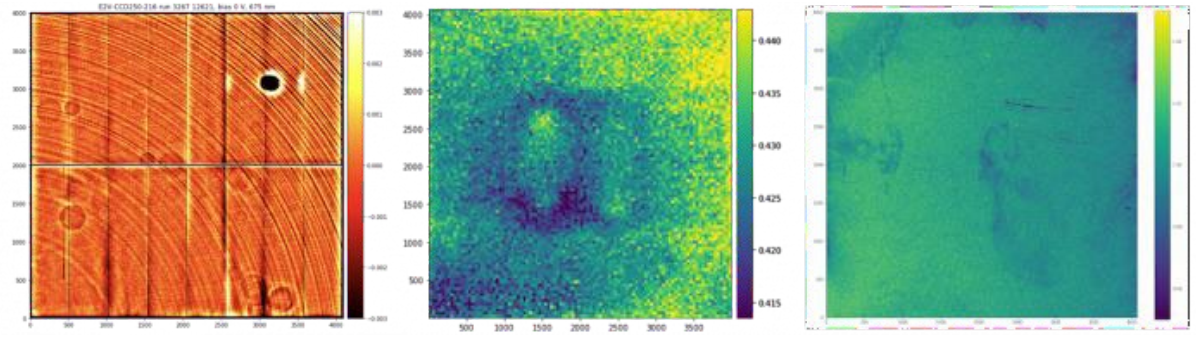

Figure 6 Example of the instrumentation effects analyses done in our group. From left to right: The "tree-rings effect", variation of 55Fe hits shape, ITL surface effects.

surface inhomogeneities. The non-uniform anti-reflection coating of the detector surface creates a pattern specific for each sensor. This induces a variation of the signal amplitude depending on the impact position and wavelength and therefore a spectrum-dependent sensitivity variation of the observed source image. The results of both these studies serve to correct for those effects or, if corrections are not possible, at least to be taken into account during image analysis.

The experimental activities of the related *Laboratory for testing and development of optical sensors for astronomy* are not only connected to LSST. Generally, they are focused on characterization of the performance of various photo-sensors such as CCD, CMOS for astronomical applications. The laboratory is now well suited for thorough testing of imaging detectors and cameras, as well as to collaborate with external groups and projects on various topics related to such detectors. In past years, the main effort has been focused on establishing a laboratory [38] suitable for performing tests under well controlled thermal and optical conditions. The setup includes a Dewar flask mounted onto a custom made vacuum chamber, which houses the tested detector. A glass window at the front allows for illumination in a wide range of wavelengths. The vacuum ensures thermal isolation and prevents water condensation, which can damage the detectors under test. The tested devices are cooled via a thermal strap connected to a liquid nitrogen container. The temperature can be precisely set by a CryoCon controller, using a PID loop and heaters. An assembly of two pumps and an anti-vibration system achieves a high vacuum (10^{-7} mbar). The light source is an APOLLO X-600 Xenon lamp connected to an ATLAS 300 monochromator. A light fibre guides the light of a selected wavelength to an integrating sphere. A dark box is mounted in front of the vacuum chamber window on an optical table. The purpose of the box is to improve the uniformity of the light when arriving at the sensors. It also allows for installing additional optical elements in the light beam. A dedicated open-source software framework, CCDLab, has been developed by the group to control and monitor the individual devices during the experiments, and to allow user-level scripts to facilitate complex experimental protocols. The framework includes a web interface for both real-time control of the test bench state, and retroactive inspection of its history. The team used this experimental setup to perform laboratory measurements of several commercially available CCD and CMOS cameras to assess their usability for sky survey applications, and to implement an instrument signature removal (ISR) pipeline for them. Thus, the researchers thoroughly studied the linearity and bias stability properties of a number of large-format G4-16000 cameras based on Kodak KAF-16803 CCD chips, to be used for sky survey applications on wide-field cameras of FRAM telescopes. To this end, a dedicated experiment protocol was implemented based on acquiring long series randomized length exposures mixed with “control” ones of fixed duration to monitor the stability of the light source, interleaved with dark frames to monitor the bias level temperature stability. As a result, the signal response non-linearity properties of all individual cameras was thoroughly characterized. All have similar characteristic piecewise shapes with different amplitudes (from a few to tens of percents), and routines were implemented for “linearizing” the data which is essential in order to use these cameras for precise photometric applications [28].

The group also performed extensive laboratory testing and characterization of an Andor Marana sCMOS camera, based on a recently developed “scientific CMOS” technology of large format extremely low-noise complementary metal–oxide–semiconductor imaging chips which are extremely promising for modern wide-field sky survey applications especially those requiring fast readouts and/or high frame rates. The experiments performed on the camera included both the laboratory testing in order to characterize the dark current properties, bias stability, gain and flatfield stability, read-out noise and the noises specificto CMOS technology (random telegraph noise and amplifier switching noise), as well as image ghosting (residual bulk images), and a dedicated on-sky testing of the camera in conditions typical for a small aperture wide-field sky survey application (e.g. similar to FRAM telescopes). The group demonstrated that the camera has quite good linearity (down to the level of a few per cent) up to approximately half of the dynamic range, acceptable dark current, read-out noise on par with best CCD chips, but some pixel level instabilities on both low and medium signal levels, along with abrupt gain and flatfield structure change at medium and high signal levels, both specific for CMOS and different from typical CCDs, thus requiring specific handling at the data processing stage in order to achieve the best possible performance [39].

Research activity and characterisation of the main scientific results

Experiments in particle physics are currently concentrated in a few large laboratories around the world. They are carried out by large international collaborations. Naturally, the main research outputs of our team are therefore published in papers with many authors. Evaluation methodology however forbids listing these large collaboration papers in the output part 3.3. The members of our team are also authors of several related phenomenology papers. We decided not to list them in part 3.3 as this would provide a highly biased representation of our results.

In the following we give a more detailed description of our scientific achievements with emphasis on our contributions. We provide a selection of our results at the extent roughly required in part 3.3. We hope that this information will help the evaluation board to understand clearly the role that our team plays in these large collaborations.

International experiments

The major experimental activities of this team are carried on within experiments and R&D projects in two laboratories, CERN and FERMILAB. Here we provide reports for each experiment.

Experiment ATLAS at CERN

FZU is a founding member of the ATLAS Collaboration. This group of about 3000 scientists from more than 180 laboratories and universities around the world has built from 1992 to 2008 the ATLAS detector, one of the most complex scientific instrument ever constructed. ATLAS and CMS are the two largest LHC experiments designed to explore the discovery potential of LHC in high energy proton-proton collisions. The most important discovery, made so far by the ATLAS and the CMS Collaborations, was the discovery of the Higgs boson in 2012. There were 24 researchers from FZU on the author list of this discovery paper.

Our researchers contributed mainly to the design and construction of the inner tracking detector and hadronic calorimeter Tilecal. New laboratories were provided in the premises of FZU for testing semiconductor sensors and for assembling Tilecal modules. Close cooperation with industry led, in the past, to concluding contracts from Czech companies with CERN, resulting in delivery of pixel sensors, various high and low voltage power supplies, and vacuum components. Our current and future activities are closely related to these past activities.

There are four ATLAS groups in FZU: Inner detector group, Tilecal group, Forward physics group, and Physics analysis group. By far, the ATLAS group is the largest experimental group in the presented team. In total, there are 11 senior physicists, 2 post-docs, 5 PhD students, 2 undergraduate students, and 6 engineers and technicians. Four PhD students defended their theses on subjects related to ATLAS during 2015-2019.

Activities of these four groups followed the schedule of LHC. Thanks to its excellent performance, LHC delivered during 2015-2018, so called Run 2, to the ATLAS experiment, 156 fb^{-1} of proton-proton collisions at a centre-of-mass energy of 13 TeV. A long LHC maintenance shutdown started in 2019 and the collider should be ready in 2022 to produce more intense proton collisions at higher centre-of-mass energies between 13.5 to 14 TeV. The ATLAS Experiment is using the shutdown to prepare for the increased LHC performance.

The next long LHC shutdown is planned for 2025-2027, during which the LHC will be upgraded to provide even more intense proton beams with a luminosity about 5-7 times higher than the original design, High Luminosity LHC (HL-LHC). This implies the need for replacement of ATLAS critical components to cope with the new harsh environment and to manage the increased data flow. As new ATLAS components should be ready for installation in 2025, their development and construction has already started. Our team participates in the construction of a new inner tracker, upgrade of readout electronics for hadronic calorimeter Tilecal, and in an upgrade of trigger and whole detector readout.

Inner Detector Group

Alongside operation and maintenance responsibilities of the current inner tracker detector, this group is involved mostly in the construction of a new Inner Tracker (ITk) capable of operating in radiation hard environments in HL-LHC. The tracker is the inner most ATLAS detector installed close to the LHC beam-pipe. ITk is made of layers of semiconductor sensors of pixel and strip types, placed in a high 2T magnetic field. Collisions of charged particles in the sensors allows reconstruction of the particle tracks and measurement of particle energies from the track curvatures.

FZU took responsibility for the construction of the ITk part, based on strip sensors [1]. In particular, about 4500 strip sensors are foreseen to be tested in Prague prior to their assembly, including radiation tests with a ^{56}Co source at UJP Praha. In addition, about 750 modules, corresponding to one-disc type layer, will be assembled at FZU. This is a major ATLAS HL-LHC task for the whole Czech ATLAS community, and it is carried out together with three other Czech ATLAS institutions: Charles University, Czech Technical University, and Palacký University. To perform this task, the group set up a new clean laboratory at FZU. Thanks to the strong support from FZU and the Academy of Sciences, the lab was equipped during 2017-2019 with the necessary devices (probe and metrology stations, bound-bonding machines, etc.) to be ready for preproduction tests in 2020 and for full production starting from 2021.

The design of a new tracker benefited from the achievements of the CERN project RD50. The aim of this project is development of new radiation hard semiconductor devices for future experiments in extremely high luminosity colliders. Our group contributed to RD50 by measuring key characteristics of newly developed sensors, including irradiation tests [2].

We are also involved in ITk project management . A member of our inner tracker group is responsible for the organization of irradiation tests for various ITk strip components at several irradiation facilities, i.e. CERN, DESY (Hamburg) and UJP Praha (cobalt source in Institute of Nuclear Fuels in Prague).

From an operational point of view, the most important contribution is support of two of our experts directly at CERN. One is responsible for the instrumentation of pixel detectors, their operation and preparation for HL-LHC upgrade. The second is an expert on pixel readout and trigger.

Tilecal Group

Tilecal is hadronic calorimeter made from passive iron plates as an absorber and plastic scintillating tiles as an active material. This group is heavily involved in Tilecal operation and maintenance [3]. In particular, during the current LHC shutdown we were responsible for the replacement of all low voltage power supplies. For the HL-LHC upgrade, we mainly contribute to the development and construction of new power supplies. The group cooperated closely with the Czech company Foton, which delivered in 2017 to ATLAS prototype power supplies for HL-LHC. Finally, however, ATLAS decided to use a different technology.

Forward Physics Group

The ATLAS experiment has two detectors in a very forward region dedicated to the measurement of protons scattered at very small angles. The ALFA spectrometer, located in the LHC tunnel about 240 m from the ATLAS interaction point, has vertical Roman Pots. Its main purpose is similar to the TOTEM experiment. It was designed to detect elastically scattered protons during dedicated LHC low luminosity runs and to measure elastic and total cross sections of proton-proton interactions.

Instrumentation of the forward region was extended recently by additional horizontal Roman Pots, located about 220 m from the interaction point. These detectors (AFP) have a good acceptance for diffractive protons, i.e. protons which survived the collision losing only a small fraction of their incident energy. Unlike ALFA, AFP operates during normal LHC runs. It consists of a tracker (several layers of pixel sensors) and a precise timing detector. Both AFP and ALFA detectors use the same housing, which was developed for the TOTEM experiment, so-called Roman Pots. These were made by the Czech company Vacuum Praha. AFP detectors were installed during shorter LHC shutdowns during 2016-2017 and are currently being commissioned and the first data, taken during Run 2, are being analysed.

Our group was involved in the AFP project from the very beginning, starting from the conceptual design, formulation of the physics program [4,5, 37], up to the installation and analysis of ATLAS data related to diffractive physics [16,21]. Two members of our team were/are physics coordinators and deputy coordinators of the AFP project [6], and our engineer was the technical coordinator for the installation of AFP in the LHC tunnel.

Physics Analysis Group

The unique ATLAS Run 2 data set of proton collisions at 13 TeV allows us to explore the properties of matter and space-time at the highest energy scales achievable in earth laboratories. ATLAS submitted, or sent for publication, more than 215 publications based on 13 TeV proton-proton data, and in total 496 papers during the evaluation period. Among them, measurements of properties of the Higgs boson, the last missing particle of the Standard Model of particle physics (SM) discovered by ATLAS and CMS experiments in 2012, are between the most cited results. The ATLAS

physics program is much broader than the physics of the Higgs boson, it includes precise measurements of other SM particle properties (top quark production rates and mass, W-boson mass, etc.), studies of CP violation mostly in decays of hadrons with b-quark, various tests of SM physics, both for electro-weak and strong force, and numerous searches for a sign of new phenomena beyond SM.

Our researchers focus on the following topics: physics of top quark, physics of b-quark, physics of electro-weak interactions, and physics of strong interactions. Here we give a short summary of ATLAS published results, which contain a direct and significant contribution from the researchers of our team. They are listed internally by the ATLAS experiment as primary authors of these measurements.

The *Top physics group* contributed to several published ATLAS results. The most recent is the measurement of the differential cross section of ttbar pair production in so-called highly boosted topology in hadron decay channels of top quark [7]. In this channel, the top quarks exhibit such large transverse momenta, that their product decays form one collimated spray of particles. We contributed to this measurement by estimation of the multijet background, propagation of systematic uncertainties, unfolding and by the development and maintenance of analysis code. An established topic widely studied by our group is the charge asymmetry in pair top quark production. This group was a driving force behind the published measurements of charge asymmetry in the dileptonic decays of top quark pairs at 7 and 8 TeV centre-of-mass energies [8-9].

The *B-physics group* concentrated on measuring various properties of decay products of mesons, which contain b quarks. The most recent activity is the search for state X(5568), a tetraquark candidate reported earlier by the D0 experiment. No sign of narrow resonance was observed in the ATLAS data [10]. The group is also involved in the measurement of CP-violating phase φ_s and B_s decay width difference in $B_s \rightarrow J/\psi+\varphi$ decays [11]. Another topic was a study of production mechanism of b-hadron pairs [12]. All three topics were the subject of three different theses, which were successfully defended.

Activities of the *electro-weak group* are represented by contributions to the three ATLAS published results. The first is the measurement of Z-boson pair production in all leptonic decays with electrons and muons [13]. Data agreed with SM predictions and were used to put constrains on the strength of anomalous triple gauge couplings in models beyond SM. The work was extended towards the final state of two jets produced in association with a Z-boson pair. Preliminary results, released recently in the form of an ATLAS conference note [14], report the first observation of electroweak production of two jets in association with a Z-boson pair. This result is an important milestone for testing interactions between gauge bosons and the interplay with the Brout-Englert-Higgs mechanism. Final publication of this important observation was submitted to Nature Physics in April 2020 [15]. Work on papers [13-15] is part of a PhD thesis, which is in preparation. Our PhD. student contributed to [13] to unfolding the cases when production of ZZ pair is accompanied by jets, for [14,15] he performed a selection of events for the measurement and estimated the most complicated background with fake leptons. He also contributed to parts of text in [14].

The second published analysis was a measurement of exclusive muon pair production in proton-proton collisions, which comes dominantly from γγ→μ+μ− scattering [16]. Photon-photon induced interactions are quite rare in the LHC proton collider. Yet, they represent a unique opportunity to study electroweak processes. For example, in the pair production of intermediate bosons γγ → WW, we can study with high precision, the quartic coupling between photons and W. The measurement of exclusive WW production is one of the future milestones of the AFP community. The measurement of exclusive dilepton production γγ → μμ is an important step in this program. It shows that we are able to identify photon-induced events on the enormous background. The group works now on exclusive γγ → WW analysis. It builds on the experience gained during their work on measurement of W-boson pair production [17]. The possibility of using LHC as photon-photon collider is a long-term subject of Oldrich Kepka's research. He was the main leader of the published γγ→μ+μ− measurement [16] and new analysis of exclusive WW production. Preliminary results have already been presented at ICHEP2020.

Most of the interactions produced in proton-proton collisions at LHC are induced by strong interaction. A good understanding of this processes is important for most of the ATLAS results, as these events constitute typically one of the leading backgrounds. Our *strong interaction group* contributed to several measurements of basic properties of average proton-proton interaction [18-21]. The contribution of two of our master students, Filip Nechansky and Matous Vozak, under supervision of Oldrich Kepka was so high that it was recognized by the ATLAS Collaboration and they were allowed to exceptionally sign papers [20] and [21].

Another important activity of the group is contribution to several measurements related to the physics program of the AFP detector. As was mentioned above, forward physics is one of our long-term research themes, where our group plays a key role at ATLAS. Besides the mentioned measurement of exclusive muon pair production, the group contributed to the measurement of dijet production associated with large rapidity gaps [22]. The work was also the base for defended PhD thesis.

For FZU, participation in the ATLAS experiment represents a unique possibility to contribute to the worldwide effort in the pursuit of fundamental laws, which govern the behaviour of the matter and universe around us. The hope is, that with increased statistics and higher collision energy, the LHC experiments can reveal new unknown phenomena outside the framework of the current Standard Model of particle physics, and that this would help us to answer open questions about the origin of dark matter and dark energy. After all, current astronomical observations are telling us that the known elementary particles from the SM constitute only 4% of the universe.

Experiment TOTEM at CERN

FZU is among the founding members of the TOTEM experiment. TOTEM is a smaller LHC experiment dedicated to measurement of elastic proton-proton cross section at LHC energies. Our physicists played an important role during construction. Vacuum parts of detectors, so call Roman Pots, were provided by the Czech company Vacuum Praha. The technology was also used later on for the ATLAS Roman Pots. The experiment is due to to finish in 2022 after it measures the proton elastic cross section at the highest LHC centre of mass energy, either 13.5 of 14 TeV. This is reflected in

the size of our TOTEM group. In 2019, it consisted of 1 senior physicist and 2 postdocs (one of them defended his thesis in 2018), today it is even smaller (1 senior physicist and 1 postdoc).

Nevertheless, as TOTEM is a much smaller than ATLAS (with about 100 authors signing papers) the group has significant impact on published papers. Besides the contribution to the operation (both postdocs were permanently at CERN, where they had responsibilities connected with operation and calibration of TOTEM detectors), the group is involved directly in the analysis of the TOTEM data and in phenomenology of proton-proton collisions. The model proposed by Kundrat and Lokajicek [23] was used by the collaboration for the analysis of the 8 TeV data [24]. Between the most interesting recent results, is possible observation of new colourless three-gluon C-odd state, so called Odderon [25], and the measurement of elastic differential cross section at 13 TeV [26].

Experiment ALICE at CERN

The ALICE experiment focuses on analysis of heavy ion collisions at LHC. One of the goals is to study matter at very high temperatures and densities, in particular new states of matter called quark gluon plasma. During the evaluation period, it published 168 papers. Our ALICE team is the smallest of our CERN groups. There are two senior physicists and one research assistant.

The group is very active. Recently they proposed utilizing pattern recognition methods developed for the analysis of heavy ion collisions in the field of astrometry [27]. They applied it for statistical analysis of binary stars from the Gaia catalogue, the resulting new atlas of binary stars was published in early 2020 [28]. Although our ALICE group is small, the overall ALICE group in FZU is larger. There is another group involved in ALICE under the leadership of Jiří Mareš from the Department of Optical Materials. Beside their contribution to the ALICE operation, they are involved in the CERN R&D project CrystalClear dedicated to the development of new scintillating materials for future generation particle detectors. Their cooperation with industry led to a contract for the Czech company Crytur from the CERN experiment LHCb for crystal scintillators.

Petr Závada from ALICE group has a long time interest in various aspects of proton structure, namely the origin of proton spin. He is author of several phenomenology papers on this subject [29]. He is also a member of COMPASS, a fixed target experiment at CERN dedicated to spin physics and proton structure.

The NOvA Experiment at Fermilab

We joined the NOvA experiment in 2011 and since then NOvA became our main intensity frontier experiment at Fermilab. NOvA, Fermilab's flagship neutrino oscillation experiment, recorded its first neutrinos in 2014 and since then has made precision measurements of electron–neutrino (ν_e) appearance and muon–neutrino (ν_μ) disappearance. This data will help unravel the remaining unknowns in our understanding of neutrino masses and mixing. NOvA uses two detectors to measure oscillation probabilities in Fermilab's NuMI (Neutrinos at the Main Injector) muon neutrino beam. When neutrinos travel the 810 km between Fermilab and Ash River in

Minnesota, through the crust of the Earth, scattering of ν_e on atomic electrons can either enhance or suppress the oscillation probability, depending on the mass hierarchy. The effect is opposite in neutrinos compared to antineutrinos, so by comparing the oscillation probability measured in neutrinos to that measured with antineutrinos, NOvA can determine the mass hierarchy, resolve the nature of mass eigenstate ν_3, and begin the study of CP violation in neutrinos. In addition to an intense beam, NOvA also requires a massive Far Detector and a functionally identical Near Detector. Like all neutrino detectors, the NOvA detector must be large to overcome the small size of the neutrino interaction cross-section and the 810 km distance from the neutrino source. Being large, however, is not enough; the detector must also be highly segmented to prevent the numerous cosmic rays, which cross the detector from interfering with neutrino events from Fermilab. The NOvA detector represents a unique solution to the particular challenge of observing ν_e appearance using the NuMI neutrino beam line. The NOvA Far Detector is a 14 000 ton detector, using 9000 tons of liquid scintillator – the largest quantity of liquid scintillator ever produced for a physics experiment – to record the tracks of charged particles. The scintillator is contained in a 15.6 × 15.6 × 64 m^3, 5000 ton PVC module structure, which segments the detector into 4 cm × 6 cm × 15.6 m channels. Light produced in these channels by the charged particles, that traverse them, bounces 10 times on average before it is captured in a wavelength shifting fibre.

The Fermilab accelerator complex provides the most powerful proton beams in the world. It currently provides a 700 kW proton beam and will rise even higher in future. During 2014 – March 2019 the complex delivered a neutrino beam with an equivalent of $8.85*10^{20}$ POT (protons on target) and antineutrino beam with $12.33*10^{20}$ POT [30]. Thanks to the large amount of neutrinos, statistical error is not dominant anymore. The precision is limited now by our knowledge of secondary charged particle interactions in the NOvA detectors. To further improve precision, the experiment built in 2019 at the testing site, studies the NOvA detector response to various charge particle beams from the acceleration complex.

Our NOvA group consists of 2 senior physicists, 1 post-doc and 7 engineers and technicians. The group closely cooperates with colleagues from Charles University and from Czech Technical University with whom we share resources, such as our Photosensors Laboratory. The same group is also involved in preparation of the future DUNE neutrino experiment described below.

The Prague laboratory with experience in avalanche photo diodes has contributed to the construction, commissioning and running of the experiment, including the test beams. The team is also involved in physics analysis of the data. In addition, we provide data processing capacities of our computing centre to the NOvA experiment as an Open Science Grid (OSG) site.

During data collection for the first combined ν_e appearance and ν_μ disappearance NOvA collaboration's analysis published in [30] and [32], a member of our team served (2015-2016) as an experiment Run Coordinator. In this high profiled collaboration position, he was charged with optimizing the use of the near and far detectors to meet the physics goals of the experiment, directing and deciding the priority and scheduling of detector systems development and maintenance. He was also reporting regularly on the experiment progress in the Fermilab director All Experiments' meeting.

After we received the new Inter-Excellence grant we hired a new post-doc, who has been participating in the analysis of seasonal variation of atmospheric multiple-muon events in the NOvA Near Detector [31] within the NOvA Exotics group. Moreover, this work led to a new method of cosmic data radiographic analysis allowing the study of overburden variations above the NOvA near detector and resulting radiographic images of its surrounding.

DUNE Experiment

The Deep Underground Neutrino Experiment (DUNE), a successor of the NOvA experiment, is being prepared in the Fermi national laboratory. DUNE is a cutting-edge next generation, international experiment for neutrino science and proton decay studies. Discoveries over the past half-century have put neutrinos, the most abundant matter particles in the universe, in the spotlight for further research into several fundamental questions about the nature of matter and the evolution of the universe — questions that DUNE will seek to answer.

DUNE will consist of two neutrino detectors placed in the world's most intense neutrino beam with an intensity of more than 1 MW. One detector will record particle interactions near the source of the beam, at the Fermi National Accelerator Laboratory in Batavia, Illinois. A second, much larger, detector will be installed more than a kilometre underground at the Sanford Underground Research Laboratory in Lead, South Dakota — 1,300 kilometres downstream of the source. These detectors will enable scientists to search for new subatomic phenomena and potentially transform our understanding of neutrinos and their role in the universe.

To test the technology of liquid argon cryostats, two prototypes of far detectors were constructed at CERN. The first one started data collection in 2018 and the second one a year later. The Long-Baseline Neutrino Facility (LBNF) will provide the neutrino beamline and the infrastructure, which will support the DUNE detectors. LBNF excavation and construction at Sanford Lab started in 2017.

FZU along with other two Czech institutions joined DUNE in 2017. We participate in the Far Detector Photon Detection Consortium under the Photo Sensor working group, where we employ our experience of photo-sensors and related electronics. Based on this, we rebuilt our photo-detector laboratory to be able to measure sensors (SiPM varieties) under cryogenic temperatures used in the planned liquid Argonne DUNE (LArTPC) detectors. The measurements of the performance of photon detectors and quality assurance is crucial during the design and construction phase.

Our team also participates in the ProtoDUNE project, a DUNE detector prototype, which is a part of CERN's neutrino platform. The detector is based on time projection chambers placed in a liquid argon and photo-detection system, which is supported by our team. We participate in all project phases, i.e. installation, component testing, commissioning, and data collection and analysis. Processed results verify the reliability of the selected measurement technology and its ability for use at larger scales for the DUNE far detector. Conclusions of these studies were reported in the main DUNE document, the Technical Design Report, which was released in early 2020 and to which our team contributed [33].

R&D in particle physics

Research and development of new techniques and technologies for particle detectors is an important activity for the preparation of future experimental projects. Our team has three major groups involved in global R&D activities coordinated through CERN.

The first activity, within the RD50 project (dedicated to the development of new semiconductor sensors for high radiation environments), was already discussed together with our main results in the ATLAS Inner Tracker section above. Another RD50 activity at FZU is within the ELI group, where they are using femtosecond lasers to measure properties of low gain avalanche detectors. This is another example of cooperation of our team with other FZU groups.

The second project connected with semiconductor technology is MEDIPIX/TIMEPIX. This project focuses on development of the application of semiconductor sensors based on silicon detectors developed at CERN for the tracking detectors. There are many interesting applications, such as radiation monitoring (e.g. on satellites), or applications based on sensors for various kinds of particles (photons, neutrons, etc.) with high spatial resolution for use in medicine, biology, art-restoration, etc. One of our researchers was a member of team which developed devices used on several satellites for monitoring radiation from space.

The last R&D activity is within the CALICE project, which exploits imaging calorimetry with an aim to improve significantly the energy resolution of particle jets, realized by highly granular calorimeters read out by semiconductor detectors preceded by accurate tracking detectors.

Our CALICE group consists of 4 senior physicists and 5 engineers and technicians. We concentrate on the scintillator tile calorimeter AHCAL equipped with silicon photomultiplier (SiPM) readout. The physics prototype of AHCAL was exposed to particle beams on accelerators at DESY, CERN and Fermilab, and jet shapes were studied for different particle initiators – electrons, pions, kaons and protons of both polarities. The results were compared to Monte Carlo simulations using Geant4 and provided input for better tuning of physical models of showers in Geant4 (see e.g. ref. [34] for the wolfram absorber in the AHCAL).

In 2015-19, the second generation of technological prototype was constructed. It should verify technologies suitable for mass production of the calorimeter. A large-scale prototype with ~22,000 channels was finished in 2018 and was used in several test beam exposures. We participated in two areas: (a) Data acquisition system (firmware and software) for data collection during the test beam campaigns (assembly and operation), either standalone or combined with other detector prototypes (CMS HGCAL, beam telescope). (b) SiPM characterization measurement with an analogue adaptive power supply, which stabilizes the gain of SiPM according to the ambient temperature [35]. The SiPM-on-tile technology has found applications in the ECAL of the DUNE New Detector and the CMS HGCAL upgrade project of the forward calorimeter for HL-LHC, where the AHCAL group participated in a combined test beam at CERN in 2018.

Computing facility

The LHC experiments use several data centres distributed on five continents to process data taken during collisions or simulated by Monte Carlo methods to compare models with measured results. These data centres are organized in a Worldwide LHC Computing Grid (WLCG). Similarly, Open Science Grid (OSG) infrastructure is used by Fermilab for experiments NOvA and DUNE.

The FZU Computing Centre is the only facility in the Czech Republic connected to WLCG and OSG and provides capacity for the LHC experiments ALICE and ATLAS and for the Fermilab experiments NOvA and DUNE. Our computing facility serves as a Tier-2 centre in the WLCG hierarchy.

The centre is run by 2 senior physicists and 4 IT specialists. The group is active in the development and testing of new data processing technologies. Main outputs of the group are reports on progress and results of tests on major conferences dedicated to the computing in high energy physics [36].

The computing resource of the centre is also shared with astroparticle physics projects Pierre Auger Observatory (Auger) and Cherenkov Telescope Array (CTA). The total capacity for these projects exceeded 9,000 computing cores and 4 PB of disk space in 2019. The centre delivered to WLCG in 2018 in total 545 million hours normalized per HS06 unit and 605 million hours in 2019.

Research activity and characterisation of the main scientific results

Research on Holographic Duality

Twenty-five years ago, 't Hooft and Susskind proposed the revolutionary idea that the gravitational force is holographic, in that it is most efficiently described in terms of a theory without gravity living on a
`holographic screen' in one dimension lower. A few years later, Maldacena showed that this concept is actually realized string theory and he was able to give a concrete meaning to their proposal. In this realization, the gravitational theory lives on an Anti-de-Sitter (AdS) background and the holographic description involves a conformal field theory (CFT) living on the boundary of AdS. Since then, this AdS/CFT correspondence has led to major insights in fields as diverse as black hole physics, condensed matter theory, the quark-gluon plasma and quantum information theory. Our own research in this field has focused on three aspects of this correspondence.

Tensionless Strings and Higher Spin Holography

To understand how AdS/CFT works, it is useful to study examples where the CFT is as simple as possible, namely where it is a free theory. For the string theory on AdS, this means that the string becomes tensionless, or in other words very `floppy'. In this limit the spectrum of the string theory consists of massless fields of all possible spins.
Since the work of Gaberdiel and Gopakumar in 2011, we know quite well how holography works in a certain subsector of the tensionless string (called the `first Regge trajectory') on AdS_3: this sector is described by Vasiliev's higher spin gravity, while the dual CFT is one of the well-studied minimal model CFTs with so-called W-symmetry.

Our research has clarified various aspects of this duality, such as the role of conical solutions, which were conjectured in the literature to describe degenerate primaries of the CFT. After providing evidence using perturbative methods in [1] we were able to prove this conjecture in [2]. To reach this result we devised a particularly simple formulation of the higher spin theory which realizes the well-known Coulomb gas formalism in the dual CFT. Our team's contribution to this international collaboration included the identification of leftover gauge freedom in the gauge used with the action of screening charges and aspects of the quantization of the model. Further research within this direction involved the construction and study of an exact solution in Vasiliev theory [3]. The solution is physically interesting as it describes a universe ending in a big crunch singularity and allows us to study it using holography. Our group's contribution consisted of calculating the explicit solution and working out the holographic dual interpretation.

Our group also contributed to the understanding of the W-symmetry underlying minimal model holography. The work [4] derived, for the first time, the explicit structure constants of the W_∞ algebra, while [5] focused on the role of triality symmetry in the W_∞-algebra and its representations, which can be encoded in terms of plane partitions and has uncovered interesting links with topological strings.

Very recently, progress was made in understanding the tensionless limit of the full string theory on AdS_3 which even led to a proof of AdS/CFT duality in this case. We contributed to this new direction by deriving the first interaction terms in a perturbative expansion of the field equations for the tensionless string, first for the untwisted sector [6], and subsequently for the full theory [7]. The latter result made use of a novel unfolded description of massive higher spin fields developed in [8]. Our contribution to this collaboration included working out group-theoretic aspects and the map to the standard formulation of higher spins.

Holography and Bulk Locality

One of the mysteries of the AdS/CFT correspondence is how local perturbations inside the AdS spacetime are encoded in the boundary theory. We investigated this question for a specific class of local perturbations, namely particles moving on helical worldliness in AdS_3. We showed [9] that these configurations are encoded in what is called the identity conformal block contribution to a specific correlation function in the CFT. Our approach includes the full backreaction of the particles on the geometry and goes beyond previously known perturbative approaches. Our team's contribution included obtaining the link with Liouville theory, working out concrete the examples and the computation of the boundary stress tensor VEV in the dual CFT. In a follow-up work [10] we extended this result to particles coupled to higher-spin gravity.

Deconstructing Black Holes

Since the work of Bekenstein and Hawking in the 1970s we know that black holes are complex thermodynamic systems which possess an entropy and should therefore correspond to a gigantic number of microscopic configurations. In one of the first applications of holographic duality, Strominger and Vafa were able to identify these black hole microstates in the holographically dual theory and thereby explain the origin of the Bekenstein-Hawking entropy. In later work, Strominger and collaborators proposed that, for a class of black holes in string theory, the typical microstates can be described geometrically as egg- shaped bound states of certain elementary constituents called D-branes.

However, the fully backreacted geometries produced by these D-brane configurations were not known. In our work [11] we constructed these geometries as solutions of supergravity, and in a follow-up [12] we clarified some technical aspects of the holographic dictionary for these solutions. The latter work revealed some tension with the originally proposed holographic interpretation of the solutions. Our team's contribution to [11] included devising a perturbative construction of the solution as well as the analysis of supersymmetry and the holographic 1-point functions. For [12] we performed the systematic survey of possible boundary conditions for the system and the application to the solutions appearing in the black hole deconstruction proposal.

[1] J. Raeymaekers, ``Quantization of conical spaces in 3D gravity," JHEP **1503**, 060 (2015)
[2] A. Campoleoni, S. Fredenhagen and J. Raeymaekers, ``Quantizing higher-spin gravity in free-field variables," JHEP **1802**, 126 (2018)
[3] C. Iazeolla and J. Raeymaekers,``On big crunch solutions in Prokushkin-Vasiliev theory," JHEP **1601**, 177 (2016)
[4] T. Procházka, ``Exploring W∞ in the quadratic basis," JHEP **1509**, 116 (2015)
[5] T. Procházka,``W-symmetry, topological vertex and affine Yangian," JHEP **1610**, 077 (2016)
[6] J. Raeymaekers, ``On matter coupled to the higher spin square," J. Phys. A **49**, no. 35, 355402 (2016)
[7] J. Raeymaekers, ``On tensionless string field theory in AdS_3" JHEP **1907**, 019 (2019)
[8] P. Kessel and J. Raeymaekers,``Simple unfolded equations for massive higher spins in AdS_3," JHEP **1808** (2018) 076
[9] O. Hulík, T. Procházka and J. Raeymaekers,``Multi-centered AdS_3 solutions from Virasoro conformal blocks," JHEP **1703**, 129 (2017)
[10] O. Hulík, J. Raeymaekers and O. Vasilakis,``Multi-centered higher spin solutions from W_N conformal blocks," JHEP **1811**, 101 (2018)
[11] J. Raeymaekers and D. Van den Bleeken, ``Microstate solutions from black hole deconstruction," JHEP **1512**, 095 (2015)
[12] J. Raeymaekers and D. Van den Bleeken, ``Chiral boundary conditions for singletons and W- branes," JHEP **1707**, 049 (2017)

String Field Theory

One of the major research lines of the theory and phenomenology department since 2009 when Dr. Schnabl joined our institute is the study of string field theory. String field theory is a particular approach to string theory, a highly mathematical theory which aims to unite purely on principles of mathematical beauty and consistency the four fundamental forces in quantum realm. Vibrating modes of a given string correspond to a spectrum of elementary particles, which in a proper quantum theory must give rise to quantum fields. The string field theory is a theory of such fields. Quantum field theory is one of the most useful and universal tools in contemporary theoretical physics, not only limited to high energy physics. In general, it becomes indispensable when we study collective phenomena (for instance, phase transitions) in a system with lots of degrees of freedom. Another example is the celebrated Higgs mechanism, which explains why in the standard model of elementary particle physics initially massless particles obtain mass. Open string field theory is in many respects very much like the gauge theory of the standard model. The analogue of the Higgs field is called for historical reasons the tachyon field. While in the standard model, the Higgs field condenses uniformly to a single value and its fluctuation behave as the recently discovered Higgs particle, in string field theory the tachyon field tends to condense in a much wider variety of ways. Often the field condenses everywhere, except in the neighbourhood of some hypersurface, which were identified by Ashoke Sen to be objects called Dirichlet membranes, or D-branes for short, introduced by Polchinski. For strings freely roaming through a flat Minkowski space these D-branes can be easily described as loci on which the string coordinate takes assumed value – a Dirichlet boundary condition. In more general situations the D-branes can be identified with the possible consistent (i.e. conformal) boundary conditions in the two-dimensional conformal field theory (CFT) on the string worldsheet.

Analytic methods in open string field theory

The topic of analytic solutions to the classical equations of motion of open string field theory has been a vibrant area of research ever since the ground-breaking solutions [26] for the tachyon vacuum and [27] for marginal deformations by Schnabl (the head of our team). An important simplification [28] has been subsequently achieved in collaboration with Erler (another team-member). Analytic methods then provided a key ingredient for the constructive proof [31] of background independence of open string field theory by Erler and Maccaferri.

In [1] we used an analytic solution describing a marginal deformation to study the non-linear relation between the SFT and BCFT moduli of the deformation. Novel algebraic solutions were found in [4] by extending the well-known KBc algebra through realizing a representation of the Virasoro algebra on string fields. The Erler-Maccaferri (EM) construction [31] was then used in [13] to construct analytic solutions corresponding to magnetized Dp-branes. In paper [15], we resolve the BCCO associativity anomaly appearing in the superstring version of the EM solution by choosing a suitable tachyon vacuum solution providing enough separation. In [17] we investigate the mysterious fate of physical fluctuations of an unstable D-brane during the process of its decay, finding (using the techniques of resurgence theory) that for late times they hide in the non-perturbative part of the solution. The original authors of the EM solution then revisit their result in [22], generalizing it to all possible reference and target D-branes (including, for instance, time-dependent backgrounds). Finally, the whole subject of analytic solutions is newly reviewed in [24].

Numerical and perturbative solutions, unconventional D-branes

While the analytic techniques represent a very important step forward in our understanding of consistent open superstring backgrounds (D-branes), they do not seem to provide a set of tools well-suited for discovering and exploration of new backgrounds: one typically has to have a prior knowledge of the corresponding conformal boundary condition in order to be able to construct the corresponding analytic OSFT solution. On the other hand, solving the equations of motion

numerically (by truncating the open string Hilbert space in a well-defined manner, the so-called “level-truncation’’), we are able to run a systematic search for new backgrounds starting from known ones. Such a program is not limited to traditional string theory backgrounds: by completing the central charge to 26 by adding a suitable auxiliary sector (whose details are unimportant), we are in this way able to look for new boundary conditions in virtually any CFT of interest. Furthermore, by employing the so-called doubling trick, we can explore the realm of conformal defects as well. Identifying the conformal boundary conditions corresponding to the given classical solution is enabled by computing suitable gauge-invariant observables, as pioneered by Kudrna, Maccaferri and Schnabl in [29].

An example of a situation where numerical OSFT yields information about highly non-trivial boundary conditions is the CFT of two free bosons (thus with a central charge c=2) compactified on a toroidal lattice. There, apart from the usual Dirichlet and Neumann boundary conditions, we have discovered a number of new ``exotic'' solutions, which persist under generic deformations of the compactification moduli. This is to be expected due to the non-rational nature of the underlying CFT (which makes it difficult to classify all possible conformally consistent boundary conditions). For special values of the torus moduli, we have subsequently constructed the corresponding boundary states analytically by realizing that the system can be described in terms of Virasoro and W_3 minimal models. It turns out that similar boundary conditions have been previously investigated in the condensed matter community and seem to be relevant to the problem of impurities and junctions of quantum wires at criticality, as well as to understanding the quantum Brownian motion on discrete lattices. The notion of such ``unconventional'' boundary conditions was then generalized in [18] to the case of open superstring in flat (toroidally compactified) space, where the worldsheet theory was decomposed as a direct product of N=2 superconformal minimal models. Doing so we were able to write down analytic expressions for the boundary states describing certain ¼-BPS bound states of Dp-branes, as well as to novel stable non-supersymmetric D-branes which do not carry any Ramond-Ramond charges. Marginally-bound ¼-BPS bound states were further investigated from the SFT point of view in [23] where it was shown that the consistency condition for the corresponding marginal deformation to solve the equation of motion up to third order exactly reproduces the well-known ADHM equations.

In [6] we show how conformal field theory topological defects can relate classical solutions of open string field theory for different boundary conditions, thus giving a realization of the fusion algebra on the open string fields. Furthermore, using numerical methods in Siegel gauge, we revisit in [5] the non-trivial relationship between the BCFT and SFT parameters of a marginal deformation (previously investigate analytically in [1]). In [14] we run a thorough numerical scan of classical solutions in the universal sector, finding candidates for double brane and ghost brane (breaking the world-record in the level to which we compute the tachyon vacuum solution in the process). Numerical solution for the tachyon vacuum in Schnabl gauge is approached in [20].

Formal aspects of (super)string field theory

In the area of investigating fundamental aspects of SFT, our group has greatly benefited from the arrival of T. Erler who is the co-author of the ground-breaking paper [30] which resolves the singularities of the cubic Witten open superstring field theory, thus providing a consistent construction of open superstring interaction vertices while remaining in the small Hilbert space. This subsequently opened up the avenue to achieving analogous constructions of the actions for the heterotic SFT, as well as for the type II closed SFT by the same authors in [32].

The construction of superstring field theory interactions were discussed in [2,3,7,9,10,12]. In [2] we have clarified the Wess-Zumino-Witten-like (WZW-like) structure of the complete open superstring field theory action (i.e. including the Ramond sector) in the large Hilbert space and established the equivalence of this theory to the small Hilbert space formulation of Erler, Konopka

and Sachs. In [3] we have presented the dual (``alternative'') action for the WZW-like heterotic and open superstring field theory. The notion of a
``higher'' WZW-like structure (consisting of two commuting A∞ algebras; one dynamical and one constraint structure) for the complete large Hilbert space formulation of open superstring field theory was entertained in [10], where it was applied to acquire a better understanding of symmetries of open superstring field theory and the structure of interactions in the Ramond sector. Similarly, the algebraic structure of the WZW-like closed superstring superstring field theory in the large Hilbert space was elucidated in [7] where it was found that it is governed by a triplet of mutually commuting L∞ algebras (one dynamical and two constraint structures). Hidden gauge reducibility of small Hilbert space superstring field theories, its implications on the BV master equation and therefore on the degrees of freedom propagating in loops was investigated in [9]. The BV formulation of open superstring field theories in the large Hilbert space was subsequently considered in [12].

Extracting low-energy physics: amplitudes and effective actions
It turns out that certain classical solutions dominantly excite only a specific subset of the full open string Hilbert space: this is in particular the example the solutions corresponding to marginal and relevant deformations, which mainly excite the corresponding marginal (or relevant) operator. The structure of such solutions then becomes much more transparent after first integrating out the remaining degrees of freedom by solving their respective equations of motion. For instance, in the case of marginal deformations, it then becomes apparent that they traverse the minima of the tree-level low-energy effective potential (whose vertices are essentially given by the on-shell S-matrix elements) which are connected to the perturbative vacuum.

In [16] we elucidate the relation between the light-cone and covariant formulations of open string field theory by integrating out the trivial excitations of the covariant theory using the homological perturbation lemma. Analytic OSFT techniques are then used in [21] to construct new gauge invariant quantities which are shown to compute on-shell scattering amplitudes for particular backgrounds. Computation of superstring scattering amplitudes is then considered in [11] where an alternative description of the so- called vertical integration (a procedure designed to avoid spurious singularities in the superstring measure) via the large Hilbert space is developed. Finally, the off-shell 1-loop tadpole amplitude in the heterotic string field theory is computed exactly in [8].

The condition for the vanishing of the third order obstruction to exact marginality of the stretched strings in the D(-1)/D3 system, which was constructed in [23] (see above for more details), can alternatively be understood as providing the expression for zero-momentum quartic part of the tree-level effective potential for such background. In the same paper, we also consider more complicated backgrounds (such as the spiked instantons of Nekrasov), reproducing in all cases the known zero-momentum effective actions (which possess N=2 supersymmetry in 4d). Finally, in [25] we investigate zero-momentum quartic tree- level effective potential computed from the WZW-like heterotic SFT, finding that it localizes on the boundary of the worldsheet moduli space whenever the background at hand admits a global N=2 superconformal symmetry (thus, in particular, avoiding the need for an explicit construction of the bosonic 3-string product).

References (team members highlighted in boldface)
[1] C. Maccaferri, **M. Schnabl**, ``Large BCFT moduli in open string field theory,'' JHEP 08 (2015) 149, arXiv:1506.03723 [hep-th]
[2] **H. Matsunaga**, ``Comments on complete actions for open superstring field theory,'' JHEP 11 (2016) 115, arXiv:1510.06023 [hep-th]
[3] K. Goto, **H. Matsunaga**, ``A∞/L∞ structure and alternative action for WZW-like superstring field theory,'' JHEP 01 (2017) 022, arXiv:1512.03379 [hep-th]

[4] N. Mertes, **M. Schnabl**, ``String field representation of the Virasoro algebra,'' JHEP 12 (2016) 151, arXiv: 1610.00968 [hep-th]
[5] **M. Kudrna**, C. Maccaferri, ``BCFT moduli space in level truncation'', JHEP 04 (2016) 057, arXiv:1601.04046 [hep-th]
[6] T. Kojita, C. Maccaferri, **T. Masuda**, **M. Schnabl**, ``Topological defects in open string field theory, JHEP 04 (2018) 057, arXiv:1612.01997 [hep-th]
[7] **H. Matsunaga**, ``Notes on the Wess-Zumino-Witten-like structure: L∞ triplet and NS-NS superstring field theory,'' JHEP 05 (2017) 095, arXiv:1612.08827 [hep-th]
[8] **T. Erler**, S. Konopka, I. Sachs, ``One Loop Tadpole in Heterotic String Field Theory,'' JHEP 11 (2017) 056, arXiv:1704.01210 [hep-th]
[9] **H. Matsunaga**, ``Hidden gauge reducibility of superstring field theory and Batalin-Vilkovisky master action'', arXiv:1706.00352 [hep-th]
[10] **T. Erler**, ``Superstring Field Theory and the Wess-Zumino-Witten Action,'' JHEP 10 (2017) 057, arXiv:1706.02629 [hep-th]
[11] **T. Erler**, S. Konopka, ``Vertical Integration from the Large Hilbert Space,'' JHEP 12 (2017) 112, arXiv:1710.07232 [hep-th]
[12] **H. Matsunaga**, M. Nomura, ``On the BV formalism of open superstring field theory in the large Hilbert space,'' JHEP 05 (2018) 020, arXiv:1802.04171 [hep-th]
[13] N. Ishibashi, I. Kishimoto, **T. Masuda**, T. Takahashi, ``Vector profile and gauge invariant observables of string field theory solutions for constant magnetic field background,'' JHEP 05 (2018) 144, arXiv:1804.01284 [hep-th]
[14] **M. Kudrna**, **M. Schnabl**, ``Universal Solutions in Open String Field Theory'', arXiv:1812:03221 [hep- th]
[15] **T. Erler**, C. Maccaferri, R. Noris, ``Taming boundary condition changing operator anomalies with the tachyon vacuum,'' JHEP 06 (2019) 027, arXiv:1901.08038 [hep-th]
[16] **H. Matsunaga**, ``Light-cone reduction of Witten's open string field theory,'' JHEP 04 (2019) 143, arXiv:1901.08555 [hep-th]
[17] **T. Erler**, **T. Masuda**, **M. Schnabl**, ``Rolling near the tachyon vacuum'', JHEP 04 (2020) 104, arXiV:1902.11103 [hep-th]
[18] **M. Schnabl**, **J. Vosmera**, ``Gepner-like boundary states on T4,'' arXiv:1903.00487 [hep-th]
[19] **T. Erler**, ``Four Lectures on Closed String Field Theory,'' Phys.Rept. 851 (2020) 1-36, arXiv:1905.06785 [hep-th]
[20] E. Aldo Arroyo, **M. Kudrna**, ``Numerical solution for tachyon vacuum in the Schnabl gauge'', JHEP 02 (2020) 065, arXiv:1908.05330 [hep-th]
[21] **H. Matsunaga**, **T. Masuda**, ``Deriving on-shell open string field amplitudes without using Feynman rules'', arXiv:1908.09784 [hep-th]
[22] **T. Erler**, C. Maccaferri, ``String field theory solution for any open string background. Part II'', JHEP 01 (2020) 021, arXiv:1909.11675 [hep-th]
[23] **J. Vosmera**, ``Generalized ADHM equations from marginal deformations in open superstring field theory,'' JHEP 12 (2019) 118, arXiv:1910.00538 [hep-th]
[24] **T. Erler**, ``Four Lectures on Analytic Solutions in Open String Field Theory'', arXiv:1912.00521 [hep- th]
[25] H. Erbin, C. Maccaferri, **J. Vosmera**, ``Localization of effective actions in Heterotic String Field Theory,'' JHEP 02 (2020) 059, arXiv:1912.05463 [hep-th]
[26] **M. Schnabl**, ``Analytic solution for tachyon condensation in open string field theory,'' Adv.Theor.Math.Phys. 10 (2006) 4, 433-501, arXiv:hep-th/0511286 [hep-th] *256 citations on INSPIRE*
[27] **M. Schnabl**, ``Comments on marginal deformations in open string field theory,'' Phys.Lett.B 654 (2007) 194-199, arXiv:hep-th/0701248 [hep-th]
102 citations on INSPIRE

[28] **T. Erler, M. Schnabl**, ``A Simple Analytic Solution for Tachyon Condensation,'' JHEP 10 (2009) 066, arXiv:0906.0979 [hep-th]
117 citations on INSPIRE
[29] **M. Kudrna**, C. Maccaferri, **M. Schnabl**, ``Boundary State from Ellwood Invariants'', JHEP 07 (2013) 033, arXiv:1207.4785 [hep-th]
30 citations on INSPIRE
[30] **T. Erler**, S. Konopka, I. Sachs, ``Resolving Witten`s superstring field theory,'' JHEP 04 (2014) 150, arXiv:1312.2948 [hep-th]
68 citations on INSPIRE
[31] **T. Erler**, C. Maccaferri, ``String Field Theory Solution for Any Open String Background,'' JHEP 10 (2014) 029, arXiv:1406.3021 [hep-th]
46 citations on INSPIRE
[32] **T. Erler**, S. Konopka, I. Sachs, ``NS-NS Sector of Closed Superstring Field Theory,'' JHEP 04 (2014) 150, arXiv:1312.2948 [hep-th]
46 citations on INSPIRE

Cosmology and gravitational physics

Cosmological phenomenology and model testing:

Determining which model best describes our universe requires a multi-faced approach to cosmology. This means to be able to accurately simulate the large-scale structure of the Universe on linear and non-linear scales, place constraints on new theories and models and investigate whether the standard cosmological model correctly describes observations. This last research direction has become particularly important in the recent years as a number of tensions –some of which are now at more than 4-sigma– show up when confronting the standard cosmological model with data.

Accurate simulations:
With other members of the cosmology community, we put forward an initiative for comparing Einstein- Boltzmann solvers for testing general relativity on linear cosmological scales, tested the precision and accuracy of various Boltzmann codes implementing modified gravity in cosmology and defined the new standard for this task [1]. As most information in the data involves modelling the non-linear scales, we created the most accurate numerical relativistic simulations of structures in a class of gravitational theories that extend General Relativity (GR) [2].

Testing the cosmological model and confronting theories with observations:
With the current and next-generation cosmological surveys providing a vast amount of data concerning galaxy clusters, our cosmology group has been active in assessing their use to constraining cosmological models. We forecasted the potential of galaxy cluster observations to constrain theories of gravity beyond GR and showed that future galaxy surveys will constrain the gravitational slip parameter down to the percent level [3]. We examined the cross-correlation of galaxy surveys seen through the cosmic infrared background and cosmic microwave background data with the goal of constraining dark energy and theories beyond GR and shown that with the next generation of galaxy surveys this method will be competitive with other methods [4]. We investigated bounds from the Integrated Sachs-Wolfe-galaxy cross-correlation observations on the two branches of the minimal theory of massive gravity [5]. We studied the cosmological phenomenology of a particular class of nonlocal corrections to GR and showed that within current observational data these models are statistically equivalent to GR [6].

Measuring redshift space distortions (RSD) has emerged as a rather good way of probing the late universe cosmology. The team has determined that vector-type perturbations in the Universe

generate RSDs and that this will be possible to measure with the next generation surveys [7,8].

Examining cosmological tensions between standard model and the data:
Low redshift measurements of the Hubble constant using supernovae have been found to be in stark contrast with its value inferred through fitting the standard cosmological model to observables associated with high redshift. The discrepancy has been increasing with every data release and has reached a level beyond 3.6-sigma. We examined the tension between the measurements of the Hubble constant using Cosmic Microwave Background and using galaxy cluster data and discussed the merits of a number of solutions to this discrepancy [9].
Discrepancies between the standard cosmological model and the data also appear when observing galaxy clusters. We examined this in detail using state-of-the-art datasets and statistical tools with the aim of determining whether this discrepancy points to new physics beyond GR or may simply be due to systematic effects in the data [10].

Testing cosmology and gravitational theories with gravitational waves:
The recent simultaneous observations of gravitational waves and electromagnetic counterparts as they were both generated by mergers of compact objects, has opened a new area in multi-messenger cosmology. Our department was amongst the leaders during the initial effort for constraining gravitational models and this has continued since. In particular, we have showed how one can use these observations to measure the variation of the Planck mass [11] and also place constraints on the size of large extra dimensions [12]. The remaining viable gravitational models lead to a number of possible effects on cosmological large-scale structure as has been investigated by our members [13]. We further calculated the effects of cosmic structure on the propagation of GW and showed that the few remaining viable generalized scalar-tensor models are in fact ruled out when considering these effects [14]. We considered the same calculations in the context of theories of modified gravity that may act as alternatives to dark matter and determined the most general set of them where the speed of GW equals the speed of light [15] as required by observations.

Dark matter and astro-particle physics:
Despite decades since its proposal, dark matter remains a deep mystery in cosmology and determining its nature is one of the most important problems in cosmology and particle physics. Progress can be made through phenomenological model testing and through model building.

Cosmological phenomenology of dark matter:
The cosmic evolution of dark matter can be very accurately probed using observations of the cosmic microwave background which is particularly sensitive to the dark matter equation of state. We have determined for the first time the evolution of the Dark Matter equation of state through cosmic history using data from the Cosmic Microwave Background and late Universe probes [16]. We have further examined the properties of cosmological dark matter by determining how dark matter forms bound structures in a general framework and used data from the WiggleZ survey to place improved constraints on the model [17].

Models of particle dark matter:
Designing new models of dark matter can always lead to new insights. One possibility investigated is that Dark Matter is composed of spin-2 fields [18]. Yet another mechanism proposed is that Dark Matter is produced during the early universe inflationary era and that this is also accompanied by the generation of baryon charge [19]. We have also investigated the emergence of Dark Matter from a spontaneously broken gauge theory of the Lorentz group [20]. Another possibility is that Dark Matter is composed of primordial black holes. We have studied the formation mechanisms of primordial black holes in the early universe and calculated their

observational signatures in cosmology [21]. We also investigated a model of super- heavy dark matter and showed the dark matter particles in this case decay slowly and have a lifetime close to the lower bounds obtained from observations of ultra-high energy cosmic rays [22].

Cosmic rays:
One of the two leading cosmic ray observatories is the Telescope Array which is located in Utah, USA and our department continued its involvement in the collaboration [23]. In the area of cosmic rays, we have shown that the cosmic ray production may be detectable in certain astrophysical conditions for *f(R)* models of gravity relevant for Dark Energy [24].

Physics of compact objects:
Testing gravity and dark matter with compact objects has been an active area of research of the cosmology group. Using a multidisciplinary approach we investigated how to use accurate measurements of the Sun's pulsations, that is, helioseismology, to place constraints on alternatives to GR relevant for cosmic acceleration. We found that departures from GR may be strongly constrained using helioseismological observations [25, 26].

Compact objects such as binary pulsars are particularly suited to testing GR. We examined the generation of GW by compact objects in a nonlocal extension of GR and showed that this extension has the same GW polarizations as GR but the effective Newton constant is rescaled and in addition that total GW energy- momentum at infinity is divergent [27]. We generalised the parameterized post-Newtonian formalism for testing gravity with compact objects to handle novel gravitational theories where part of the field is screened and imposed constraints on the parameters [28]. We also placed constraints on vector fuzzy Dark Matter using observations of binary pulsars [29].

Investigating new theories of gravity as a way to explain cosmic acceleration:
Our department specializes in constructing theories and models of gravitational theories beyond GR. We invented a novel Weyl-invariant and generally covariant formulation of unimodular gravity which leads to a global dynamical degree of freedom: the cosmological constant [30]. We constructed a novel parity- violating theory beyond GR which provides an explanation for dynamical dark energy, determining its Hamiltonian formulation and finding cosmological solutions [31]. We examined the localised version of a nonlocal dark-energy motivated extension of GR and determined that only the set of initial conditions corresponding to the original nonlocal version lead to a well-defined theory [32]. We expanded Ashtekar's formulation of GR plus pressure-less fluid as a spontaneously broken gauge theory of the Lorentz group by proposing a model with a larger symmetry [33].

Physics of the early Universe:
The team is very active in studies of classical and quantum gravity and Early Universe cosmology. We have studied quantum entanglement from multi-field inflation [34]. In the area of modified gravity, we compared the local and non-local formulations of the Deser-Woodard Dark Energy model [35]. We have presented the construction of the so-called P(X) theories using as a basis a canonical complex scalar field [36]. We studied a particular realization of the cosmological bounce scenario proposed recently by Ijjas and Steinhardt and uncovered a number of pathologies [37]. We examined the ultra-violet implications of theories that exhibit Vainshtein screening and performed a general study of derivatively coupled scalar theories using non-perturbative exact renormalisation group techniques [38]. We worked on GW sourced by scalar fluctuations in the early universe which can give information on the small-scale primordial fluctuations [39]. We considered an inflationary model involving interactions between axions and gauge fields and constrained the resulting parameter space [40]. We investigated the effective field theory of

preheating which implies three types of derivative couplings between the inflaton and the reheating field and explored the variety of low energy regimes, showing that some models led to nontrivial sound speed for both the inflation and reheating sectors [41]. We explored a version of Affleck-Dine baryogenesis which neither requires low reheating temperatures in the Universe nor leads to large isocurvature perturbations of baryonic matter [42]. Scalar-Gauss-Bonnet theories lead to scalarisation of black holes and neutron stars in a certain range of parameters. We showed that for this range of parameters these theories are in conflict with the existence of an inflationary era at the beginning of the Universe [43]. We also demonstrated how to avoid tachyonic instabilities in the early universe in another theory which leads to scalarisation [44]. We showed that in a nonlocal extension of GR the big bang singularity can be replaced with a bounce and thus is never reached [45]. We investigated the fine-tuning problem of scalar-driven inflation arising from coupling the inflaton to ordinary matter so that reheating of the Universe takes place [46]. Finally, we calculated the bispectrum that results from quantum entanglement between the inflaton and spectator fields and found distinctive signatures in the bispectrum which can be used to constrain these models with observations [47].

References:

[1] E. Bellini et al., Phys. Rev. D97, 023520 (2018).
[2] **L. Reverberi** and D. Daverio, JCAP, 1907, 035 (2019)
[3] L. Pizzuti, **I.D. Saltas**, *et al.*, Mon. Not. Roy. Astron. Soc. 486, 596 (2019).
[4] A. Maniyar, G. Lagache, M. Bethermin and **S. Ilić**, A&A, 621, A32 (2019).
[5] **N. Bolis,** A. De Felice and S. Mukohyama, Phys.Rev. D98**,** 024010 (2018).
[6] L. Amendola, Y. Dirian, H. Nersisyan and **S. Park,** JCAP 1903, 045
(2019). [7] C. Bonvin et al., JCAP 1802, 028 (2018).
[8] V. Tansella at al., Phys.Rev. D98, 103515 (2018).
[9] Z. Sakr et al., Astron.Astrophys. 620**,** A78 (2018).
[10] **S. Ilić,** Ziad Sakr and Alain Blanchard, Astronomy & Astrophysycis, 631, A96 (2019).
[11] L. Amendola, **I. Sawicki,** M. Kunz and **I. Saltas**, JCAP 1808, 030 (2018).
[12] L. Visinelli, **N. Bolis** and S. Vagnozzi, Phys. Rev. D97, 064039 (2018).
[13] L. Amendola, M. Kunz, **I. Saltas** and **I. Sawicki**, Phys. Rev. Lett. 120, 131101 (2018).
[14] E. J. Copeland, **M. Kopp,** A. Padilla, P. M. Saffin & **C. Skordis,** Phys. Rev. Lett. 122,
061301 (2019).
[15] **C. Skordis** and **T. Zlosnik**, Phys.Rev. D100, 104013 (2019).
[16] **M. Kopp, C. Skordis,** D. Thomas and **S. Ilic**, Phys. Rev. Lett. 120, 221102 (2018).
[17] D. B. Thomas**, M. Kopp** and K. Markovič, Mon.Not.Roy.Astron.Soc. 490, 813
(2019). [18] **F. Urban**, Universe, 4, 90 (2018); ibid, Int.J.Mod.Phys. A33, 1845010
(2018).
[19] E. Babichev, D. Gorbunov and **S. Ramazanov**, Phys.Rev. D**97**, 123543 (2018).
[20] **T. Zlosnik, F. Urban**, L. Marzola and T. Koivisto, Class. Quant. Grav. 35, 235003
(2018). [21] V. De Luca *et al.*, JCAP 1907, 048 (2019).
[22] E. Babichev, D. Gorbunov and **S. Ramazanov**, Phys.Lett. B794, 69 (2019).
[23] Abbasi et al., Astrophys. J. 858**,** 76 (2018); ibid, ApJ 858, 76 (2018); ibid, ApJ 862, 91
(2018); ibid,
ApJ 865, 74 (2018); ibid, Phys. Rev. D 98, 022002 (2018); ibid, Phys. Rev. D99, 022002 (2019);
ibid,
Astropart. Phys. 110, 8 (2019).
[24] E. Arbuzova, A. Dolgov and **L. Reverberi**, Eur. Phys. J. C 78, 481 (2018).
[25] **I. Saltas, I. Sawicki** and I. Lopes, JCAP 1805, 028 (2018).
[26] **I. D. Saltas** and I. Lopes, Phys. Rev. Lett. 123, 091103 (2019)
[27] Y-Z. Chu and **S. Park**, Phys. Rev. D 99, 044052 (2019).
[28] **N. Bolis, C. Skordis**, D. Thomas and **T. Zlosnik**, Phys.Rev. D99, 084009 (2019)
[29] D. Nacir and **F. Urban**, JCAP 1810, 044 (2018).
[30] **P. Jiroušek and A. Vikman**, JCAP 1904, 004 (2019).

[31] J. Magueijo and **T. Zlosnik**, Phys.Rev. D100, 084036 (2019).
[32] **S. Park** and R. P. Woodard, Phys. Rev. D 99, 024014 (2019).
[33] T. Koivisto, M. Hohmann and **T. Zlosnik**, Universe 5, 153 (2019).
[34] **N. Bolis**, T. Fujita, S. Mizuno and S. Mukohyama, JCAP 1809, 004
(2018). [35] **S. Park**, Phys. Rev. D97, 044006 (2018).
[36] E. Babichev, **S. Ramazanov and A. Vikman**, JCAP 1811, 023
(2018). [37] Dobre et al., JCAP 1803, 020 (2018).
[38] A. Padilla and **I. Saltas**,
[39] **C. Unal**, Phys. Rev. D99, 041301 (2019)
[40] A. Papageorgiou, M. Peloso and **C. Unal**, JCAP 1907, 004
(2019). [41] **G. Sengor**, Phys. Rev D100, 043503 (2019)
[42] E. Babichev, D. Gorbunov and **S. Ramazanov**, Phys.Lett. B792, 228 (2019).
[43] T. Anson, E. Babichev, C. Charmousis and **S. Ramazanov**, JCAP 1906, 023 (2019).
[44] T. Anson, E. Babichev and **S. Ramazanov**, Phys.Rev. D100, 104051 (2019).
[45] C-Y Chen, P. Chen and **S. Park**, Phys. Lett. B 796, 112 (2019).
[46] S. P. Miao, **S. Park** and R. P. Woodard, Phys. Rev. D100, 103503 (2019).
[47] **N. Bolis**, A. Albrecht and R. Holman, JCAP 1907, 021 (2019]

Research activity and characterisation of the main scientific results

Functional Materials and Composites research group

In the period 2015-19, researchers of this group have focused on investigation of **thermomechanical fatigue of superelastic NiTi shape memory alloys** [1-5] by a variety of experimental methods (Fig. 1). Key results concern the description of experimental conditions under which fatigue degradation of martensitically transforming NiTi accelerates [1]. The research also involves development of new experimental methods and theoretical approaches applicable to the experimental analysis of thermomechanical fatigue of SMAs relying on the combination of strain analysis via Digital Image Correlation and Infrared Camera Analysis of heat generated by cyclically loaded NiTi [1] (*share 90%*).

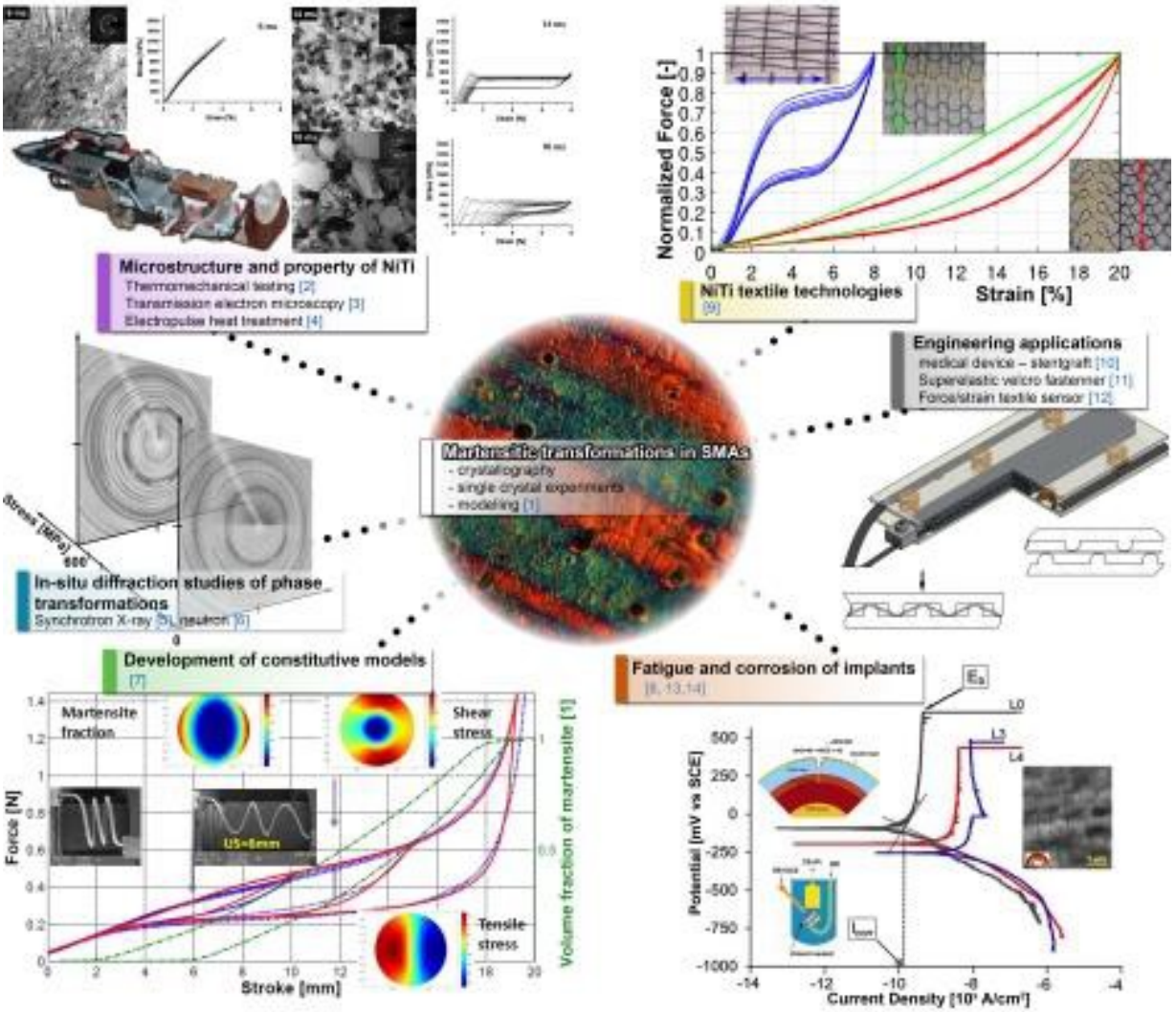

Figure 1: Fatigue of thin superelastic NiTi filaments investigated by a variety of experimental and theoretical methods covering shape setting and tensile testing, in-situ synchrotron x-ray diffraction during thermomechanical loads, in-situ electrochemical characterization of fatigued surfaces, transmission electron microscopy of lattice defects created by tensile deformation, mechanics modelling and finite element simulation, application in smart textiles.

Further key results consist of identification of the origin of the instability of cyclic superelastic response of NiTi in accumulation of internal stress via in-situ synchrotron x-ray diffraction [2] (*share 90%*) and revealing the key role of deformation twinning in martensite in the mechanics of NiTi deformation through systematic thermomechanical

loading experiments on thin NiTi wires with controlled microstructures and complimented by detailed TEM characterization of lattice defects generated by martensitic transformation [4,5].

Very interesting results have been obtained by the development of a new in-house developed technique combining mechanical testing in aggressive fluids with in-situ electrochemical characterization of changes occurring within the mechanically loaded material surface. The electrochemical method enables detection of the accumulation of surface damage of the cyclically loaded metal before it can be detected by conventional means. The method was successfully applied to NiTi wires and springs deformed cyclically in aggressive biofluids. A unique hydrogen-based mechanism of mechanochemical damage occurring within the TiO2 surface oxide cracks was revealed [3].

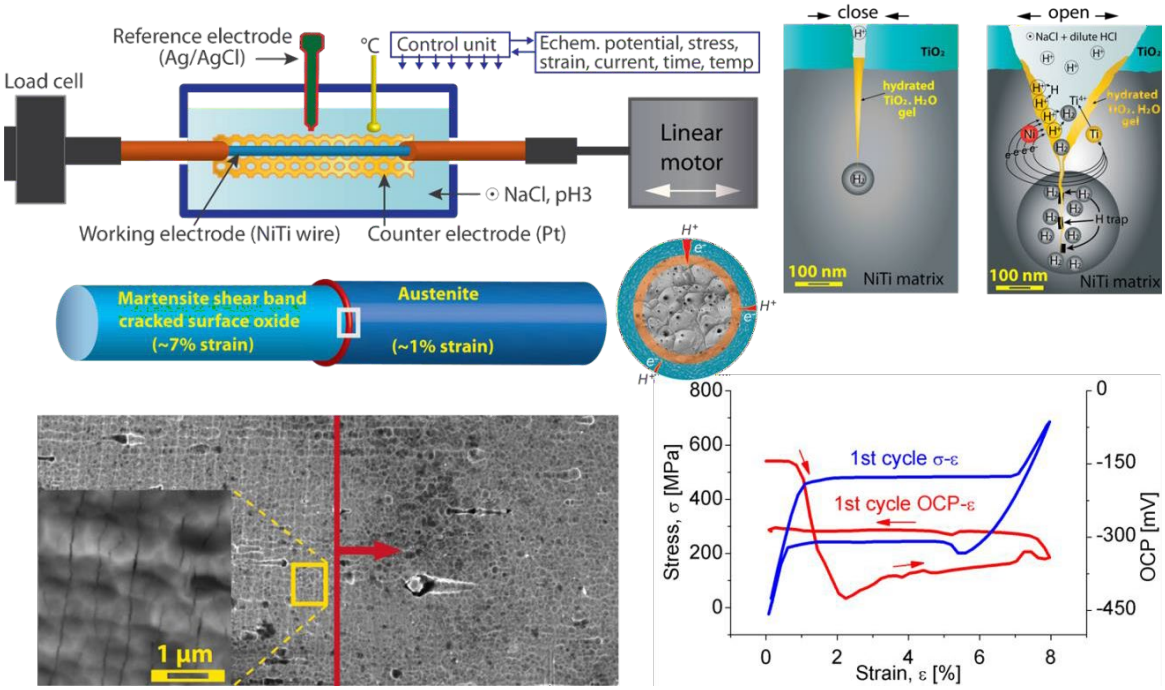

Figure 2: Two exciting properties of NiTi SMAs (superelasticity due to martensitic transformation and biocompatibility due to the protective TiO_2 surface oxide layer) when combined together, lead to excessive fatigue damage during cyclic mechanical loading of NiTi filaments in biofluids [3].

The most prestigious result of the team in the 2015-19 period was achieved by the application in-situ 3D x-ray diffraction (3D-XRD)method combined with mechanics modelling to solve the problem of localized tensile deformation of NiTi wires in tension (*share 80%*). The method enabled determination of full strain and stress tensors in ~15000 grains of polycrystalline wire undergoing stress induced martensitic transformation during the tensile test. We have succeeded in evaluating internal stresses surrounding the cone shaped martensite band fronts propagating during tensile test on 0.1 mm thin NiTi wire. The physical origin of the observed redistribution of internal stress and strain was rationalized through FE simulation of tensile deformation of phase transforming NiTi wire using the original SMA model. The result was published in the prestigious journal Science [6]. It drew wide attention from the SMA field and was awarded the Werner for Siemens 2016 medal.

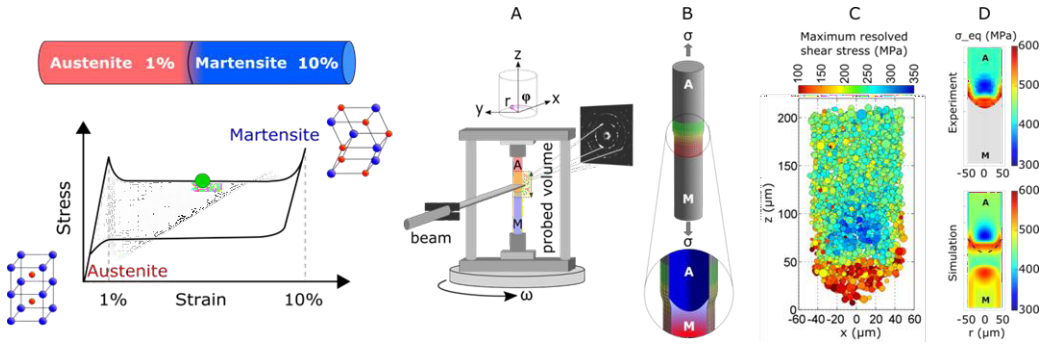

Figure 3: In-situ 3D synchrotron x-ray diffraction method was successfully applied to evaluate grain microstructure and grain resolved internal stresses within a martensite band front propagating in 0.1 mm thin NiTi wire subjected to the tensile test on beamline ID11 at ESRF Grenoble [6].

Taking advantage of the original in-house developed electropulse heat treatment method allowing precise manipulation of the microstructure of superelastic NiTi wire, systematic experimental and theoretical research of the coupling between martensitic transformation and dislocation plasticity in NiTi was carried out [7-9]. It was found that the material deforms at high temperatures and large strains by a **unique TRIP like deformation mechanism** involving dislocation slip assisted deformation twinning in martensite (*share 80%*).

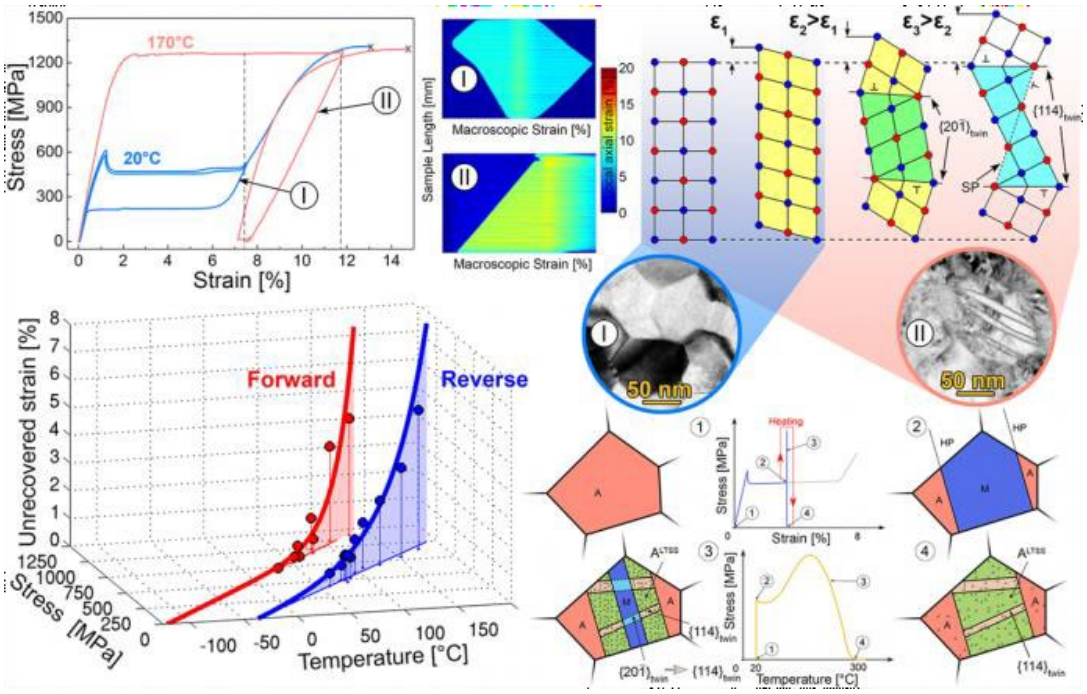

Figure 4: Review summarizing the state-of-the-art knowledge on the deformation mechanism of NiTi SMAs due to martensitic transformation combined with plastic deformation via dislocation slip and martensite twinning published in the prestigious journal Progress in Materials Science [8].

An important part of the group's research was further development of the original mechanics model accounting for this deformation mechanism and finite element simulation of NiTi components carried out in collaboration with colleagues from IT ASCR [10] (*share 50%*).

Finally, new a research program, started in the 2015, aiming at the development of nanocantilevers incorporating **NiTi thin films and multilayered structures for smart sensors** utilizing the nonlinear mechanical properties of NiTi has brought very

promising results [11]. It was theoretically predicted and experimentally verified that nanocantilevers with tuneable resonance frequencies can be successfully fabricated using smart functional materials such as NiTi.

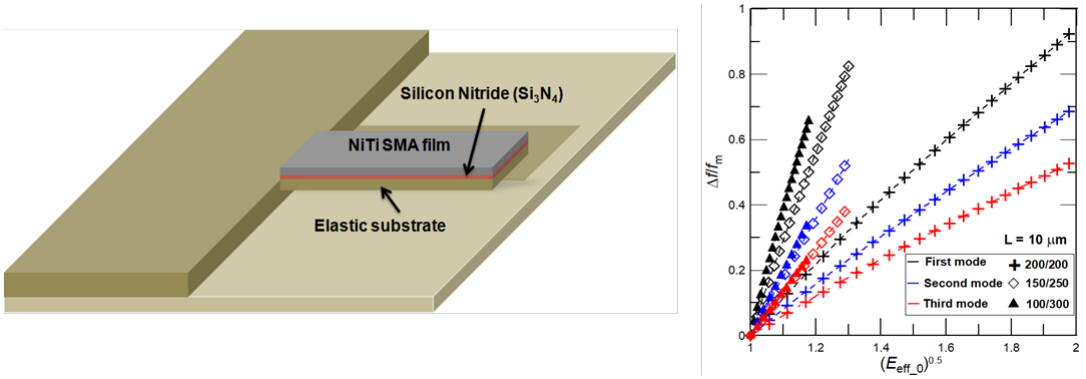

Figure 5: Scheme of a NiTi/Si nanocantilever containing NiTi thin film layer and absolute frequency shift Δ*f* of the nanoresonator calculated as a function of effective elastic modulus $(E_{eff\_0})^{0.5}$ for the length of the nanocantilever L = 10 μm [11].

Materials for Nanosystems and Biointerfaces research group

During 2015-19, researchers from the group have focused on the science and technology of diamond materials. Research was initially oriented on the luminescent nanodiamond particles in biological environments, and then shifted towards boron-doped diamond film growth and characterisation of its properties, particularly to the application of boron-doped diamond in protective coatings, photovoltaics, electrochemistry, biomedicine, sensors and electronics.

The research and development of fluorescent nanodiamond (FND) particles for bio-medical applications, which started in the previous review period has continued in collaboration with several Czech research institutions and Hasselt University (Belgium). The MNB research group contributed to the development of an innovative mass production method for fluorescent nanoparticles with homogeneous distribution of nitrogen-vacancy (NV) centres per particle. V. Petrakova et al. [12] demonstrated a possible optical detection mechanism based on modulation of NV centre fluorescence in nanodiamond induced by changes of surface charge, which occurs upon noncovalent interaction with charged molecules on the surface of nanoparticles. NV centres exist in two electronic states: Neutral (NV^0) and negatively charged (NV^-). The NV^0 state emits orange luminescence with a zero-phonon line (ZPL) at 575 nm; the NV^- state emits in the red region with a ZPL at 637 nm. Both ZPLs are followed by a broad phonon replica side band luminescence. The shape of the fluorescence spectra depends on the occupancy of the NV^- and NV^0 energy states, i.e. on the position of the Fermi level. Near the (nano)diamond surface, these levels are bent and their occupancy changes resulting in a change in fluorescence due to the presence of a surface potential. Fluorescent nanodiamonds were successfully used as a biocompatible DNA carrier and monitoring optical probe for intracellular non-labelled DNA release [13]. This multidisciplinary work led to several publications with a FZU team share from 15 to 40%.

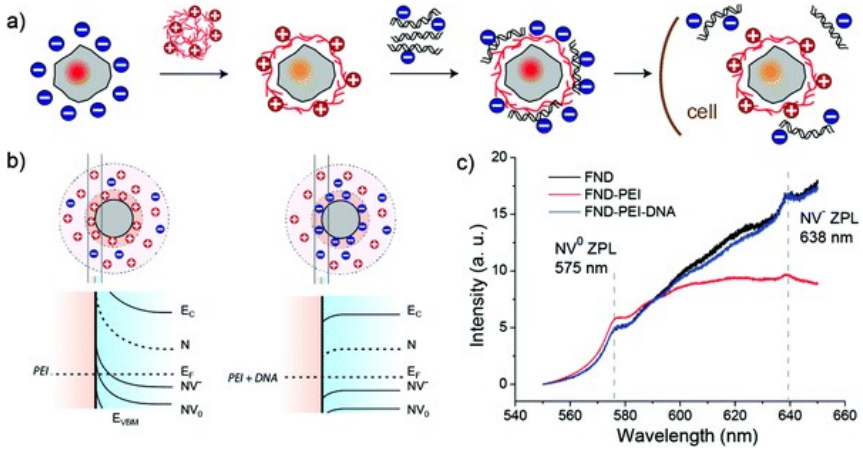

Figure 6: Principle of simultaneous vectoring, imaging and tracking of DNA payload release with an FND-based device. (a) Schematic of formation of the FND–PEI–DNA complex based on electrostatic interactions and the release of DNA from the complex after entering the cell. [13]

Additionally, the group has intensely studied growth and properties of boron-doped diamond layers for their potential use in electronics and electrochemistry. The group reported on several important aspects, such as the growth of conductive nanocrystalline diamond over large area using microwave plasma enhanced chemical vapour deposition with linear antenna delivery (LA MW PECVD), developed new coatings (silicon carbide, silicon carbide/diamond composite, and porous diamond layers), and updated analysis of characteristic boron-doped diamond Raman spectrum. Careful analysis of the precursor gas composition effect on the growth of diamond by LA MW PECVD demonstrated the important role of the presence of oxygen (CO2) in the plasma in the competitive formation of boron-doped nanocrystalline diamond (BNCD) and silicon carbide (SiC). BNCD layers were successfully grown over large areas by LA MW PECVD with high boron concentrations, up to 2×10^{21} at/cm^3 with electrical conductivity levels akin to layers prepared in conventional MW PECVD systems (> 30 S.cm^{-1}) (Fig. 7) and electrochemical properties suitable for industrial applications [14] (*share 65%*). Fabrication of either pure silicon carbide or silicon carbide / diamond composite layers was found to be possible at low CO2 concentrations with mechanical properties comparable to nanocrystalline diamond (NCD) layers and superior scratch resistivity and wear resistance [15,16] (Fig. 7).

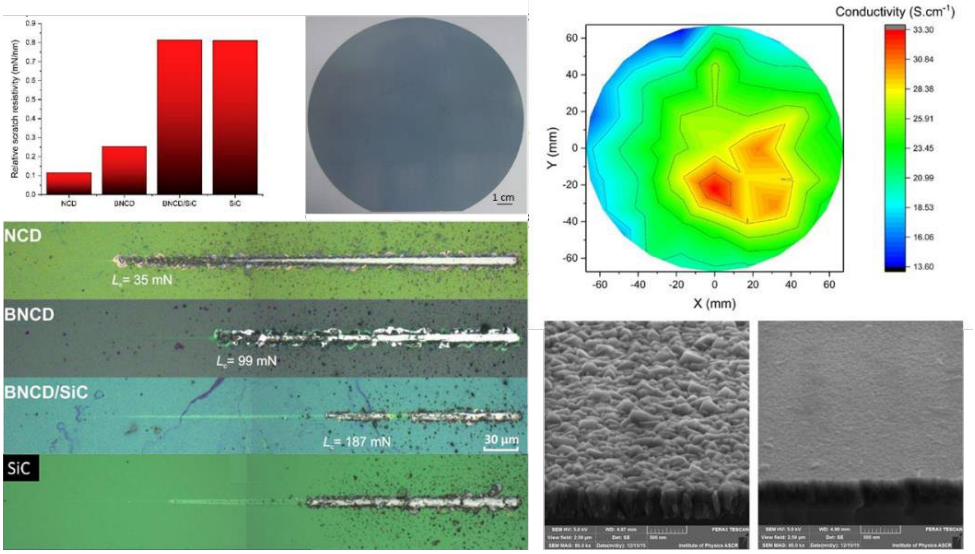

Figure 7: (Upper middle) picture of a BNCD coated 6-inch diameter fused silica wafer with a characteristic blue colour; (lower left) Comparison of the on-load depth residual scratch grooves and

(upper left) the relative scratch depth resistivity (=critical load/layer thickness) of SiC, SiC/BNCD composite, BNCD and NCD coating; (Upper right) Four point probe conductivity map of a BNCD coated 6-inch in diameter fused silica wafer; (lower right) Scanning electron microscopy images of BNCD (left) and silicon carbide (right) layers.

Analysis of BNCD layers grown at temperatures ranging from 250 up to 750 °C [17] indicate a partial compensation of boron acceptors attributed to hydrogen passivation in layers deposited a low temperature. BNCD was also successfully deposited on silicon solar cells as a transparent anode and corrosion protection layer used for water splitting. BNCD layers deposited onto Si solar cell act as an anode and allows for photogenerated charge carrier transfer from the underlying Si toward the electrolyte solution to participate in water oxidation (Fig. 8a). Upon functionalization of the diamond surface with CoPi oxygen evolution catalyst, the fabricated Si|BNCD photoelectrodes effectively oxidize water under simulated light conditions (Fig. 8b). The underlying Si solar cell is effectively protected from corrosion by the diamond layer, i.e. the photocurrent output from the Si solar cell remained constant upon recurrent electrochemical operation (Fig. 8c) [17].

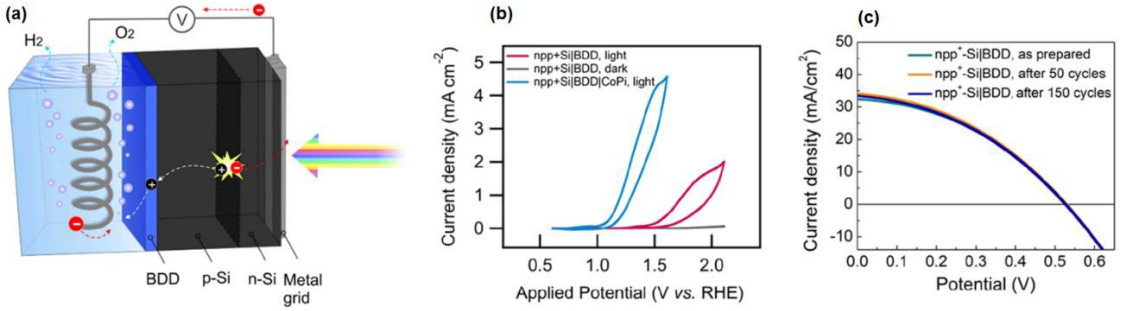

Figure 8: (a) Schematic illustration of a photoelectrode based on a BNCD electrode and buried pn-junction Si solar cell for water oxidation and reduction. (b) Cyclic voltammetry curves of the Si|BNCD photoelectrodes upon light illumination. (c) Current−voltage curves of the Si|BNCD photoelectrodes.

We developed and patented, with the J. Heyrovsky Institute of Physical Chemistry, a new simple and reproducible method for producing porous boron doped diamond (p-BDD) diamond layers using electrospun SiO2 fibres as a template deposited by spin coating [18,19] (*share 50%*). This process was successfully transferred to the LA MW PECVD system, allowing synthesis of this new material over large area (Fig. 9). This patented fabrication process is, in principle, unlimited and allows the preparation of thick p-BDD electrodes.

Originally developed for water treatment, this work opened a new pathway toward fabrication of diamond based electrochemical devices and has been successfully used in neural cell growth and electrochemical sensing [20]. Considering the wide range of its potential electrochemical applications, the method may easily become a ground-breaking innovation in the field. Careful optical and electrical characterization of BNCD layers allowed the fabrication of transparent and conductive electrodes used, for instance, in photovoltaic organic devices [21]. The integration of a Ti metal grid (Fig. 9) allowed the fabrication of composite diamond electrodes with enhanced optical transparency (up to 80%) and conductivity (with a sheet resistance of 200 $\Omega.sq^{-1}$) (*share 77%*). These electrodes are stable at elevated temperatures [22] and against electrochemical corrosion [17] (*share 65%*).

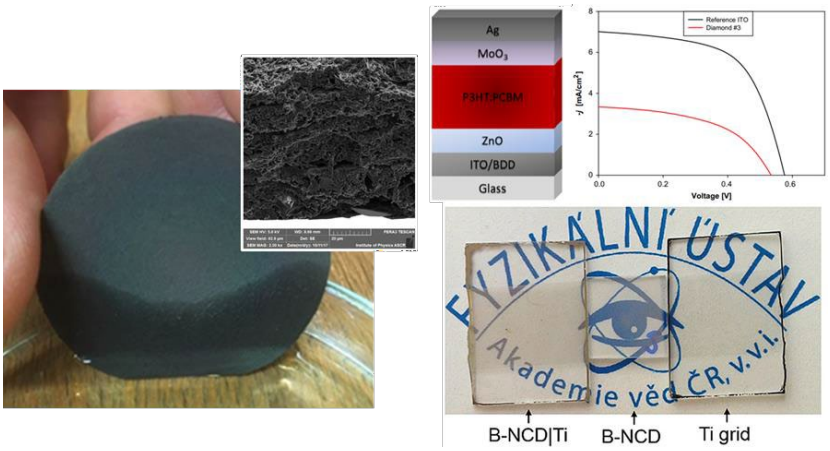

Figure 9: Schematic illustration of a bulk-heterojunction (BHJ) organic solar cell **(**upper centre). Current-voltage characteristics of the BHJ solar cell based on ITO and BNCD electrodes (upper right); Picture showing absorption of porous diamond layer in contact with acetone with cross-section SEM picture of a thick porous boron-doped diamond layer (left);) photograph of optically transparent and electrically conductive electrodes (right: boron-doped diamond and titanium grid composite (BNCDTi), boron-doped diamond electrodes (BNCD) and titanium grid (Ti grid).

Although Raman spectroscopy is a simple and widely used characterization method for diamond, there has not been a good description of the characteristic Raman spectrum of BDD until now. By reviewing and comparing a large amount of Raman data from the literature enabled us to conclude that characteristic Raman lines correspond to carbon vibration modes, whose position is sensitive to the concentration of boron defects [23] (*share 65%*). By introducing the new concept of decoupled multiple Fano-function, we have been able to: 1- evidence the electronic Raman contribution in the spectrum [24], and 2- describe in detail the effect of the atomic boron concentration on the zone centre phonon and the phonon density of state maximum (at ca. 1200 cm^{-1}) lines [25]. In contrary to previously empirical studies, this new analytical method is robust and allows unprecedented precision for determination of boron concentration (Fig.10).

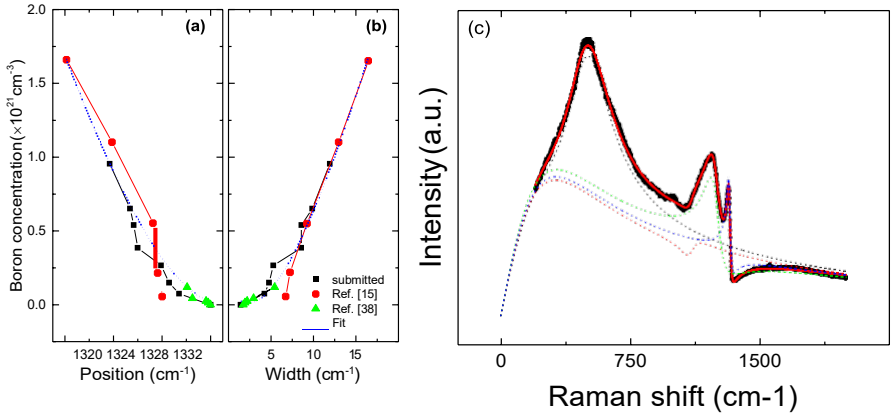

Figure 10: Experimental and fitted variation of the boron concentration with position (a) and width (b) of the diamond ZCP line in epitaxial diamond layers; (c) Experimental and fitted Raman spectra measured at room temperature of boron-doped diamond layers grown with B/C of 2000 ppm in the gas phase with the modelled contribution of the different peaks.

Materials with Controlled Microstructure research group

Researchers from this group have performed a complex multiscale study of the microstructure of iron
– a representative metal exhibiting diffusionless solid-state phase transformations – produced by **additive manufacturing** (or 3D printing). This study showed that even in such a simple material, additive manufacturing produces a hierarchical microstructure consisting of (i) large, nearly equiaxed grains separated by high-angle grain boundaries; (ii) micrometre-sized subgrains with low-angle grain boundaries inside these grains; and (iii) nanometre-sized cells inside the subgrains, which are mutually separated by dislocation walls (Fig. 11). We explain the microstructure as well as occurrence of nearly equiaxed grains instead of columnar grains, originally formed during the SLM process, due to steep temperature changes when the laser scans over the studied location, thus inducing quick α→γ→α transformations (Fig. 12) [26].

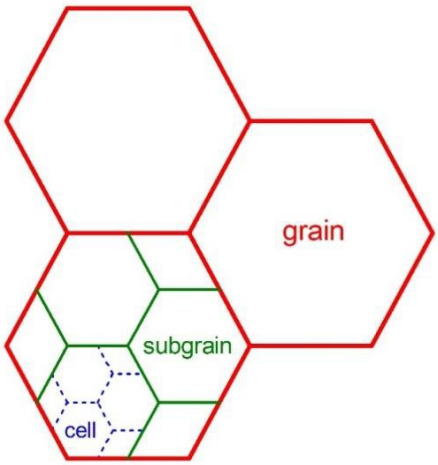

Figure 11: Schematic depiction of the microstructural hierarchy in SLM iron.

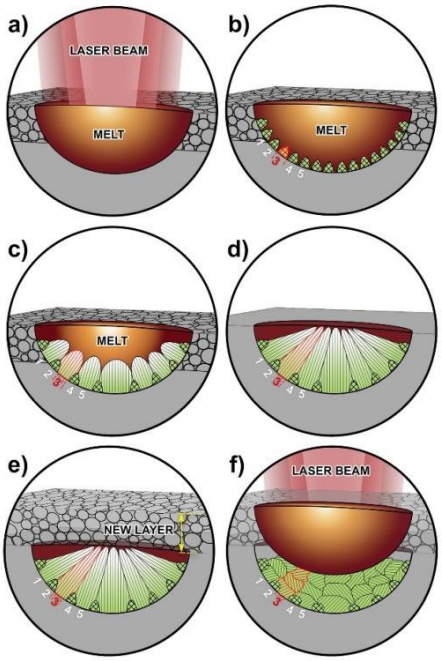

Figure 12: Model of melt pool solidification. (a) Melt pool with the melt; (b) nucleated grains on the melt pool border; (c) preferential growth of a few grains (1 and 5); (d) solidified melt pool with prevailing columnar grains; (e) addition of a new powder layer; (f) partial re-melting of the melt pool and break down of the columnar grains into a number of equiaxed grains via α↔γ solid state transformations.

The group has proposed a simple method for prediction of the binary interaction coefficients in grain boundary segregation based on the knowledge of the volume solid solubility, the maximum possible concentration of the solute at the grain boundary, and an additional parameter representing an activity exponent of both the solute and the host metal [27]. **We discovered a new method for predicting grain boundary segregation at any grain boundary, in any alloy at any temperature**. The crucial points are prediction of (i) the enthalpy, (ii) the entropy of grain boundary segregation, both related to ideal behaviour, and (iii) the binary interaction coefficient describing the real contribution. The procedure is schematically shown in Fig. 13 [28]. We also summarized the current knowledge of grain boundary segregation and its relationship

to intergranular brittle fracture, which was published in a prestigious scientific journal, Progress in Materials Science [29]. Here, we compared experimental and calculated values of the segregation enthalpy/energy available in the literature. This comparison showed that the data corresponding to segregation of well soluble solutes in the host metal exhibit excellent agreement, while in the case of less soluble solutes, there is an extreme discrepancy between experimental and calculated values. We explained these discrepancies on the basis of the relationship between the size of the calculation cell and the solid solubility (*share 90%*).

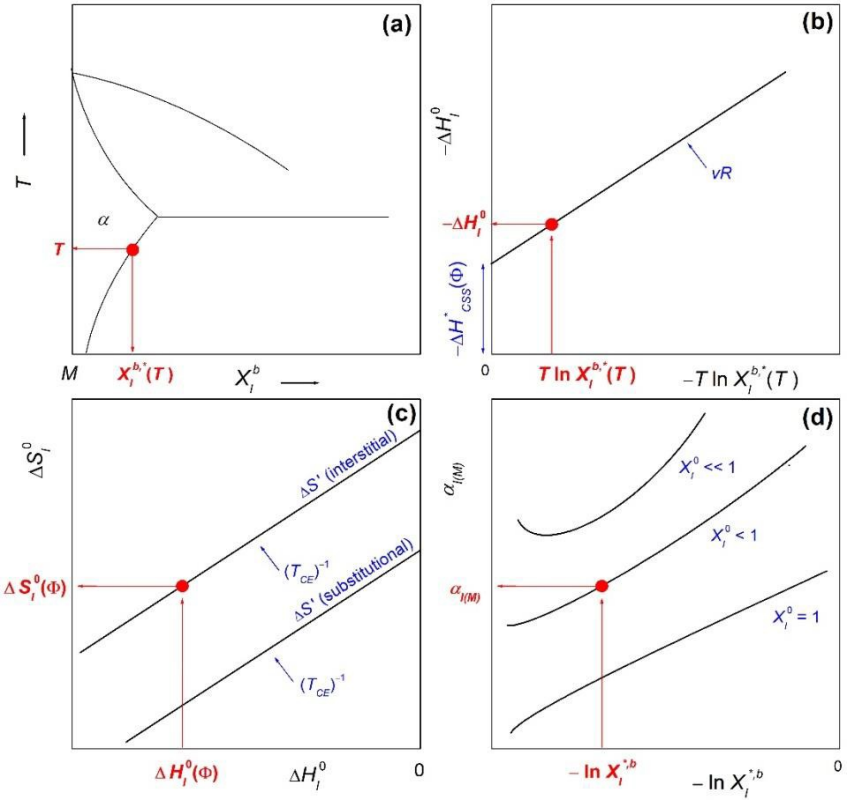

Figure 13: Scheme of procedure for obtaining parameters of grain boundary segregation.

An interesting project, with a possible quick application, was completed in cooperation with the University of Chemistry and Technology and the 1st Faculty of Medicine of the Charles University. The main aim was to design **zinc-based materials possessing suitable properties for applications in orthopedics**. Zinc and its alloys are materials with elastic moduli close to that of human bones. Additionally, zinc-based alloys are biodegradable with suitable corrosion rates and the products are incorporating well in the human body. Porous zinc, prepared by thermal plasma spraying, was characterized from the point of view of mechanical and corrosion properties, and viability of cells. These results show the potential of these materials, and the potential of this process for production of such materials [30]. Further, the study focused on mixtures of hydroxyapatite representing the inorganic part of bones, and biocompatible Zn-Mg-Ca/Sr alloys, which enable tuning of the mechanical properties and corrosion rate (Fig. 14). Modern techniques, such as equal channel angular pressing, were applied for preparation of parts. Also demonstrated was double twinning $\{10\bar{1}2\}/\{10\bar{1}2\}$ occurring in zinc. A relatively simple explanation of double twinning in crystals with hexagonal symmetry based essentially
only on the crystal geometry was elaborated in [31] (*share 90%*).

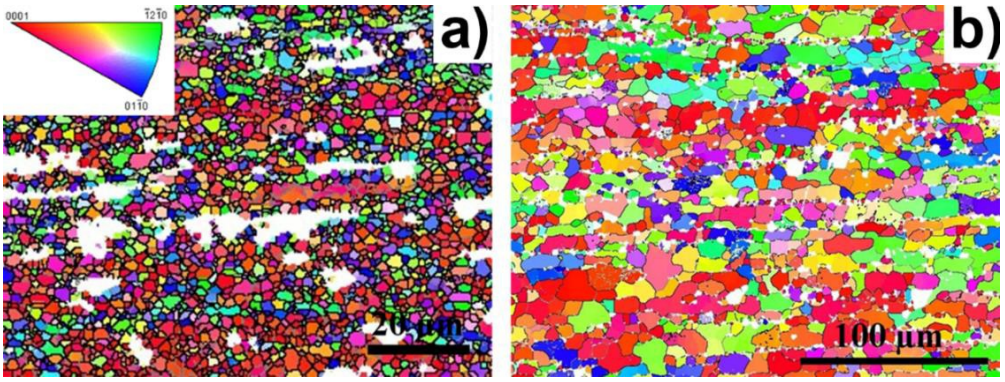

Figure 14: 0001 inverse pole figures of extruded ZnMg0.8Ca0.2 alloy, extruded at a) 150 °C and b) 300 °C.

Researchers in the FIB-SEM FUNBIO-SAFMAT central laboratory perform research services for users across the whole of FZU, consisting of material characterization using scanning electron microscopy, plasma focus ion beam (P-FIB) micromanipulation and electron back-scattered electrons diffraction techniques (EBSD). The lab collaborates closely with all three research groups FMC, MNB and MCM of the team. A good example (Fig. 15) is the application of modern 3D characterization techniques in SEM by combination of FIB and EBSD in 3D-EBSD mapping of grain microstructure of polycrystalline materials [6] (*share 80%*) or the application of P-FIB for preparation of NiMnGa micropillars, which were further used for investigation of functional properties [32] (*share 20%*).

Besides of the research services, the head of the laboratory J. Kopeček, who is personally interested in the research of intermetallics, such as Fe-Al, Fe-Al-Si, Ti-Al-Si, Ni-Mn-Ga, Co-Ni-Al, Co-Ni-Ga, Ni-Ti, various silicides of transient metals, Bi2Se3 and similar topological insulators, has developed a wide range of research collaborations and collaborative projects in this area.
.

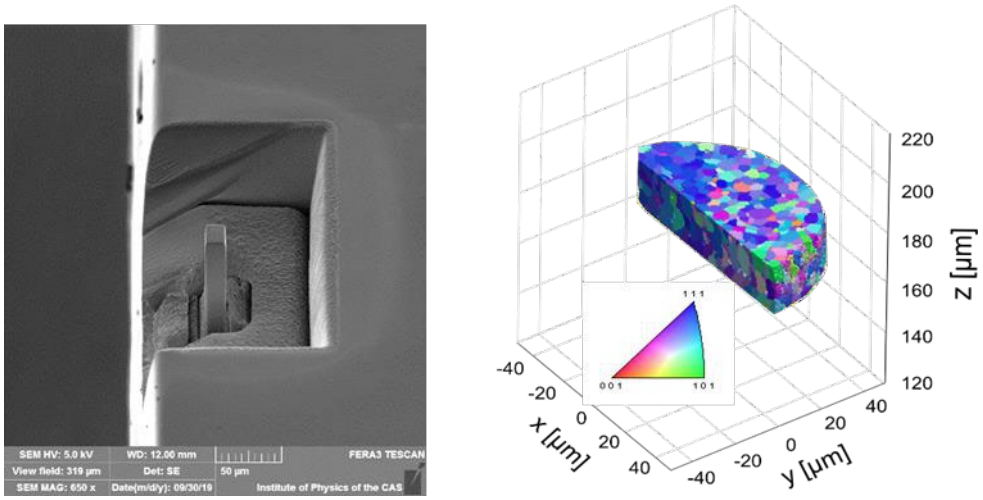

Figure 15: Single crystalline Ni-Mn-Ga cuboid micropillars with dimensions of 15 × 15 × 60 µm^3 prepared by P-FIB (left) 3D-EBSD reconstruction of grain orientation in NiTi annealed wire (right). Colour scale gives the orientation of normal in plane x-z.

Finally, there is a very important methodological collaboration of the team with the Department of Structure Analysis in FZU. Originally, FUNBIO researchers prepared a wide set of silicides of transient metals as bulk comparative materials. These samples

were later used to describe three new phases in a Cu-Si system after re-work of system phase diagram. The Ni2Si sample was used as an example to show the ability of precession electron diffraction tomography [33] (*share 10%*).

References

[1] E. Alarcon, L Heller, S.A. Chirani, P. Šittner, J. Kopeček, L. Saint-Sulpice, Fatigue performance of superelastic NiTi near stress-induced martensitic transformation, *International Journal of Fatigue* **95** (2017) 76-89
[2] P. Sedmák, P. Šittner, J. Pilch, C. Curfs, Instability of cyclic superelastic deformation of NiTi investigated by synchrotron X-ray diffraction, *Acta Materialia* **94** (2015) 257-70
[3] J. Racek, M. Stora, P. Šittner, L. Heller, J. Kopeček, M. Petrenec, Monitoring tensile fatigue of superelastic NiTi wire in liquids by electrochemical potential, *Shape Memory and Superelasticity*, **1** (2015) 204-230
[4] Y. Chen, O. Tyc, L.Kadeřávek, O. Molnárová, L. Heller, P. Šittner, Temperature and microstructure dependence of localized tensile deformation of superelastic NiTi wires, *Materials & Design* **174** (2019) 107797
[5] Y Chen, O Molnárová, O Tyc, L Kadeřávek, L Heller, P Šittner, Recoverability of large strains and deformation twinning in martensite during tensile deformation of NiTi shape memory alloy polycrystals Acta Materialia 180, 243-259
[6] P. Sedmák, J. Pilch, L. Heller, J. Kopeček, J. Wright, P. Sedlák, M. Frost, Grain-resolved analysis of localized deformation in nickel-titanium wire under tensile load, *Science* **353** (2016) 559-562, L. Heller, H. Seiner, P. Šittner, P. Sedlák, O. Tyc, L. Kadeřávek , On the plastic deformation accompanying cyclic martensitic transformation in thermomechanically loaded NiTi, *International Journal of Plasticity* **111** (2018) 53-71
[7] P. Šittner, P. Sedlák, H. Seiner, P. Sedmák, J. Pilch, R. Delville, L. Heller, L. Kadeřávek, On the coupling between martensitic transformation and plasticity in NiTi: experiments and continuum based modelling, *Progress in Materials Science* **98** (2018) 249-298
[8] L. Heller, P. Šittner, P. Sedlák, H. Seiner, O. Tyc, L. Kadeřávek, P. Sedmák, M. Vronka, Beyond the strain recoverability of martensitic transformation in NiTi, *International Journal of Plasticity*,**116** (2019) 232-264
[9] M. Frost, P. Sedlák, L. Kadeřávek, L. Heller, P. Šittner, Modeling of mechanical response of NiTi shape memory alloy subjected to combined thermal and non-proportional mechanical loading: a case study on helical spring actuator, *Journal of Intelligent Material Systems and Structures* **27** (2015) 1927-1938
[10] I. Stachiv, P. Sittner, Nanocantilevers with adjustable static deflection and significantly tunable spectrum resonant frequencies for applications in nanomechanical mass sensors, *Nanomaterials* **8** (2018) 116
[11] V. Petrakova, I. Rehor, J. Stursa, M. Ledvina, M. Nesladek, and P. Cigler, Nanoscale 7, 12307 (2015).
[12] V. Petrakova, V. Benson, M. Buncek, A. Fiserova, M. Ledvina, J. Stursa, P. Cigler, and M. Nesladek, Nanoscale 8, 12002 (2016).
[13] A. Taylor, P. Ashcheulov, P. Hubík, L. Klimša, J. Kopeček, Z. Remeš, Z. Vlčková Živcová, M. Remzová, L. Kavan, E. Scheid, J. Lorinčík, and V. Mortet, Carbon 128, 164 (2018).
[14] A. Taylor, L. Klimša, J. Kopeček, Z. Remeš, M. Vronka, R. Čtvrtlík, J. Tomáštík, and V. Mortet, Journal of Alloys and Compounds 800, 327 (2019).
[15] A. Taylor, J. Drahokoupil, L. Fekete, L. Klimša, J. Kopeček, A. Purkrt, Z. Remeš, R. Čtvrtlík, J. Tomáštík, O. Frank, P. Janíček, J. Mistrík, and V. Mortet, Diamond and Related Materials 69, 13 (2016).
[16] P. Ashcheulov, A. Taylor, V. Mortet, A. Poruba, F. Le Formal, H. Krýsová, M. Klementová, P. Hubík, J. Kopeček, J. Lorinčík, J.-H. Yum, I. Kratochvílová, L. Kavan, and K. Sivula, ACS Applied Materials & Interfaces 10, 29552 (2018).
[17] V. Petrák, Z. Vlčková Živcová, H. Krýsová, O. Frank, A. Zukal, L. Klimša, J. Kopeček, A. Taylor, L. Kavan, and V. Mortet, Carbon 114, 457 (2017).
[18] S. Sedlakova, A. Taylor, Z. V. Zivcova, V. Renciukova, J. Kopecek, L. Klimsa, L. Kavan, M. Ledvina, and V. Mortet, 9th International Conference on Nanomaterials - Research and Application, NANOCON 2017; Hotel Voronez IBrno; Czech Republic; 18 October 2017 through 20 October 2017 2017-October, 2018, 277 (n.d.).
[19] S. Baluchová, A. Taylor, V. Mortet, S. Sedláková, L. Klimša, J. Kopeček, O. Hák, and K. Schwarzová-Pecková, Electrochimica Acta 327, 135025 (2019).
[20] A. Kovalenko, P. Ashcheulov, A. Guerrero, P. Heinrichová, L. Fekete, M. Vala, M. Weiter, I. Kratochvílová, and G. Garcia-Belmonte, Sol. Energy Mater Sol. Cells 134, 73 (2015).
[21] Z. Remes, J. Stuchlik, H. T. Stuchlikova, K. Dragounova, P. Ashcheulov, A. Taylor, V. Mortet, and A. Poruba, Phys. Status Solidi A 216, 1900241 (2019).
[22] V. Mortet, Z. Vlčková Živcová, A. Taylor, O. Frank, P. Hubík, D. Trémouilles, F. Jomard, J. Barjon, and L. Kavan, Carbon 115, 279 (2017).
[23] V. Mortet, A. Taylor, Z. Vlčková Živcová, D. Machon, O. Frank, P. Hubík, D. Tremouilles, and L. Kavan, Diamond and Related Materials 88, 163 (2018).

[24] V. Mortet, Z. V. Živcová, A. Taylor, M. Davydová, O. Frank, P. Hubík, J. Lorincik, and M. Aleshin, Diamond and Related Materials 93, 54 (2019).
[25] P. Lejček, M. Roudnická, J. Čapek, D. Dvorský, J. Drahokoupil, D. Šimek, J. Čížek, P. Svora, O. Molnárová, D. Vojtěch: Selective laser melting of pure iron: Multiscale characterization of hierarchical microstructure. *Mater. Charact.* 154 (2019) 222-232.
[26] P. Lejček, S. Hofmann: Prediction of binary interaction coefficients in grain boundary segregation. *Surf. Interface Anal.* 50 (2018) 640-647.
[27] P. Lejček, S. Hofmann: Modeling grain boundary segregation by prediction of all the necessary parameters, *Acta Mater.* 170 (2019) 253-267.
[28] P. Lejček, M. Šob, V. Paidar: Interfacial segregation and grain boundary embrittlement: An overview and critical assessment of experimental data and calculated results. *Prog. Mater. Sci.* 87 (2017) 83-139.
[29] J. Čapek, J. Pinc, Š. Msallamová, E. Jablonská, P. Veřtát, J. Kubásek, D. Vojtěch: Thermal plasma spraying as a new approach for preparation of zinc biodegradable scaffolds: A complex material characterization. *J. Thermal Spray Technol.* 28 (2019) 826-841.
[30] V. Paidar, J. Čapek, A. Ostapovets: Secondary twinning in zinc. *Phil. Mag. Lett.* 98 (2018) 437-445.
[31] D. Musiienko, A. Saren, L. Straka, M. Vronka, J. Kopeček, O. Heczko, A. Sozinov, K. Ullakko, Ultrafast actuation of Ni-Mn-Ga micropillars by pulsed magnetic field, Scripta Mat., 162, 482-485, (2019);
[32] L. Palatinus, C. A. Corrêa, G. Steciuk, D. Jacob, P. Roussel, P. Boullay, M. Klementová, M. Gemmi, J. Kopeček, M. C. Domeneghetti, F. Cámara, V. Petříček, Structure refinement using precession electron diffraction tomography and dynamical diffraction: tests on experimental data, Acta Cryst. B, 71:(6), 740-751

Research activity and characterisation of the main scientific results

Most of the research output of the Department was published in impact factored peer-reviewed journals (in 2015–2019, over 250 articles including 20 articles in Physical Review Letters and other journals with an impact factor over 7). Here we list examples from its priority research activities. Unless otherwise stated, all the selected results and data described here are chiefly obtained within the Department and within disciplines where the Department is recognized as the world leader.

1. Frustrated ferroelectrics

Spatio-temporal distribution of relative Ti–O_6 displacements in cubic $BaTiO_3$. $BaTiO_3$ is often considered as a model ferroelectric material in which the dielectric properties are defined by the displacements of Ti ions with respect to surrounding oxygen atoms. However, despite the decades of a dedicated research, certain controversies have remained as to the description of collective movements of the Ti ions. Members of the Department and collaborators approached this problem using nanoscale-oriented X-ray scattering methods and large-scale atomistic simulations [1]. Together these showed that the Ti dynamics can be exhaustively explained by phonons excited on a picosecond timescale. X-ray diffuse scattering by $BaTiO_3$ has been recorded in a synchrotron experiment and simultaneously computed using molecular dynamics simulations of a shell model. Together, these approaches have allowed us to clarify the details of the disorder in paraelectric $BaTiO_3$.The narrow sheets of diffuse scattering, related to the famous anisotropic longitudinal correlations of Ti ions, are shown to originate from the overdamped anharmonic soft phonon branch. This finding demonstrates that the occurrence of narrow sheets of diffuse scattering agrees with a displacive picture of the cubic phase of this textbook ferroelectric material. The developed methodology allows one to go beyond the harmonic approximation in the analysis of phonons and phonon-related scattering. Using a similar approach, the Department could get very detailed insights into diffuse scattering patterns of antiferroelectric lead zirconate [2] or a relaxor lead magnesium niobate [3].

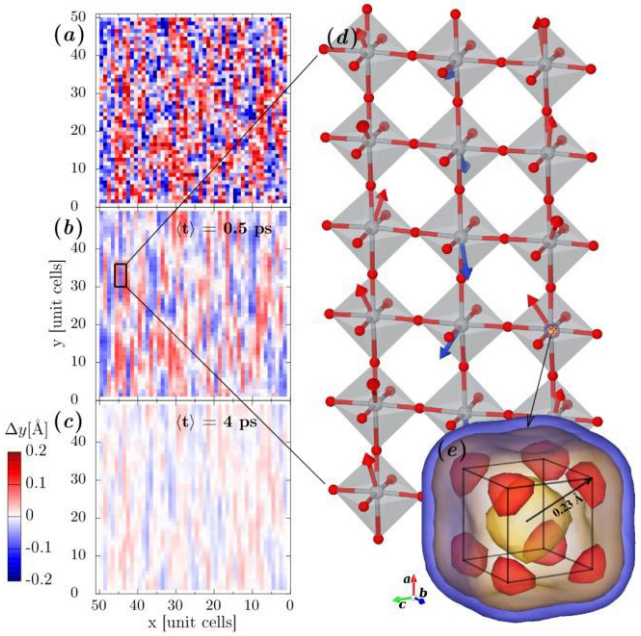

Figure 1: One component of the relative Ti–O_6 displacement is mapped within one layer of the material using different time averages (a–c) which clearly shows that chain correlations exist on a timescale of picoseconds. The displacements averaged over the simulation time and all unit cells of the crystal have a cuboidal distribution with shallow minima along diagonal directions [1].

Perhaps the most advanced methodological breakthrough has been achieved in the **analysis of the neutron scattering pair distribution function of a tetragonal tungsten bronze** material – strontium barium niobate ($Sr_xBa_{1-x}Nb_2O_6$; SBN) from the relaxor ferroelectric family. There, in order to interpret the original experiments performed entirely within the Department, and to extract the microscopic mechanisms of the extraordinary dielectric response, the Department member M. Paściak employed ab-initio molecular dynamics to study ps scale finite temperature dynamics in supercells with over 1000 atoms and partial site occupancy [4].

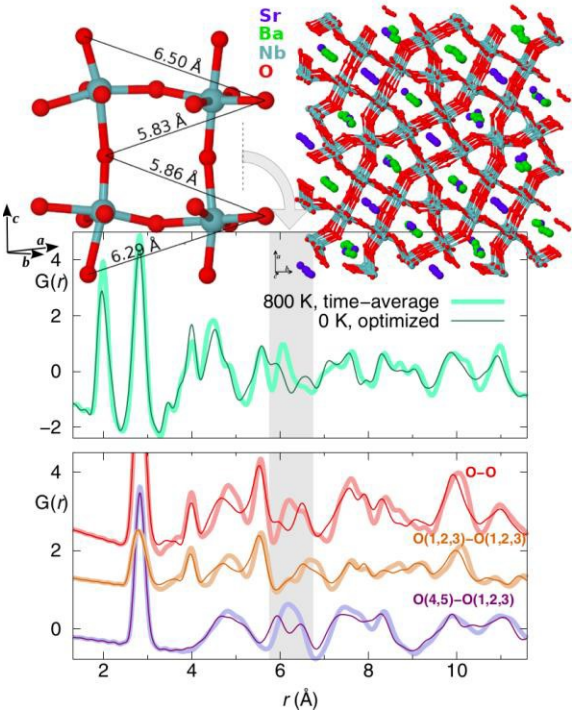

Figure 2: Finite-temperature ab-initio calculations and the neutron pair-distribution function, G(r), have shown that the most visible structural change in the $Sr_xBa_{1-x}Nb_2O_6$ structure upon cooling can be attributed to tilting of rigid oxygen octahedra [4].

Polarization mechanisms in uniaxial ferroelectrics. The same ($Sr_xBa_{1-x}Nb_2O_6$) system has been thoroughly studied by various spectroscopic techniques within the project of E. Buixaderas [5,6]. The high-frequency dielectric response of uniaxial strontium barium niobate ($Sr_xBa_{1-x}Nb_2O_6$) crystals was studied from 1 kHz to 30 THz in a wide temperature interval [6]. Four main excitations were ascertained below the phonon frequencies. These fast polarization mechanisms take place at THz, GHz and MHz ranges and show different temperature evolution. Altogether, the four mechanisms explain, above the kHz range, the ferroelectric transition as well as its relaxor character.

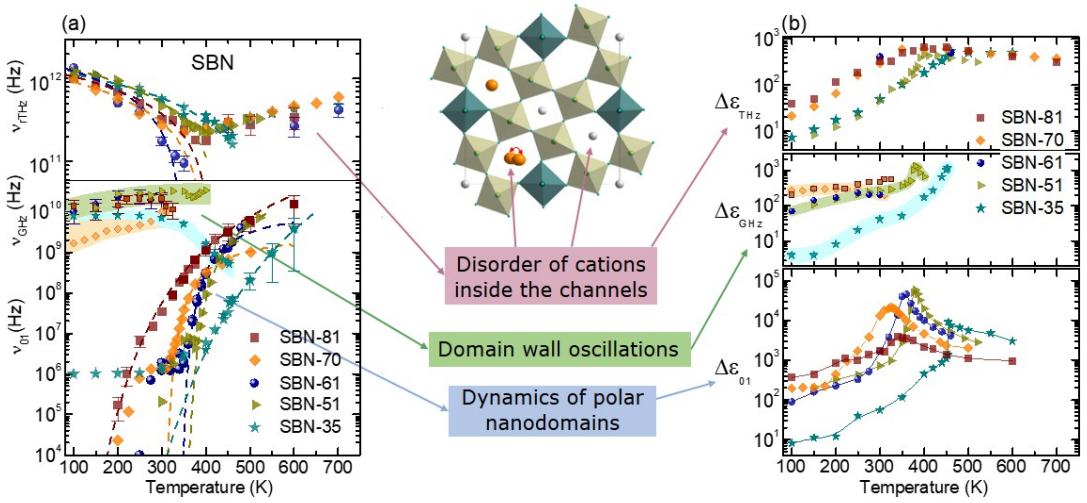

Figure 3: (a) Temperature dependences of the frequencies of the main excitations found in SBN crystals of different compositions and (b) contribution to the permittivity of the main excitations, related to the crystal microstructure shown in the middle (unit cell) [6].

Local ferroelectric transition in lead-based relaxors. In order to clarify the universal nature of relaxor effects, materials with different characteristics have been investigated. For example, perovskite relaxors have a completely different structure and dynamics to SBN. In order to have sound evidence for sub-THz excitations in the perovskite relaxor $Pb(Mg_{1/3}Nb_{2/3})O_3$ (PMN), hyper-Raman scattering spectroscopy investigations have been carried out in collaboration with our long-term partners at Univ. Montpellier [7]. Subsequently, investigation of infrared (IR) and terahertz (THz) spectra using the Bruggeman effective medium approach allowed the authors from the Department to claim that the mesoscopic structure of PMN and $Pb(Mg_{1/3}Ta_{2/3})O_3$ (PMT) consists of dynamic, randomly oriented, uniaxially anisotropic polar nanoregions with harder transverse optical polar modes in the direction along the local dipoles [8,9]. The lowest-frequency phonon of the *E* symmetry, polarized perpendicular to the local dipole moments, undergoes a softening towards $T^* \approx 400$ K, which provides evidence for a local structural phase transition [7,8,9].

2. Semiconductor nanostructures

Conductivity and ultrafast photoconductivity in semiconductor nanostructures. A strong research focus of the Department is put on the quantitative understanding of the conductivity and ultrafast photoconductivity in semiconductor nanostructures (see the scheme in Figure 4). In this field we largely benefitted from our previous developments: namely, from the classical Monte-Carlo calculations, describing the motion of confined carriers, and from effective medium approaches. In collaboration with T. Ostatnický from the Charles University in Prague we developed the first quantum model of the THz conductivity of confined carriers [10]. Indeed, the Kubo formula for the optical conductivity in the relaxation time approximation is not valid in the THz spectral range due to a broken translation symmetry at nanoscale. Probing by the THz field causes a net displacement of the carrier concentration within the nanostructure; the relaxation time approximation then inherently erroneously assumes that a scattering event of the charge carrier leads to the relaxation of this inhomogeneous charge density via an *instantaneous* restoration current,

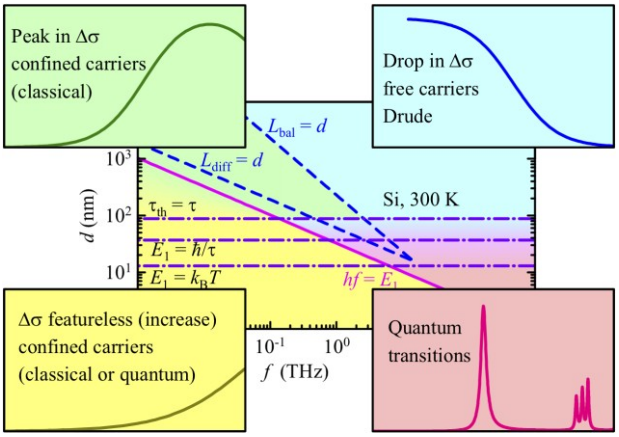

Figure 4: Schemes of confinement regimes for model silicon nanocrystals in the form of cubes with a side length *d* and with a probing frequency *f*; momentum scattering time $\tau = 150$ fs, temperature $T = 300$ K. In the region I (cyan) the charge carriers show a delocalized (Drude-like) response; the region II (green) is roughly delimited by the lines indicating the carrier transport distance in the ballistic (L_{bal}) and diffusion (L_{diff}) regimes within a single period of the probing radiation and it features a conductivity peak interpreted within the framework of the classical physics. Region III (yellow) is below the lowest quantum transition energy denoted as E_1; here the conductivity signal is small, the spectra are featureless and typical for the localized response (Drude–Smith-like behavior). The three dash-dot horizontal lines ($\tau_{th} = \tau$, $E_1 = \hbar/\tau$ and $E_1 = k_B T$) delimit a zone marking the crossover from the classical to the quantum regime. Finally, in regime IV (red), several quantum transitions will appear in the spectra; naturally, this triangle broadens toward the optical region where these phenomena are usually observed. The figure was adapted from [18].

which leads to unphysical results. Our theory then properly takes into account the *finite* duration of the thermalisation regime and yields correct THz conductivity spectra. Experimentally, we frequently complement the THz results with the dc conductivity measurements, with the conductive AFM characterization and with the multi-THz results; this allows us to achieve a deeper understanding of the underlying phenomena on a microscopic level well beyond the frequently used phenomenological approaches. Sb-doped SnO_2 nanoparticles were studied from the viewpoint of their intra-nanoparticle conductivity and inter-nanoparticle electrical connectivity in relation with the technological steps of their fabrication and post- processing [11,12].

Ultrafast charge carrier transport. Ultrafast charge carrier transport has been studied in bulk TiO_2 under very strong photoexcitation and in anodic TiO_2 nanotubes (see Figure 5) [13,14,15]. Ultrafast photoconductivity has been thoroughly studied in silicon nanocrystal networks prepared by thermal separation of Si nanocrystals from SiO_2 matrix with an enhanced control of the nanocrystal size. The quantum theory of the THz conductivity has been employed to explain the charge carrier transport both

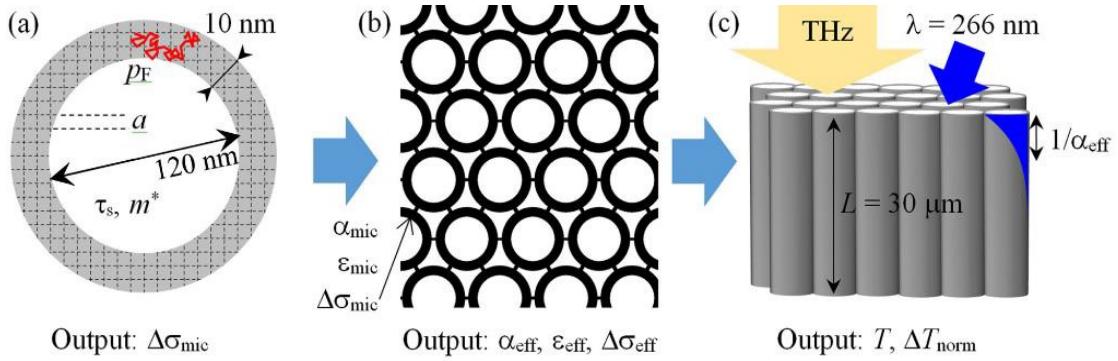

Figure 5: (a) Monte-Carlo calculations are used to determine the microscopic terahertz response of the charges in the TiO_2 nanotubes. It is found that charges are confined by the nanotube boundaries, but also by grain boundaries. (b) The microscopic conductivity enters the effective-medium calculations, which provide effective terahertz conductivity and effective optical absorption of the nanotube structure. (c) Finally, using the knowledge of the effective properties, the transient terahertz signal is calculated. A combination of all these steps thus links microscopic charge transport properties with a measurable terahertz signal [15].

at high and low temperatures over several orders of magnitude of the carrier concentration [16,17]. A careful data analysis made it possible to assess the distribution of sizes of nanocrystals participating to the photoconduction in samples with various nominal sizes of nanocrystals. We showed and justified that a conductivity-weighted distribution of sizes may differ from the size distribution obtained by standard analysis of transmission electron microscopy images. In 2019, our competence in this field allowed us to publish a comprehensive review involving both theoretical and experimental aspects of the state-of-the-art achievements in charge-carrier transport in nanomaterials [18].

3. New liquid crystal phases

Members of the Department are also strongly involved in characterization of phase diagrams, mesomorphic phases and functional properties of completely new types of liquid crystal molecules and phases. Examples of unique achievements (see Figures 6 and 7) include a discovery of **new type of bent-core molecule dimers** [19], **light-**

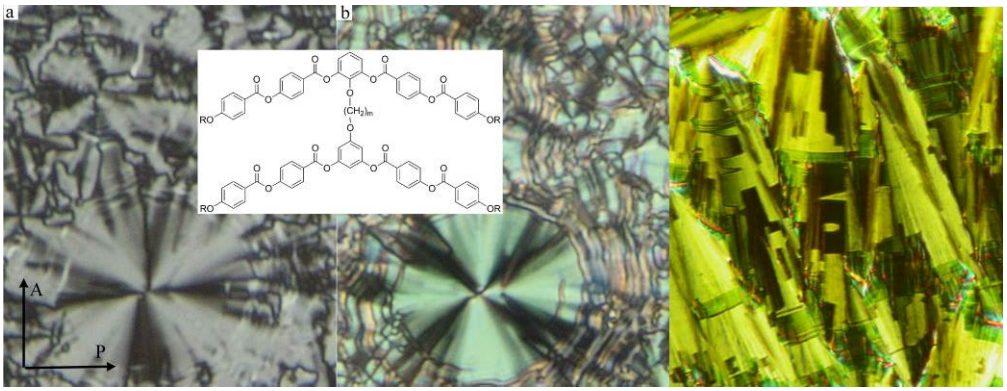

Figure 6: Liquid crystals under a polarizing microscope. A bent-molecule liquid crystal without (left) and with electric field on (middle). It was found that the length of the terminal chain selects the mesophase type. The shortest homologue forms a smectic A phase, dimers with intermediate chains form a columnar phase. Still longer chain yields a phase with an antiferroelectric electric switching [19]. Right: A photosensitive rod-like molecule material forming a ferroelectric phase [20].

sensitive rod-like molecules also showing a ferroelectric liquid crystal phase [20], or **new cholesteric liquid crystals with extremely short pitch** [21,22]. The Department also contributed to the **discovery of a facile route of preparation of organic nanotubes from chiral rod-like mesogens** [23]. The mechanism of the observed rolling-up was traced back to the difference of the surface tension between the opposite crystallite surfaces [23].

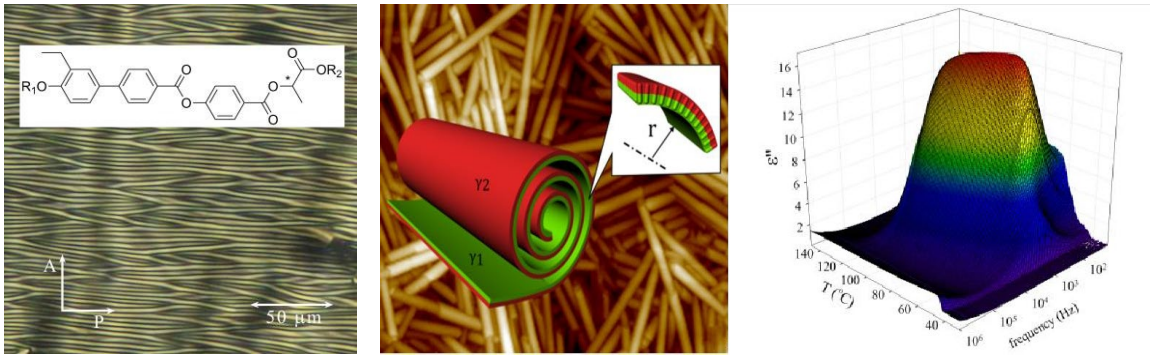

Figure 7: Left: Texture of a new cholesteric liquid crystal in electric field. These materials form a cholesteric phase with the helix pitch length in the interval of 120–200 nm within a broad temperature range. Due to a positive dielectric anisotropy and a short pitch, the applied electric field causes reproducible and reversible optical changes in the planar cell. In the inset: the chemical formula of the studied compound [21,22]. Middle: AFM image shows nanotubes with a diameter of 50–60 nm. The inset illustrates the original scrolling-up mechanism discovered with a contribution from the Department [23]. Right: Dielectric response of the mesogen.

4. Multiferroic materials

Multiferroics are materials with simultaneous orderings of different nature and, as such, they obviously promise new functional properties related to the plethora of possible property combinations. The Department has an internationally recognized reputation in the study of dynamical magnetoelectric phenomena. Observation of electrically active spin waves – **electromagnons in $SrMn_7O_{12}$ and in Y-type hexaferrite $BaSrCoZnFe_{11}AlO_{22}$** is an example of successful studies.

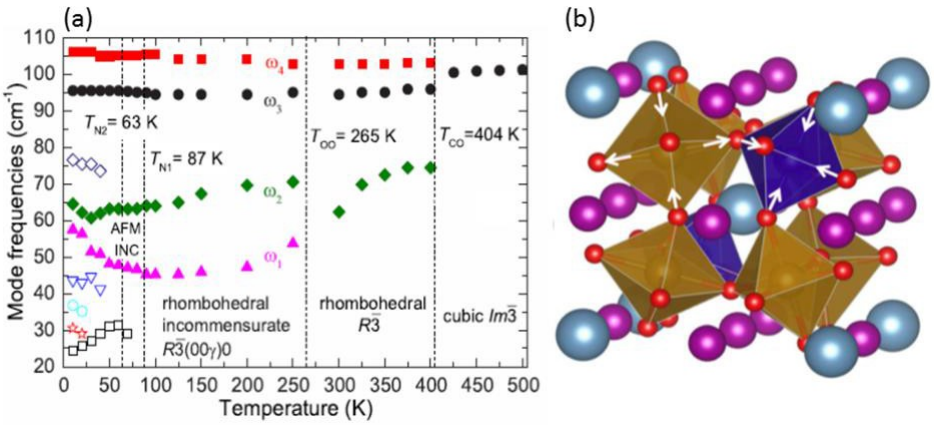

Figure 8: (a) Temperature dependence of the low-frequency excitations observed in THz and IR spectra of $SrMn_7O_{12}$. The open symbols correspond to spin excitations or phonons activated by breaking of the inversion center, whereas the remaining phonons are marked with solid symbols. (b) Rhombohedral quadruple perovskite crystal structure of $SrMn_7O_{12}$ [24].

Upon cooling, $SrMn_7O_{12}$ undergoes a series of structural and magnetic phase transitions from cubic to rhombohedral symmetry, and to an incommensurately modulated crystal structure, which is connected with the charge and orbital ordering of the Mn cations. The Department reported IR, THz, and Raman spectra of $SrMn_7O_{12}$ ceramics reflecting new phonons appearing in spin-order-induced ferroelectric phases. The strongest variations occur in the THz spectra near the two magnetic phase transitions, at T_{N1} = 87 K and T_{N2} = 63 K. The observed transfer of oscillator strengths from low-frequency phonons to these excitations below T_{N2} allows us to assign them as electromagnons [24].

An even more striking manifestation of electromagnons was documented in a

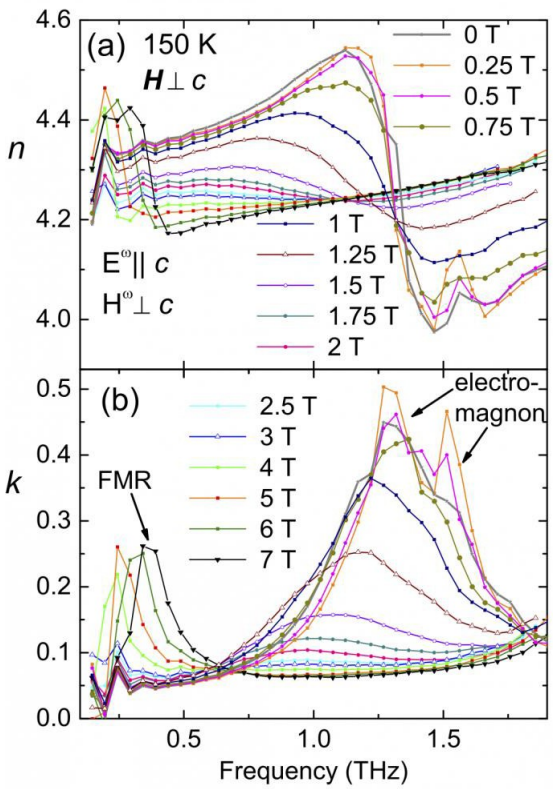

Figure 9: Electromagnon and ferromagnetic resonance (FMR) in THz spectra of a complex index of refraction for $BaSrCoZnFe_{11}AlO_{22}$ [25].

room-temperature multiferroic crystal with a Y-type hexaferrite structure (see Figure 9). There THz and Raman spectra reveal an electromagnon below 300 K at ≈ 1.2 THz. The Department members have demonstrated that the electromagnon is activated due to the magnetostriction mechanism involving spin vibrations along the hexagonal axis, while the static polarization is induced by the inverse Dzyaloshinskii–Moriya interaction. Moreover, the authors from the Department derived selection rules for electromagnons activated in infrared spectra in other magnetic phases of Y- type hexaferrites [25].

Theory of multiferroic materials. The Department is also heavily involved in developing the theory of multiferroic materials. Using purely a symmetry analysis, they have constructed a set of tools for searching new multiferroic phases. In particular, 212 species of structural phase transitions with a macroscopic symmetry breaking were inspected with respect to a simultaneous occurrence of ferroelastic, ferroelectric, and ferroaxial properties. For each species, a matrix of representative equilibrium property tensors in both high- and low symmetry phases, showing emergence of spontaneous components, were explicitly worked out [26]. The results can serve as a useful tool in the search of fundamentally new material properties, such as so-called ferroaxial materials [27].

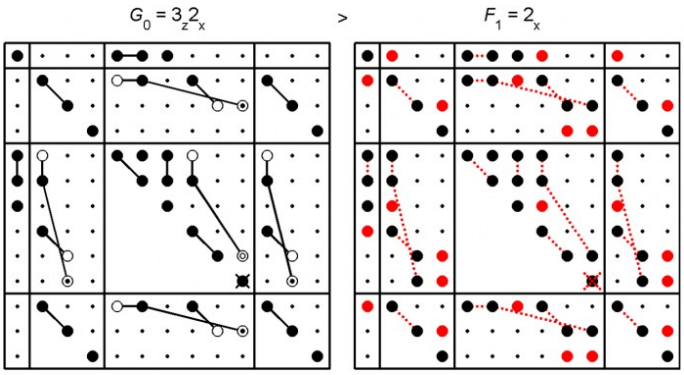

Figure 10: Symmetry relations among components of property tensors at a symmetry-breaking phase transition. Red points stand for spontaneous components [26].

The Department has also developed a **novel strategy for ab-initio determination of the Landau–Devonshire potentials**. In contrast to the usual approaches based on the soft mode eigenvectors of the parent phase, the new method exploits the configuration space attached to the eigenvectors of the modes frozen in the ground state. This enables a much better description of the energy surface in the vicinity of the ground state, which is relevant for most applications. This procedure was demonstrated on multiferroic $BiFeO_3$ in order to determine the potential energy associated with strain, polarization, and oxygen octahedra tilt [28].

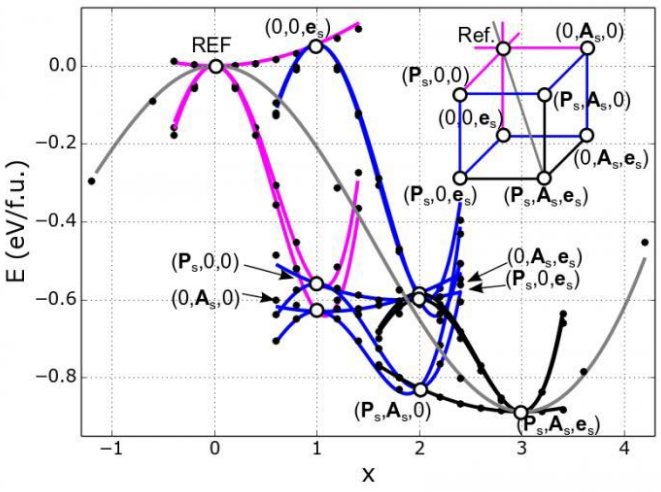

Figure 11: Energy profiles along selected paths in theorder parameter space of $BiFeO_3$, connecting the cubic reference state (REF) and the ground state with spontaneous strain, polarization, and oxygen octahedra tilt ($\mathbf{P}_s$, $\mathbf{A}_s$, $\mathbf{e}_s$). Point symbols are from a direct first-principles calculation, lines are evaluated from the proposed Landau– Devonshire potential [28].

5. Ferroelectric interfaces

Exceptional electromechanical properties of modern ferroelectric materials can often be related to their domain structure. The Department is traditionally investigating various domain- wall related phenomena.

For example, the authors from the Department have shown by means of atomistic modelling that a suitable configuration of interfaces can result in the **formation of a terahertz resonant mode in a $BiFeO_3$** thin film. These findings can be used in a design of new materials [29].

Experimentally, researchers from the Department have discovered a method of natural growth of ferroelectric

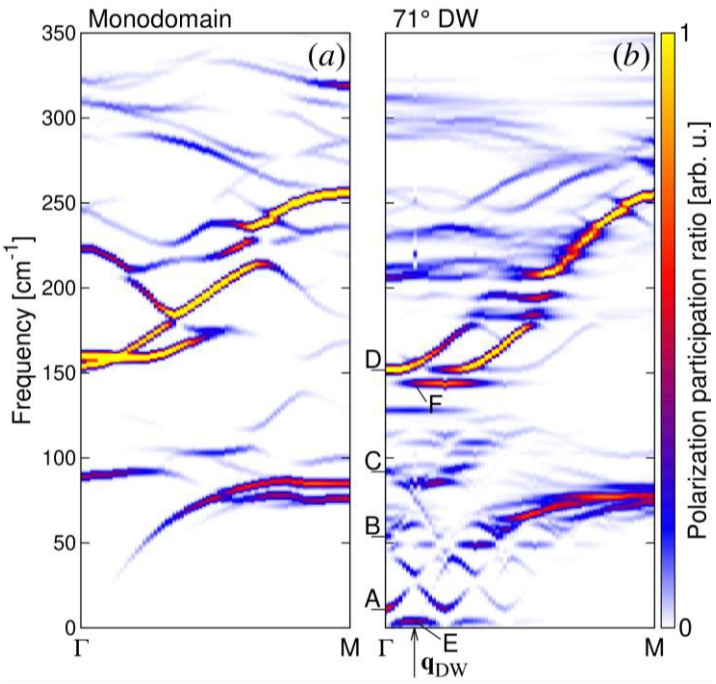

Figure 12: Phonon spectrum due to a dense domain structure (b) in $BiFeO_3$ crystal compared to the monodomain case (a). The domain-wall mode labelled A is responsible for a 25x enhancement of the dielectric permittivity [29].

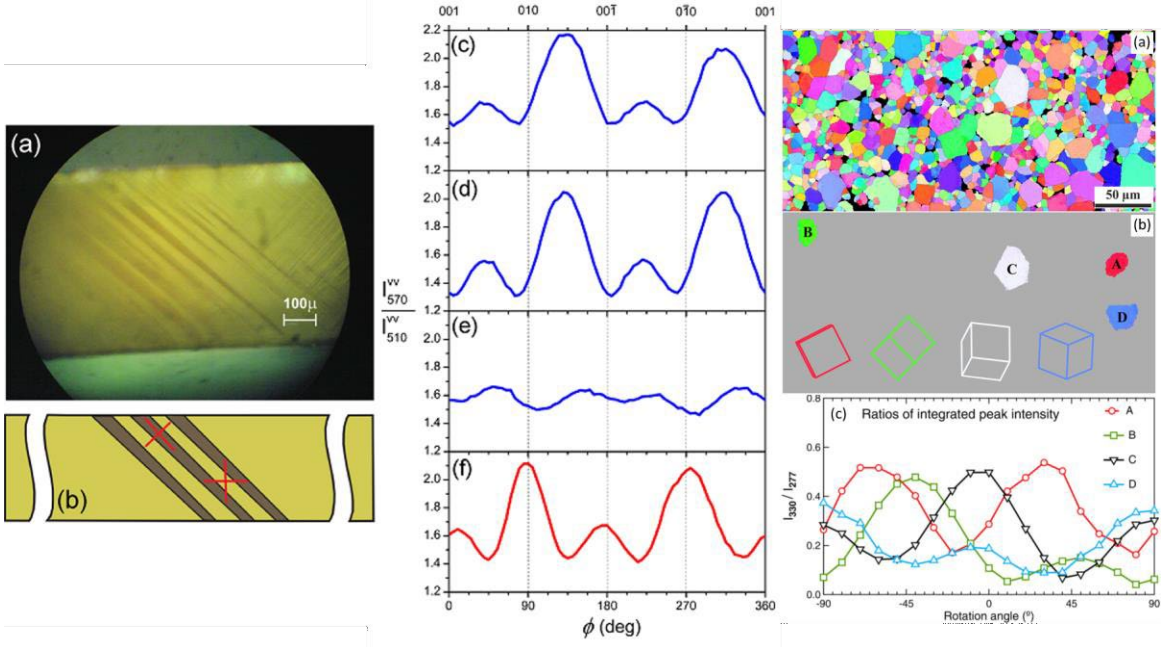

Figure 13: Optical micrograph (a) of phase coexistence in $Pb(Mg_{1/3}Nb_{2/3})O_3xPbTiO_3$ crystal. In the illustration (b), red crosses in the dark and light stripe indicate extinction of cross- polarized Raman intensity at 570 cm^{-1}. The angular dependence of the I_{570}/I_{510} intensity ratio for the parallel-polarized Raman scattering is detected from the dark stripe (c), from a single-domain ($[111]_{pc}$-poled) crystal (d), from a $[100]_{pc}$-poled crystal (e), and from the light stripe (f) [30]. Right: Novel all-optical method of crystal grain orientation is tested in the Department on GaV_4S_8 ceramics [31].

lamellar superstructures in $Pb(Mg_{1/3}Nb_{2/3})O_3$–$PbTiO_3$ single crystals (see Figure 13) that allowed a new insight into the tuning of piezoelectric properties of these materials. A spatially resolved polarized Raman scattering technique confirmed that the stripe pattern is due to the coexistence of the phases attached to the opposite sides of the morphotropic phase boundary in the temperature−composition phase diagram [30].

References:

[1] M. Paściak, T. R. Welberry, J. Kulda, S. Leoni, and J. Hlinka, Dynamic displacement disorder of cubic $BaTiO_3$, *Phys. Rev. Lett.* 120, 167601 (2018).
[2] N. Zhang, M. Paściak, A. M. Glazer, J. Hlinka, M. Gutmann, H. A. Sparkes, T. R. Welberry, A. Majchrowski, K. Roleder, Y. Xie, and Z.–G. Ye, A neutron diffuse scattering study of $PbZrO_3$ and Zr-rich $PbZr_{1-x}Ti_xO_3$, *J. Appl. Crystallography* 48, 1637 (2015).
[3] M. Kopecký, J. Kub, J. Fábry, and J. Hlinka, Nanometer-range atomic order directly recovered from resonant diffuse scattering, *Phys. Rev. B* 93, 054202 (2016).
[4] M. Paściak, P. Ondrejkovic, J. Kulda, P. Vaněk, J. Drahokoupil, G. Steciuk, L. Palatinus, T. R. Welberry, H. E. Fischer, J. Hlinka, and E. Buixaderas, Local structure of relaxor ferroelectric $Sr_xBa_{1-x}Nb_2O_6$ from a pair distribution function analysis, *Phys. Rev. B* 99, 104102 (2019).
[5] E. Buixaderas, C. Kadlec, M. Kempa, V. Bovtun, M. Savinov, P. Bednyakov, J. Hlinka, and J. Dec, Fast polarization mechanisms in the uniaxial tungsten-bronze relaxor strontium barium niobate SBN-81, *Sci. Rep.* 7, 18034 (2017).
[6] E. Buixaderas, M. Kempa, Š. Svirskas, C. Kadlec, V. Bovtun, M. Savinov, M. Paściak, and J. Dec, Dynamics of mesoscopic polarization in the uniaxial tetragonal tungsten bronze $(Sr_xBa_{1-x})Nb_2O_6$, *Phys. Rev. B* 100, 184113 (2019).
[7] B. Hehlen, M. Al-Sabbagh, A. Al-Zein, and J. Hlinka, Relaxor ferroelectrics: back to the single-soft-mode picture, *Phys. Rev. Lett.* 117, 155501 (2016).
[8] D. Nuzhnyy, J. Petzelt, V. Bovtun, S. Kamba, and J. Hlinka, Infrared, terahertz, and microwave spectroscopy of the soft and central modes in $Pb(Mg_{1/3}Nb_{2/3})O_3$, *Phys. Rev. B* 96, 174113 (2017).
[9] D. Nuzhnyy, J. Petzelt, V. Bovtun, S. Kamba, and J. Hlinka, Soft mode driven local ferroelectric transition in lead-based relaxors, *Appl. Phys. Lett.* 114, 182901 (2019).
[10] T. Ostatnický, V. Pushkarev, H. Němec, and P. Kužel, Quantum theory of terahertz conductivity of semiconductor nanostructures, *Phys. Rev. B* 97, 085426 (2018).
[11] K. Peters, P. Zeller, G. Stefanic, V. Skoromets, H. Němec, P. Kužel, and D. Fattakhova–Rohlfing, Water-dispersible small monodisperse electrically conducting antimony doped tin oxide nanoparticles, *Chem. Mater.* 27, 1090 (2015).
[12] V. Skoromets, H. Němec, J. Kopeček, P. Kužel, K. Peters, D. Fattakhova–Rohlfing, A. Vetushka, M. Müller, K. Ganzerová, and A. Fejfar, Conductivity mechanisms in Sb-doped SnO_2 nanoparticle assemblies: DC and terahertz regime, *J. Phys. Chem. C* 119, 19485 (2015).
[13] V. Zajac, H. Němec, and P. Kužel, Picosecond charge transport in rutile at high carrier densities studied by transient terahertz spectroscopy, *Phys. Rev. B* 94, 115206 (2016).

[14] M. Krbal, J. Kuchařík, H. Sopha, H. Němec, and J. M. Macák, Charge transport in anodic TiO_2 nanotubes studied by terahertz spectroscopy, *Phys. Status Solidi RRL* 10, 691 (2016).
[15] J. Kuchařík, H. Sopha, M. Krbal, I. Rychetský, P. Kužel, J. M. Macak, and H. Němec, Photoconductive, dielectric and percolation properties of anodic TiO_2 nanotubes studied by terahertz spectroscopy, *J. Phys. D: Appl. Phys.* 51, 014004 (2018).
[16] H. Němec, V. Zajac, P. Kužel, P. Malý, S. Gutsch, D. Hiller, and M. Zacharias, Charge transport in silicon nanocrystal superlattices in the terahertz regime, *Phys. Rev. B* 91, 195443 (2015).
[17] V. Pushkarev, T. Ostatnický, H. Němec, T. Chlouba, F. Trojánek, P. Malý, M. Zacharias, S. Gutsch, D. Hiller, and P. Kužel, Quantum behavior of terahertz photoconductivity in silicon nanocrystals networks, *Phys. Rev. B* 95, 125424 (2017).
[18] P. Kužel and H. Němec, Terahertz spectroscopy of nanomaterials: a close look at charge-carrier transport, *Adv. Opt. Mater.* 8, 1900623 (2019).
[19] M. Horčic, J. Svoboda, V. Novotná, D. Pociecha, and E. Gorecka, Core-to-core dimers forming switchable mesophase, *Chem. Commun.* 53, 2721 (2017).
[20] M. Cigl, A. Bubnov, M. Kašpar, F. Hampl, V. Hamplová, O. Pacherová. and J. Svoboda, Photosensitive chiral self-assembling materials: significant effects of small lateral substituents, *J. Mater. Chem. C* 4, 5326 (2016).
[21] V. Novotná, V. Hamplová, M. Glogarová, L. Lejček, and E. Gorecka, Effect of the applied electric field on new cholesterics with extremely short pitch, *Liq. Cryst.* 45, 634 (2018).
[22] L. Lejček, V. Novotná, and M. Glogarová, A model of field induced stripe texture in the cholesterics with extremely short pitch, *Liq. Cryst.* 46, 1280 (2019).
[23] V. Novotná, V. Hamplová, L. Lejček, D. Pociecha, M. Cigl, L. Fekete, M. Glogarová, L. Bednárová, P. Majewski, and E. Gorecka, Organic nanotubes created from mesogenic derivatives, *Nanoscale Adv.* 1, 2835 (2019).
[24] S. Kamba, V. Goian, F. Kadlec, D. Nuzhnyy, C. Kadlec, J. Vít, F. Borodavka, I. S. Glazkova, and A. A. Belik, Changes in spin and lattice dynamics induced by magnetic and structural phase transitions in multiferroic $SrMn_7O_{12}$, *Phys. Rev. B* 99, 184108 (2019).
[25] J. Vít, F. Kadlec, C. Kadlec, F. Borodavka, Y.S. Chai, K. Zhai, Y. Sun, and S. Kamba, Electromagnon in the Y-type hexaferrite $BaSrCoZnFe_{11}AlO_{22}$, *Phys. Rev. B* 97, 134406 (2018).
[26] http://palata.fzu.cz/species/13x13axial
[27] J. Hlinka, J. Privratska, P. Ondrejkovic, and V. Janovec, Symmetry guide to ferroaxial transitions, *Phys. Rev. Lett.* 116, 177602 (2016).
[28] P. Marton, A. Klíč, M. Paściak, and J. Hlinka, First-principles-based Landau–Devonshire potential for $BiFeO_3$, *Phys. Rev. B* 96, 174110 (2017).
[29] J. Hlinka, M. Pasciak, S. Körbel, and P. Márton, Terahertz-range polar modes in domain-engineered $BiFeO_3$, *Phys. Rev. Lett.* 119, 057604 (2017).
[30] I. Rafalovskyi, M. Guennou, I. Gregora, and J. Hlinka, Macroscopic lamellar heterophase pattern in $Pb(Mg_{1/3}Nb_{2/3})O_3$–$PbTiO_3$ single crystals, *Phys. Rev. B* 93, 064110 (2016).
[31] K. Tesar, I. Gregora, P. Beresova, P. Vanek, P. Ondrejkovic, and J. Hlinka, Raman scattering yields cubic crystal grain orientation, *Sci. Rep.* 9, 9385 (2019).

Research activity and characterisation of the main scientific results

The chapter is divided according to the research activity and the main scientific results with references in the end of the chapter.

A. Magnetic shape memory materials

It is expected that the investigated materials, mostly based on Heusler compounds, can thanks to their functional behaviour replace complicated machines fulfilling the motto "material is a machine". Such material provides simultaneous action and self-sensing and, therefore, belongs to the class of smart or intelligent materials. The distinct advantage over other smart materials is its contactless remote control by a magnetic field, plus the phenomenon scales well from macroscale to microscale. As there are many unknowns in this field, we strive to combine basic research to the effect with application driven one. There are still many unresolved but essential issues in basic research of MSM materials and these are addressed by the group according their research urgency and the group personnel capacity. The motivation behind all the effort is at the first place basic understanding of the material and the physics behind it but we also keep in mind the practical properties of the material and the importance in bridging the gap between basic research and potential material applications. To provide institutional basis and to have a well-defined direction, we formed a **Laboratory of magnetic shape memory materials (MSM)**. Initially, we were part of the other department and only in 2017 a new department of Magnetic Measurement and Materials was formed and the Laboratory became an integral part of it.

During the evaluated period, the research in this field was performed mainly within the frame of five awarded research grants related to magnetic shape memory alloys, four of them granted by the Czech Science Foundation, including Multidisciplinary Research Centre of Modern Materials (CSF–excellence in basic research) and one coming from the European Commission (MSCA-IF).

In the recent period, the group's focus was on extreme mobility of martensite twin boundaries and martensite microstructures in MSM materials, on the extraordinary modulated structure of the material, on the role of material doping and scale, and on novel functionalities of MSM materials for the case of significant magnetic hysteresis. In detail, we described several topics following the publications submitted to evaluation.

A.1 Twin boundary mobility and martensite microstructure

The understanding of high twin boundary mobility and martensite microstructure is a key prerequisite for understanding and designing a functional behaviour of MSM materials. Two publications are related to high twin boundary mobility and martensite microstructure[1-2].

The first paper [1] is a successful attempt to explain the appearance of hierarchical twin patterns in thin films of Ni-Mn-Ga. By combining a theoretical concept of an adaptive martensite developed by our team and by careful experimental observation of martensite transformation in thin films we were able to identify and explain the features on various scales from microscopic to meso- or macroscopic, particularly its anisotropic morphology. Our approach differs from the common approach used to explain twinned martensite. This complex result originated from a long-standing cooperation with IFW Dresden, where the author from FZU spent two years. The first author is a postdoc, co-supervised in his doctoral studies by the FZU author. Contribution of FZU was smaller, however, decisive, as it is based on previous work and joint studies.

The second example paper [2] can be considered as a case study of a branched needle microstructure, a specific complex martensitic microstructure of an MSM alloy. Such

microstructure can result in pseudoelastic and magnetoelastic behaviour of magnetic shape memory alloys. We investigated the branched needle microstructure in Ni-Mn-Ga in great detail, showing and explaining its large complexity with four types of twinning identified, including type I and II, modulation and compound a/b twins. The study provides important guidelines for understanding and designing complex microstructures in magnetic shape memory alloys. Contribution of FZU is corresponding proportionally to the fact that two abroad laboratories were involved.

A.2 Modulated structure in MSM alloys

The true character of the modulated structure of MSM materials has been a long-standing puzzling problem of the MSM field, a subject of many disputes, and consequently an attractive research topic. The investigation of extraordinary modulated structure of the MSM materials is the subject of several publications [3-6]. In [3], unique in-situ studies of martensite under tensile stress in a transmission electron microscope using in-house built holder developed in FZU (Prague) and following high resolution TEM (Helsinki) reveal the mechanism of the transition between a modulated and a non-modulated martensite of magnetic shape memory alloy. The discovered mechanism indicates that modulated martensite is in fact a nanotwinned structure, decisively contributing to the heated discussion about the nature of modulated phases in Ni-Mn-Ga. The experimental work done in Prague and Helsinki stemmed from a long-lasting cooperation between the institutions involved. Both teams in Prague and Helsinki (Aalto University) contributed equally.

Although the TEM studies were very successful, they cannot fully replace the bulk experiments, as there is always doubt about the effect of foil thickness. Thus, in [4], we used an advanced technique of reciprocal space mapping by XRD to study the modulation in Ni- Mn-Ga single crystal exhibiting magnetic shape memory effect. Apart from confirming the twin hierarchy and distribution, we showed that, by analysis of modulation satellites, the modulation can be considered equally a modulation or nanotwinning and it can be hardly discerned due to intrinsic physical limitation arising from the yet unknown disorder in the single crystals. Based on diffraction peak broadening and estimated coherence length, we assumed an existence of antiphase boundaries, which was later confirmed in [7] and [8]. The experimental work was done in cooperation with the Institute of Physics and Faculty of Mathematics and Physics of the Charles University. Both teams contributed equally. Systematic characterization made at the Institute was complemented by a high resolution X- ray study at the Charles University.

The actual existence of nanotwinning in a bulk MSM alloy, albeit only in a narrow temperature range near martensitic transformation, was later confirmed indirectly by XRD, by an analysis of the main peak splitting instead of a diffusive peak analysis, and directly by SEM [9]. Thus, for the first time, we presented the direct and indirect observations of twin refinement and nanotwinning near martensite transformation. The observations strongly support relevance of the nanotwinning concept and give important directions for further research of the crystal structure of Ni-Mn-Ga. The refinement of the particular twin structure is demonstrated in Fig. 1. The work was initiated, guided, and mostly performed by the authors of the team and contribution of the team authors constituted a large percentage. The first author guiding the work and the corresponding author is a member of the team.

Publication [6] deals with a so-called a/b-laminate, i.e. the laminate of {110} compound twins, which is very important as it is linking the modulated structure at an atomic scale and martensite microstructure at a microscale. The full twin hierarchy of modulated Ni-Mn-Ga martensite was predicted by us before, but confident experimental proof of its existence was missing. By systematic search we were able to demonstrate for the first

time how a-b laminate in a bulk material can be discerned using scanning electron microscopy. Not only did we reveal the full twinning hierarchy and size of the a-b laminate in the vicinity of large twins but we were also able to confirm the a-b laminate branching predicted in the theoretical model of twinning. The work was performed in our group using in house facilities.

Fig. 1. Observation of nanotwinned phase evolution close to martensite phase transformation in Ni- Mn-Ga magnetic shape memory alloy [9].

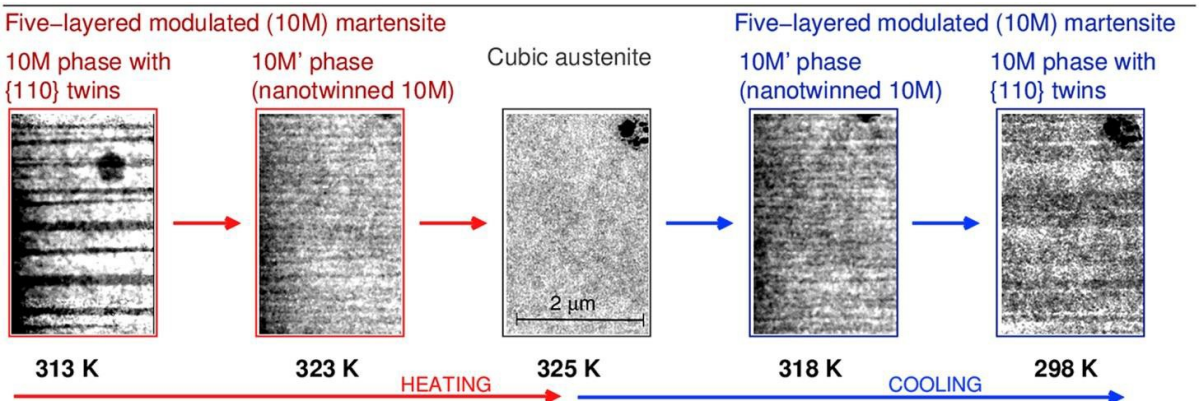

A.3 Properties engineering by doping

The material doping or alloying is one of the possible ways how the properties of MSM alloys can be modified. To give an example, the material can be doped in order to shift the transformation temperatures from low to environmental ones, which is beneficial both for research (simplification of observations with less need for cryocooling) as well as for practical applications. The topic is represented by publication [10], where we studied Ni-Mn-Ga-Co-Cu alloys, which are new exciting materials in the magnetic shape memory field as they exhibit giant magnetic field induced strain up to 12%. For the first time we characterized the effect of composition and temperature on the magnetic properties of Ni-Mn-Ga-Co-Cu. We studied magnetocrystalline anisotropy of single-crystalline Co- and Cu- doped non-modulated Ni-Mn- Ga-Co-Cu martensite $Ni_{50-x}Mn_{28-y}Ga_{22}Co_xCu_y$ with x and y ranging between 3 and 5 at.%. Samples were investigated in nearly single-variant microstructure. From magnetic hysteresis loops measured along hard axis anisotropy, constant K_1 was obtained as a function of dopant concentration and temperature. With increasing dopant concentration $|K_1|$ decreased. The decrease was influenced mostly by Co doping, whereas Cu doping played a minor role here.

The findings are important for exploitation and further research of the very novel material. Moreover, this study is only the second world report on the giant magnetic field induced strain in Ni-Mn-Ga-Co-Cu. The work was initiated, guided, and mostly performed by the authors of the team. The percentage contribution of the team authors is more than 80%. The first and corresponding author is a member of the team.

A.4 Novel functionalities of MSM alloys

The topic of the novel functionality of MSM alloys based on interaction of magnetic domains and magnetic martensite twin structure in a material with significant magnetic coercivity was brought to the group through the MSCA-IF fellowship of Ladislav Straka, current group member. Understanding of and control of the magnetic coercivity was the key issue of the project and a prerequisite of obtaining the novel functionality. Publications [11–13] are related to this topic. Antiphase boundaries (APBs) have been suspected as one of the reasons of the enlarged susceptibility in MSM alloys. In [11] we found a new method of visualization of antiphase boundaries (APBs) in magnetic

shape memory alloys as illustrated in Fig. 2. The conventional visualization method using TEM did not work due to large extinction coefficients of Mn and Ga. The important finding of the magnetic force microscopy-based alternative opened the possibility of research of APBs in magnetic shape memory alloys for us as well as for a broad research community. The work was initiated, guided, and mostly performed by the authors of the team. The percentage contribution of the team authors is more than 80%. The first and corresponding author is a member of the team.

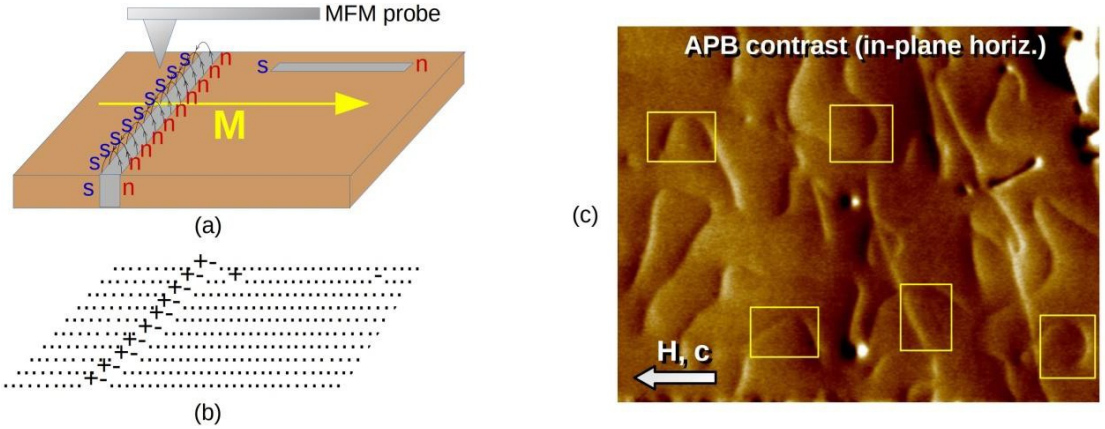

Fig. 2. Visualization of antiphase boundaries using magnetic force microscopy (MFM): a) Modeled expected contrast for perpendicular interfaces; b) Experimental observation shown in [11].

In publication [12], based on the observation described in [11] we used the novel method to reveal and understand how to control the magnetic coercivity. We confirmed that the APBs are the main reason behind the enlarged coercivity, and we were able to exclude the previous suggestion that B-doping was causing the effect. The finding is very important, as it opens a new avenue in the magnetic shape memory field – by controlling the magnetic coercivity a spectrum of interesting novel functionalities (such as mechanically induced demagnetization or remanent magnetization rotation) can be obtained, exploited, and further studied in magnetic shape memory alloys. The work was initiated, guided, and mostly performed by the authors of the team. The percentage contribution of the team authors was more than 90%. The first and corresponding author is a member of the team.

Publication [13] presents a complementary work to [11] and [12]. It uses the Lorentz TEM method to reveal APBs and especially the width of magnetic domain walls in all possible configurations (on APBs, away of APBs, in an austenite, etc.). The illustrative figure of an APB and magnetic domains is shown in Fig. 3. The results are important not only for the magnetic shape memory effect but also for theoretical considerations of domain wall behaviour in the presence of APBs and twins. The work was initiated by the team at FZU. The experimental part was performed at the Carnegie Mellon University by the first author (corresponding author) on his postdoctoral stay after finishing his thesis in the group. He is now a member of the team. M. De Graef guided the work at the Carnegie Mellon University.

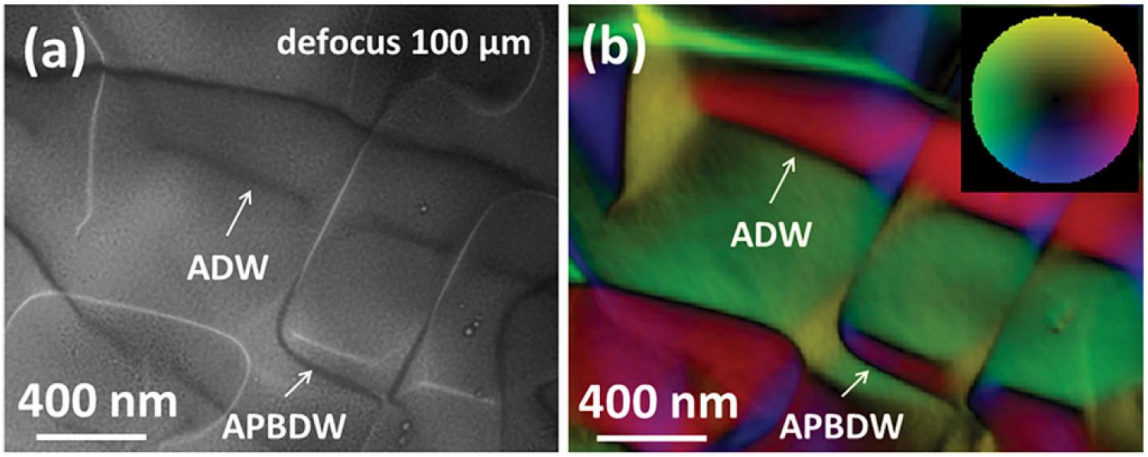

Fig. 3. Comparison of different types of magnetic domain walls in Ni-Mn-Ga austenite showing domain walls free from an APB [austenite domain wall (ADW)] and pinned on APBs (APBDW). (a) Under-focus Lorentz micrograph showing the position of magnetic domain walls with the corresponding magnetic induction color map (b). [13].

A.5. Novel topics for future

Publication [14] presents a new promising direction in MSM research, which is microscale and nanoscale functionality of MSM alloys. The microscale functionality of magnetic shape memory (MSM) materials is often suggested but has not been demonstrated as such. The work proves experimentally, for the first time, the ability of MSM alloys to function as magnetic actuators in microscale 3D microdevices. Novel Xe-ion beam micro-milling is used for the first time on an MSM alloy. The work forms an important bridge between basic research of MSM alloys and their exploitation in applied research and applications. The examples of the prepared shapes are shown in Fig. 4. Authors of the team (L.Straka, O.Heczko) initiated the research and provided scientific expertise for the work, and participated significantly in manuscript preparation and editing, as well as in tutoring visiting student. The contribution of the team authors is about one half. The first author, who was a visiting PhD student at the time when the publication was being written, joined the team as a postdoc in the end of 2018.

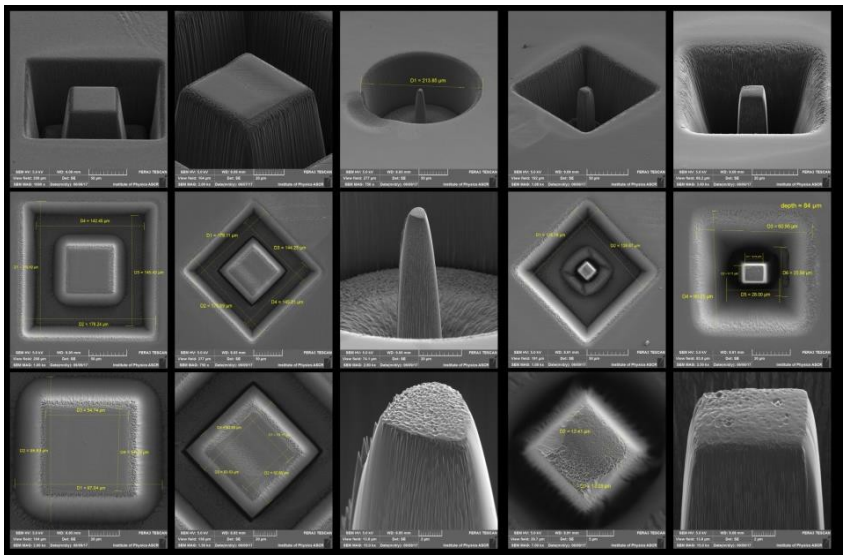

Fig. 4. An example set of different magnetic shape memory micropillars prepared using focused Xe-ion beam milling and observed through a scanning electron microscope.

B. Physics of lathanides and actinides compounds

In the frameworks of searching for new or poorly studied highly anisotropic intermetallic compounds, a group $R_3Ru_4Al_{12}$ (R = rare-earth metal or uranium) was found to be very interesting from the viewpoint of magnetism as described in publications [15, 16]. The R atoms form a distorted kagome net in this hexagonal structure resulting in geometrical frustration in the R sublattice. This leads to very complicated magnetic properties characterised by spontaneous and field-induced transitions. High anisotropy requires single- crystalline samples and high magnetic field. Single crystals of several $R_3Ru_4Al_{12}$ (R = Pr, Nd, Tb, Dy, Ho) were prepared for the first time, their magnetism and magnetoacoustics were studied in fields up to 60 T. Ultrasound technique is an extremely sensitive probe of magnetoelastic interactions. Its extreme sensitivity to structural and magnetic changes makes it a proper tool to investigate spin-lattice effects. This is especially important near phase transitions. Using magnetoacoustics, phase diagrams were prepared and both equilibrium and non-equilibrium phenomena were studied. In 2015–2019, 10 papers (including 5 in Physical Review) were published (currently having 98 citations). All work wasdone in a broad international (High field laboratory Helmholtz-Zentrum Dresden- Rossendorf, Germany and University of Hiroshima, Japan) and domestic cooperation with the Faculty of Mathematics and Physics, Charles University.

Various combinations of magnetic materials based on 3d-4f elements in bulk are important for electronics and information storage, while 5f thin films are the key to surface science of actinides at present but can also become, due to the very strong spin-orbit interaction, promising in various applications. The research activity has two parts. The first deals with the studies of magnetic properties of 3d-4f intermetallics under extreme conditions such as high and ultra-high magnetic fields, low temperatures, high pressures. It focuses on the studies of structure and magnetic properties of rare earth (R) intermetallics, both parent and modified by hydrogenation [17]. The second part of research concerns uranium-based thin films, for instance, uranium hydrides and determination of the conditions favourable for formation of recently discovered UH_2 on the account of conventional UH_3 films (5]. Studies of effects of disorder on conducting properties of the films and recent attempts to employ uranium-based magnetism in the modern technologies such as exchange bias have been proven promising.

C. Superconductive materials

he superconducting materials stand in the front of present theoretical and application physics as a theoretical challenge combined with their quite straightforward practical applicability. While the applicability of high-T_c superconductors was evident just since the moment of their discovery, their real introduction to market was hindered by many problems. As electromagnetic properties are in each case a prior qualification factor, we were quite often asked to participate in international teams for our main expertise, magnetism, e.g. [18– 23].

Superconducting cuprate tapes of the second generation possess much higher critical currents and irreversibility fields than classical metallic superconductors and any other nowadays known materials. The main research topic has been the response of high-T_c superconducting tapes intended for magnet coils wiring in future thermonuclear fusion reactors to neutron irradiation. A set of 22 tapes from 4 main world suppliers was tested inductively (vibrating sample magnetometry, VSM) in an intact state. The survey of the results was published in [24]. This publication was selected as one of the highlights of Superconductor Science and Technology in 2017. The subject is rather complex and requires several further neutron irradiation steps. As each such step is

quite time consuming due to the need of the samples' radiation decay, this subject is a theme for a few years. It was found that all the tapes satisfy the basic requirement for use in practice, carrying critical current higher than 50 A at 77 K and in zero magnetic field (self-field). The data obtained after a series of neutron irradiations supplied an optimistic evidence that the best tapes are able to carry a sufficient critical current up to 15 T, provided they are cooled to temperatures below 30 K. Importantly, the temperature range 5–30 K is nowadays accessible by cryogen- free refrigerator cooling, which offers a more economical operation than cooling of classical superconductors into their superconducting state by liquid helium.
Our expertise in magnetic levitation, low temperature physics, and vacuum has also been utilized in the joint project of the Institute of Thermomechanics and the Institute of Physics for study of loss-less bearings for use in flywheel energy storages.
The other part of the research is focused on a study of phenomena related to nonlinear response of superconductors and magnetic materials, particularly at phase transitions. Experiments are carried out in both DC and AC weak magnetic field using a unique custom- made continuous reading SQUID magnetometer [25]. Recently we have experimentally proved validity of the models to the critical state in type II superconductor thin films. These models are particularly important in connection with coated HTS conductors, novel products of a wide application potential. Using these models, critical depinning current density, one of the crucial parameters, and its temperature dependence can be estimated in a contactless way. These theoretical and experimental results open new opportunities in physics and application of nonlinear phenomena.

D. Mössbauer spectroscopy

The laboratory of Mössbauer spectroscopy is important part of Joint Laboratory of Low Temperature Physics. In the evaluated period, the most significant results were achieved in the field of perovskite multiferroics (Pb/Ba(Fe1/2Nb1/2)O3, Pb(Fe1/2Sb1/2)O3), iron oxide nanomagnets ((*X*,Fe)2O3, (*X*,Fe)3O4) interacting with biological systems, Heusler alloys (Fe/Mn/Ga etc.), properties of stainless steels for nuclear applications, amorphous and nanocrystalline metallic glasses, iron accumulation in biological tissues (liver and brain), and hexaferrites (BaFe12O19 doped by Ti/Zn, LaFe12O19).
Multiferroics exhibit simultaneously several types of spontaneous ordering, which can be utilized in spintronics, memory elements, as sensors or detectors. The understanding of the microscopic mechanism of cross-coupling effects and their tailoring by modifications at atomic scale was enhanced by thorough studies of hyperfine interactions. The results from Mössbauer spectroscopy provide detailed information about structural and magnetic transitions, local arrangement of atoms in Fe surroundings and the type of magnetic order [26,27]. The magnetic order is well visible by MS as demonstrated in Fig. 5. In near future, we would like to exploit multiferroic properties of skyrmion and magnetic shape memory materials.

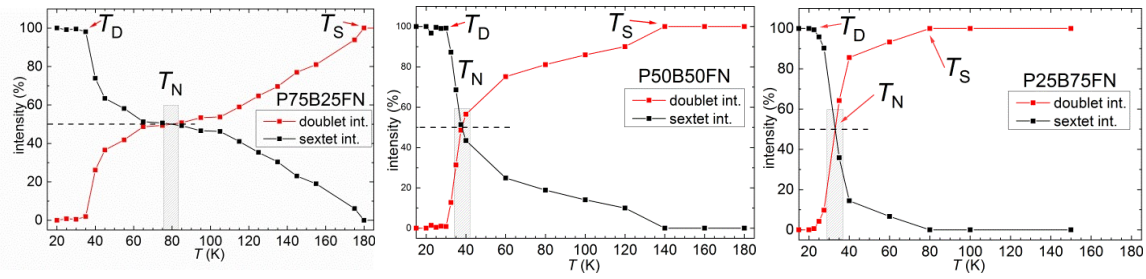

Fig. 5. Transition from antiferromagnetic to paramagnetic state – temperature dependence of the intensities of sextet (black) and doublet (red) in Mössbauer spectra of the samples $Pb_{1-x}Ba_x(Fe_{0.5}Nb_{0.5})O_3$, x=0.25 (left), 0.5 (middle), 0.75 (right).

Harsh conditions such as intense radiation, high temperature, and presence of corrosion agents jeopardize normal function of construction materials operating in nuclear facilities. Consequently, there is a serious technological, economic, and environmental demand for advanced metallic glasses and nanocrystalline alloys for particle accelerators and for construction steels for nuclear reactors with long-term reliability. Thorough study of novel materials by means of hyperfine interactions is under go to elucidate the relationship between structural arrangement and magnetic state, and structural transformations (amorphous to nanocrystalline) and modifications imposed by thermal treatment and irradiation by ions and neutrons [28, 29].
Beyond technological applications, the Mössbauer group aims at development and applications of magnetic nanoparticles in biomedical and biophysical research (synergic water splitting, environmental catalysis). Our contribution to the field of contrast-increase agents for magnetic resonance imaging is well documented in recent publications [30]. Biogenic formation and degradation of iron-based minerals is also investigated as a possible explanation of the occurrence of some compounds in nature, or as a sustainable way to produce high amounts of material for environmental use.

E. Magnetic domains observation and magnetic inspection

Mechanical stress affects magnetic properties of ferromagnetic materials. We have finished investigation and modelling of bulk magnetic hysteresis loops of differently oriented Fe-3%Si Goss-textured steels exposed to compressive and tensile stress [31-33] with high accuracy using an effective field concept. The observation of magnetic domains (Fig. 6) in such stressed steel helped us to understand the nature of that effective field [34].
After that, we studied hysteresis loops of non-oriented Fe-3%Si steel under tensile and compressive elastic stresses [35], where the magnetic domains are very complex and are hardly possible to observe. Hysteresis loops on such steel also followed an effective field concept. The complex hysteresis loop behaviour under tension and compression was explained. These results are interesting not only from the physical point of view but also for use in non-destructive testing of ferromagnetic materials under stress.

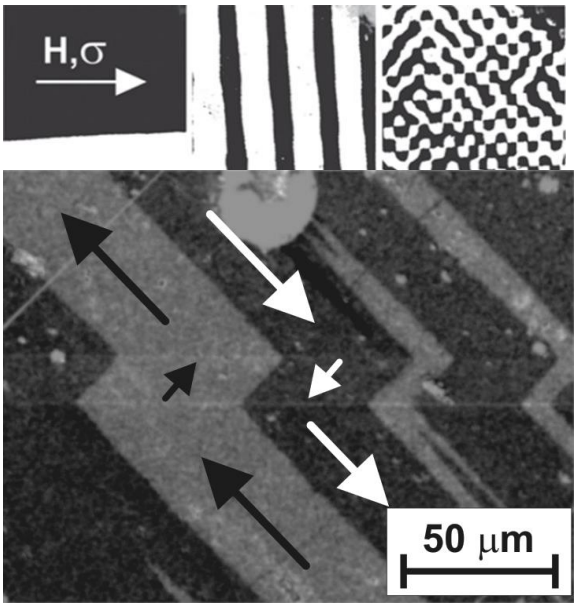

Fig. 6. Magnetic domains in a demagnetized state for compressed Goss-textured (110) [001] Fe-3%Si steel.

Fig. 7. A detailed view of magnetic domains of the twin microstructure with only three twins separated by two twin boundaries (weak horizontal lines) in a demagnetized state. The magnetization direction is indicated by arrows.

During manufacturing and processing of steels the material surface is often modified – plastically deformed by machining [36], nitrided layer [37] or decarburized [34]. We applied different magnetic surface-sensitive techniques: Barkhausen noise, Eddy currents, and incremental permeability. All methods were sensitive to changes of magnetic properties of the surface layer, but the the one revealed as the most promising was the incremental permeability, in which sensitivity to the thickness of the detected layer can be easily changed from less than 1 μm to 1 mm by varying the magnetizing frequency.
The study of the Barkhausen noise (BN) and magnetoacoustic emission (MAE) on steels is interesting not only from the physical point of view but also for use in non-destructive testing. For these purposes, it was necessary to develop reliable measuring techniques to obtain repeatable results on magnetically open samples. Then we could study the dependence of BN and MAE on the magnetizing frequency and the magnetic field waveform properly and developed the correct signal normalization procedure as the result [38–40].
Using the knowledge of observation domains in stress, we focused on the study of domains in magnetic shape memory Ni-Mn-Ga single crystals. The magnetic domains in magnetic shape memory Ni-Mn-Ga alloy were observed for the first time by magneto-optical Kerr microscopy using monochrome blue LED light and active sample position stabilization [41]. High-contrast images were obtained (Fig. 7).

F. Magnetic nanoparticles

Although the research of magnetic nanoparticles was discontinued in our Team in 2017 as the group leader Jana Vejpravova moved to Charles University with an ERC grant, we also include one result from her group in this survey [42]. The work was done in a broad international and domestic cooperation concerning both the particle preparation and measuring methods used. The obtained data were in conflict with the established knowledge, consequently, careful reasoning and detailed experiment was demanded for successful publication.

G. Joint Laboratories

Researchers in MGML work mainly on topics of condensed matter physics, materials R&D, and they develop and enhance new techniques and instruments in order to extend experimental conditions and methods and sample environment following the modern trends in materials R&D. These laboratories are described in detail later.

References

Results selected for evaluation are in bold

[1] R. Niemann, A. Backen, S. Kauffmann-Weiss, C. Behler, U.K. Rossler, H. Seiner, O. Heczko, K. Nielsch, L. Schultz, S. Fahler. Nucleation and growth of hierarchical martensite in epitaxial shape memory films. Acta Materialia, vol. 132, pp. 327-334, 2017.
[2] R. Chulist, L. Straka, A. Sozinov, T. Tokarski, W. Skrotzki. Branched needle microstructure in Ni-Mn-Ga 10M martensite: EBSD study. Acta Materialia, vol. 128, pp. 113-119, 2016.
[3] Y. Ge, N. Zarubova, O. Heczko, S-P. Hannula. Stress-induced transition from modulated 14M to non-modulated martensite in Ni-Mn-Ga alloy. Acta Materialia, vol. 90, pp. 151-160, 2016.
[4] O. Heczko, P. Cejpek, J. Drahokoupil, V. Holy. Structure and microstructure of Ni-Mn-Ga single crystal exhibiting magnetic shape memory effect analysed by high resolution X-ray diffraction. Acta Materialia, vol. 115, pp. 250-258, 2016.
[5] V.B. Chzhan, I.S. Tereshina, A.Y. Karpenkov, E.A. Tereshina-Chitrova. Persistent values of magnetocaloric effect in the multicomponent Laves phase compounds with varied composition.

Acta Materialia, vol. 154, pp. 303-310, 2018.
[6] O. Heczko, L. Klimša, J. Kopeček. Direct observation of a-b twin laminate in monoclinic five-layered martensite of Ni-Mn-Ga magnetic shape memory single crystal. Scripta Materialia,vol. 131, pp. 76-79, 2017.
[7] O. Heczko, H. Seiner, P. Stoklasova, P. Sedlak, J. Sermeus, Ch. Glorieux, A. Backen, S. Fahler, M. Landa. Temperature dependence of elastic properties in austenite and martensite of Ni-Mn-Ga epitaxial films. Acta Materialia, vol. 145, pp. 298-305, 2018.
[8] G. Vértesy, I. Tomáš. Nondestructive magnetic inspection of spot welding. NDT & E International, vol. 98, pp. 95-100, 2018.
[9] L. Straka, J. Drahokoupil, P. Veřtát, J. Kopeček, M. Zelený, H. Seiner, O. Heczko. Orthorhombic intermediate phase originating from {110} nanotwinning in Ni50Mn28.7Ga21.3 modulated martensite. Acta Materialia, vol. 132, pp. 335-344, 2017.
[10] M. Rameš, O. Heczko, A. Sozinov, K. Ullakko, L. Straka. Magnetic properties of Ni-Mn-Ga-Co-Cu tetragonal martensites exhibiting magnetic shape memory effect. Scripta Materialia, vol. 142, pp. 61-65, 2015.
[11] L. Straka, L. Fekete, O. Heczko. Antiphase boundaries in bulk Ni-Mn-Ga Heusler alloy observed by magnetic force microscopy. Applied Physics Letters, vol. 113(17), p. 172901, 2015.
[12] L. Straka, L. Fekete, M. Rameš, E. Belas, O. Heczko. Magnetic coercivity control by heat treatment in Heusler Ni-Mn-Ga(-B) single crystals. Acta Materialia, vol. 169, pp. 109-121, 2019.
[13] M. Vronka, O. Heczko, M. De Graef. Influence of antiphase and ferroelastic domain boundaries on ferromagnetic domain wall width in multiferroic Ni-Mn-Ga compound. Applied Physics Letters, vol. 115(3), p. 032401, 2019.
[14] D. Musiienko, L. Straka, L. Klimša, A. Saren, A. Sozinov, O. Heczko, K. Ullakko. Giant magnetic-field-induced strain in Ni-Mn-Ga micropillars. Scripta Materialia, vol.150, pp. 173-176, 2018.
[15] K. Prokeš, D.I. Gorbunov, M. Reehuis, B. Klemke, A. Gukasov, K. Uhlířová, X. Fabrèges, Y. Skourski, F. Yokaichiya, S. Hartwig, A.V. Andreev. Anisotropic physical properties of single-crystal U2Rh2Sn in high magnetic fields. Phys. Rev. B, vol. 95, p. 174433, 2017.
[16] D.I. Gorbunov, C. Strohm, M.S. Henriques, P. van der Linden, B. Pedersen, N.V. Mushnikov, E.V. Rosenfeld, V. Petříček, O. Mathon, J. Wosnitza, A.V. Andreev. Microscopic nature of the irst-order field-induced phase transition in the strongly anisotropic ferrimagnet HoFe5Al7. Phys. Rev. Lett., vol. 122, p. 127205, 2019.
[17] N.V. Kostyuchenko, A.K. Zvezdin, E.A. Tereshina, Y. Skourski, M. Doerr, H. Drulis, I.A. Pelevin, I.S. Tereshina. High-field magnetic behavior and forced-ferromagnetic state in an ErFe11TiH single crystal. Phys. Rev. B, vol. 92, p. 10423, 2015.
[18] M. Rameš, V. Železný, I. Gregora, T. Wolf, M. Jirsa. Interaction of phonons with intraband electronic excitations and crystal field transitions in Raman spectra of (Nd,Eu,Gd)Ba2Cu3Oy crystals. Mat. Sci. Eng. B, vol. 197, pp. 10-17, 2015.
[19] M. Muralidhar, T. Hanai, K. Furutani, P. Diko, M. Jirsa, M. Murakami. Processing and Characterization of Bulk FeSe. J. Electr. Eng., vol. 4, pp. 109-115, 2016
[20] M. Jirsa, M. Rameš, M.R. Koblischka, A. Koblischka-Veneva, K. Berger, B. Douine. Relaxation and pinning in spark-plasma sintered MgB2 superconductor. Supercond. Sci. Tech., vol. 29, p. 025006, 2016.
[21] S. Pavan Kumar Naik, M. Muralidhar, M. Jirsa, M. Murakami. Growth and physical properties of top-seeded infiltration growth processed large grain (Gd, Dy)BCO bulk superconductors. J. Appl. Phys., vol. 122, p. 193902, 2017.
[22] M. Jirsa, M. Rameš, I. Ďuran, L. Viererbl. Effect of Neutron Irradiation on Critical Currents of REBaCuO Superconducting Tapes Considered for Magnets in Fusion Reactors. IEEE Trans. Appl. Supercond., vol. 28, p. 6601505, 2018.
[23] M. Jirsa, M. Rameš, I. Ďuran, T. Entler, L. Viererbl. Critical currents in REBaCuO superconducting tapes in response to neutron irradiation. Supercond. Sci. Tech., vol. 32, p. 0550007, 2019.
[24] M. Jirsa, M. Rameš, I. Ďuran, T. Melíšek, P. Kováč, L. Viererbl. Electric Currents in REBaCuO Superconducting Tapes. Supercond. Sci. Technol., vol. 30, p. 045010, 2017.
[25] Z. Janů, F. Soukup, Reduction in energy dissipation rate with increased effective applied field. Supercond. Sci. Technol., vol. 28, p. 085016, 2015.
[26] B. Argymbek, T. Kmječ, V. Chlan, J. Kohout, S.E. Kichanov, D.P. Kozlenko, B.N. Savenko. The crystal and magnetic structures of the ordered perovskite Pb_2FeSbO_6 studied by neutron diffraction and Mössbauer spectroscopy. J. Magn. Magn. Mater., vol. 477, pp. 334-339, 2019.
[27] T. Kmječ, M. Adamec, D. Kubániová, J. Plocek, M. Dopita, M. Cesnek, V. Chlan, J. Bednarčík, K. Závěta, M. Maryško, J. Kohout. ^{57}Fe-enriched perovskites $M(Fe_{0.5}Nb_{0.5})O_3$ (M – Pb, Ba) studied by Mössbauer spectroscopy, NMR and XRD in the wide temperature range 4.2–533 K. J. Magn. Magn. Mater., vol. 475, pp. 334-344, 2019.

[28] A. Lančok, T. Kmječ, M. Štefánik, P. Bezdička, M. Klementová, M. Miglierini. Mössbauer spectrometry of LC 200N steel. AIP Conf. Proc., vol. 1781, p. 020017, 2016.
[29] A. Lančok, T. Kmječ, M. Štefánik, Ľ. Sklenka, M. Miglierini. Structural characterization of highly corrosion-resistant steel. Croat. Chem. Acta, vol. 88(4), pp. 355-361, 2015.
[30] O. Kaman, J. Kuličková, M. Maryško, P. Veverka, V. Herynek, R. Havelek, K. Královec, D. Kubániová, J. Kohout, P. Dvořák, Z. Jirák. Mn-Zn ferrite nanoparticles with silica and titania coatings: Synthesis, transverse relaxivity, and cytotoxicity. IEEE Trans. Magn., vol. 53, p.5300908, 2017.
[31] O. Perevertov, R. Schafer. Influence of applied tensile stress on the hysteresis curve and magnetic domain structure of grain-oriented Fe–3%Si steel. J. Phys. D-Appl. Phys., vol. 47, p.185001, 2014.
[32] O. Perevertov, J. Thielsch, R. Schaefer. Effect of applied tensile stress on the hysteresis curve and magnetic domain structure of grain-oriented transverse Fe-3%Si steel. J. Magn. Magn. Mater., vol. 385, pp. 358-367, 2015.
[33] O. Perevertov, R. Schäfer. Magnetic properties and magnetic domain structure of grain-oriented Fe-3%Si steel under compression. Mater. Res. Express, vol. 3, p. 096103, 2016.
[34] O. Perevertov, M. Neslušan, A. Stupakov. Detection of milled 100Cr6 steel surface by eddy current and incremental permeance methods, NDT & E International, vol. 87, pp. 15-23, 2017.
[35] O. Perevertov. Influence of the applied elastic tensile and compressive stress on the hysteresis curves of Fe-3%Si non-oriented steel. J. Magn. Magn. Mater., vol. 428, pp. 223-228, 2017.
[36] O. Heczko, O. Perevertov, D. Král, M. Veis, I.V. Soldatov, R. Schäfer. Using Kerr Microscopy for Direct Observation of Magnetic Domains in Ni–Mn–Ga Magnetic Shape Memory Alloy. IEEE Trans. Magn., vol. 53, p. 2502605, 2017.
[37] A. Stupakov, M. Neslušan, O. Perevertov. Detection of a milling-induced surface damage by the magnetic Barkhausen noise. J. Magn. Magn. Mater., vol. 410, pp. 198-209, 2016.
[38] A. Stupakov, R. Farda, M. Neslušan, A. Perevertov, T. Uchimoto. Evaluation of a Nitrided Case Depth by the Magnetic Barkhausen Noise. J. Nondestruct. Eval., vol. 36, p. 73, 2017.
[39] A. Stupakov, O. Perevertov. Dynamic properties of micro-magnetic noise in soft ferromagnetic materials. J. Magn. Magn. Mater., vol. 456, pp. 390-399, 2018.
[40] O. Perevertov, A. Stupakov. Magnetoacoustic measurements on steel samples at low magnetizing frequencies. J. Electr. Eng., vol. 66(7), pp. 58-61, 2015.
[41] O. Perevertov, O. Heczko, R. Schäfer. Direct observation of magnetic domains by Kerr microscopy in a Ni-Mn-Ga magnetic shape-memory alloy. Phys. Rev. B, vol. 95, p. 144431, 2017.
[42] B. Pacáková, S. Kubíčková, G. Salas, A. Mantlíková, M. Marciello, M.P. Morales, D. Nižňanský, J. Vejpravová. The internal structure of magnetic nanoparticles determines the magnetic response. Nanoscale, vol. 9(16), pp. 5129-5140, 2017.

Research activity and characterisation of the main scientific results

We have at our disposal theoretical methods and computer codes based on the density functional theory of the electronic structure, which are aimed at a comprehensive study of materials properties. We use several complementary approaches, namely the TB-LMTO- CPA method suitable for systems with atomistic disorder (alloys, solids with impurities) and full-potential methods as implemented in our in-house LAPW code as well as in codes developed elsewhere (WIEN2k, VASP). When the electron-electron correlations are significant, the density-functional calculations are complemented with Hubbard models that are solved either in the static mean-field approximation (LDA+U method) or in the framework of the dynamical mean-field theory (LDA+DMFT method).

Using these methods we are able to determine the lattice geometry, formation energies of lattice defects, relative stability of various crystallographic and magnetic phases, or the magnetic anisotropy. The computed electronic structure can be used to parametrize low- energy models, for instance, we can calculate the exchange integrals entering the Heisenberg model. The low-energy models are then used to determine the magnon spectra or transition temperatures between magnetic or more exotic phases. Furthermore, we investigate transport properties such as the conductivity tensor, magnetoresistance, Hall conductivity and anomalous Hall conductivity, or Gilbert damping.

Transport in metals and semiconductors, materials for spintronics

V. Drchal, J. Kudrnovský, F. Máca, A. Shick

The FeRh alloy was suggested as a room-temperature **antiferromagnetic resistor**. The prominent feature of this alloy is a large decrease of the resistivity accompanying the antiferromagnetic (AFM) to ferromagnetic (FM) phase transition. We have explained the resistivity drop quantitatively by first-principles methods as due to the **strong spin disorder** present between Fe-sublattices in the AFM phase, which is not present in the FM phase. The spin disorder is induced by the finite temperature [1].

We have investigated the influence of native defects on magnetic and transport properties of the **topological insulator Bi_2Te_3 doped with Mn**. We demonstrated for the first time that the geometry relaxations and also Mn atoms located in the interstitial positions play an important role, and that additional defects, for instance antisite impurities (Bi_{Te} donors and Te_{Bi} acceptors) must also be present in order to explain the experimental observations of resistivity and Curie temperature [2].

The tetragonal CuMnAs alloy is a promising material for antiferromagnetic spintronics. Resistivity measurements indicate the presence of defects, the origin and concentrations of which are unknown. Using computational tools we found that vacancies on Mn or Cu sites, and Mn_{Cu} and Cu_{Mn} antisites are **the most probable defects in CuMnAs**. Our theoretically estimated Néel temperatures and also resistivities for such samples agree well with experimental results, indicating our good understanding of the material [3].

Mn-doped GaAs is a prototype of diluted ferromagnetic semiconductors. Although it was intensively studied both experimentally and theoretically in the past, several

problems remained that had not been explained. We theoretically investigated the properties connected with exchange interactions (Curie temperature and spin stiffness) and with spin- orbit coupling (**anomalous Hall effect**, anisotropic magnetoresistance, and **Gilbert damping**). We employed the first-principles Lichtenstein's mapping to construct an effective Heisenberg Hamiltonian and to estimate the Curie temperature and spin stiffness in the real- space random-phase approximation. We obtained a good agreement of calculated quantities with experiments on well-annealed samples containing a small amount of compensating defects [4].

Development of the magnetic materials for **applications in magnetic tunnel junctions** used in magnetic random access memory (MRAM) devices is a key ingredient for success in the emerging non-volatile memory technologies. In collaboration with theorists from TU Wien, we performed electronic structure calculations to estimate the **magnetic anisotropy** energy and the **tunnelling anisotropic magnetoresistance** effect in two candidate materials – Mn_3Ge and Mn_3Ga ferrimagnets. We found the tunnelling anisotropic magnetoresistance to be sizable and we discussed the prospects of these compounds for applications in magnetic tunnel junctions [5].

The electronic and thermal resistivities of the **Earth's core** are crucial ingredients for understanding the Earth's magnetic field. We report the first ab initio calculation of the resistivity caused by random magnetic moments present in the Earth's core at high temperatures. The magnitude of this **spin-disorder resistivity** is comparable to contributions from impurity disorder and electron-phonon scattering. Our results can serve as an **input for modelling in geophysics**, in particular for geodynamo and magnetic field reversals [6].

Strongly correlated electrons – new concepts

I. Janiš, J. Kuneš

Strong electron correlations in transition metals and heavy-fermion materials lead to unexpected and unusual phenomena that cannot be explained by simple arguments and standard (typically mean-field) techniques. Nowadays, large-scale numerical simulations are used to obtain quantitative agreement with experimental data, but they typically offer only a limited microscopic understanding of the origin of the macroscopically observed behaviour. The applicability of the standard perturbation theory based on dynamical corrections to the quasiparticle parameters of Fermi liquid is restricted to weak and intermediate coupling. In the **strong-coupling regime**, one has to introduce a **dynamical renormalization** of the interaction strength and to use the diagrammatic perturbation theory for the response and vertex functions.

We developed a renormalization scheme of the interaction strength by using two-particle Green's functions and multiple scatterings of electrons on electrons and on holes, appropriately balanced to allow only for real quantum critical behaviour and to suppress spurious phase transitions appearing in the weak-coupling approaches. We used the non- perturbative parquet construction of the **two-particle self-consistency** needed for the dynamical renormalization of the interaction strength. We reduced the original set of the parquet equations to a **mean-field-like approximation for the**

screened interaction. The major challenge of this two-particle approach is how to reconcile the two exact relations between the one-particle self-energy and the two-particle vertex. We demonstrated that the two relations cannot be satisfied in any approximate scheme and suggested that the only way **to avoid spurious critical points is to introduce two self-energies**, thermodynamic and spectral [7]. The thermodynamic self-energy is used in the diagrammatic expansion and determines the thermodynamic properties, the spectral self-energy determines the spectral properties. Both self-energies share the same critical behaviour. This construction was used in the strong-coupling regime of the single-impurity Anderson model where it qualitatively correctly reproduced the exact Kondo behaviour [7,8]. We succeeded in fully formalizing this approach and explained that the two self-energies are anomalous and normal parts of a single physical self-energy. The anomalous part is related to the vertex via the Ward identity and the normal part via the Schwinger–Dyson equation. We also detailed the approximations needed to reduce the full set of the parquet equations to obtain the renormalized interaction strength in **quantum criticality** [9].

Spontaneous symmetry breaking leading to states of matter with long-range order is one of the central topics in condensed matter physics. Common types of order, such as ferromagnetic and antiferromagnetic, are characterized by spin or charge densities modulated at the inter-atomic scale, therefore well studied thanks to various scattering experiments. Order parameters that are not of this type are much more difficult to detect, giving rise to names such as hidden order or electronic nematicity. We investigated **excitonic condensation** in systems with strongly correlated electrons as a new mechanism leading to unconventional ordered states. The investigation followed two threads: an analysis of the two-band Hubbard model as a minimal model of the **excitonic magnet**, and a search for possible manifestations of this concept in various materials.

We have mapped out the phase diagram of the two-band Hubbard model as a function of bandwidth asymmetry, crystal field, doping and temperature. We have characterized distinct excitonic phases (polar condensate and ferromagnetic condensate) and studied their response to an external magnetic field [10]. These studies were facilitated by the development of impurity solvers that enabled calculations for low-symmetry Anderson impurity models. We have described a new physical mechanism of interaction between excitonic condensate and free charge carriers, the generalized double-exchange interaction.

Most recently, we have developed computer codes to calculate dynamical **susceptibilities within the DMFT framework**. To achieve this, we came up with an efficient representation of the two-particle propagators and vertices in the **tensor product form**. We used these tools to study Goldstone and Higgs modes in excitonic condensates [11]. This was the first study to demonstrate that **DMFT fulfils the Goldstone theorem**. We also demonstrated the relationship between the collective modes and approximate symmetries.

Most interestingly, we have found a crossover between Higgs-like amplitude mode and gapped Goldstone mode, which is controlled by the relative strength of the Weiss field compared to the explicit symmetry-breaking term in the Hamiltonian.

To find examples of **material realization of excitonic magnetism** we have focused on the d^6 system in certain cobaltites. We have shown that excitonic condensate with

a complex 18-component order parameter is obtained as the **mean-field ground state of $LaCoO_3$** for realistic interaction parameters [12]. We have performed several studies that addressed the question of competing orders and ways to eliminate them. Another family of materials we studied was 5d double-perovskites. We have predicted the $J = 0$ ground state of Sr_2YIrO_6 and excluded the possibility of tentative excitonic magnetism in this compound [13].

Magnetism at the nanoscale

J. Kolorenč, A. Shick

Motivated by technological advances achieved in the fabrication of nanoscale devices with properties tightly controlled down to single atoms (using lithography and scanning-probe techniques), we studied the magnetic behaviour of various nanoscale objects, which is often substantially influenced by strong correlations among electrons. Single magnetic atoms or their small clusters adsorbed on non-magnetic surfaces enable fundamental insights into the origin of magnetic properties and are candidates for high-density/high-capacity information processing and information storage. We used exact diagonalization of the Anderson impurity model with parameters extracted from the density- functional theory to analyse the electronic structure and magnetic properties of adatoms (transition metals or rare-earth metals) on various surfaces. In collaboration with the group of
A. Lichtenstein (University of Hamburg), analogous problems were investigated with the aid of the quantum Monte Carlo method.
In particular, we were involved in the theoretical interpretation of scanning tunnelling microscopy (STM) experiments on an iron atom adsorbed on the platinum surface, which were performed at the University of Hamburg. This adatom setting corresponds to a **magnetic moment in the presence of strong charge fluctuations**. The observed behaviour was linked with the concept of the so-called **Hund's impurity**, a system where electron correlations are driven mainly by the intra-atomic Hund's-rule exchange instead of the Hubbard repulsion. The idea that the Hund's exchange can be more important than the Hubbard repulsion was introduced in the context of iron-based high-temperature superconductors and the investigated adatom system could be viewed as a realization of the basic constituent of these bulk materials [14]. In a somewhat different context of rare-earth and actinide compounds, we proposed a **generalization of the Hund's metal to a Racah metal**, where the conduction bands, formed out of partially localized electronic states, retain remnants of the multiplet structure of fully localized atomic shells [15].
We took part in a detailed study of the magnetic properties of Fe and Co adatoms placed on $Cu_2N/Cu(100)$ surface. In this setup, the magnetic adatoms are decoupled from the scattering by conduction electrons in copper by a monolayer of insulating nitride to increase the lifetime of the magnetic states. The investigation combined x-ray magnetic circular dichroism (XMCD) measurements with our density functional theory calculations. The obtained results were critically compared to the properties previously deduced from inelastic tunnelling spectra, acquired with scanning-probe methods. Both XMCD measurements and DFT calculations indicate a relatively **large orbital contribution** to the total magnetic moment of the adatoms, **contrary to the**

often assumed spin-only magnetism [16].
Besides the transition-metal adatoms, we also studied rare-earth adatoms where the orbital magnetism plays a yet more important and often even dominant role. Using non- magnetic Sm atoms and magnetic Nd atoms adsorbed on graphene as test cases, we explored the **limits of applicability of the static mean-field** approximation (LDA+U) by comparison with a more accurate method of solving the Anderson impurity model corresponding to the 4f shells of the adatoms [17]. It turned out to be crucially important that the (approximate) solution correctly captures the **multi-reference character** of the adatom ground state, a feature that the LDA+U method does not possess.
Finally, we addressed a controversy about the magnetic state of a holmium adatom placed on a platinum surface that arose from conflicting results of several independent experiments. Using first-principles theoretical modelling we showed that measurements performed with and without an external magnetic field can indeed yield different conclusions about the size of the magnetic moment of the holmium adatom [18]. In that study, we discussed the importance of the **intra-atomic 5d–4f exchange polarization**, which we elaborated in our later works concerning rare-earth adatoms, for instance dysprosium on an iridium surface [19].

Transport in nanosystems

V. Janiš, A. Kalvová

Quantum dots attached to metallic or **superconducting leads** have a potential for applications in quantum computing or superconducting electronics. They have been attracting the attention of both experimentalists and theorists for decades. A prominent feature of the dots with superconducting leads is a quantum phase transition from the spin singlet to a spin doublet, accompanied by an abrupt change of the Josephson current. As the Josephson current is driven by a phase difference instead of a voltage bias, equilibrium methods can be employed to study this phase transition. It turns out that the static mean-field description is unable to describe this transition – it fails even in the weak coupling. We have been working in a collaboration with the group of T. Novotný (Faculty of Mathematics and Physics, Charles University) on a **systematic inclusion of dynamical corrections** via many-body perturbation expansion that would eliminate the deficiency of the mean-field description. Already the second-order corrections significantly improved quantitative agreement with the exact numerical solution [20,21]. This second-order approximation can be used for fast scans of the parameter space to localize the quantum phase transition **without the need of computationally expensive methods**. The model was later generalized for the presence of a third, non-superconductive lead that smears out the sharp phase transition and gives rise to new phenomena such as the Kondo effect. We used a numerically exact quantum Monte Carlo method to study transport in these setups to obtain the current-phase characteristics in the crossover region between the singlet and doublet ground states at finite temperatures [22].
Our research on time-dependent electron transport was performed on an analogous nanostructure, a **molecular bridge** placed between two massive metallic leads. The bridge was represented by an Anderson impurity, the leads were ferromagnetic, specifically, made of nickel. The electronic structure of the leads translated into a

complex spectral form of the tunnelling functions. The non-equilibrium processes we studied were **transient spin- resolved currents** induced by a sudden change of the strength of the tunnelling junctions under an external bias as the control parameter. Three separate but interwoven problems were investigated. First, the transients were shown to depend sensitively on the control parameters and on the details of the spectral functions, and it was found that the magnetic currents for the individual spin orientations are qualitatively different. This has been achieved by the technique of non-equilibrium Green's functions (NGF). Second, there is a long-standing problem of reducing the full NGF equations to **quantum transport equations** for the quantum distribution function, which can be used for the late stages of the transients, where the use of the full NGF is computationally prohibitive. The reduction based on the generalized Kadanoff–Baym ansatz (GKBA) was found to be unreliable in the investigated application. This was clarified by establishing quantitative criteria for the use of the ansatz.

We succeeded in overcoming the problem by including vertex corrections in an asymptotic approximation. The resulting **corrected generalized Kadanoff–Baym ansatz** yields the magnetic currents in excellent agreement with the exact numerical solution of the full

NGF [23]. The third direction of our study led to a weak non-equilibrium form of the fluctuation-dissipation theorem suitable for NGF and linked to quantum transport equations. The connection between the non-equilibrium fluctuation-dissipation theorem and the GKBA has been established [24]. These results were obtained in collaboration with V. Špička (FZU, **Team 12**).

Strongly non-equilibrium processes

M. Kotrla, K. Netočný, F. Slanina

We have extensive expertise in the field of **stochastic thermodynamics**, which is a modern approach towards modelling strongly non-equilibrium processes, both in the incoherent and the quantum regimes. In the evaluated period, we mainly focused on general problems which arise whenever **several well-separated time scales** are present, typically due to the interaction between a driven non-equilibrium system (made of forced or active colloid particles, for example), one or more thermal baths, and some external macroscopic probes. The developed theoretical techniques may be applied to the analysis as well as to a controlled manipulation of the non-equilibrium system via appropriately designated external probes. Our results were obtained in collaboration with the group of C. Maes (KU Leuven) and with P. Kalinay (SAV Bratislava).

As a realistic model of strongly non-equilibrium dynamics, we studied the movement of **colloidal particles driven by fluid flow** in non-trivial geometries. The flow of colloidal solutions is interesting for technical as well as medical applications. We have had in mind mainly applications for the **lab-on-a-chip technology**, a medical example would be blood flowing in capillaries. We developed approximative analytical procedures, using exact projections to lower dimensions and power expansion in a small parameter characterizing the flow geometry, which enabled an assessment of the applicability and efficiency of these systems for **particle separation** according to their size [25,26].

Furthermore, we investigated the emergent mechanical forces from a non-equilibrium system, such as driven colloids in a fluid, acting on attached macroscopic probes. Our aim was to extend the standard thermodynamic scheme of entropic forces, which is not available out of equilibrium. Interestingly, we have found a close-to-equilibrium extension which still resembles the familiar thermodynamic formulas, yet it includes new genuinely stochastic-thermodynamic quantities such as excess work and heat [27,28]. We explained how the kinetic features play an important role far from equilibrium, and discussed various **intrinsically non-equilibrium properties of the emergent forces** such as their non- additivity [27], the non-gradient structure [29], and certain non-equilibrium variational principles. We also investigated the phenomenon of macroscopic probe stabilization induced by non-equilibrium driving in the ambient system [30,31].
In addition to the mechanical forces from non-equilibrium systems, we studied their thermal response to slow variations of the ambient temperature. We have improved the previous theoretical scheme for **non-equilibrium steady heat capacity** [32]. In particular, we have shown how to tackle the fluctuations by applying suitable time-periodic protocols, which should be suitable for measurement purposes. We also focused on extending the formalism to quantum systems with coherent contacts. Our recent study, still to be finalized, predicts that the interplay between non-equilibrium and quantum features leads to several distinct operational modes at low temperatures.

Non-linear optics in semiconductor heterostructures
M. Pereira

Our research has focused on **semiconductor superlattices** (SSLs) and their utilization in different spectroscopic schemes. The superlattices have received and continue to attract much attention as nonlinear media due to their electro-optical properties, which can be tuned to cover both the GHz and THz ranges. Several important questions regarding the design of efficient SSL devices remain or have been only partially addressed. We have developed methods, combining non-equilibrium Green's functions and the Boltzmann equation, which we use for understanding the microscopic phenomena underlying the SSLs' nonlinearities, for the quantitative modelling of electron transport, and for providing guidelines for designing components with application potential, such as SSL **frequency multipliers** (SSLMs). In particular, we investigated the realistic **high harmonic generation efficiencies** that can be achieved by coupling unbiased SSLMs with the most relevant compact GHz input sources [33]. Furthermore, we showed that asymmetric currents affect the spontaneous emission and can result in a significant enhancement of even harmonics by tuning the interface quality of the heterostructures [34].
Our approach has been further extended to describe the SSLs both as nonlinear sources and as mixers for heterodyne detection. The numerical simulations revealed a strong and unexpected interplay between asymmetric flow, applied static voltages, and oscillating input power that occur when Bloch oscillations in an SSL are modulated by GHz field with output in the GHz-THz range. The complex nature of harmonic mixing process in SSLs was studied to identify the mechanisms responsible for the control and the enhancement of the odd and even harmonics. These results are

supported by experimental measurements performed in the group of Vladimir Vaks (Institute for Physics of Microstructures, Russian Academy of Sciences, Nizhny Novgorod), unlocking the dual potential of SSL devices as **compact**, room temperature, **controllable sources and detectors**.

Development of computational methods and tools

J. Kolorenč, A. Shick, J. Vackář

Many of the investigations discussed so far would not be possible without continued development and improvements of the computational tools. Here we summarize our achievements in this area.

We pushed forward our development of **ab-initio real-space approach to the electronic structure calculations**, which is based on the density functional theory, the finite-elements method, and the self-consistent environment-reflecting pseudopotentials. This approach is filling the gap between the well-established k-space methods based on the Bloch theorem for structures with translational symmetry and the real-space methods using special bases to represent the single-electron wave functions. Our approach aspires to be a counterpart to the plane-wave basis for **non-crystalline, non-periodic structures** without translational symmetry. Another asset of this approach is that it neither assumes nor requires charge neutrality, making it possible to calculate properties of electrically charged structures. The precise, fully non-local, environment-reflecting ab-initio pseudopotentials increase efficiency by treating the core-electrons separately, without imposing any kind of frozen-core approximation. A novel, very **accurate and efficient** method for evaluation of **Hellmann– Feynman forces** has been developed and recently published [35], and improving the computational efficiency making it possible to pursue complex structures and large samples [36] is going on continuously.

In the dynamical mean-field theory that we use to investigate strongly correlated electrons, an important element is an **accurate solution of the multi-orbital impurity model.** In the investigations of excitonic magnets, this solution was found by the continuous- time quantum Monte Carlo method, in the studies of adatoms and rare-earth or actinide compounds, we used exact diagonalization (ED) in a reduced many-electron basis (configuration-interaction method in the language of quantum chemistry). In our applications, the Anderson impurity model often had a **very low symmetry**, in part due to an **interplay of the spin-orbit coupling with the crystal field**. In the case of ED, the impurity model has to be explicitly constructed, which involves extraction of many parameters from the ab-initio electronic structure. We devised a method that is applicable in such low-symmetry situations and tested it successfully on actinide dioxides [37].

We demonstrated that our tools originally developed for the valence electronic structure can be used also for **first-principles investigation of core-level spectra**. The LDA+DMFT study of actinide oxides was complemented with an analogous analysis of rare-earth oxides, for which the filling of the 4f orbitals and its relation to the 4f–oxygen covalency are well established by means of the core-level photoemission (XPS). Comparing the results of our calculations and critically examining the corresponding experimental spectra we concluded that actinide compounds are considerably more difficult when it comes to inferring the fingerprints of covalency from

the spectra, mainly because the core-valence Coulomb interaction is not strong enough [37,38].

Encouraged by the successful calculations of XPS, we extended our tools to enable calculations of the x-ray absorption, the x-ray magnetic circular dichroism, and, finally, the **resonant x-ray emission spectra (RXES)**. A full calculation of RXES is computationally very demanding since it amounts to evaluation of the three-particle Green's function (as opposed to the single-particle Green's function in the case of XPS). We demonstrated that under certain conditions, the **computational complexity of RXES can be reduced to the complexity of XPS**. We formulated a theory which allowed us to interpret pressure- dependent RXES data measured a few years ago on elemental praseodymium, and to show how important it is to accurately take into account hybridization effects in such analysis (as opposed to the standard practice of neglecting most of these effects) [39].

References

[1] **J. Kudrnovský**, **V. Drchal**, I. Turek, *Physical properties of FeRh alloys: The antiferromagnetic to ferromagnetic transition*, Phys. Rev. B **91**, 014435 (2015).

[2] K. Carva, **J. Kudrnovský**, **F. Máca**, **V. Drchal**, I. Turek, P. Baláž, V. Tkáč, V. Holý, V. Sechovský, J. Honolka, *Electronic and transport properties of the Mn-doped topological insulator Bi_2Te_3: A first-principles study*, Phys. Rev. B **93**, 214409 (2016).

[3] **F. Máca**, **J. Kudrnovský**, **V. Drchal**, K. Carva, P. Baláž, I. Turek, *Physical properties of the tetragonal CuMnAs: A first-principles study*, Phys. Rev. B **96**, 094406 (2017).

[4] **J. Kudrnovský**, **V. Drchal**, I. Turek, *Exchange and spin-orbit induced phenomena in diluted (Ga,Mn)As from first principles*, Phys. Rev. B **94**, 054428 (2016).

[5] S. Khmelevskyi, **A. B. Shick**, P. Mohn, *Prospect for tunneling anisotropic magneto- resistance in ferrimagnets: Spin-orbit coupling effects in Mn_3Ge and Mn_3Ga*, Appl. Phys. Lett. **109**, 222402 (2016).

[6] **V. Drchal**, **J. Kudrnovský**, D. Wagenknecht, I. Turek, S. Khmelevskyi, *Transport properties of iron at Earth's core conditions: The effect of spin disorder*, Phys. Rev. B **96**, 024432 (2017).

[7] **V. Janiš**, **A. Kauch**, **V. Pokorný**, *Thermodynamically consistent description of criticality in models of correlated electrons*, Phys. Rev. B **95**, 045108 (2017).

[8] **V. Janiš**, **V. Pokorný**, **A. Kauch**, *Mean-field approximation for thermodynamic and spectral functions of correlated electrons: Strong coupling and arbitrary band filling*, Phys. Rev. B **95**, 165113 (2017).

[9] **V. Janiš**, **P. Zalom**, **V. Pokorný**, A. Klíč, *Strongly correlated electrons: Analytic mean- field theories with two-particle self-consistency*, Phys. Rev. B **100**, 195114 (2019).

[10] **A. Sotnikov**, **J. Kuneš**, *Field-induced exciton condensation in $LaCoO_3$*, Sci. Rep. **6**, 30510 (2016).

[11] D. Geffroy, J. Kaufmann, A. Hariki, P. Gunacker, A. Hausoel, **J. Kuneš**,

Collective Modes in Excitonic Magnets: Dynamical Mean-Field Study, Phys. Rev. Lett. **122**, 127601 (2019).

[12] **J. F. Afonso**, **J. Kuneš**, *Excitonic magnetism in d^6 perovskites*, Phys. Rev. B **95**, 115131 (2017).

[13] K. Pajskr, P. Novák, **V. Pokorný**, **J. Kolorenč**, R. Arita, **J. Kuneš**, *On the possibility of excitonic magnetism in Ir double perovskites*, Phys. Rev. B **93**, 035129 (2016).

[14] A. A. Khajetoorians, M. Valentyuk, M. Steinbrecher, T. Schlenk, **A. Shick**, **J. Kolorenč**, A. I. Lichtenstein, T. O. Wehling, R. Wiesendanger, J. Wiebe, *Tuning emergent magnetism in a Hund's impurity*, Nature Nanotechnology **10**, 958–964 (2015).

[15] **A. B. Shick**, L. Havela, A. I. Lichtenstein, M. I. Katsnelson, *Racah materials: role of atomic multiplets in intermediate valence systems*, Sci. Rep. **5**, 15429 (2015).

[16] M. Etzkorn, C. F. Hirjibehedin, A. Lehnert, S. Ouazi, S. Rusponi, S. Stepanow, P. Gambardella, C. Tieg, P. Thakur, A. I. Lichtenstein, **A. B. Shick**, S. Loth, A. J. Heinrich, H. Brune, *Comparing XMCD and DFT with STM spin excitation spectroscopy for Fe and Co adatoms on Cu_2N/Cu(100)*, Phys. Rev. B **92**, 184406 (2015).

[17] **A. L. Kozub**, **A. B. Shick**, **F. Máca**, **J. Kolorenč**, A. I. Lichtenstein, *Electronic structure and magnetism of samarium and neodymium adatoms on free-standing graphene*, Phys. Rev. B **94**, 125113 (2016).

[18] **A. B. Shick**, D. S. Shapiro, **J. Kolorenč**, A. I. Lichtenstein, *Magnetic character of holmium atom adsorbed on platinum surface*, Sci. Rep. **7**, 2751 (2017).

[19] **A. B. Shick**, A. I. Lichtenstein, *Electronic structure and magnetic properties of Dy adatom on Ir surface*, J. Magn. Magn. Mater. **454**, 61–65 (2018).

[20] M. Žonda, **V. Pokorný**, **V. Janiš**, T. Novotný, *Perturbation theory of a superconducting 0-π impurity quantum phase transition*, Sci. Rep. **5**, 8821 (2015).

[21] M. Žonda, **V. Pokorný**, **V. Janiš**, T. Novotný, *Perturbation theory for an Anderson quantum dot asymmetrically attached to two superconducting leads*, Phys. Rev. B **93**, 024523 (2016).

[22] T. Domański, M. Žonda, **V. Pokorný**, G. Gorski, **V. Janiš**, T. Novotný, *Josephson- phase-controlled interplay between correlation effects and electron pairing in a three- terminal nanostructure*, Phys. Rev. B **95**, 045104 (2017).

[23] **A. Kalvová**, B. Velický, V. Špička, *Generalized master equation for a molecular bridge improved by vertex correction to the Generalized Kadanoff-Baym Ansatz*, EPL **121**, 67002 (2018).

[24] V. Špička, B. Velický, **A. Kalvová**, *Non-equilibrium dynamics of open systems and fluctuation-dissipation theorems*, Fortschritte Der Physik - Progress of Physics **65**, 1–23 (2017).

[25] **F. Slanina**, *Movement of spherical colloid particles carried by flow in tubes of periodically varying diameter*, Phys. Rev. E **99**, 012604 (2019).

[26] **F. Slanina**, P. Kalinay, *Hydrodynamic separation of colloidal particles in tubes:*

Effective one-dimensional approach, Phys. Rev. E **100**, 032606 (2019).

[27] U. Basu, C. Maes, **K. Netočný**, *How Statistical Forces Depend on the Thermodynamics and Kinetics of Driven Media*, Phys. Rev. Lett. **114**, 250601 (2015).

[28] U. Basu, C. Maes, **K. Netočný**, *Statistical forces from close-to-equilibrium media*, New J. Phys. **17**, 115006 (2015).

[29] C. Maes, **K. Netočný**, *Nonequilibrium corrections to gradient flow*, Chaos **29**, 073109 (2019).

[30] U. Basu, P. De Buyl, C. Maes, **K. Netočný**, *Driving-induced stability with long-range effects*, EPL **115**, 30007 (2016).

[31] T. Demaerel, C. Maes, **K. Netočný**, *Stabilization in the Eye of a Cyclone*, Annales Henri Poincaré **19**, 2673–2699 (2018).

[32] C. Maes, **K. Netočný**, *Nonequilibrium calorimetry*, J. Stat. Mech. Theory Exp. 114004 (2019).

[33] **A. Apostolakis**, **M. F. Pereira**, *Potential and limits of superlattice multipliers coupled to different input power sources*, J. Nanophotonics **13**, 036017 (2019).

[34] **A. Apostolakis**, **M. F. Pereira**, *Controlling the harmonic conversion efficiency in semiconductor superlattices by interface roughness design*, AIP Adv. **9**, 015022 (2019).

[35] **M. Novák**, **J. Vackář**, R. Cimrman, *Evaluating Hellmann–Feynman forces within non- local pseudopotentials*, Comput. Phys. Commun. **250**, 107034 (2020).

[36] R. Cimrman, **M. Novák**, R. Kolman, M. Tůma, J. Plešek, **J. Vackář**, *Convergence study of isogeometric analysis based on Bezier extraction in electronic structure calculations*, Appl. Math. Comput. **319**, 138–152 (2018).

[37] **J. Kolorenč**, **A. B. Shick**, A. I. Lichtenstein, *Electronic structure and core-level spectra of light actinide dioxides in the dynamical mean-field theory*, Phys. Rev. B **92**, 085125 (2015).

[38] **J. Kolorenč**, *Metal-Oxygen Hybridization and Core-Level Spectra in Actinide and Rare- Earth Oxides*, MRS Advances **1**, 3007–3012 (2016).

[39] **J. Kolorenč**, *Theory of resonant x-ray emission spectra in compounds with localized f electrons*, Physica B **536**, 695–700 (2018).

Research activity and characterisation of the main scientific results

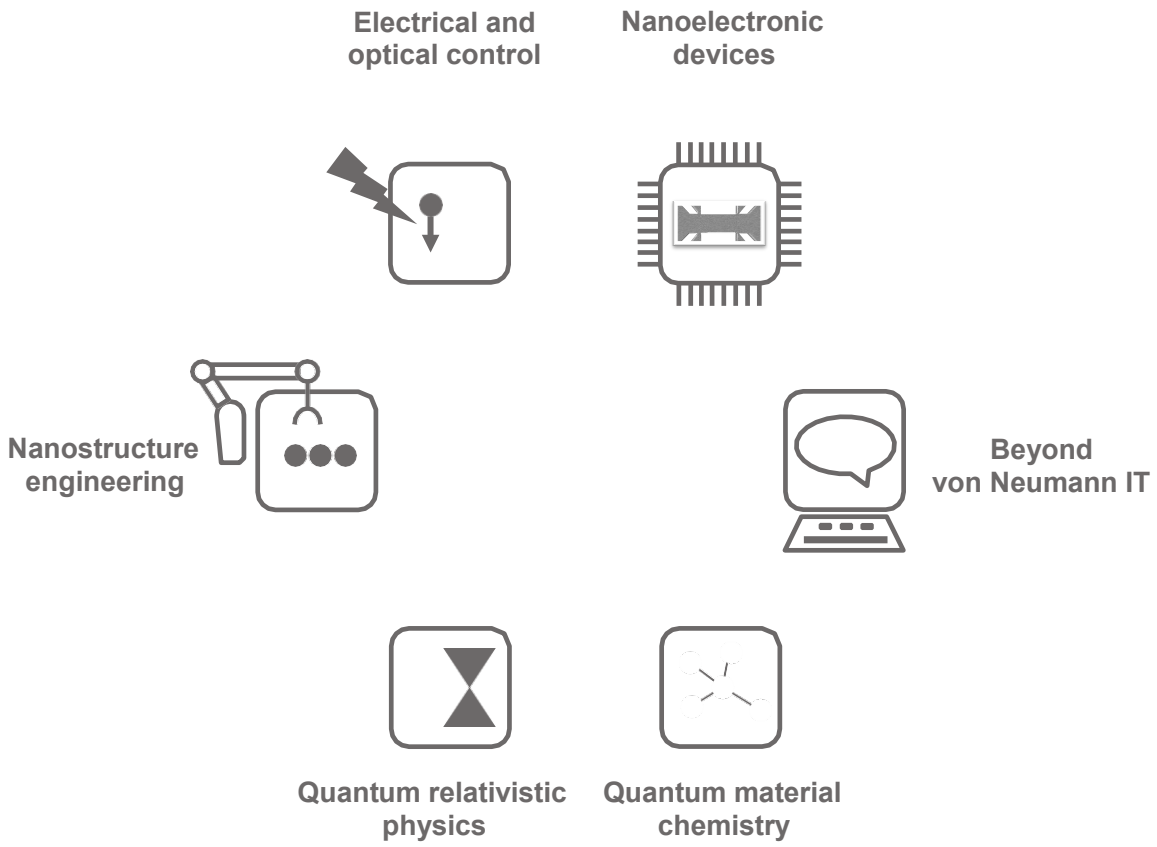

Figure 1 *Interdisciplinary research in spin physics and nanoelectronics of the team includes a range of science and development fields shown in the diagram.*

Based on its track record, expertise, and infrastructure, the team has demonstrated the capability of delivering, in-house, highly interdisciplinary projects spanning a wide range of research and development disciplines (Fig. 1). Simultaneously, the world-wide recognition of the team's pioneering role in the fields of relativistic and antiferromagnetic spintronics has opened the door for its involvement, often as a coordinator, to numerous international collaborative projects. A snapshot of the research area and of the team's major achievements is given in the following two sections.

Brief account of the status of the field and the team's track record prior to the reporting period

According to relativistic quantum mechanics, electron and its charge-conjugate positron components are separated by the huge energy gap of $2mc^2$, which allows electronics to rely on perfect charge conservation. This does not apply to spin components, which poses both opportunities and challenges for spin-electronics (spintronics): On one hand, the electron spin degree of freedom greatly enlarges the potential range of device functionalities. On the other hand, spin is in general a non-conserving elusive property, which can limit control and efficiency of spintronic devices.

Apart from charge-conjugation, parity and time-reversal symmetries play a crucial role

in physics. Breaking the latter symmetry by a collective ferromagnetic order, which introduces an energy gap between up and down spins, is the driving principle behind, the Nobel Prize winning, giant and tunnelling magnetoresistance phenomenon. This electrical-current switch controlled by the ferromagnetic order vector is among the cornerstones of spintronics. The energy separation of up and down spins in ferromagnets, reinforced by carefully engineered spin-filtering through tunnelling in nanostructured material stacks (Fig. 2), makes the spin, transported through the device, a well conserved quantity. The high degree of spin protection gave these nanostructures superior on-off switching characteristics and allowed spintronics to revolutionize the storage and memory industry, made the internet possible, and turned data into the oil, fuelling the economy of the 21st century.

The team's entry point into spintronics, fifteen years ago, was including the parity symmetry breaking and connecting structure, and magnetism by relativistic spin-orbit coupling. This led to the team's discovery of the spin Hall effect. Here spin builds up at the edges of a conductor under the applied electric field and the resulting transient magnetization can efficiently rewrite a magnetic bit. The spin Hall effect opened a development path toward non-volatile magnetic random-access memories 10 times faster than the existing limit, making them competitive with the fastest volatile semiconductor cache memories.

Apart from the immediate consequences for memory technology, the spin Hall effect evolved into a new condensed matter physics discipline owing to its topological ultra-relativistic variants. Here the central problem of spin conservation is solved by separating, at opposite sample edges, co-propagating up and down spin channels (Fig. 2). The resulting spin protection can act without requiring ferromagnetic order in the system. However, conventional conductors used in existing commercial spintronic devices do not show ultra-relativistic topological effects. Quantum chemistry had to enter the research scene to bring these advanced physical concepts to life by discovering new material with the required characteristics.

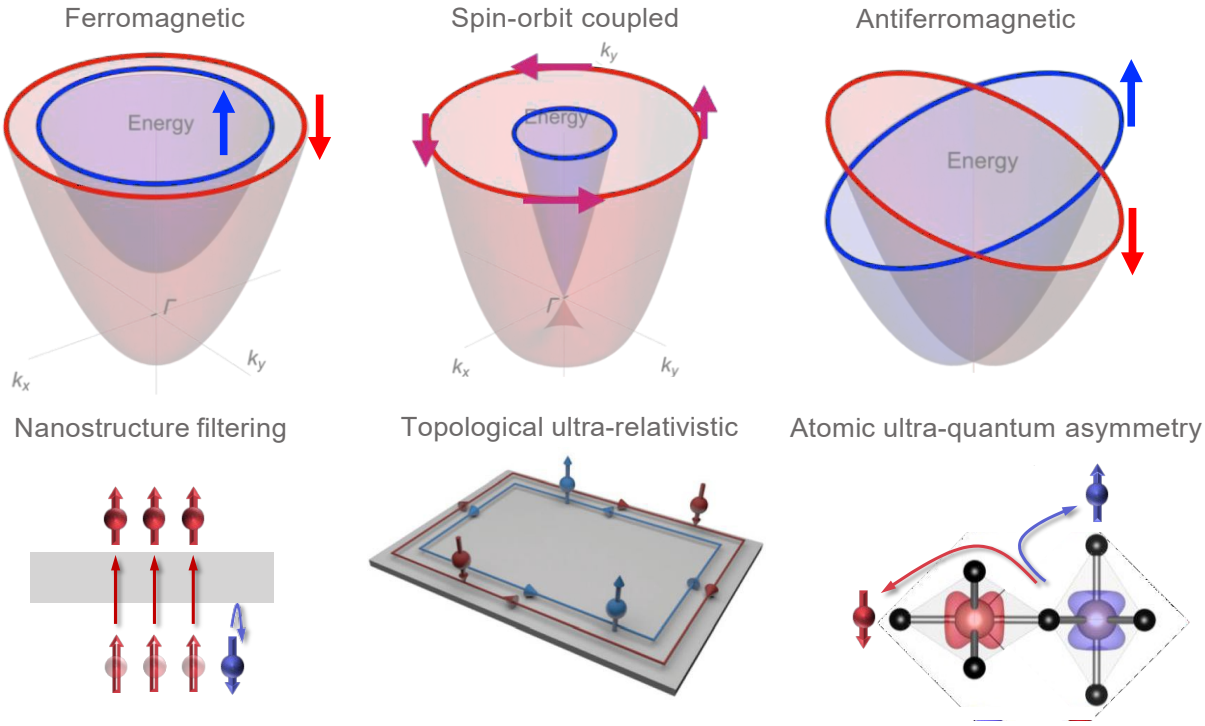

Figure 2 *Left: Spin-splitting of electronic bands by ferromagnetic exchange combined with spin filtering by nanostructure engineering results in spin protection in ferromagnetic spintronics. Middle: Spin-splitting by relativistic spin-orbit coupling combined with topological separation of counter-propagating spin channels at opposite sample edges results in spin protection in relativistic spintronics. Right: Spin-splitting by collinear antiferromagnetism with zero net moment combined with asymmetry of atomic magnetization densities results in spin protection in antiferromagnetic spintronics.*

Despite the many scientific and technological achievements on the path from classical to relativistic and topological spintronics, the team started, a decade ago, a process which evolved into a common perception in the research community, that not all fundamental elements were in place to realize the full potential of spin physics and nanoelectronics. Specifically, ferromagnetic order generates stray fields, which limit the density of integration of memory bits; characteristic spin-dynamics scales in ferromagnets are in the gigahertz range, which limits their speed; and ferromagnetic bits are binary, which makes them unfavourable for realizing analog functionalities in computer architectures beyond von Neumann neuromorphic. In addition, the ultra-relativistic states demand materials with rare heavy elements, and topology and ferromagnetism are mutually poorly compatible, making the corresponding hybrid memory elements fragile.

The team responded to these challenges by opening a new field of spintronics based on antiferromagnets, or complex magnets in general, whose aim is to remedy the inherent limitations arising from invoking the commonly explored and exploited ferromagnetic order. Several preliminary results were already obtained during the previous reporting period, but the key breakthroughs have been made over the past five years. As we elaborate on, in more detail, in the following section and in the Activity plan for the upcoming period section, the team has demonstrated experimental antiferromagnetic memory devices showcasing the absence of stray fields, electrical and optical switching scaled down to ultra-fast femtosecond laser pulses, and analog memory-logic functionalities mimicking neurons and synapses in biological neural networks. A further advantage of this field, highlighted by the team's recent studies, is a much broader material symmetry and chemistry landscape for antiferromagnets compared to ferromagnets, which opens new means for integrating magnetism and topological phenomena.

Besides directly addressing the limitations of ferromagnets, the research of the team in antiferromagnetic spintronics has recently uncovered a new, third concept of spin protection. Instead of ferromagnetic nanostructure or ultra-relativistic, the new spin protection in antiferromagnets is of an ultra-quantum atomic asymmetry nature (Fig. 2). It is based on collinear antiferromagnetism, which can separate spin states while conserving spin and generate fundamental interactions in solids, which are not available in conventional ferromagnetic or broken-parity systems. Among the series of predicted physical consequences of this new spin-protection principle is the anomalous Hall effect, spin conserving spin-splitter, or giant magnetoresistance effect reaching 1000% in fully compensated antiferromagnets. Since these phenomena were identified by the team toward the end of the reporting period and in 2020, they are discussed in more detail in the section on the Activity plan for the upcoming period. They are another illustration, that while already firmly established in the research community, the field of antiferromagnetic spintronics is still in its infancy and we expect its significant expansion in the decades to come.

Introducing antiferromagnets into spintronics has another important implication not

covered so far. Building the complex ferromagnetic nanostructure stacks with tunnel barriers serves, besides the spin- filtering, an additional key purpose. Ferromagnets tend to be metallic, and low-resistivity metallic conductors provide only weak ohmic readout signals, which limits their compatibility with semiconductor microelectronics. Introducing a high-resistive tunnel barrier was the way around this limitation of ferromagnets, which made spintronic memory devices commercially successful. However, these complex multilayer stacks represent a significant challenge to properly engineer and control their properties. Antiferromagnets, on the other hand, range from superconducting and metallic to semiconducting and insulating. Building analogous devices to conventional silicon electronics with a simple thin-film transport channel is, therefore, more accessible in antiferromagnets than ferromagnets. Moreover, semiconducting antiferromagnets open a route toward magnetic transistors for integrated memory-logic. Future research and development of these devices can benefit from the emerging advanced concepts of spin-protection available in antiferromagnets. The team has already achieved first results along this line of research, which we mention in the following section.

As illustrated above, antiferromagnetic spintronics is driving research to the ultimate atomic length- scales and femtosecond time-scales, which makes ultra-high-resolution imaging techniques of paramount importance. Apart from synchrotron facilities, a major role is played here by electron- microscopy and near-field scanning-probe techniques. They can now offer high structural sensitivity including light elements, combined structural and magnetic contrasts down to the atomic scale, and simultaneous high spatial and temporal resolution. Antiferromagnetic spintronics can not only benefit, but also stimulate research and development of these cutting-edge techniques beyond their existing resolution limits. The development of imaging at ultimate temporal and spatial scales is among the key on-going efforts of the team. Several initial results in this area are mentioned in the following section and future projects in this direction are detailed in the section on the Activity plan of the team for the upcoming period.

Finally, as another illustration of the team’s potential to impact science well beyond the domain of spin, we point out that the topological spin-charge coupling phenomena mentioned above represent one facet of a general physics concept, which in ferroelectrics is referred to as magneto-electric coupling or in particle physics as the axion electrodynamics. The latter connection has led to the theoretical proposal put forward jointly with astrophysicists for detecting dark matter by axionic topological antiferromagnets.

Activities and scientific results during the reporting period

Over the reporting period, the team has published 36 papers in Q1* journals, allowing for the size of the team only 18 of those are submitted in phase 1 of this evaluation. Publications include 3 articles in Reviews of Modern Physics, an article in Science, Science Advances, Nature Photonics, 3 articles in Nature Nanotechnology, 4 articles in Nature Physics, and 8 articles in Nature Communications. Within the limited space of this report, we can therefore mention only brief selected highlights of the team’s results.

Spin Hall effect, Rev. Mod. Phys. 87 (2015) 1213 – 1259.

This article gives a review of basic and applied aspects of the spin Hall effect, a field that the team co- initiated a decade earlier (Fig. 3). It includes original data analyses

and connections to fields ranging from quantum and topological phenomena to memories and opto-electronics. It also anticipated the key role of relativistic charge-spin conversion for antiferromagnetic spintronics. According to WoS, the paper has 975 citations, is labelled as a Highly Cited Paper and is the most cited paper out of 11,000 papers published in 2015-2019 on the topic "Hall effect". The team members led this work both conceptually and in all practical aspects.

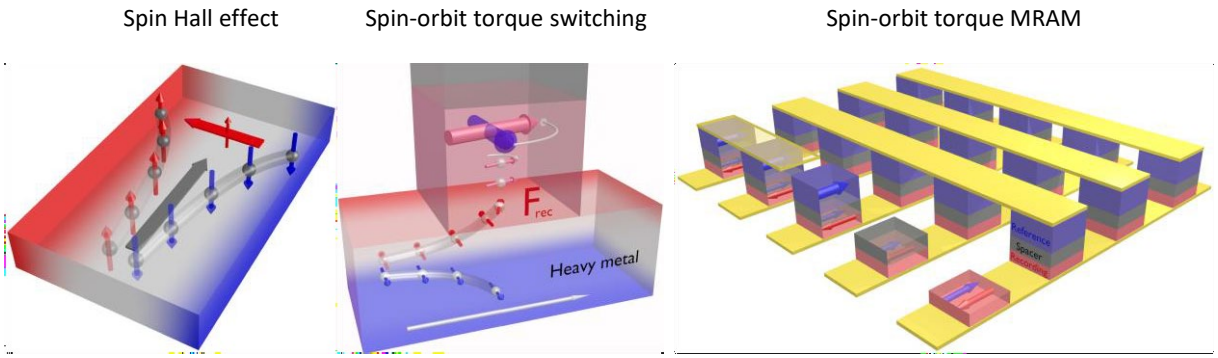

Figure 3 *Left: Longitudinal charge current generates a transverse pure spin current due to the spin Hall effect. Middle: The spin-Hall current is absorbed in the adjacent recording ferromagnetic bit and causes spin-orbit torque switching of the bit's magnetization. Right: Spin-orbit torque magnetic random-access memory.*

Electrical switching of an antiferromagnet, Science 351 (2016) 587 - 590.

Here the team reported the initial experimental demonstration of an antiferromagnetic memory device with electrical writing and readout (Fig. 4). It is based on the team's earlier material synthesis of metallic antiferromagnet CuMnAs, prediction of a staggered relativistic current-induced field which can switch the staggered antiferromagnetic order, and on relativistic magneto-resistive detection of switching. According to WoS, the paper has 510 citations, is labelled as a Highly Cited Paper and is the 2nd most cited paper out of 16,000 papers published in 2015-2019 on the topic "Antiferromagnet". The team members led this work conceptually, performed ab initio theory calculations, together with the University of Nottingham developed epitaxial growth of this new antiferromagnetic compound and fabricated microdevices, and with contributions from additional partners performed electrical and magnetic measurements.

Antiferromagnetic spintronics, Nature Nanotech. 11 (2016) 231 - 241.

Shortly after the above experimental demonstration of the antiferromagnetic memory, in this article the team formulated the basic concepts of the emerging field of antiferromagnetic spintronics. The article summarized the already demonstrated methods and proposed new basic schemes for the operation of antiferromagnetic devices, highlighted that information stored in antiferromagnets is insensitive to disturbing magnetic fields and the consequences of zero stray-fields generated by antiferromagnets, and highlighted that the THz dynamic scale in antiferromagnets should allow for orders of magnitude faster devices than in ferromagnets. All these predicted concepts and consequences have been subsequently demonstrated by the team and further explored by the growing research community in the field world-wide. According to WoS, the paper has 670 citations, is labelled as a Highly Cited Paper and in is the most cited paper out of 16,000 papers published in 2015-2019 on the topic "Antiferromagnet". The team members led this work both conceptually and in all practical aspects.

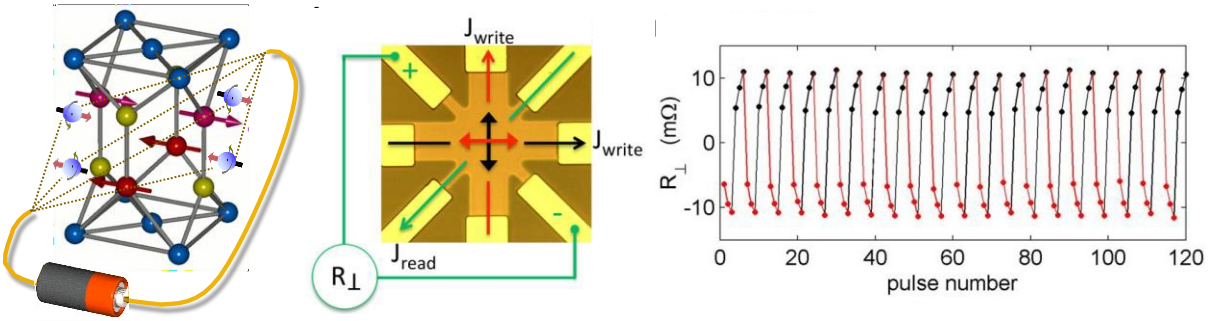

Figure 4 *Left: Electrons with opposite spins accumulate at lattice sites of the opposite antiferromagnetic sublattices and by this generate the staggered relativistic current-induced field that can switch the antiferromagnetic order. Middle: An antiferromagnetic memory cell with double-arrows representing the two memory states with orthogonal Néel vectors and with depicted writing and readout electrical currents. Right: Corresponding electrical readout signals showing that the memory can store multiple states for each of the two writing current directions.*

High antiferromagnetic domain wall velocity induced by Néel spin-orbit torques, Phys. Rev. Lett. 117 (2016) 017202(1) - 017202(5).

This work provided further elaboration on the staggered current-induced field and ultra-fast switching concept in antiferromagnets mentioned above. It predicted that electrically driven antiferromagnetic domain walls can reach velocities two orders of magnitude larger than in ferromagnets. The high domain wall velocity in antiferromagnets arises from the low domain wall mass and the absence of the domain wall breakdown at large driving currents. According to WoS, the paper has 110 citations and is labelled as a Highly Cited Paper. The team members led this work conceptually and performed the theory analysis and calculations in collaboration with the University of Mainz.

Electric control of Dirac quasiparticles by spin-orbit torque in an antiferromagnet, Phys. Rev. Lett. 118 (2017) 106402(1) - 106402(5).

In this article the team opened a new chapter in antiferromagnetic spintronics connecting it to the fields of topological phenomena and relativistic quasiparticles in condensed matter. The work identified Dirac bands, considered earlier only in non-magnets (e.g. graphene), in a collinear antiferromagnet. It predicted topological metal-insulator transition and magnetoresistance associated with Dirac band crossings, who's on and off switching is mediated by the Néel vector reorientation (Fig. 5). According to WoS, the paper has 60 citations and all authors were members of the team.

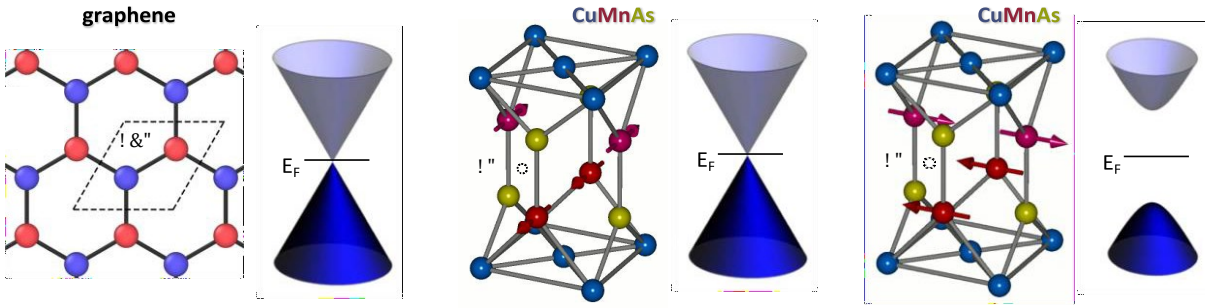

Figure 5 *Left: Dirac crossing of two doubly-degenerate bands in graphene with parity (P) and time-reversal (T) symmetry. Middle & Right: Dirac crossing in an antiferromagnet with broken P and T but preserved combined PT symmetry. In contrast, the combined PT symmetry and corresponding*

topological Dirac states are not allowed in ferromagnets. The gap at the Dirac point can be controlled by the direction of the Néel vector of the antiferromagnet – a functionality that is absent in graphene or other Dirac paramagnets.

Imaging current-induced switching of antiferromagnetic domains in CuMnAs, Phys. Rev. Lett. 118 (2017) 057701(1) - 057701(5).

This article presents a complementary work to the electrical detection of switching of an antiferromagnet mentioned above. It reported direct imaging of switching of antiferromagnetic domains by synchrotron X-ray microscopy. The measurement confirmed that electrical writing pulses can reorient the antiferromagnetic Néel vector in CuMnAs and excluded any ferromagnetic or non-magnetic impurity contribution to the magnetoresistive switching signal. According to WoS, the paper has 70 citations. The team members led this work conceptually and together with the University of Nottingham partner prepared samples for the synchrotron measurements, performed in collaboration with the Diamond Light Source partner.

Optical determination of the Neel vector in a CuMnAs thin-film antiferromagnet, Nature Photon. 11 (2017) 91 - 96.

In this work the team reported the determination of the Néel vector in antiferromagnetic CuMnAs by a table-top time-resolved femtosecond-laser experiment (Fig. 6). It demonstrated a considerably more accessible technique than measurements at synchrotron mentioned above. This was also the initial work that allowed the team to venture into the field of ultra-fast opto-spintronic devices using the antiferromagnetic materials platform. According to WoS, the paper has 50 citations. The team members led this work conceptually, performed ab initio calculations, together with Charles University performed optical experiments, and together with the University of Nottingham prepared samples.

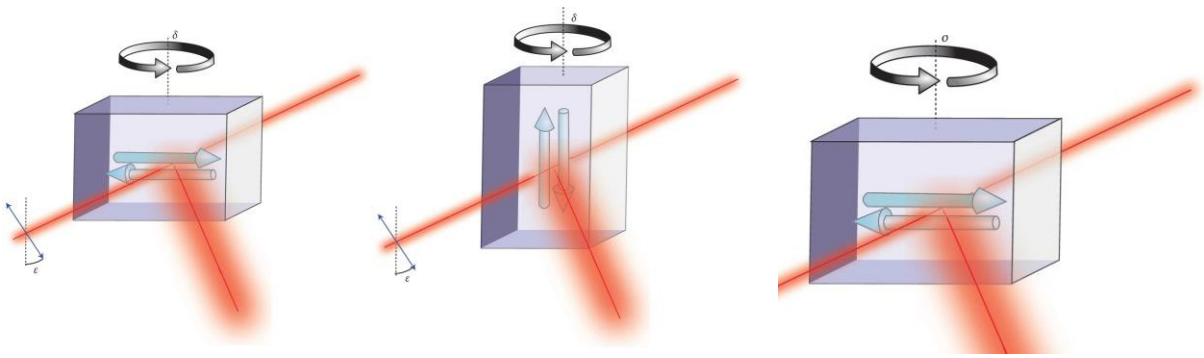

Figure 6 *Left & Middle: Schematics showing that the sample rotation about an axis perpendicular or parallel to the antiferromagnetic Néel vector can be used to detect the Néel vector direction optically. In the former case, the projection of the Néel vector to the light propagation axis varies while in the latter case it remains fixed. Right: Experimental magneto-optical signal variations corresponding to the sample rotation geometry of the left panel.*

Antiferromagnetic CuMnAs multi-level memory cell with microelectronic compatibility, Nat. Commun. 8 (2017) 15434(1) - 15434(7) and EU patent applications EP17197856

Following the initial laboratory experiments, the team demonstrated in this work memory cells fabricated from antiferromagnetic CuMnAs deposited on III–V or Si substrates compatible with common microelectronic circuitry. The antiferromagnetic bit cells were implemented in a standard printed circuit board managed and powered at ambient conditions by a computer via a USB interface (Fig. 7). This prototype antiferromagnetic

spintronic device prompted a long-term collaboration contract with Hitachi Ltd. in antiferromagnetic spintronics, and was awarded the Vodafone Technological Prize. According to WoS, the paper has 70 citations. The team members led this work both conceptually and in all major practical aspects, illustrating the capacity within the team to cover the full range of activities from ab initio theory to prototype “plug-and-play” demonstrator devices. Supporting electrical measurements were performed in collaboration with ETH Zurich and materials were co-developed jointly with the University of Nottingham. The prototype devices were tested not only in the team’s research laboratories but also at the internet of things development sites run by the team at the premises of the Czech Academy of Sciences or jointly with other national and international academic and industry partners. More details on the intensifying tech-transfer activities of the team are given below in the section on the Activity plan for the upcoming period.

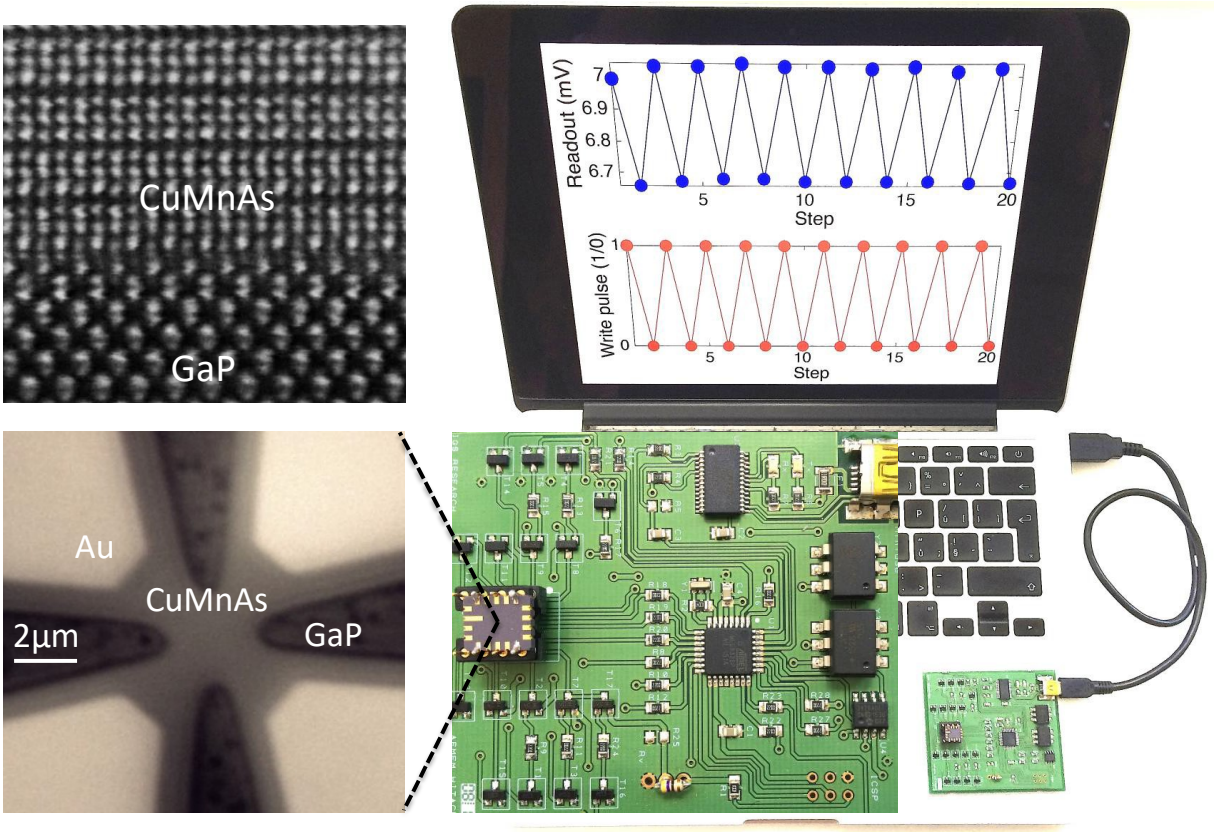

Figure 7 *Top left: Transmission electron microscopy image of the antiferromagnetic CuMnAs film deposited on a GaP substrate. Bottom left: Scanning electron micrograph of the device containing the antiferromagnetic bit cell. Right. An antiferromagnetic memory is implemented in a printed circuit board and controlled by a PC via a standard USB interface.*

Interface-induced phenomena in magnetism, Rev. Mod. Phys. 89 (2017) 025006(1) - 025006(79).

This work was a U.S. led initiative to identify the most exciting scientific results and highlight promising future research directions in the very broad field of static and dynamic interfacial effects in magnetism. The article provides a deep analysis of charge and spin transport through and near interfaces and how these can be used to control the properties of the magnetic layers. According to WoS, the paper has 280 citations and is labelled as a Highly Cited Paper. While the above-mentioned work highlighted the range of activities that the team can encompass internally, this output illustrates the

team's collaborative potential, including high-profile projects of consortia from outside Europe. In this particular work, the leader of the team was responsible for the fifteen-page Chapter III of the article. As one of the few non-
U.S. contributors, he provided the expertise in relativistic magnetotransport and interfaces involving antiferromagnets.

Terahertz electrical writing speed in an antiferromagnetic memory, Science Advances 4 (2018) eaar3566(1)

This work provided an experimental demonstration of the speed of reversible electrical writing in an antiferromagnetic memory device scaled up to the THz range, which is elusive in ferromagnets (Fig. 8). Since the memory bits also showed analog multi-level switching characteristics, the work opened a development path to memories beyond the conventional digital technologies toward neuromorphic applications, combined with the ultra-fast operation. According to WoS, the paper has 70 citations and is labelled as a Highly Cited Paper. The team members led this work both conceptually and in all practical aspects. THz measurements were performed in collaboration with the Fritz Haber Institute of the Max Planck Society in Berlin. Supporting electrical measurements were performed with ETH Zurich and materials were co-developed jointly with the University of Nottingham.

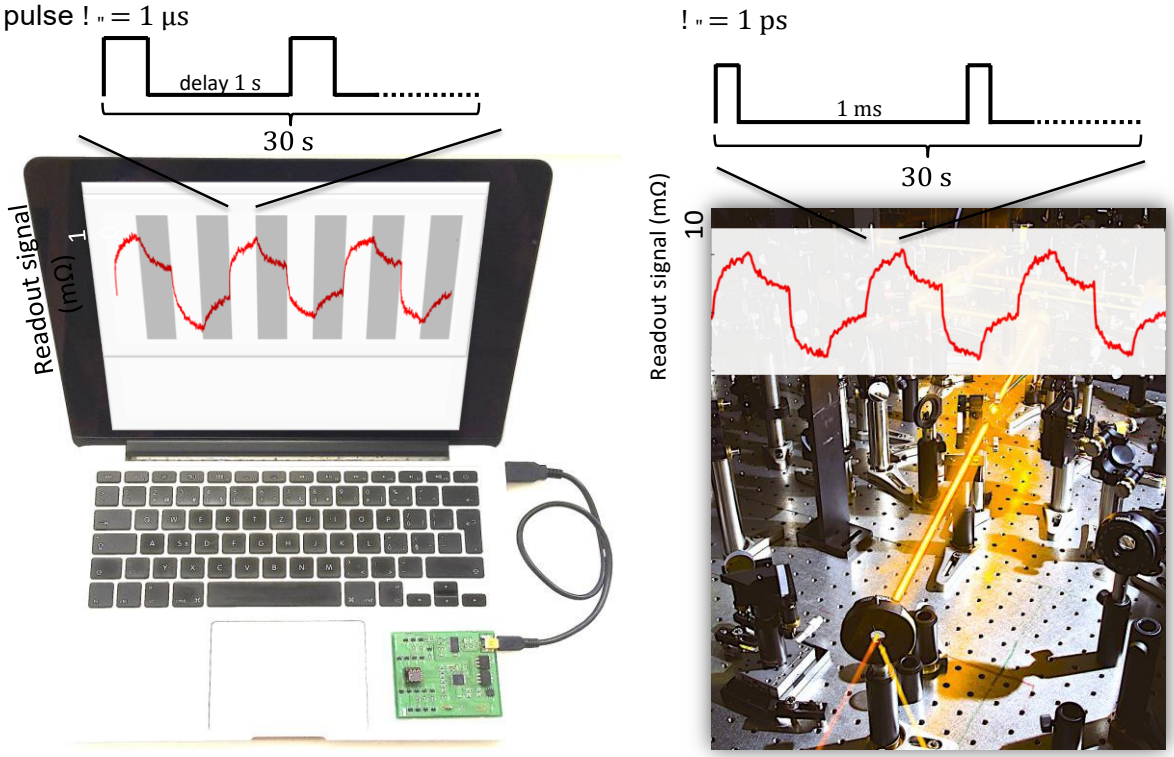

Figure 8 *Left: A sequence of 1 µs electrical current pulses writes multi-level states in the antiferromagnetic memory cell. Right: The same antiferromagnetic bit cell can be written by 1 ps THz field electrical pulses.*

Writing and reading antiferromagnetic Mn_2Au: Néel spin-orbit torques and large anisotropic magnetoresistance, Nat. Commun. 9 (2018) 348(1) - 348(7).

This work reports the demonstration of electrical switching in antiferromagnet Mn2Au for which the team members made the initial theory prediction in 2014. The article also reports evidence of the manipulation of the Dirac band crossing by the antiferromagnetic order vector, as predicted for this symmetry-type antiferromagnet in

the above-mentioned theory work on topological Dirac bands in collinear antiferromagnets. According to WoS, the paper has 130 citations and is labelled as a Highly Cited Paper. The team members proposed this research project and performed ab initio theory calculations. Experiments were performed jointly with the Mainz University.

The multiple directions of antiferromagnetic spintronics, Nature Phys. 14 (2018) 200 - 203. Spin transport and spin torque in antiferromagnetic devices, Nature Phys. 14 (2018) 220 - 228. Topological antiferromagnetic spintronics, Nature Phys. 14 (2018) 242 - 251.

Here the team was invited to co-edit a special issue of Nature Physics on the emerging field of antiferromagnetic spintronics, collecting contributions to six articles from more than twenty academic or industrial institutions around the globe. The team then led the work on three articles from this special issue. The first one gave an overview of new developments in spintronics based on antiferromagnets and the next one discussed a range of spin-torque and magnetoresistance phenomena suitable for writing and reading in ohmic or tunnelling antiferromagnetic devices. The third article went beyond the team's initial study of Dirac quasiparticles in antiferromagnets and elaborated on the connection between topology and antiferromagnetism in a broad context including superconductivity or quantum Hall effect. According to WoS, the papers jointly have 360 citations and are labelled as Highly Cited Papers.

Current-polarity dependent manipulation of antiferromagnetic domains, Nature Nanotech. 13 (2018) 362-365.

This work reports on a demonstration of stable switching of the Néel vector in CuMnAs via domain wall motion. The work was inspired by the theory prediction mentioned in the above work on domain wall dynamics. The experimental verification was carried out using X-ray imaging techniques (Fig. 9) developed in the experimental work also already mentioned above. The experiment provided the decisive confirmation of the switching mechanism by the staggered spin-orbit torque. Switching was observed at current densities an order of magnitude lower than in the counterpart spin-orbit torque devices made of conventional transition metal ferromagnets. According to WoS, the paper has 40 citations. Team members developed the concept and prepared samples jointly with the University of Nottingham while the synchrotron measurements where performed in collaboration with the Diamond Light Source.

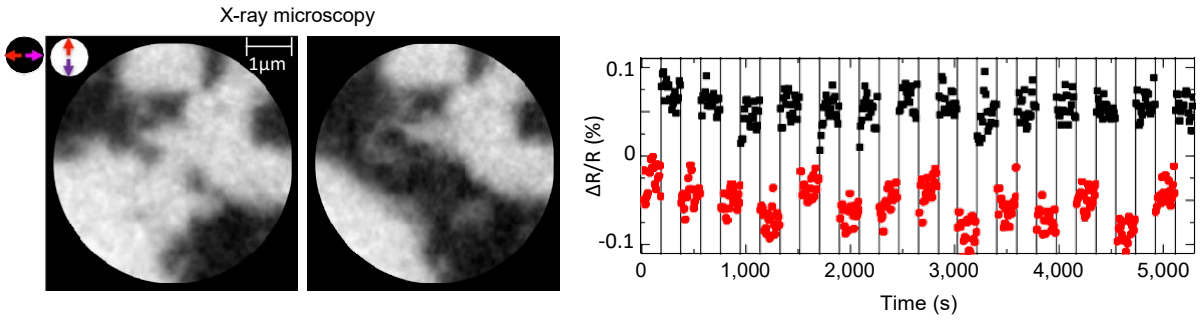

Figure 9 *Left: Current-induced switching of the Néel vector in a micron-size domain imaged by X-ray magnetic linear dichroism photoemission electron microscopy. Right: Corresponding electrical switching signal.*

Current-induced spin-orbit torques in ferromagnetic and antiferromagnetic systems, Rev. Mod. Phys. 91 (2019) 035004(1) - 035004(80).

This is an extensive review reflecting the team's knowledge gained over the fifteen years of research into relativistic non-magnetic, ferromagnetic, and antiferromagnetic spintronics. It focuses on the spin- orbit torque phenomenon whose roots are in the team's work on the spin Hall effect and which is now in the development phase for memory chips in major semiconductor companies. Basic and applied aspects of the field are discussed, as well as major challenges and envisaged future research. According to WoS, the paper has 130 citations and is labelled as a Highly Cited and Hot Paper. Team members were in charge of chapters I-III and V, significant portions of chapter IV and VII, and some portions of chapter VI.

Imaging and writing magnetic domains in the non-collinear antiferromagnet Mn3Sn, Nat. Commun. 10 (2019) 5459(1) - 5459(6).

This work gives an illustration of team's recent research interests beyond collinear antiferromagnets CuMnAs and M2Au. Here the team studied a non-collinear antiferromagnet Mn3Sn, which, despite the vanishing net magnetic moment, has a strong anomalous Hall and Nernst effect. The importance of this work is also in the demonstration of the laser-beam thermo-voltage imaging of antiferromagnetic domains in Mn3Sn based on the Nernst effect, opening up the prospect of studying spintronic phenomena in antiferromagnets with high spatial and temporal resolution (Fig. 10). Team members led the work conceptually, provided the theory analysis, and prepared devices for measurements which were completed in collaboration with the Technical University of Dresden. The materials were grown by the Max Planck Institute in Dresden.

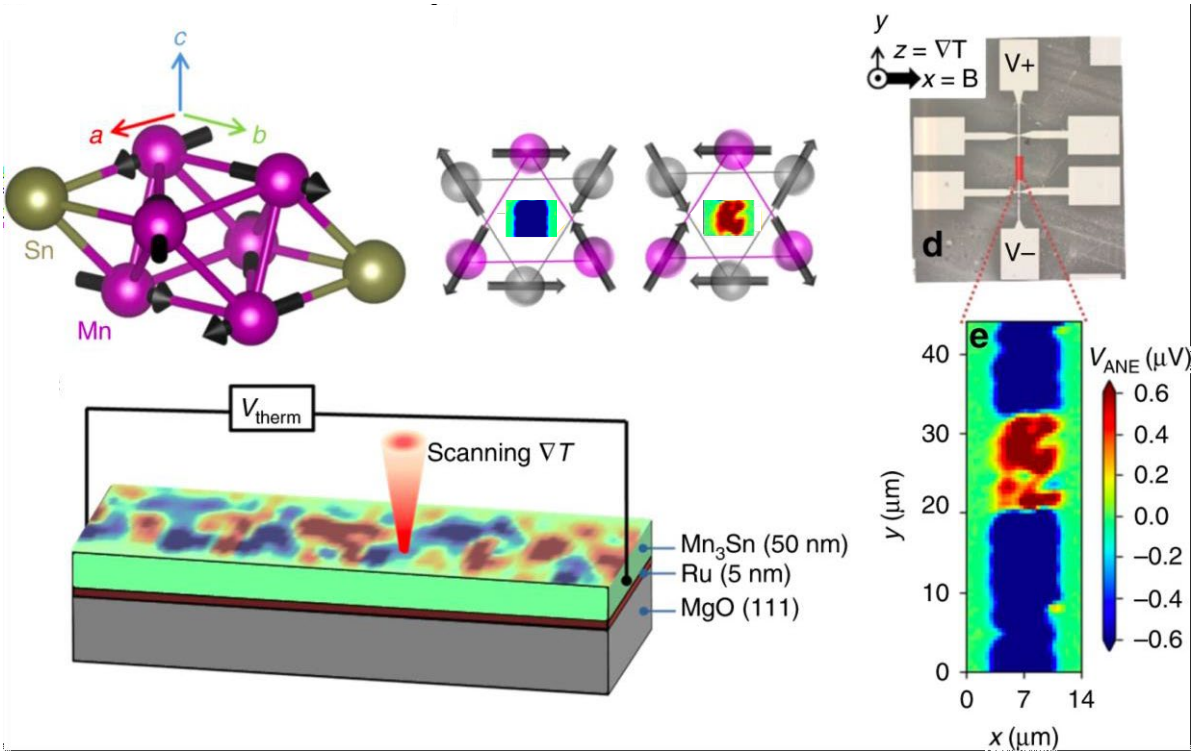

Figure 10 *Top left: Non-collinear antiferromagnet Mn3Sn and its two time-reversed antiferromagnetic domains. Bottom left: The technique of spatially-resolved thermo-voltage imaging of antiferromagnetic domains based on the anomalous Nernst effect. Right: Experimental device realization and domain imaging.*

Research activity and characterization of the main scientific results

The team was primarily involved in an investigation of physical and chemical processes of molecular systems, surfaces and prospective 2D materials. We frequently employed a combination of experimental and theoretical techniques, which allowed us to get detailed insight into the underlying processes and origin of the physical and chemical properties of the studied systems. Besides this, we also developed new experimental and theoretical tools, which enabled us to perform research beyond the state-of-the-art. Several papers resulted from joint action of groups within the team, synergizing the complementary expertise of each group. The main research lines presented in this report can be divided into 4-four categories: 1/ High-resolution scanning probe imaging; 2/ On-surface UHV synthesis of novel molecular structures; 3/ Electron transport and mechanical properties of single-molecule system; and 4/ Prospective 2D materials.

A. High-resolution SPM imaging

One of the most remarkable and exciting achievements in the field of SPM in recent years is the unprecedented sub-molecular resolution of single molecules deposited on surfaces under UHV conditions. In 2014 the team published two theoretical papers, which established a solid basis for theoretical understanding of the origin of the sub molecular SPM imaging with functionalized tips. Early in 2015, the NANOSURF Lab also adopted experimental skills to acquire the sub molecular AFM/STM images using the functionalized tips. This put the group in strong position to further advance the technique beyond the state-of-the-art. A few examples of such resolution acquired by the team are shown in Fig. 1, where the chemical structure of distinct molecules on surfaces is clearly resolved. In the autumn2018, a former member of the NANOSURF Lab Dr. Švec established his own research SPLM group, which quickly demonstrated its capability to conduct independent and high-quality research, merging the capabilities of high-resolution SPM imaging and single molecule photoluminescence measurements.

The possibility to simultaneously acquire the tunneling current (STM) and force (AFM) between the tip and the sample opens up new ways to characterize charge transport through molecular junctions as well as their mechanical stability. Recently, the high-resolution AFM/STM technique has advanced to the point, where it provides not only exciting images with unprecedented resolution, but it might be used to obtain new information not yet available through other techniques. The members of this team have contributed significantly to further develop such capabilities of the high-resolution images and to push further their current limits employing synergy between experimental and theoretical expertise available within the team. This statement can be demonstrated by several achievements, which significantly contributed to advances in the SPM field (see next) including a review article on this topic written by one of the team members[1].

[1] *P. Jelínek J. Phys.-Condens. Mat. 29, 343002 (2017)*

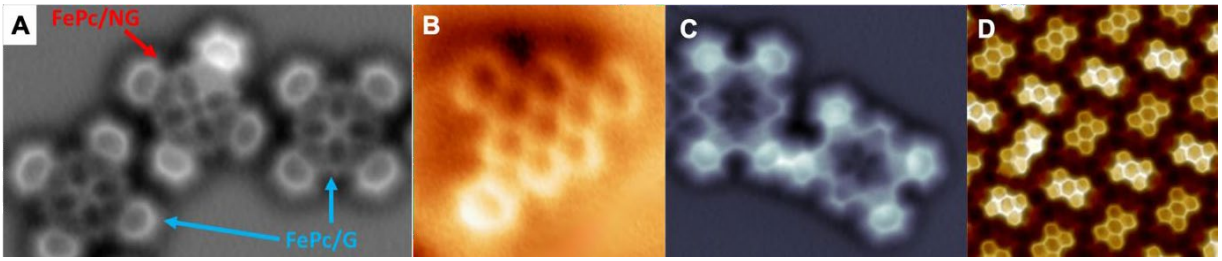

Fig. 1: High-resolution AFM imaging with CO-tip. *Examples of submolecular AFM images of molecules on surfaces obtained in Nanosurf Lab a) FePc on gr/SiC(0001) b) 6-phenyldibenzo[a,g]coronene on Ag(111); c) planarized Au-porphyrin dimer on Au(111); and d) assembly of PTCDA molecules on Au(111) surface.*

Mapping of the electrostatic potential within a single molecule

Originally, the high-resolution SPM technique was mostly used to visualize chemical structures of molecules on surfaces, but this did not provide quantitative information saving the bond-order analysis. From the perspective of chemistry or physics, the capability to measure the charge distribution of a molecule is an extremely useful as this property determines the chemical reactivity of a molecule, as well as many other material properties. Precise determination of the charge distribution in molecules is a highly non-trivial task. Kelvin Probe Force Microscopy (KPFM) has so far been the only technique that can measure a quantity that is related to the charge distribution of an individual molecule with sub- molecular resolution. However, this method has several drawbacks: i) demanding data acquisition; ii) unclear definition of the measured quantity interpretation (do we measure charges, dipoles, electrostatic field or potential?); iii) presence of artefacts at small tip-sample distances; iv) moderate spatial resolution; and (v) last but not the least the impossibility to extract quantitative information. Therefore, there was a high demand to establish a new technique that provides straightforward data acquisition, interpretation, and the ability to extract quantitative information.

We demonstrated how the electrostatic field, originating from the inhomogeneous charge distribution in a molecule, can be measured with sub-molecular resolution[2]. The technique exploits the fact that image distortions typically observed in high-resolution SPM images mostly stem from the electrostatic force acting between the tip and the charge distributed in the molecule of interest, see Fig. 2. We showed that by finding a geometrical transformation between two high-resolution AFM/STM images acquired with two different tips, the electrostatic potential over the molecule can be quantitatively reconstructed with unprecedented spatial resolution.

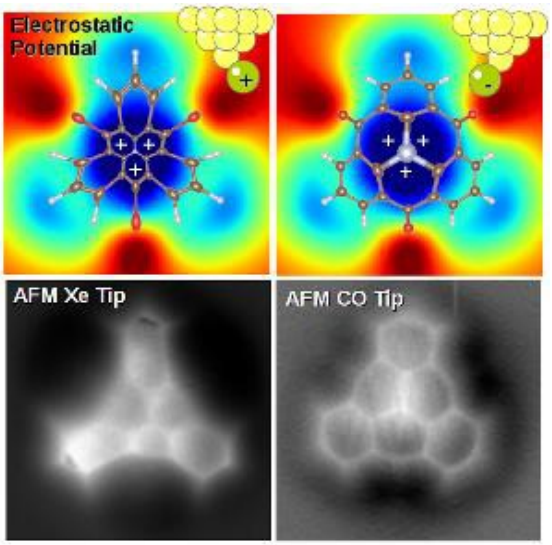

Fig. 2: *Local electrostatic potential of molecule causes a lateral distortion of a probe decorated with a single molecule or atom. This lateral bending introduces deformation of the submolecular image of inspected molecule, enabling reconstruction of the electrostatic field of the molecule.*

Imaging of weakly coupled hydrogen bonded clusters on surfaces

By understanding the importance of the electrostatic forces in determining the submolecular contrast, we were able to further push spatial resolution of the SPM technique with functionalized probes. We showed that the submolecular resolution of weakly bound water clusters on salt using CO-tip can be achieved. We predicted theoretically that the quadrupole charge distribution of a CO-tip acts as a high- pass filter, which allows the discrimination of weakly H-bonded water clusters at some distance from the sample tip without disturbing their atomic arrangement. This was later confirmed experimentally by

colleagues from Beijing University[3]. Later on, this non-invasive imaging technique enabled us to study the mobility of water clusters on an insulating thin film layer[4].

---

[2] *P. Hapala et al, Nat. Commun. 7, 11560 (2016)*

Discrimination of distinct spin state of a single molecule

High-resolution SPM imaging with functionalized probes revealed clear differences in submolecular contrast between iron(II) phthalocyanine (FePc) molecules located on pristine graphene and those in the vicinity of an N dopant. We demonstrate that these differences in submolecular contrast originate from the redistribution of the total density distribution across the molecule due to triplet-to-singlet spin transition[5]. This is a remarkable result because it shows that high-resolution AFM can distinguish between different molecular spin states without using a spin-polarized tip. The ability to explore changes in electron density and their correlation to spin states extends the outstanding capabilities of this technique beyond merely observing the chemical structures of molecules on surfaces.

Moreover, the spin states of single molecules have now been modified by applying external stimuli such as changes in temperature, illumination, and magnetic or electric fields. This work introduced a new strategy involving a weak non-covalent interaction between FePc and nitrogen-doped graphene, which causes a redistribution of electron density between iron(II) d-orbitals. Because of this effect, FePc molecules that exist in the triplet state (S=1) when adsorbed on pristine graphene transition to a singlet state (S=0) when placed near a graphitic N-defect. To our knowledge, this is the first example of a molecular spin crossover driven solely by weak non-covalent interactions resulting from the positioning of a molecule on a 2D surface, with no reliance on external stimuli.

Understanding of the common origin of IETS/STS/AFM imaging with a CO-tip

We demonstrated, for the first time, that AFM, STM and IETS images can be acquired simultaneously at 5K confirming the common imaging mechanism[6]. Our theoretical analysis provided a detailed understanding of the IETS signal with unambiguous identification of the effects of each vibrational mode. On top of this, we provided a methodology to map where inside the molecular junction each IETS peaks was generated by analysing the electron-vibration interaction, the localization of vibrational modes, and the extent of the electron scattering states. We applied this methodology to an adsorbed FePc molecule measured with a CO-functionalized tip to explain why submolecular resolution from the IETS amplitude was possible with one CO vibrational mode but not another. Moreover, we developed a new efficient tool for simulating IETS images, which has been incorporated into home-built PP-SPM code, which is now able to simulate all AFM, STM and IETS images.

Light spectroscopy of single molecules combined with submolecular resolution
In the SPLM group, we have implemented a light-detection path for investigation of single-molecular emitters using the tip-enhancement effect in the UHV AFM/STM instrument. The new instrumentation uses a focusing lens, fiber waveguides and a low-noise/high-sensitivity CCD-based spectrograph to detect photons originating from the tip-sample nanocavity. Inspired by the most recent progress in the light-SPM field, we have chosen ZnPc molecules on NaCl layers on clean crystalline Au and Ag surfaces to perform benchmarks of the optical setup performance. We have successfully reproduced the results from the literature and proceeded to further enhance knowledge of the ZnPc/NaCl system[7]. The most important result published so far is achievement of submolecular resolution with CO-functionalized tips and correlation of the photon maps with high-resolution images from AFM, see Fig. 3. This combination represents a paradigm in scanning probe microscopy, by demonstrating that a simultaneous AFM, STM and light spectroscopy are feasible.

[3] *J. Peng et al, Nat. Commun. 9, 122 (2018)*
[4] *J. Peng et al, Nature 557, 701 (2018).*
[5] *B. de la Torre et al, Nat. Commun. 9, 2831 (2018)*

[6] *B. de la Torre et al, Phys. Rev. Lett. 119, (2017) 166001 (2017)*
[7] *J. Doležal et al, s, Nano letters 19 (12), 8605 (2019)*

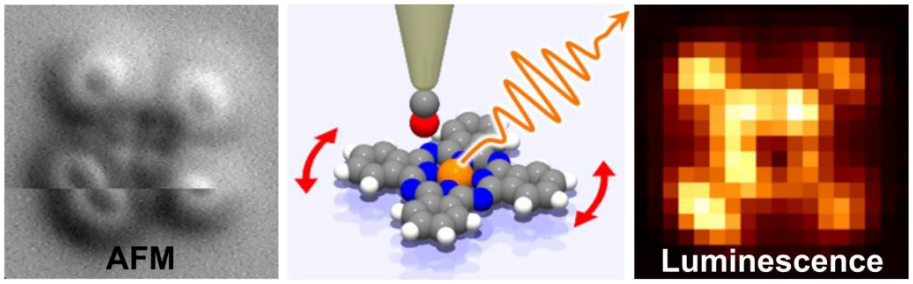

Fig. 3: Simultaneous atomic force and electroluminescence mapping on a single molecule, performed using a scanning probe microscope at cryogenic temperatures and ultra-high vacuum conditions.

B. On-surface UHV synthesis of novel molecular structures

Recent progress in ultra-high vacuum (UHV) on-surface chemistry and scanning probe microscopy with the unprecedented submolecular resolution (see above), which enables the precise determination of molecular products, opened up new possibilities to synthetize and characterize new molecular species not available via traditional solution chemistry. The team contributed to the recent progress not only employing its expertise in high-resolution SPM imaging but also exploring new relevant chemical processes on surfaces and developing a new simulation toolkit based on QM/MM strategy, which enables more realistic simulations of reaction pathways including the search of the optimal free energy profiles including the temperature effect.

Transformation of chirality
Effective control of chirality is one of the greatest achievements of chemistry in solution over the last half century. However, targeted manipulation of chirality in surface reactions has remained a major challenge. We demonstrated a novel method that enables the creation of large 2D layers of molecules with a chiral orientation of choice. This is the first practical example of how molecules on the surface of a substance can assume the same either left-handed or right-handed orientation[8]. We achieved identical chirality of molecules in the whole layer by controlled thermal transformation of specially synthesized spiral helicene molecules on the surface of silver crystal, see Fig.

4. In addition, we were able to accurately describe the chemical transformation of molecules using high-resolution scanning probe microscopy. Specifically, we were able to visualize both the intermediate and final products of the process and to identify the phenomenon as a chemically known Diels-Alder cycloaddition reaction. Nature Chemistry journal highlighted this work in a news & views article. This work was done by a joint effort with partners from the Institute of Organic Chemistry and Biochemistry, who provided molecular precursors.

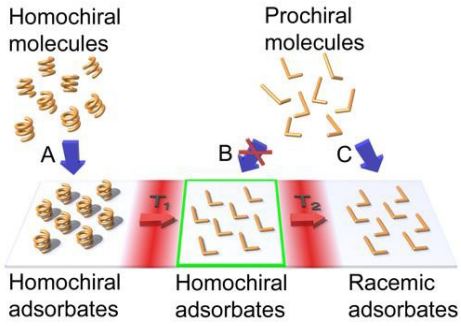

Fig. 4 The proposed concept of global mirror-symmetry breaking in the system of prochiral molecules on an achiral substrate. *(**A**) Vacuum deposition of homochiral molecules (represented here by helices of the same handedness) onto an achiral substrate provides homochiral adsorbates. (**B**) Vacuum deposition of prochiral molecules (represented here by L-shaped objects) onto an achiral substrate does not lead to homochiral (or enantioenriched) adsorbates as spontaneous global mirror-symmetry breaking is unlikely. (**C**) Vacuum deposition of prochiral molecules onto an achiral substrate delivers racemic adsorbates.*

Synthesis of 1D chains on surfaces

We employed on-surface chemistry under UHV conditions to synthetize different kind of well-defined molecular chains with lengths of tens to hundreds of nanometers. We analysed the chemical structure of 1D chains by high-resolution SPM with functionalized probes and theoretical simulations.

---

[8] *O. Stetsovych et al, Nat. Chem. 9, 213 (2017)*

We introduce a new chemical route based on the dehalogenation, homocoupling and aromatization of quinoid anthracene precursors to synthetize long, defect-free flexible polymers with a low bandgap[9]. This represents a new synthetic pathway to engineer a novel class of π-conjugated polymers on surfaces in UHV, where the band gap is directly modulated by the proximity of topological phase transition. We have been involved in both experimental (high-resolution imaging) and theoretical analysis of the atomic and electronic structure of polymers.

Next, we employed supramolecular chemistry on surfaces as a methodology to create polynuclear coordination complexes with novel local charge distribution properties. By a combination of state-of-the- art scanning probe microscopy techniques and density functional theory, we provide direct evidence of on-surface synthesis of atomically precise trinuclear coordination complexes, based on well-defined iron clusters in a mixed (positive) valence configuration[10]. We also demonstrated nontrivial, site-specific redistribution and accumulation of electrons at the metal-organic interface, resulting from the trinuclear coordination. The atomic-scale morphology and resulting electronic/chemical properties of this unusual tri-iron coordination motif have not been achieved via conventional synthetic chemistry; they result from the on-surface metal-organic self-assembly. Our findings are of crucial importance for designing hybrid

interfaces, where nanoscale control over local charge distribution can allow for tailored, site-specific chemical activity. In this study, we performed theoretical DFT simulations and detailed analysis of chemical and atomic structures of the 1D chains.

We also use mechanical strain to steer chemical reactions, which creates entirely new opportunities for a solution- and solid-phase synthesis of functional molecules and materials. This strategy is not readily applied in the bottom-up on-surface synthesis of well-defined nanostructures. We reported an internal strain-induced skeletal rearrangement of 1D metal–organic chains (MOCs) via a concurrent atom shift and bond cleavage on Cu(111) at room temperature[11]. We introduced a novel computational scheme which enables us to calculate the free energy activation on a surface at a given temperature of a given chemical reaction. These simulations together with bond-resolved non-contact atomic force microscopy imaging (performed by partners from NUS) showed that the relief of substrate-induced internal strain drives the skeletal rearrangement of MOCs via 1,3-H shifts and shift of Cu adatoms that enable migration of the monomer backbone toward an energetically favorable registry with the Cu(111) substrate. Our findings on this strain-induced structural rearrangement in 1D systems will enrich the toolbox for on-surface synthesis of novel functional materials and quantum nanostructures. The work was selected as hot-paper by editors of Angew. Chemie journal.

On-surface synthesis and characterization of magnetic triangulene molecule

There is a requirement to synthetize polycyclic aromatic hydrocarbons (PAH) with open shell electronic structure featuring magnetic properties. So far, however, room-temperature stable magnetic carbon nanostructures have only been theoretical constructs. Here we participated in a research project with partners from NUS, which succeeded in producing such a structure in practice. The zigzag-edged triangular graphene molecules (ZTGMs) have been predicted to host ferromagnetically coupled edge states with the net spin scaling with the molecular size, which affords large spin tunability crucial for next-generation molecular spintronics. However, the scalable synthesis of large ZTGMs and the direct observation of their edge states have been long-standing challenges because of the molecules' high chemical instability. Here, we report the bottom-up synthesis of π-extended [5]triangulene with atomic precision via surface-assisted cyclodehydrogenation of a rationally designed molecular precursor on metallic surfaces[12]. Atomic force microscopy measurements unambiguously resolve its ZTGM-like skeleton consisting of 15 fused benzene rings, while scanning tunneling spectroscopy measurements reveal edge-localized electronic states. Bolstered by density functional theory calculations, our results show that [5]triangulenes synthesized on Au(111) retain the open shell π-conjugated character with magnetic ground states.

[9] *A. Sánchez-Grande et al, Angew. Chem. Int. Ed. 58. 6559 (2019)*
[10] *C. Krull et al, Nat. Commun. 9, 3211 (2018)*
[11] *M. Telychko at al, Angew. Chem. Int. Ed. 58, 18591 (2019)*
[12] *J. Su et al, Science Advances 5, eaav7717 (2019)*

On-surface synthesis of novel aromatic compounds from aryl azides precursors

We studied the chemical transformation of 9-azidophenanthrene on the Ag(111) surface by nc-AFM in UHV, which was provided by partners from IOCB CAS. High-resolution imaging supported by first- principle calculations revealed the structure of the final products that originated from a common and elusive 9-phenanthryl nitrenoid intermediate chemisorbed on the Ag(111) surface[13]. A formal nitrene insertion into the C−H bond along with its dimerization and hydrogenation were identified as main

reaction channel. Thus, the ability of aryl azides to form covalent σ- and π-bonds between their transformation products on a solid surface was demonstrated at the single-molecule level. The work was highlighted on the cover page and selected as hot-paper of Angew. Chemie journal.

C. Electron transport and mechanical properties of single molecules

The main focus of the Molecular Transport group was the **calculation of charge transport properties at single molecule junctions**. In these systems, individual molecules are placed between two (usually metallic) electrodes. The ability of the junction to sustain an electrical current depends sensitively on the chemical structure of the molecule but also on how the molecule is bonded to the electrodes. Calculations must therefore properly describe the molecular properties and the binding of the molecule to the electrodes including, of course, quantum effects. The standard methodology involves a combination of **Density-Functional Theory** (DFT) and Non-Equilibrium Green's Functions (NEGF). The electronic structure of the metal-molecule-metal junction is calculated within DFT, and this is used as input for the transport problem (within the NEGF formalism). Atomistic simulations unveil the **main mechanisms that govern charge transport** through single molecules, thus **rationalizing experiments and making predictions** or establishing design rules at the molecular level. We worked on several aspects of single molecule systems.

Single-molecule electron transport theory.

We investigated how the **molecular backbone** (which contains the functionality of the molecule) influences charge transport, in particular conductance, which is defined as the inverse of electrical resistance. We studied two closely related kinds of molecular backbone. In collaboration with partners from chemical synthesis and break-junction experiments, we investigated the conductance of an **antiaromatic** molecular backbone (Fig. 5 a). This was the culmination of decades-long research in this area by the community. Aromaticity is a key concept in chemistry, describing the stability of conjugated molecules. According to Hückel's rule, if the number of π electrons is 4n+2 (where n is any integer), the molecule is aromatic, and if this number is 4n, the molecule is antiaromatic. Antiaromatic compounds are known for being unstable and reactive, and thus very hard to synthesize. Indeed, most conjugated molecules in surface science and molecular transport studies are aromatic molecules. Antiaromatic molecules had been predicted to show exceptional conducting properties in the 1970s[14], however, efforts to synthesize and study their conductance had failed. In collaboration with partners from experiments and chemical synthesis, we studied the **single molecule conductance of an antiaromatic compound for the first time**[15]. We found that it is approximately 20 times more conducting than its aromatic analogue, which is structurally similar. Atomistic calculations, which were done by our group, revealed why the antiaromatic molecule was more conducting than its aromatic counterpart. We found that the relevant frontier molecular orbital was much closer to the Fermi level in the antiaromatic case, thus explaining its higher conductance. Our work settled a longstanding debate and showed the potential of antiaromatic compounds as remarkable molecular conductors.

New metal-molecule linker groups for single molecule transport

In addition to the backbone, molecular conductance depends strongly on the nature of end groups of the molecule which bind it to the electrodes, including the interface geometry. This has long troubled molecular electronics, especially if molecules are functionalized with thiolate (sulphur) end groups. These groups have been used since the birth of molecular electronics due to their strong binding to Au, a widely used

electrode material. However, there are several possible ways for thiolate-terminated molecules to bind to Au, depending on whether S binds to one, two, or more Au atoms, or in other conformations. Importantly, each of these binding motifs significantly changes the electron transport properties, such that conductance can change by more than two orders of magnitude depending

[13] *J. Hellerstedt et al, Angew. Chem. Int. Ed. 58, 2266 (2019)*
[14] *R. Breslow et al, J. Am. Chem. Soc. 95, 6688 (1973)*
[15] *S. Fujii et al, Nature Commun. 8, 15984 (2017)*

on the geometry of the metal-molecule interface[16]. To complicate matters further, interface structure cannot be measured easily in single molecule junctions due to several experimental challenges, such as the impossibility of carrying out x-ray measurements or to the breaking of the junction under standard experimental conditions. In collaboration with an experimental team from the Tokyo Institute of Technology, we studied a paradigmatic molecular junction. Simultaneous Raman measurements at the junction of molecular vibrations and conductance measurements correlated Raman shifts with conductance values. Our group performed the theoretical modelling (Fig. 5 b). Through simulations, we could ascribe the measured Raman shifts and conductance values to specific binding sites at the metal- molecule interface[17]. In this way, we could **identify the adsorption site of the molecule** in a nanoscale circuit, **helping overcome a major obstacle in the field**.

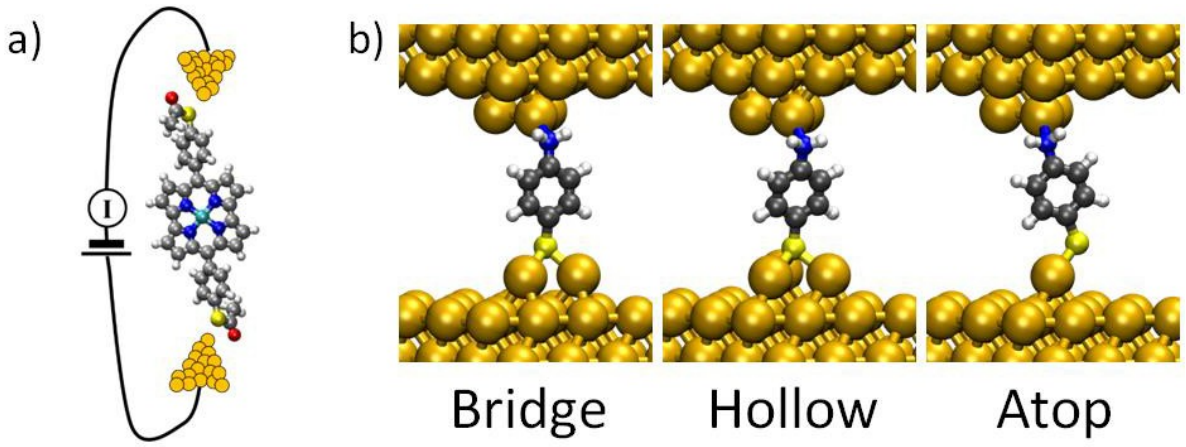

Fig. 5 *a) Structure of a single molecule circuit containing an antiaromatic compound between two nanoelectrodes. b) Three representative molecular adsorption structures for a paradigmatic molecular junction. Notice the different binding geometries of the bottom contact.*

We also provided the theoretical modelling for a **new class of metal-molecule linker**. **N-Heterocyclic Carbenes** (NHCs) are relatively new molecules, first isolated in the 1990s, which contain a divalent C atom with a six-electron shell. NHCs have shown high thermal and chemical stability as films on metallic surfaces, and it seemed natural to extend this study to single molecule circuits. Our work was the **first study** of the electron transport properties of NHC-based single molecules[18]. This work was carried out with partners from chemical synthesis and break-junction experiments from Columbia University, USA. Our group performed all theoretical modelling. Our work illustrated the role of NHC groups in the conducting properties of the molecule and demonstrated their strong electronic coupling to the electrodes.

Inelastic Electron Tunnelling Spectroscopy theory

The interaction between tunnelling electrons and vibrations localized in the molecule opens new pathways for electron transport, and results in signatures in the second derivative of the tunnelling current with applied voltage. This is the basis of **Inelastic Electron Tunnelling Spectroscopy** (IETS). In a theoretical paper we proposed a molecular system that exhibits a transition from dips to peaks in the IETS. We considered a series of oligophenyls (having 1-4 benzene rings) bonded to the electrodes via highly-conducting Au-C bonds. The short molecule showed near resonant elastic transmission (almost the full conductance quantum) and exhibited IETS dips, while in longer oligomers conductance is in the tunnelling regime and IETS peaks were obtained (Fig. 6a). We showed that this family of molecules is an ideal system to tune the interplay between electronic structure and vibrational properties and realize the **transition between IETS dips to peaks** by simply increasing the length of the molecular backbone.

[16] *Y. Kim et al, Nano Lett. 11, 3734 (2011)*
[17] *S. Kaneko et al, Chem. Sci. 10, 6261 (2019)*
[18] *E.A. Doud et al, J. Am. Chem. Soc. 140, 8944 (2018)*

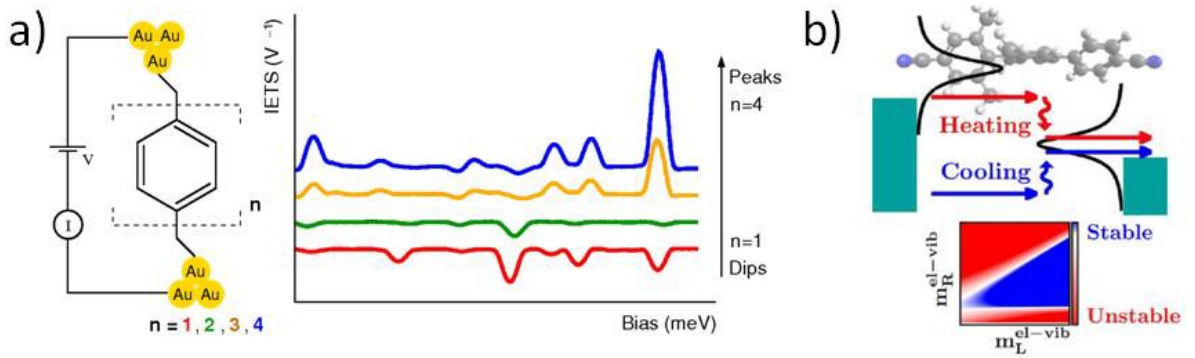

Fig. 6 *a) Molecular system consisting of a series of benzene rings with Au-C links to electrodes. Calculated IETS spectra predicting a transition from dips to peaks with increasing number of rings. b) Schematic current-induced heating and cooling processes, and calculated stability diagram for a general molecular system.*

Current-induced excitation of vibrational modes

In molecular electronics, the **stability of metal-molecule-metal junctions with respect to current flow** is essential. Electronic and vibrational degrees of freedom exchange energy. Energy transferred from electrons to vibrations locally heats the conducting molecule, which can become unstable and break if these processes are not counterbalanced by dissipation mechanisms. An increase in the population of molecular vibrational modes due to the **current will locally heat the junction**. Conversely, a net energy transfer from vibrations to tunnelling electrons will **locally cool the molecule**, as this energy is dissipated far from the junction. Absorption and emission processes depend on the electronic structure of the junction under bias. Thus, accurate and computationally demanding calculations of the junction out of equilibrium (ie. with a large applied bias and self-consistently calculating the potential drop across the interface) are necessary. These calculations open the way to **tuning current-induced energy exchange** by modifying the molecular junction. It is easy to expect that the molecular junction will heat as the voltage is increased. However, an interesting result of our work is that, by tuning the metal-molecule interface, an applied voltage can also locally cool the junction if the net energy transfer at a given bias voltage is from molecular vibrations to the tunnelling electrons. We predicted a molecular system where this current-induced cooling could be observed by tuning the metal-molecule

coupling[19]. We also studied the conditions for junction breakdown due to the applied voltage and passing current. In a theoretical paper by our group alone, **we extended previous predictions to a less restrictive regime and to a wider class of molecular systems**[20]. Understanding and controlling the conditions under which molecular-scale circuits will break down is critical in the field of molecular electronics. Our work showed that these current-induced instabilities (Fig. 6b) are a more general phenomenon than previously thought.

Demonstration of piezoelectric effect on single molecule

The converse piezoelectric effect is a phenomenon, in which a mechanical strain is generated in a material due to an applied electrical field. However, demonstration of the piezoelectric effect at the nanoscale has remained elusive so far. We demonstrated, for the first time to our knowledge, the piezoelectric effect on a single molecule[21]. How does the converse piezoelectric effect work at the nanoscale? The screw-like molecule 2,17-Bis(acetylsulfanyl) heptahelicene (BA7H) endowed with an inner dipole stretches or squeezes itself depending on the strength and polarity of the outer electric field. It arises by applying a voltage bias between the silver surface and atomically sharp tip of the scanning microscope that resides over the studied molecule, see Fig. 7. We can monitor the corresponding change in a molecule height with very high accuracy, so by measuring force-distance spectroscopy by means of scanning probe microscopy (shown in Fig. 7 b), it is possible to see a molecule deformation induced by the electric field. We can corroborate the experimental evidence by the total energy DFT simulations. The calculations reveal strong charge transfer between the BA7H molecule and the metallic substrate, which gives rise to a vertical electric dipole. The presence of the electric dipole coupled with

[19] *G. Foti and H. Vázquez, J. Phys. Chem. C 121, 1082 (2017)*
[20] *G. Foti and H. Vázquez, J. Phys. Chem. Lett. 9, 2791 (2018)*
[21] *O. Stetsovych et al, J. Am. Chem. Soc. 140, 940 – 946 (2018)*

a soft vibrational mode steaming from a helical structure of the molecule originates the strong piezoelectric effect. The demonstration of the piezoelectric effect on a single molecule represents a breakthrough in the understanding the electromechanical behaviour of individual molecules and provides a new concept of the design of molecular motors, sensors and electricity generators at the nanoscale.

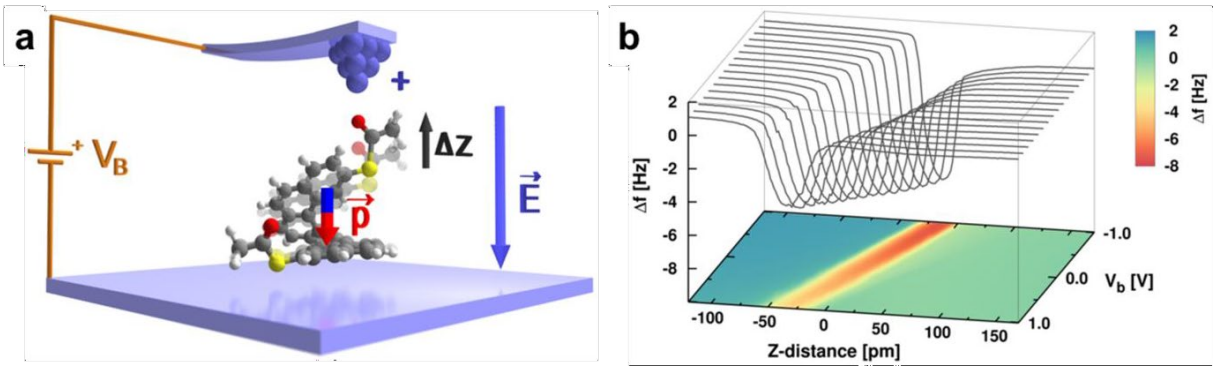

Fig. 7*. Measurements of the piezoelectric effect on helicene molecule by means of scanning probe microscopy. (a) Ball-and-stick model of the experiment. (b) Measured df(z,V_B) the frequency shift ⊗f vs. z-distance spectroscopies acquired for different bias voltages V_B acquired over a single 7HdiET molecule with the same tip.*

D. Synthesis and characterization of prospective 2D materials

We launched a project on graphene doping, especially to develop ways to incorporate B atoms into graphene grown on SiC, in order to provide p-type centres and compare properties directly to the N doping described previously. We have successfully achieved this goal and characterized their fundamental properties, using our state-of-the-art AFM/STM instrumentation and various experiments at synchrotron Elettra[22]. We have found a very interesting quantum interference effect that is useful for discrimination between the B and N dopants. (e.g. by measuring the 3D volumes of individual dopants in Fig. 8).

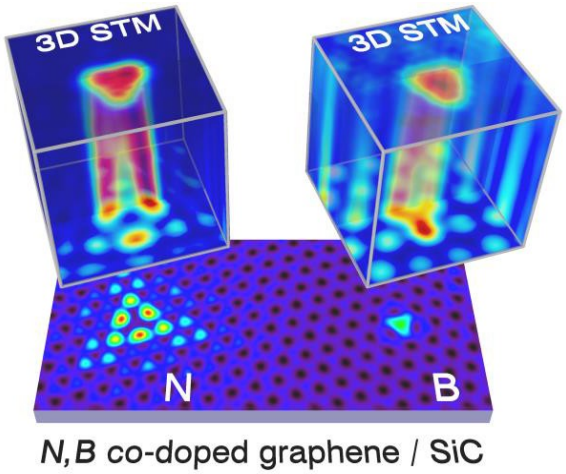

Fig. 8: 3D-volume measurements with atomic resolution of the tunnelling current over N and B graphitic dopants in graphene/SiC. The quantum interference effect, manifested by a hollow-triangle appearance of the N-dopant allows us to distinguish the N and B dopants very easily.

[22] *M. Telychko et al, ACS Nano 9, 9180 (2105)*

Our work on N- and B- dopants inspired new synchrotron experiments, in which our members actively participated both in the experimental and theoretical parts[23, 24]. In these works, we performed atomically precise structural characterization by X-ray standing-wave technique of N-doped graphene on SiC sample. The doping effect on the Dirac-like electron behavior has been determined using angle- resolved ultraviolet photoemission spectroscopy and rationalized using DFT simulations. Boron incorporation into graphene mesh during the formation of graphene on SiC has been studied in detail using X-ray absorption spectroscopy technique.
We have built upon our previous knowledge of graphene growth on SiC substrates and created an infrastructure to provide high-quality single-layer graphene samples for further research. The reactor for graphene growth has been described in a dedicated publication[25]. Samples have been used for various experiments addressing the elementary properties of dopants and their interaction with the environment,
e.g. the non-covalent spin state modification of the FePc molecule due to the presence of a dopant in its vicinity[26].

In an independent line of research dedicated to new prospective insulating substrates for molecular deposition, on-surface chemistry and photochemistry, a new 2D-oxide has been discovered by us, after being grown on natural hematite crystals of the (0001) orientation[27]. The FeO_2 layer was chemically and structurally identified using the atomically-resolved images from STM, and the mesoscopic real-space and k-space

imaging by the LEEM and micro-LEED instrument. Complementary data from XPS and LEIS techniques together with DFT+U simulations allowed us to unambiguously determine the atomic structure and magnetic ordering of this new material. By publishing these results, it was thereby possible to settle one of the long-standing disputes about the termination of oxidized hematite substrates.

Research activity and characterisation of the main scientific results

The detailed description below follows not only from G1 to G5, but also to smaller studied objects – from thin films through to nanowires and nanoparticles. Material-wise, the narrative starts with classical silicon devices (photovoltaic solar cells) and progresses to light emitting silicon, carbon allotropes and 2D materials. The story also develops from traditional, application-oriented topics to fundamental exploratory research.

G1 Thin Films (group of Martin Ledinský)

Thin films of amorphous or nanocrystalline silicon have been at the core of our research for decades, being developed for thin film solar cells (one of the team members, T. Mates, is a co-author of a current record efficiency of 12.34% for a large scale thin-film silicon tandem solar panel [1] developed at TEL Solar). Thin film solar cells require much less semiconductor material (several micrometres instead of ~150 μm wafers), but they were left behind due to the enormous progress of wafer-based cells. Nevertheless, the Group of Thin Films found two avenues for keeping abreast of the field, namely i) the use of very thin Si films in heterojunction-based solar cells and ii) thin films of hybrid organometallic perovskites. Both approaches lead to high efficiencies and both present challenges, some of which we were able to address.

i) Thin films for Silicon Heterojunction Solar Cells

The current world record of 26.7 % photovoltaic efficiency of a silicon-based solar cell is held by the Japanese company Kaneka, using the so-called Interdigitated Back Contact Silicon Heterojunction (IBC-SHJ) design. These cells use a few nanometres of a-Si:H to passivate the crystalline silicon surface, enabling low surface recombination velocity and high voltage. The back contacted cells have no front contacts and collect charges using interdigitated strips of n- or p-doped a-Si:H at the back. Kaneka fabricated these cells using photolithography, a sophisticated process too costly for mass production.

The European H2020 project NextBase, „Next-generation interdigitated back-contacted silicon heterojunction solar cells and modules by design and process innovations", aimed at developing a low-cost process with comparable performance.

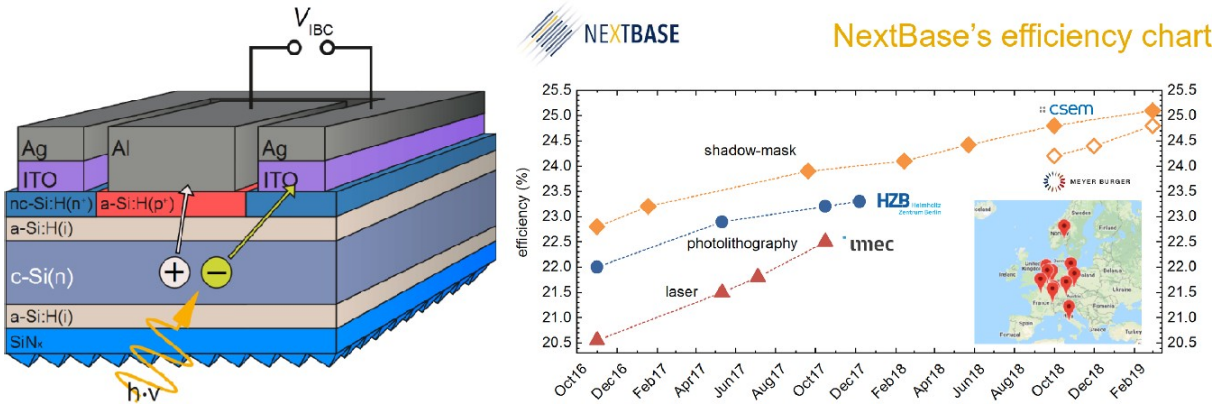

Fig. 1 (Left): Scheme of interdigitated back contacted silicon heterojunction solar cell (shown with back contacts on the top and illuminated side in the bottom). (Right) Progress in resulting cells' efficiency results of the H2020 NextBase consortium.

The € 5.7 M project funded by the European Commission and Swiss government via the Research and Innovation Action ID 727523 ran from 2016 to 2019. The project brought together European leaders in the field; Forschung Zentrum Julich, EPFL Neuchatel, TU Delft, IMEC, CEA, CSEM, Helmholtz Zentrum Berlin, Fraunhofer ISE, and industrial partners Meyer Burger, Norwegian Crystals and Enel Green Power, from 8 European countries (see the inset of Fig. 1). The FZU thin film group led the Characterization and Modelling work package. The project goal was to realize IBC-SHJ solar cells with efficiency above 26.0% using stencil masks (instead of photolithography) and the corresponding solar modules with efficiency above 22.0%.

We contributed to the project by developing a new method for checking the interdigitated back contacts. The challenge lies in the need to measure the thickness of ~10 nm thin strips of amorphous silicon on textured silicon wafers. No practical tool to verify the quality of these contacts was available. Our approach was a new optical profilometry based on Raman spectroscopy [2], in which Raman scattering from the underlying wafer was attenuated by the a-Si:H strip. Using a suitable Raman excitation wavelength, it is possible to detect thin film profiles with a precision better than 1 nm on both flat as well as textured wafers, leading to 3D maps as shown in Fig. 2. Even though the paper has received little attention (7 citations), the method was identified as one of three **Key Exploitable Results** of the NextBase project because it could serve as a real-time diagnostic tool for IBC SHJ production lines. We have further elaborated the method, using photoluminescence imaging excited by 2 different wavelengths instead of Raman scattering, thus shortening the measurement time for one cell from hours to ~ 20 seconds. A patent application for this solution has been filed and we are looking for possible technology transfer to the industry.

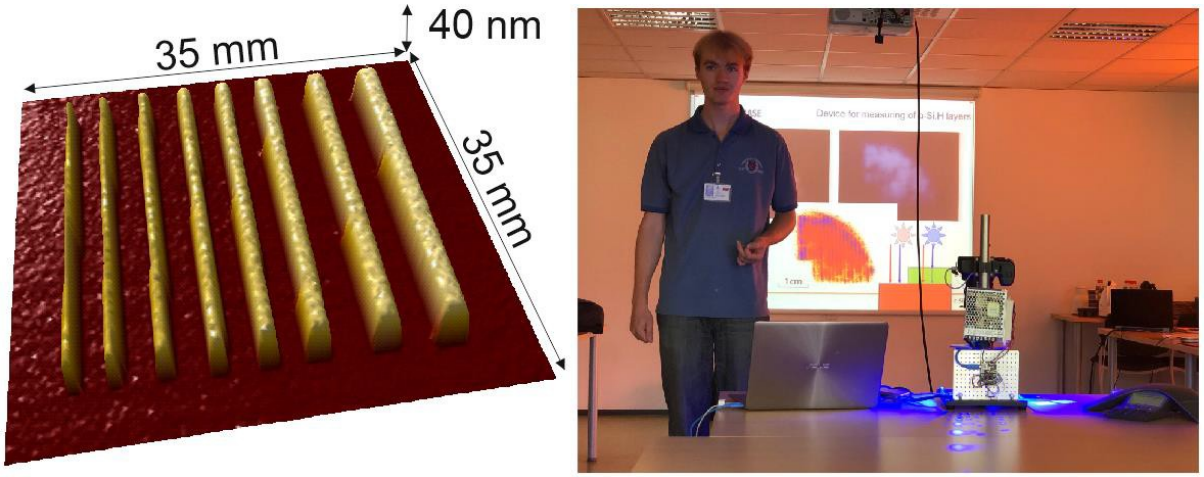

Fig. 2 Left: Three-dimensional map of amorphous strips on top of Si wafer. Right: Demonstration of a prototype instrument for rapid imaging of the contact scheme based on photoluminescence at the final NextBase meeting.

The European Commission has included the NextBase project among its Success Stories. A solar cell efficiency of 25.4 % has been achieved and industrial partners (Swiss Meyer Burger & Italian Enel Green Power) announced plans to renew the production of solar cells. The NextBase project has thus brought a competitive advantage, which makes it possible to restart production of photovoltaic panels in Europe. In this way we helped to address a paradoxical situation, i.e. when Europe plans to produce at least 30% of electricity from renewable sources by 2030, but imports a vast majority of solar panels from Southeast Asia.

ii) thin films of hybrid organometallic perovskites

The strongest competitor to Si wafer-based cells are now hybrid organometallic perovskites (methylammonium lead iodide, $CH_3NH_3PbI_3$ or $MAPbI_3$). Since the fabrication of the first perovskite solar cells in 2009, this class of material has been researched intensively, leading to a solar cell power conversion efficiency currently exceeding 25% (reported by the joint KRICT and MIT team in October 2020). Making full perovskite cells is beyond our reach, but we have cooperated with the foremost teams of EPFL Neuchatel, Switzerland and KAUST, Thuwal, Saudi Arabia, and we used our characterization methods to explore some relevant fundamental properties of this fascinating class of materials. The cooperation has led to several high-profile publications, with three of them receiving the status of Highly Cited in Field on the Web of Knowledge. The most prominent of them is paper [3] from 2014 with over 1500 citations on the sharp optical absorption edge, which is visible in the spectra in the left part of the Fig. 3. The result required a method for measuring low absorptance, in this case by Fourier-transform Photocurrent Spectroscopy, FTPS, developed at FZU [4]. Please note the log scale of the y axis in the left plot of the Fig. 3, in which the drop follows a straight line, so called Urbach edge, with a slope corresponding to so called Urbach energy. Urbach energy for $MAPbI_3$ is as low as 15 meV. Such a low value proves high electronic quality of these films, which enables high voltages in solar cells.

We also contributed to a highly cited paper [5] on Organic–inorganic halide perovskite/crystalline silicon four-terminal tandem solar cells, one of the first attempts at such a type of tandems.

The third of the highly cited papers [6] from 2019 completes the investigation of the optical spectra by focusing on the temperature dependence of optical absorption spectra for MAPbI3, with specific attention to its Urbach energy, see the central panel of Fig. 3. Firstly, we found clear further evidence for the universality of the correlation between the Urbach energy and the open-circuit voltage losses of solar cells. Secondly, we found that the temperature-independent contribution of the Urbach energy (proportional to the static defects density) of MAPbI3 is 3.8 ± 0.7 meV, which is smaller than that of crystalline silicon (Si), gallium arsenide (GaAs), indium phosphide (InP), or gallium nitride (GaN). The right part of the Fig. 3 compares the values and underlines the remarkable optoelectronic properties of perovskites.

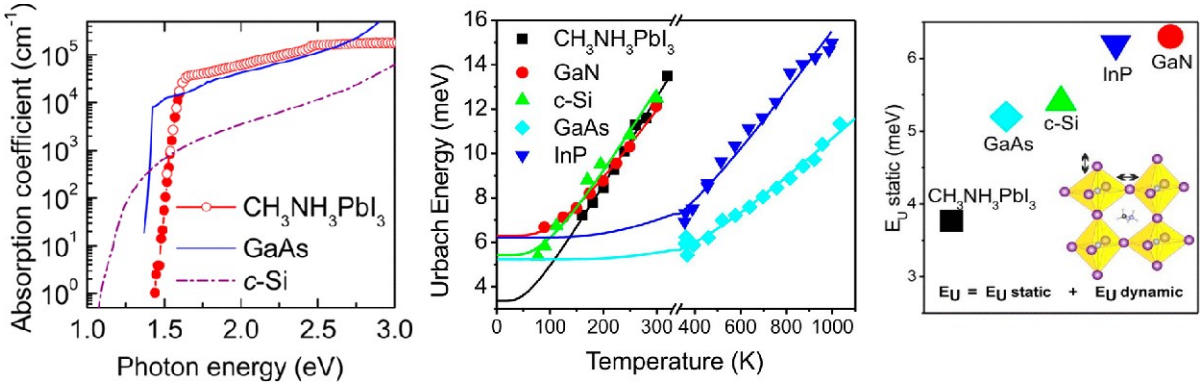

Fig. 3 Left: spectra of Optical absorption in $CH_3NH_3PbI_3$ in comparison with GaAs and crystalline silicon (c-Si). Middle: Comparison of the Urbach energy temperature dependences for selected standard bulk crystalline semiconductors and $MAPbI_3$ thin films. The temperature scale is split into two parts with different ranges. Right: the comparison of the static Urbach energy values, obtained from the temperature measurement, for opto-electronically most relevant semiconductor mono-crystals and $MAPbI_3$ thin film.

G2. Nanoscale Materials and Systems (group of Jiří Červenka)

Thin films described above are nanostructures confined in one dimension only. With small modifications of the deposition system, the PECVD can produce nanostructures confined in 2 (nanowires) or 3 (nanoparticles) dimensions. The growth of silicon nanowires (SiNWs) is mediated by catalytic metal nanoparticles previously prepared on the substrate. Nanowires may have diameters from 10 to 100 nm and lengths up to several μm. Nanowires can be coated by a thin amorphous silicon layer forming a radial p-n junction. We have studied the role of different catalysts [7], lateral growth of nanowires and other growth parameters [8] in order to explore an alternative design of photovoltaic cells [9], in which the **geometrically thin but optically thick solar cell design** is realized (see Fig. 4).

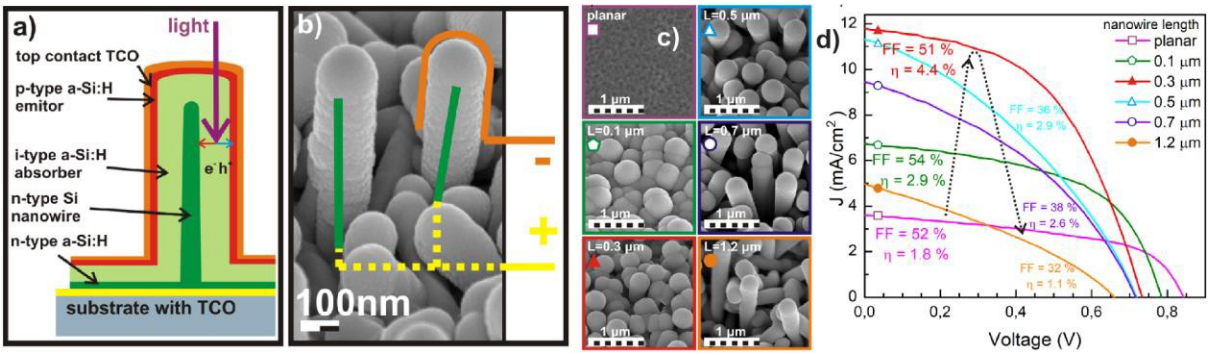

Fig. 4 a) Design of solar cells based on SiNWs, b) contacting design, c) SiNWs at different lengths and d) corresponding PV characteristics

PECVD is also used in our lab for the synthesis of crystalline and amorphous Si nanoparticles in a glass tube reactor system using a non-thermal plasma. This synthesis method enables the preparation of large quantities of luminescent Si nanoparticles, with sizes of 5-20 nm. This topic will be described below as a joint activity with the G3. The possibility to produce SiNCs has also enabled hitherto unpublished electrochemical experiments on lithium intercalation into SiNCs, for which a patent application has been filed.

The scope of G2, however, does not include only the synthesis of silicon nanomaterials, but also research into carbon-based materials, such as graphene. The research of graphene has been done predominantly in collaboration with The University of Melbourne, where J. Červenka worked for 4 years. Together with our Australian colleagues, we have developed ultrasensitive electronic sensors using graphene field-effect transistors [10] and liquid gated Hall effect sensors [11]. We have also developed novel nanoporous biocompatible membranes for single-molecule-level detection and purification of circulating nucleic acids [12].

G3. Laser Spectroscopy of Silicon Based Nanostructures (group of Kateřina Kůsová)

Silicon nanocrystals can be made to emit light relatively efficiently (even though bulk Si crystal does not emit light), which makes them promising candidates for optical and biological applications. Following a breakthrough discovery of porous silicon luminescence in 1991, Si nanoparticles are studied by laser spectroscopy in G3. Much of the research in the past had been focused on **oxide-covered SiNCs**, prepared by electrochemical etching in our laboratory. Later, using our original approach, these

SiNCs (with indirect bandgap) were **re-passivated** and capped **by methyl groups** using a photochemical treatment in a mixture of aromatic hydrocarbons in order to **tensile-strain** them and to achieve a **switch-over to direct bandgap**. The resulting modified SiNCs are characterized by 10,000x faster emission rates, implying a 10,000x increase in the overall emitted intensity. Further research of these modified SiNCs included low-temperature single-nanocrystal photoluminescence spectroscopy [13]. These measurements, carried out in cooperation with the Faculty of Mathematics and Physics of Charles University in Prague, revealed, after careful analysis, a somewhat controversial radiative recombination channel, namely the radiative recombination of a trion quasiparticle, see Fig. 5. Both sample preparation and the analysis of the measurement results were performed by our group. K. Kůsová received a **prize from the Czech Science Foundation** for the results of her research project.

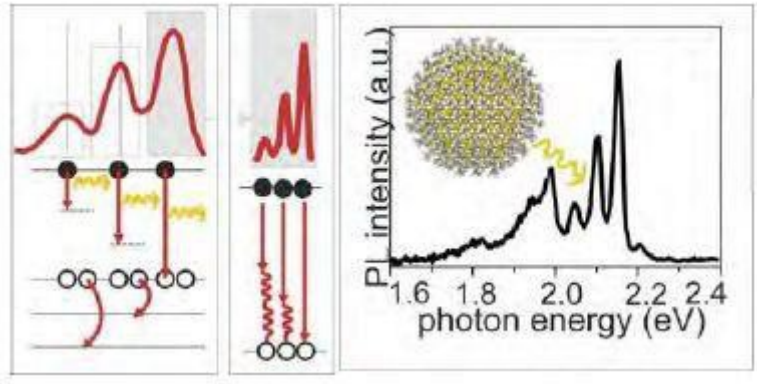

Fig. 5 Direct-band silicon nanocrystals coated with methyl groups -CH3: Scheme of the formation of a trion emission line by radiant recombination of an electron with one of two holes occupying the surface near the top of the valence band (left panel), part of the recombination energy is passed to the second hole. Diagram of phonon replicas of each line by passing a part of the electron-hole energy to the oscillations of the crystal lattice of the nanocrystal (middle panel) and the experimentally obtained spectrum (right panel).

The main drawback of this line of research was a very small amount of the modified, highly emissive, sample. Therefore, further research was directed at using the experience of the G2 team with PECVD systems and building a chamber dedicated to the synthesis of SiNCs in a non-thermal plasma, based on published protocols, which yields much higher amounts of SiNCs. These synthesized SiNCs are then to be further surface-modified by a plasma-based treatment to optimize their light emission properties.

The first success in this line of research was the novel method we proposed for surface modification of nanoparticles, which, in the case of oxidized SiNCs, leads to a several-times increase in the emitted intensity. This method is unique, because it relies only on using water and air, with no other chemicals being necessary, for the incorporation of air-originating nitrate and nitrite complexes onto the surface layer of nanoparticles. It is the subject to a **pending international patent** [14].

Our capability to synthesize larger amounts of SiNCs has also led to a new collaboration aimed at using silicon nanostructured anodes in lithium ion batteries. This line of research is currently in its very first stages.

G4. Nanophotonics and Quantum Optics (group of Lukáš Ondič)
The G4 group grew out of G3 after L. Ondič was awarded the **Lumina Quaeruntur prize**, which also includes substantial funding for 5 years for starting a new research direction, namely the use of Si vacancy (SiV) centres in diamond photonic crystals as a single photon source for quantum optics. The distinction of G3 and G4 is thus very recent and made for clarity only, as both groups use the same research tools (ultrafast optical spectroscopies) and have a joint history of research.

Light-emitting optical centres such as nitrogen-, silicon- or germanium- vacancies in diamond are well-known for their single-photon properties. Combining these centres with photonic nanostructures is an essential step for their practical application in photonics or sensing. Most of the diamond-based photonic devices studied so far have been fabricated on mono-crystalline diamond. On the other hand, we have shown that for some applications polycrystalline diamond, which is far cheaper and more easily up-scalable compared to the monocrystalline diamond, also can be used to successfully manipulate light-emission from the SiV centres. One of the issues we have tackled is that most of the light generated in diamond is trapped inside due to the phenomenon of total internal reflection. We have prepared two-dimensional photonic crystal slabs from polycrystalline diamond thin layers with a high density of SiV centres employing bottom-up growth on quartz templates (Fig. 6). More than 14-fold extraction enhancement of the SiV centres photoluminescence was achieved compared to an uncorrugated sample (Fig. 6) [15]. Furthermore, most of the extracted light was outcoupled in the normal direction, which simplifies the collection of the emission. Computer simulations confirmed that the extraction enhancement originated from the efficient light-matter interaction between the light emitted from the SiV centres and the photonic crystal slab (Fig. 6).

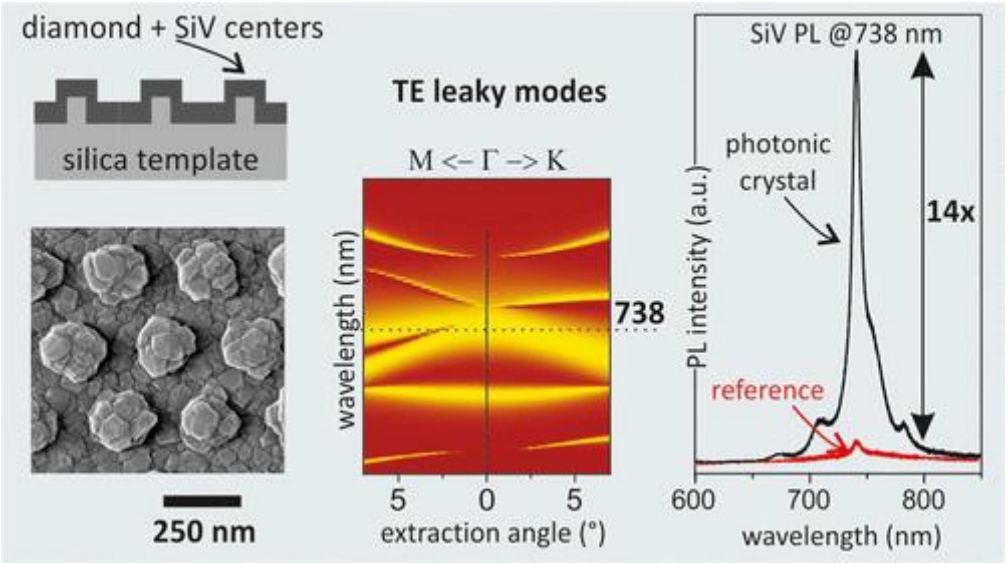

Fig. 6 Top left shows a cross section of a photonic structure. The actual 2D photonic crystal imaged by scanning electron microscopy is below. In the middle is the so-called band structure of light modes of a given structure, demonstrating the existence of a mooring channel at 738 nm. On the right is a comparison of the photoluminescence spectrum of a 2D photonic crystal and a planar reference showing a 14-fold increase in the photoluminescence signal intensity at 738 nm.

As a second step of the performance optimization of such a photonic crystal structure, the vertically-extracted photoluminescence intensity was maximized by also employing the resonant excitation of the SiV centres. A more than 100-fold enhancement in the

emission intensity was obtained using the resonant excitation and extraction scheme [18].

It should be noted that a close collaboration exists between G4 and the group of carbon nanostructures led by A. Kromka, part of the neighbouring department 27, which produces the polycrystalline diamond thin films. Very close cooperation on diamond nanoparticles exists also with G5.

G5. Nanomaterials and Functional Interfaces (group of Bohuslav Rezek and later of Štěpán Stehlík).

In the past five years the group has focused on modifications and detailed understanding of nanodiamond (ND) properties toward their molecular size. In 2015 we published a highly cited work [16] where we introduced an efficient way for obtaining pure sub-10 nm high-pressure high-temperature nanodiamonds (HPHT NDs) by simple annealing in the air followed by centrifugation of ND colloids. Most importantly, the work demonstrated the **stability of the diamond crystalline structure down to 1 nm**, which was experimentally confirmed by scanning transmission electron microscopy for the first time (Fig. 7). The work also provided the first comparison of monocrystalline HPHT NDs and defective detonation nanodiamonds (DNDs) at the comparable, sub-10 nm size scale, which revealed overestimation of the phonon confinement effect so far routinely applied to explain the broad and shifted diamond Raman peak of DNDs. In following work, we demonstrated the possibility to **reduce the size of individual DNDs from 5 nm to 2 nm controllably and with a high yield** by annealing in air [17,18]. The work [18] also showed insensitivity of the DND Raman diamond peak parameters to the size reduction of DNDs, as well as the fact that the diamond structure of such molecular-sized DNDs is preserved. It was concluded that the broadened and shifted Raman diamond peak routinely observed in DNDs should be attributed to ~2 nm scattering domains despite the typical 5 nm mean size. The significance of these results was acknowledged by the **Otto Wichterle Prize in 2016** for Š. Stehlík.

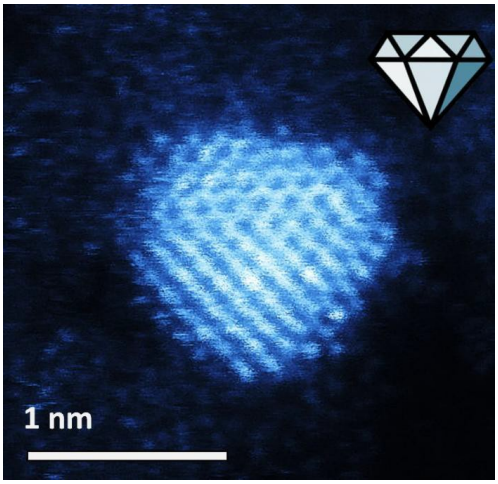

Fig. 7 One of the smallest nanodiamonds observed by STEM.

The field of molecular-sized NDs was further advanced in 2017 in [19] where 2 nm hydrogenated DNDs with positive zeta potential were prepared and used to form nucleation layers with world record parameters (in terms of density, thickness and flatness) for the subsequent growth of **unique ultra-thin, sub-10 nm nanocrystalline**

diamond films (NCD) with switchable SiV photoluminescence (see the G4 above). The critical thickness (or size) of the diamond film within which the SiV PL can be fully switched between on and off states by oxygen and hydrogen surface chemistry terminations was experimentally determined to be 10 nm. Focus on this topic is due to Š. Stehlík's role as the principal investigator of a junior-GACR grant (18-11711Y) titled "*A way to quantum-sized diamonds"*, which focuses on ultra-small NDs, their preparation, isolation, characterization, understanding and investigation of their physico-chemical properties.

The latest achievement of the group came from the cooperation with the Czech Technical University, the Military Research Institute in Brno and Uppsala University, Sweden. We have demonstrated the promising **potential of TiO_2/ND composites toward photocatalysis** [20]. The work introduced NDs as water-compatible, stable, nontoxic and readily available material, which can be easily applied in synergy with TiO_2 to achieve an efficient (photo)degradation of toxic organophosphate compounds. Thanks to suitable ND surface chemistry the TiO_2/ND nanocomposites were achieved in the form of a homogeneously inter-grown nanostructure of TiO_2 matrix with embedded primary and aggregated NDs (Fig. 8). Several **structural and electronic effects at the TiO_2/ND interface** were proposed and the appropriate model was presented. The work also **gained significant media attention** (national TV networks), which is understandable as the organophosphate compounds include dangerous chemical warfare agents. An example cited was Soman, listed by the UN resolution as a weapon of mass destruction, along with Sarin and Tabun, all nerve agents of the organophosphate class.

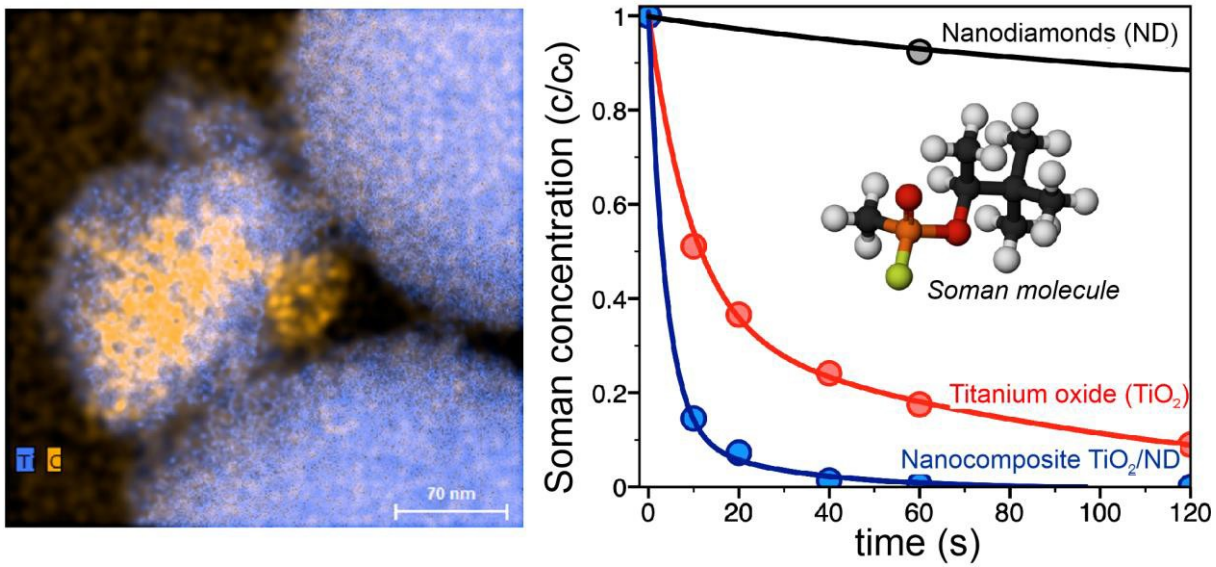

Fig. 8 Left: an image taken with transmission electron microscope shows the nanodiamonds (orange) dispersed in the titania matrix (blue) in the nanocomposite. Right: The decomposition of warfare agent Soman using pure titania, nanodiamonds and their nanocomposite, which was the most efficient.

Other research

In order to present a coherent story, we have skipped a number of results. For example, the joint work with EPFL on Passivating electron contacts based on highly crystalline nanostructured silicon oxide layers for silicon solar cells [21], an alternative route towards heterojunction solar cells, which by now has achieved over 60 citations. We have not described other works on microscopies of PV structures [22] or first

experimental quantification of useful and parasitic absorption of light in plasmon-enhanced thin silicon films for solar cells application [23], performed in cooperation with IMM CNR at Catania, which received 32 citations. We have only touched on the cooperative research on alternative uses of graphene [24–26].

Our groups are also part of the institute-wide Solid21 project (Solid state physics for the 21st century), with activities in three of the five work packages. Within this project we have undertook to install and operate a new setup for atomic layer depositions (ALD), which will be become a part of the technological base of the institute.

Finally, let us mention one more topic explored in cooperation with the industry, namely with HVM Plazma, s.r.o.. We started our cooperation through contractual research in 2015, at first exploring nitride or carbide protective thin films for various uses. This grew into a research supported by several projects of the Technological Agency of the Czech Republic. Since 2018 we take part in collaborative research building on our experience with plasma treatments, but this time for a different purpose. The cooperation takes place within a National Centre of Competence Matca, subproject PlasGas with the goal to perform plasma **waste treatment of hazardous substances**, including biological waste from hospitals. The heat of a plasma torch (operated at 1200 °C) can fully gasify both inorganic and organic materials, yielding mainly a mixture of H_2 and CO (the synthetic gas) and vitrified solid slag. The prototype setup, nicknamed GOLEM, (Fig. 9) is being operated at the Institute of Plasma Physics for tests with a capacity of around 100 kg per hour. Besides the guaranteed removal of biological hazard, the setup is able to partially recycle also the energy stored in the chemical compounds. We point this out in order to highlight the potential of the team for achieving not only excellent scientific results, but also to take part in the technology transfer and practical applications in everyday life.

Fig. 9 Prototype setup GOLEM explored for Plasma Gasification of hazardous waste, with T. Mates, responsible researcher at FZU and HVM Plazma (in the left) and M. Jeremiáš, head of department of Plasma Chemical Technologies, Insitute of Plasma Physics (in the right)

Research activity and characterisation of the main scientific results

Outline

Our primary concern in the current evaluation period 2015-2019, concerning the excellent rating obtained in the previous evaluation, was to keep the exclusive position of the team in the field of method development for structure analysis. To this aim, we had to reinforce our traditional tools and react to the latest challenges in our field. Our tasks in the current evaluation period were as follows:

1) Development of the long-awaited program JANA2020, the successor of the successful software JANA2006.
2) Development of experimental and computational methods for 3D electron diffraction.
3) Development of methods for magnetic structure analysis and description. Theoretical investigation towards understanding the interactions leading to magnetic order. Establishment of a group dedicated to magnetic structures.
4) Further development of methods for modulated structures.
5) Enhancement of mineralogical crystallography with particular regard to the nano-crystalline uranium minerals.
6) Establishing a new field of mathematical crystallography.
7) Enhancement of chemical crystallography utilising the laboratory ASTRA established in the previous evaluation period. Advancement of pharmaceutical crystallography. Opening a new field of sponge crystallography.
8) Dissemination of our methods.

JANA2020

The JANA program (Petříček et al., 2014) is a comprehensive tool for the analysis of crystal structures from x-ray, neutron and electron diffraction. For our team, it represents an essential computational tool, to which we gradually add other programs solving partial problems, such as SUPERFLIP (Palatinus and Chapuis, 2007) and DYNGO (Palatinus et al. 2015a, 2015b). The program is used worldwide by around 3,000 users, mainly for solving complicated structures. The latest version of the program, JANA2006, was continuously developed until the end of 2019. However, it became strongly evident that the technical solution of the user interface based on in-house developed graphic objects is no longer sufficient for the requirements of a modern computer program. The work on the new version, JANA2020, began in 2018 as part of the Czech Science Foundation project No 18-10504S. Our goal is to create a universal crystallographic toolbox, applicable for the most demanding tasks of modern crystallography, yet at the same time furnished with the most intuitive user interface. The intuitive graphics-driven user control will be based on a new visualisation scheme for crystal structures. The user, while editing structure parameters by clicking on visualised parts of the crystal structure, will be able to see the changes of the crystal structure or the residual density immediately during refinement cycles. The existing tools of JANA2006 will be improved and extended by an indexing tool for powder diffraction data, graphical editing of modulation functions, and full support for higher-dimensional nuclear and magnetic structures. The resulting software, JANA2020, will have a complete undo/redo system and the possibility to switch between the primary and advanced modes. These possibilities will facilitate all tasks of modern structure analysis and will be especially useful for intuitive analysis of modulated structures.

Given that the JANA2006 code is very complex, the conversion of graphical tools into the OpenGL environment was a difficult task. During the years 2018-19, it was possible

to convert all graphic tools, create a drawing tool for crystal structures and revise most of the computational methods included in the program. As of December 31st 2019, the development of the 2006 program has been completed, wherefrom this date on only errors are eliminated. The JANA2020 program exists in the alpha version tested by several selected users. The program will be made available to all users by the end of 2020.

In parallel with the development of the JANA2020 program, we implemented part of the planned documentation project, where the methods of the JANA program are described in a series of publications following the introductory article from 2014 (Petříček et al., 2014). In the period under review, we described the way the JANA program handles twin structures (Petříček et al., 2016a), as well as the original concept of discontinuous modulation functions (Petříček et al., 2016b). Furthermore, several exciting modulated phases were solved: a study of hydrophobic amino acids as a rare example of single- crystal structures where two phases are present simultaneously (Görbitz et al., 2016); a study of the high-pressure silicate K1.5Mg2Si2O7H0.5 formally looking like (3+2)d commensurately modulated structures but finally confirmed to be an orthorhombic (3+1)d commensurately modulated three-fold twin(Welch et al., 2016); and a study contributing to the problem of solution and refinement of modulated structures of protein crystals (Lovelace et al., 2019).

Electron crystallography

Electron diffraction is a technique that allows crystal structure analysis to be performed on tiny crystals, down to about 10 nm in size. Although the principles of the technique were known for decades, it was only about 15 years ago that the instrumentation and computational methods had progressed sufficiently to make structure determination by electron diffraction feasible. Since the first reports (Kolb et al., 2007, Kolb et al., 2008), the technique has quickly become very popular, and this technique now solves many crystal structures. Several flavours of the technique exist, and each of them bears a particular name. However, all are based on the collection of the three-dimensional distribution of electron diffraction patterns, and therefore the approach is generally called three-dimensional electron diffraction (3D ED). Our department has been active in the development of this method since 2009. We have developed a complete suite of software starting from the software for data collection through data processing (Palatinus et al. 2019) to the solution and accurate refinement of crystal structures (Palatinus et al., 2015a, 2015b).

The main emphasis of our research has been on the inclusion of so-called dynamical diffraction effects in the calculation of model diffracted intensities. Dynamical diffraction is an important effect present in electron diffraction, while it is almost absent in standard x-ray diffraction on small crystals. Dynamical effects modify the diffracted intensities with respect to the expectation of the simpler, x-ray-like kinematical approximation. However, including dynamical effects in the calculations is mathematically and computationally challenging. Therefore, it is customary to ignore the dynamical diffraction effects and use only the kinematical approximation. This results, however, in less accurate structure models and a decreased sensitivity to fine structural details.

We have succeeded in implementing the calculation of dynamical scattering effects in the program DYNGO, which acts as a service program used by JANA2006 to assist with these complicated calculations. The user can then use JANA2006 to determine the structure from electron diffraction in almost the same manner as with other radiation sources, and still achieve quite a good accuracy of the structure model. The

implementation and test results were described in a mini-series of two papers (Palatinus 2015a, 2015b). They marked the start of the “dynamical era” in structure determination from electron diffraction.

Figure 2: Front-cover of the magazine Science highlighting publication of Palatinus et al., 2017.

In the following years, we developed our research in two directions: further development of methods of electron crystallography, and applications to interesting scientific problems. In the methodological part, we focused on exploring the limits of the dynamical refinement and showing that it can solve previously unsolvable problems. One of the breakthroughs was a demonstration of the possibility to detect the positions of hydrogen atoms in both organic and inorganic nanocrystals (Palatinus et al., 2017), (Fig. 2). This work marked a change in perception of the capabilities of electron diffraction methods, and the ability to “see” hydrogen atoms has changed, very quickly, from something considered almost impossible to a mark of the quality of structure analysis by 3D electron diffraction.

The second crucial methodological breakthrough was the demonstration that 3D ED can be used to determine the absolute structure of a non-centrosymmetric crystal. The indication that this is not only possible but very straightforward was given already in the original paper about the dynamical refinement (Palatinus, 2015b). However, the real breakthrough came with the proof that the method is sufficiently robust and sensitive to be used in the analysis of beam sensitive organic materials. This proof was convincingly demonstrated by the determination of the absolute structure of a cocrystal of a pharmaceutical molecule sofosbuvir and an amino acid L-prolin (Brazda et al., 2019). This result is of utmost importance for pharmaceutical research and industry, as the determination of absolute structure is a crucial part of the characterisation of pharmaceutical compounds, and these compounds often form only tiny crystals unsuitable for analysis by other methods than 3D ED.

Other methodological works include the implementation of dynamical refinement to twinned crystals (Steciuk et al., 2019) and the implementation of dynamical refinement of modulated structures (Weidemann et al., 2017). Significant progress has also been obtained in the analysis of electron diffraction data (Palatinus et al., 2019). The contribution of our group to the development of 3D ED methods was also reflected in the invitation to contribute to the review paper on the history of 3D ED methods (Gemmi et al., 2019). This work summarises the key developments in the field and which is becoming a standard reference paper in this field.

The 3D ED method finds application in many fields. We have applied the 3D ED methods and dynamical refinement to a wide range of materials and problems, resulting in more than 30 publications in the period 2015-2019. Here we give a short account of some of the results. We have contributed to the analysis of new extra hard carbon-containing Fe-Ni-Cr-Si alloy (Bowden et al., 2018). Here the dynamical refinement method turned out to be of central importance because the analysis required the localisation of a small number of carbon atoms, which turned out to be impossible with other methods. We have solved the structure of vaterite – an elusive polymorph of calcium carbonate, which resisted the correct structure description for many decades (Steciuk et al., 2019). We could show that the real structure is an incommensurately modulated one regarding the stacking of CaCO3 layers. We also

contributed to the structural analysis of orthorhombic CuMnAs thin film – an important antiferromagnetic material studied thoroughly for its potential applications in spintronics. 3D ED analysis also helped us to understand the structure of TaS_3 – a material studied by physicists for a very long time, but lacking a correct structural description until our work (Mayorga-Martinez et al. 2017). Another work demonstrating the power of the 3D ED technique in combination with dynamical refinement was the structure analysis of the intermetallic Ni_8Ti_5 – a new phase in the Ni-Ti system. Thanks to the advanced analysis, we were able to identify the distribution of Ni and Ti in the structure despite their close scattering powers. In a long-term collaboration with the chemists from the Institute of Inorganic Chemistry of the CAS, we have determined several structures of a new class of metal-organic framework material (Hynek et al. 2018). Last but not least, several new mineral structures have been solved by 3D ED, mostly in collaboration with the group of mineralogical crystallography (see section Mineralogical crystallography), but also in collaboration with other researchers (Skacha et al. 2016, Gemmi et al. 2016).

Magnetic structures and magnetic crystallography

Magnetic phases and transitions are essential in various research fields, from fundamental to applied physics or materials science. Experimentally, the fundamental interactions that govern the neutron scattering by ordered magnetic phases lead to nuclear and magnetic scattering. The measured diffracted intensities and the direction of the magnetic scattering with respect to the incident neutron beam are used to determine the amplitude and orientation of the ordered spins within the material. The ordering of magnetic moments in a crystalline material is intrinsically linked to the underlying symmetry of the crystal lattice that characterises the positional periodicity of the atoms carrying magnetic moments within the material. The translational periodicity of the magnetic phase either corresponds to one of the paramagnetic phases, or it is violated in a commensurate or incommensurate manner.

The description of a magnetic structure includes the assignment of the relevant symmetry modes for the spin configuration and its constraints consistent with the parent paramagnetic phase and the magnetic propagation vector(s). In this context, two well-established methods are mostly used. Representation analysis is a method in which the set of possible magnetic configurations is given by the spin modes transforming as one or more physically irreducible representations (*irreps*) of the paramagnetic space group (Bertaut, 1968). In the second concept, the magnetic symmetry can be expressed in the form of a magnetic (Shubnikov) space group (commensurate ordering) (Koptsik, 1966; Bradley and Cracknell, 1972) or magnetic superspace group (incommensurate ordering) (Janner & Jansen, 1980; Petříček et al., 2010; Perez-Mato et al., 2012).

These two approaches are not equivalent in general, but they can be efficiently used in a complementary way (Petříček et al., 2010). This innovative, combined approach is implemented in the magnetic option of JANA2006. It allows the construction of possible alternative magnetic models for the symmetries given by each *irrep* epikernels and kernel for both commensurate and incommensurate magnetic structures. This approach is similar to the one used in the program ISODISTORT (Campbell et al., 2006), which can be run separately from JANA2006. Currently, the routine for magnetic structures within the program JANA2006 is capable of handling different sets of diffraction data to consistently solve and describe commensurate and single-*k* incommensurate magnetic structures based on symmetry considerations. For each magnetic space (or superspace) group, the symmetry information is systematically

used to derive the magnetic structure factors, analyse the symmetry of the diffraction data, and constrain magnetic and nuclear parameters. In the latest versions, the modulated magnetic waves can be restrained to keep an elliptical or cycloidal form. The user can explore this listing to check the different magnetic configurations to be tested against the experimental data. The analysis of the different models can be done through simulation of powder profiles or by visualisation in external programs. The magnetic option of JANA2006 is one of only a few existing tools capable of handling modulated magnetic structures coupled (or not) with structural modulations.

In the period 2015-2019, the magnetic option in JANA2006 was continuously developed and tested by experimental data and feedback from the neutron users and instrument experts worldwide. During the last five years, we have fine-tuned the previously developed tools (Petříček et al., 2010; Perez-Mato et al., 2012) and presented the resulting new possibilities of JANA2006 at the most important neutron facilities such as Oak Ridge National Laboratory (16-18.6.2015 and 22-23.10.2019), Institute Laue- Langevin (12-16.12.2016), MLZ (26-27.10.2017), ISIS neutron source (11-13.4.2018), and European Spallation Source (12.9.2018). We also participated in the Erice School on magnetic crystallography (31.5.-9.6.2019) and at the Neutron Diffraction and Imaging for Newcomers – Satellite meeting of the 32nd European Crystallographic Meeting (14-17.8.2019). The use of the magnetic option was also presented in invited lectures at the Aperiodic 2018 – the ninth conference on Aperiodic Materials (8- 13.8.2018), at the ILL-ESS European User Meeting 2018 (10-12.10.2018), and the 77th Pittsburgh Diffraction Conference (24-26.10.2019). This concentrated effort helped us to establish JANA2006 and its “symmetry approach” as the now recommended tool among the neutron diffraction user community.

Our own most essential contributions to the practical solution of magnetic structures were published in Gorbunov et al. (2018a) (Fig. 1) and Gorbunov et al. (2019) and resulted from a post-doctoral stay at the Institute Laue-Langevin (Grenoble, France) to study the magnetic ground-states of f-based intermetallic systems by neutron scattering techniques.

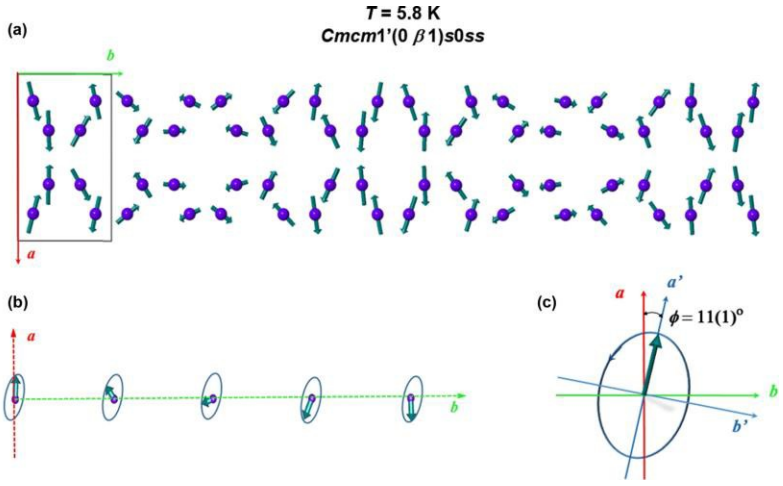

***Figure 1**: The incommensurate magnetic structure of Dy2Co3Al9 at 4.5 K: (a) the Dy atoms (purple spheres) and their magnetic moments (green arrows); (b) the magnetic moments describe a collinear transverse oblique spin wave that propagates parallel to the b axis. (c) Within the ab plane, the magnetic moments are inclined from the a axis (Gorbunov et al., 2018a).*

12 2018b). On another family of compounds, it was shown for the first time how the microscopic rotation of individual magnetic moments from two distinct sublattices occurs through a field-induced phase transition in a ferrimagnet (Gorbunov et al., 2019). The experiment used a unique combination of x-ray magnetic circular dichroism experiments in pulsed fields up to 30 T, supported on the zero-field structure solved from neutron scattering data. The powerful combination of x-ray magnetic circular dichroism using synchrotron hard x-rays in pulsed magnetic fields and neutron scattering is pioneering.

To further develop these results, MH was awarded a Junior project, No 19-07931Y of the Czech Science Foundation to study 'Magnetic structures and electronic properties of low-dimensional and frustrated intermetallic *f*-systems'. One of the main goals of this project is to establish a research group on magnetic structures within the group of Structure Analysis. The ongoing work is a result of an outstanding international collaboration among some of the best European research facilities as ESRF (Grenoble, France), LNCMI (Toulouse, France), HMFL-HZDR (Dresden, Germany), DESY (Hamburg, Germany), MLZ (Munich, Germany), FZU (Prague, Czech Republic), and Charles University (Prague, Czech Republic), and Hiroshima University (Hiroshima, Japan).

Fundamental aspects of magnetic order

Magnetic order arises from the interaction between magnetic moments as well as from the interaction between magnetic moments and the crystal field. Magnetic order has profound implications for the macroscopic properties of materials. The energetic aspects of the anisotropy of the magnetic order are of paramount importance for magnetic recording.

The interaction between individual magnetic moments has its origin in the Pauli exclusion principle. In the ground state, the magnetic moments are usually collinear. However, in the excited state, various non-collinear configurations may arise. This is the case of spin waves. Our interest was the spin-wave stiffness, which is a quantity needed for multi-scale modelling of the domain structure of magnetic materials. Specifically, we studied how the spin-wave stiffness of permalloy ($Fe_{19}Ni_{81}$) is affected by doping by atoms of a different kind (Šipr et al., 2019). We found that the rate of change of the spin-wave stiffness upon introducing the dopants can be described by just considering the influence of the atoms in the first coordination shell. This is important not only for principal reasons but also from the technical point of view because the accurate evaluation of the spin-wave stiffness constant is quite demanding computationally and our results show a way to by-pass it. Another fundamental finding is that the hybridisation between impurity and host states is more important for the stiffness than the polarizability of the impurity.

The interaction between magnetic moments and the crystal field (i.e., the Coulombic field generated by the crystal lattice) gives rise to the magnetocrystalline anisotropy (MCA), which is a phenomenon hotly studied because of implications, among others, for magnetic recording. First, we focused on understanding the physical picture. Although it has been known for decades that MCA is linked to spin- orbit coupling (SOC), the mechanism of how it arises for specific systems is still a subject of debate. We focused in our work (Šipr et al., 2016a) on finding markers of SOC in the density of states and on using them to understand the source of MCA for the case of adatoms and monolayers. We found that a significant contribution to MCA for adatoms comes from pushing the SOC-split states above or below the Fermi level. As a result of this, the MCA energy depends crucially on the position of the energy bands of the adatom

with respect to the Fermi level of the substrate. In a related work (Šipr et al., 2016b) we studied the influence of SOC on the magnetic dipole term $T\alpha$, which is important for analysing x-ray magnetic circular dichroism spectra via the spin moment sum rule. We found that the dimensionality of the system is the crucial factor for deciding whether the influence of the SOC on $T\alpha$ can be neglected or not. For 3*d* adatoms, the influence of SOC on $T\alpha$ can be significant, whereas for monolayers it is always practically negligible.

We also dealt with the practical aspect of the magnetocrystalline anisotropy. Namely, it is a tiny (albeit very important) quantity, and its evaluation is often at the limits of accuracy of numerical ab-initio calculations. We undertook a comprehensive study of the MCA of a layered compound FePt, comparing two different computational approaches, to identify critical factors affecting its accuracy (Khan et al., 2016). Finally, we also investigated the interplay between magnetic order and crystal order or, more specifically, the influence of local environment effects on magnetic properties of a substitutional alloy (Khan et al., 2017).

Mineralogical crystallography

Mineralogical crystallography has a very long tradition in our team, with emphasis on the description of twinning, polytypism, order-disorder (OD) phenomena and modulated structures. Furthermore, in recent decades Mineralogy itself has changed to be a less purely descriptive and more interdisciplinary research discipline. Along with the description of new minerals, which we still consider as challenging (because structures are unknown), a precise crystal structure is a necessary input for advanced solid- state physics and chemistry methods. These involve the calculation of thermodynamic and other properties from first-principles using density-functional theory (DFT).

We fully benefit from the computational power of the program JANA2006, which has been specially developed for the refinement of challenging structures. During the past five years, our mineralogical research has developed continuously, due primarily to the capabilities of the laboratory ASTRA, established during the previous evaluation period. Availability of a powerful microfocus x-ray source at the single-crystal x-ray diffractometer SuperNova enables the structure analysis of relatively small crystals. The limitation now lies either in the diffraction capabilities of the material itself (e.g., absorption, presence of stacking faults) or in the possibilities of preparation of tiny crystals for the analysis. The smallest crystals successfully analysed by our team measured only ~10 micrometres in diameter (Sejkora et al. 2017). The other great advantage that we possess now is the possibility of 3D electron diffraction methods enabling structure analysis of nano-sized or poorly diffracting minerals. Special preparation of samples for the analysis, involving the handling of the samples at liquid N2 temperature, enable structure analysis of thermally unstable samples, such as highly hydrated oxysalts.

As a significant success, we want to highlight that more than 30 new uranyl minerals (approximately 20% of all known U^{VI} minerals on Earth) have been discovered with the essential contribution of our team. Among them, there are several exciting phases such as the mineral ewingite Mg8Ca8(UO2)24(CO3)30O4(OH)12(H2O)138 (Olds et al. 2017) (Fig. 2). Ewingite is currently the most complex known mineral structure on Earth and represents a novel class of structures, containing nano- sized cages, which have not been reported in natural conditions. Another complicated structure solved by our team is of the mineral swamboite-(Nd), representing a rare (3+3) modulated structure (Plášil et al. 2018).

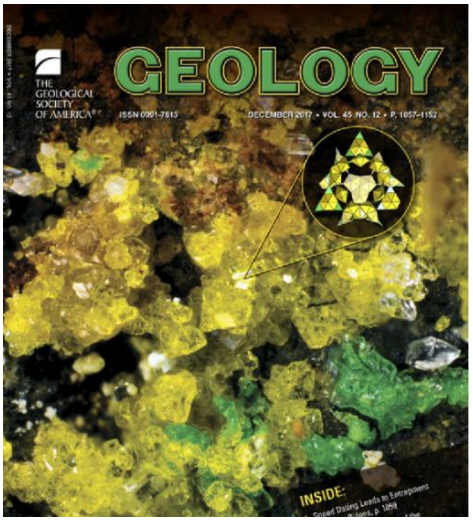

Figure 2: *Front-cover of the magazine Geology (no#1 in Geosciences according to Thompson Reuters) with the photo of mineral ewingite.*

We have contributed to the development of a relatively simple (compared to the requirements of DFT methods) computational technique that we call Torque (Ghazisaeed et al. 2018), which is based on zero-net torque, where their rotational equilibrium constrains the predicted orientations of molecular H2O. This technique allows a refinement of H-atom positions in cases in which they cannot be located appropriately from experimental data. The Torque method has been successfully applied to several U-containing structures (Ghazisaeed et al. 2019; Steciuk et al. 2019; Plášil et al. 2020), including the particularly interesting U(IV) mineral vyacheslavite, U(PO4)(OH). Employing DFT calculations optimising precise x-ray data have yielded several important results (Colmenero et al. 2019a, b, c, 2020a, b, c).

We have co-authored a purely descriptive, popular-scientific book on minerals from Jáchymov (Škácha et al. 2020; J. Plášil, ed.), which is considered as one of the most prolific and famous mineralogical localities in the world. The book was released in September 2019 by the publisher Academia.

We continued studies of cronstedtite polytypism with the aid of the single-crystal x-ray diffraction and 3D electron diffraction. A new six-layer non-standard polytype denoted as 6*T*2 was identified (Hybler et al., 2016), in the new occurrence in Pohled, Czech republic, and its structure was determined (Hybler, 2016). Polytypes 2*H*1, 2*H*2 and 3*T* in mixed crystals with 1*M* were also found. Some crystals of polytypes of the subfamily A (3*T*, 1*M*, 6*T*2) were affected by twinning by reticular merohedry. The same twinning was revealed in samples of the 3*T* polytype of cronstedtite from Nižná Slaná, Slovakia (Hybler et al., 2017). In the occurrence of Chyňava, Czech Republic, mostly 2*H*1 and 2*H*2 polytypes were present. A rare mixed crystal containing 1*T*, 3*T* and possible 6*T*2 polytypes was also found (Hybler and Sejkora, 2017). We also investigated synthetic cronstedtite crystals using 3D electron diffraction. The studies revealed the rare 1*M* polytype as the most common in the material. Other rare polytypes 2*M*1 and triclinic 3*A*, as well as a unique mixed 1T+1M crystal, were also found. The study required a generalization of standard identification diagrams for monoclinic and triclinic polytypes (Hybler et al., 2018).

Mathematical crystallography

Mathematical crystallography is a promising research field, which has been newly established in our team, in order to expand our ability to analyse and compare solved structures and find broader connections between them. To this end, within the Czech Science Foundation project No 18-10438S, we started the development of quantitative structure descriptors based on the uniform distribution theory, applicable to both standard and modulated crystals. To date, we have been able to calculate these descriptors and the ongoing research is focused on their predictive power (finding or predicting structures with similar physical properties).

We have also continued work on 'structures of structures', namely the complex microstructures of intermetallic alloys. The crystalline phases constituting a microstructure of an alloy ultimately determine its physical properties One example

from our work is the elucidation of the atomic structure of a twinned NiZr crystal (Fig. 3) from the non-equilibrium-solidified microstructure of its heavily undercooled melt by purely theoretical means (Hornfeck, 2018) and its experimental confirmation by atomic resolution electron microscopy (Hornfeck et al., 2014, 2018). This research was done in collaboration with researchers of the Institute of Materials Physics in Space, located at the German Aerospace Center (DLR) in Cologne, Germany, employing their state-of-the-art electrostatic levitation facility for alloy processing (which currently has an electromag- netic counterpart in use on the International Space Station). Our work contributes to the physical understanding of this glass-forming intermetallic compound (Kobold et al., 2017/2018).

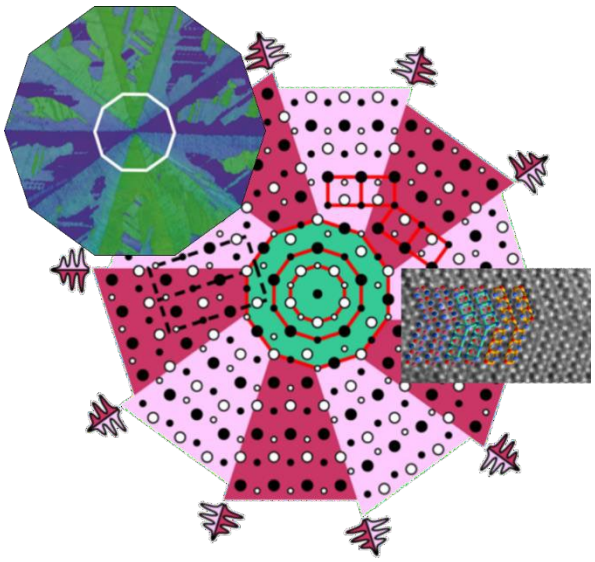

Figure 3: *Shown are the tenfold twin structure of NiZr together with its microstructure (analyzed by means of electron backscatter electron diffraction, top left) and an atomically resolved twin boundary (analyzed by means of high angle annular dark field scanning transmission electron microscopy, middle right).*

Chemical and pharmaceutical crystallography

Crystallography, at its frontier, undoubtedly belongs to basic research. On develop crystallography have a single goal, namely to provide other branches of science with a detailed knowledge of the atomic structure of crystalline substances. We are therefore developing a field where the requirements and demands of other fields are of fundamental importance. For this reason, the development of crystallography is not conceivable without the continuous supply of a wide range of samples for structure analysis.

During the period under review, we were able to program a unique web-based tool for managing requirements, results and publications of structurenalysis. This system, called LabTidy, (https://labtidy.com/) was partly created within the Gamma project of the Technology Agency of the Czech Republic, The Institute of Physics now offers it on a commercial basis. According to statistics from LabTidy, 2600 measurement requests were registered in the evaluated period, 880 samples passed tests, were measured, and their structure was solved, and in 90 cases a publication was created. These statistics are incomplete because the system has not been fully operational for the entire period, but illustrates the breadth in which we provide (academic or commercial) chemical crystallography services. Quite predictably, there are challenging cases in this volume of substances that help to develop further and tune our crystallographic programs.

The most interesting results in chemical crystallography were the determination of novel Co/Ni and Co/Zn inorganic precursors for Fischer–Tropsch synthesis (Saheli et al. 2019, Saheli et al. 2018); studies of calix[4]arenes and thiacalix[4]arenes (Kortus et al. 2019, Slavík et al. 2019, Tlustý et al. 2019, Landovský et al. 2018); determination of sulfoxide based boronates (Čubiňák et al. 2018); and determination of Schiff base complexes (Zarei et al. 2019, Barfeie et al. 2018, Hosseini-Yazdi et al. 2017). We have also collaborated intensely in research into the solid-state of pharmaceutical compounds. Examples include crystallographic studies on ibrutinib solvates (Zvoníček et al., 2017) and polymorphs (Zvoníček et al. 2018) and determination of structures of

sofosbuvir polymorphs formed by grinding (Chatziadi et al., 2019) and of sofosbuvir L-proline cocrystal (Brázda et al., 2019, see the section on electron diffraction). Several published structures were based on powder diffraction, which remains a more challenging approach compared with the analysis of single crystals (Holaň et al., 2016; Tieger et al., 2016a-b; Valach et al., 2018; Kočí et al., 2019). Within the field of powder analysis, we were able to determine the organic molecular structure of Selexipag Form I with 38 degrees of freedom, which is one of the most complex substances that has ever been determined ab initio from powder diffraction data (Hušák et al., 2019).

Within powder structure analysis, we also focused on the description of phase transformations and the in-situ study of solid-state reactions. We developed a new sample holder (Rohlíček et al., 2020 – submitted 2019) for the reaction capillary, where the controlled solid-state reaction takes place. During the reaction, the powder diffraction is collected, and the reaction is recorded in real-time. Important collaborations in this field were started with the Department of Physical Chemistry and with the Department of Chemical Engineering at the University of Chemistry and Technology in Prague (Štejfa et al., 2019).

The study of polymorphism, solvatomorphism and phase transitions is connected with the study of similarity between investigated crystalline compounds. The similarity of compounds can also be used during the determination of crystal structure from powder diffraction data to decrease the computational complexity of the refinement of the studied compound. The most straightforward method is to fix the starting model on known conformations of the studied compound. We introduced a new approach, and we have developed software for a fast and automated crystal structure comparison of molecular compounds called CrystalCMP (Rohlíček et al., 2016; Rohlíček & Skořepová, 2020 – submitted 2019).

Active pharmaceutical compounds (APIs) and natural compounds are typical examples where high- quality crystals, necessary for single-crystal x-ray diffraction, are often unavailable. To overcome this difficulty and broaden the scope of our possibilities, we started with a new method called Crystal Sponge, an approach where a stable metal-organic framework (MOF) with sufficient channel space is used as a crystalline matrix. The MOF channels are filled with an inert solvent, and the studied compound is then infused into the channels. The resulting crystal can reveal the molecular structure of the target compound without the need for its crystallisation. This method will be implemented within a new Junior project No 20-14770Y of the Czech Science Foundation awarded to V. Eigner.

Training activities

In order to spread knowledge about our methods and attract young scientists, we continued the tradition of so-called Ad Hoc Workshops on JANA2006 with topics selected by the users through the web page http://jana.fzu.cz. In the period 2015-2019, 12 such workshops took place with a total attendance of 170 people. As well as these workshops, we were invited to many external workshops and schools to speak about JANA2006, e.g. three workshops at the Shanghai Institute of Ceramics, and workshops organized at facilities in Garching, Oak Ridge, Oxford and Grenoble. In total, during the evaluation period, more than 1200 people visited our workshops (see Pedagogical activities for details). The workshops had an impact on the visibility of our methods and citations of our programs (558 citations in 2014, 936 citations in 2019, for JANA, Superflip and electron diffraction programs altogether). Besides the activities to promote JANA, people from our group are also involved in student supervision and

teaching. Altogether, in the evaluation period, seven bachelor, master and doctoral students had either the consultant or the supervisor specialist from our department.

Conclusions

During the evaluation period, we further developed the fields in which our team already belongs in the world's top crystallographic research. In the field of electron crystallography, after several years of development of experimental and computational methods, we determined the positions of the hydrogen atoms of an organic and inorganic compound. The result attracted much attention in the domestic media as being the first work of a Czech author highlighted on the cover of the journal Science. In the next step, we were able to determine for the first time the absolute structure of an unstable organic molecule from its electron diffraction data. In the field of magnetic structures, we have further improved the methods implemented in the JANA2006 program. Thanks to the user-friendliness of the methods and our broad promotional activity, we have reached the point where the JANA program is widely used in the field of magnetic structures. The program was also used for our own research of magnetic structures, where frustrated *f* ion networks were studied. Theoretical research of magnetic arrangements took place in parallel.

Last few years, we were creating a new version of the JANA program, JANA2020, which will make it possible to streamline and simplify structure analysis significantly. The new program exists in the alpha version and will be published in 2021. Another novelty is the introduction of the field of mathematical crystallography, from which we intend to gain better opportunities for comparing structures and predicting their properties. Towards the end of the period, we began work on the implementation of a sponge crystallography method that will allow structure analysis of molecules that do not crystallise.

In the field of mineralogical crystallography, we have made full use of new experimental possibilities for measuring tiny mineral samples. We managed to determine the structure of the mineral ewingite, which is the most complex mineral known so far. We contributed to the development of the Torque method for determining the orientation of H2O molecules in the crystal and published a comprehensive 800-page book on minerals in the Jáchymov region. In the field of chemical crystallography, we continued with the support of the newly created LabTidy system in the massive application of our methods to samples of various research groups. In the field of powder diffraction, we have created a sample holder for real- time monitoring of solid-state reactions. We have strengthened our collaboration with the pharmaceutical industry and created a new CrystalCMP program for comparing pharmaceutical structures.

References

Barfeie, H., Grivani, G., Eigner, V., Dusek, M., Khalaji, A.D. (2018). Polyhedron, 146, 19-25

Bowden, D., Krysiak, Y., Palatinus, L., Tsivoulas, D., Plana-Ruiz, S., Sarakinou, E., Kolb, U., Stewart, D., Preuss, M. (2018). Nat. Comm. 9, Art. Nr. 1374

Bradley, C.J. and Cracknell, A.P. (1972). The mathematical Theory of Symmetry in Solids. Oxford: Clarendon Brázda, P., Palatinus, L., Babor, M. (2019). Science **364**, 667-669.

Campbell, B.J., Stokes, H.T., Tanner, D.E., Hatch, D.M. (2006). J. Appl. Cryst., **39**, 607-614.

Chatziadi, A., Skořepová, E., Rohlíček, J., Dušek, M., Ridvan, L. (2019). Crystal

Growth & Design, **20**, 1, 139-147. Colmenero, F., Plášil, J., Cobos, J., Sejkora, J., Timón, V., Čejka, J., Bonales, L. J. (2019a). RSC Adv. **9**, 15323– 15334.
Colmenero, F., Plášil, J., Cobos, J., Sejkora, J., Timón, V., Čejka, J., Fernández, A. M., Petříček, V. (2019c). RSC Adv. **9**, 40708–40726.
Colmenero, F., Plášil, J., Němec, I. (2020b) Journal of Physics and Chemistry of Solids 141, 109400. Colmenero, F., Plášil, J., Škácha, P. (2020c) Spectrochimica Acta Part A: Molecular and Biomolecular Spectroscopy 234, 118216.
Colmenero, F., Plášill, J., Sejkora, J. (2019b). Dalton Trans. **48**, 16722–16736. Colmenero, F., Sejkora, J., Plášil, J. (2020a). Sci. Rep., **10**, 7510.
Čubiňák, M., Eigner, V., Tobrman, T. (2018). Adv. Synth. Catal., **360** (23), 4604-4614
Gemmi, M., Merlini, M., Palatinus, L., Fumagalli, P., Hanfland, M. (2016). American Mineralogist 101, 2645-2654 Gemmi, M., Mugnaioli, E., Gorelik, T., Kolb, U., Palatinus, L., Boullay, P., Hovmoller, S., Abrahams, J. P. (2019). ACS Cent. Sci. 5, 1315-1329
Ghazisaeed, S., Kiefer, B., Plášil, J. (2019). RSC Adv. **9**, 10058–10063.
Ghazisaeed, S., Majzlan, J., Plášil, J., Kiefer, B. (2018). J. Appl. Cryst., **51**, 1116–1124. Görbitz, C.H., Karen P., Dušek, M. & Petříček, V. (2016). IUCRj **3**, 341-353.
Gorbunov, D.I., Henriques, M.S., Qureshi, N., Ouladdiaf, B., Salazar Mejía, C., Gronemann, J., Andreev, A.V., Petříček, V., Green, E.L., Wosnitza, J. (2018a). Phys. Rev. Mat., **2**, 084406.
Gorbunov, D.I., Nomura, T., Ishii, I., Henriques, M.S., Andreev, A.V., Doerr, M., Stöter, T., Suzuki, T., Zherlitsyn, S., Wosnitza, J. (2018b). Phys. Rev. B, **97**, 184412.
Gorbunov, D.I., Strohm, C., Henriques, M.S., van der Linden, P., Pedersen, B., Mushnikov, N.V., Rosenfeld, E.V., Petříček, V., Mathon, O., Wosnitza J., Andreev, A.V. (2019). Phys. Rev. Lett., **122**, 127205.
Henriques, M.S., Gorbunov, D.I., Andreev, A.V., Fabrèges, X., Gukasov, A., Uhlarz, M., Petříček, V., Ouladdiaf, B., Wosnitza, J. (2018). Phys. Rev. B, **97**, 014431.
Holaň, J., Skořepová, E., Heraud, L., Baltes, D., Rohlíček, J., Dammer, O., Ridvan, L., Štěpánek, F. (2016). Org. Process Res. Dev. **20**, 1, 33–43.
Hornfeck, W. (2018). Acta Cryst. A**74**, 659–672.
Hornfeck, W., Kobold, R., Kolbe, M., Conrad, M., Herlach, D. (2018). Nature Comm. **9**, art. no. 4054 (6 p.). Hornfeck, W., Kobold, R., Kolbe, M., Herlach, D. (2014) arXiv:1410.2952 [cond-mat.mtrl-sci].
Hosseini-Yazdi, S.A., Mirzaahmadi, A., Khandar, A.A., Eigner, V., Dušek, M., Mahdavi, M., Soltani, S., Lotfipour, F., White, J. (2017). Polyhedron, **124**, 156-165
Hušák M., Jegorov, A., Czernek, J., Rohlíček, J., Žižková, S., Vraspír, P., Kolesa, P., Fitch, A., Brus, J. (2019). Cryst. Growth Des. **19**, 8, 4625–4631.
Hybler, J. (2016). European Journal of Mineralogy, **28**, 777–788.
Hybler, J., Klementová, M., Jarošová, M., Pignatelli, I., Mosser-Ruck, R., Ďurovič, S. (2018). Clays and Clay Minerals, **66**, 379–402.
Hybler, J., Sejkora (2017). Journal of Geosciences, **62**, 137–146.
Hybler, J., Sejkora, J., Venclík, V. (2016). European Journal of Mineralogy, **28**, 765–775. Hybler, J., Števko, M., Sejkora, J. (2017). European Journal of Mineralogy, **29**, 91–99.
Hynek, J., Brazda, P., Rohlíček, J., Londesborough, M. G. S., Demel, J. (2018).

Angew. Chem., Int. Ed. 57, 5016− 5019.
Ishii, I., Mizuno, T., Takezawa, K., Kumano, S., Kawamoto, Y., Suzuki, T., Gorbunov, D.I., Henriques M.S., Andreev, A.V., (2018). Phys. Rev. B, **97**, 235130.
Janner, A. & Jansen, T. (1980). Acta Cryst. A36, 399-408
Khan, S. A., Blaha, P., Ebert, H., Minár, J., Šipr, O. (2016). Phys. Rev. B, **94**, 144436.
Khan, S. A., Minár, J., Ebert, H., Blaha, P., Šipr, O. (2017). Phys. Rev. B, **95**, 014408.
Kobold, R., Kolbe, M., Hornfeck, W., Herlach, D.M. (2018). J. Chem. Phys. **148**, art. no. 114502 (6 p.).
Kobold, R., Kuang, W.W., Wang, H., Hornfeck, W., Kolbe, M., Herlach, D.M. (2017). Phil. Mag. Lett. **97**, 249–256. Kočí, E., Rohlíček, J., Kobera, L., Plocek, J., Švarcová, S., Bezdička, P. (2019). Dalton Trans. **48**, 12531-12540. Kolb, U., Gorelik, T., Kübel, C., Otten, M.T., Hubert D. (2007). Ultramicroscopy, **107**, 507-513.
Kolb, U., Gorelik, T., Otten, M. T. (2008). Ultramicroscopy, **108,** 763-772.
Koptsik, V A. (1966). Shubnikov Groups. Handbook on the Symmetry and Physical Properties of Crystal Structures. Moscow: Moscow University Press.
Kortus, D., Mikšátko, J., Kundrát, O., Babor, M., Eigner, V., Dvořáková, H., Lhoták, P. (2019). J. Org. Chem., **84**
(18), 11572-11580
Landovský, T., Eigner, V., Babor, M., Tichotová, M., Dvořáková, H., Lhoták, P. (2019). Cem. Comm., **56** (1), 78- 81
Lovelace, J, Petříček, V., Murshudov, G. & Borgstahl, G.E.O, (2019). Acta Cryst. **D75**, 852-860.
Mayorga-Martinez, CC., Sofer, Z., Luxa, J., Huber, S., Sedmidubsky, D., Brazda, P., Palatinus, L., Milkulics, M., Lazar, P., Medlin, R., Pumera, M. (2017). ACS Nano 12, 464-473
Olds, T.A., Plášil, J, Kampf, A.R., Simonetti, A., Sadergaski, L.R., Chen, Y.-S., Burns, P. (2017). Geology, **45**, 1007–1010.
Palatinus, L., Brázda, P., Boullay, P., Perez, O., Klementová, M., Petit, S., Eigner, V., Zaarour, M., Mintova,S. (2017). Science **355**, 166-169.
Palatinus, L., Brazda, P., Jelinek, M., Hrda, J., Steciuk, G., Klementova, M. (2019). Acta Crystallogr. B 75, 512- 522
Palatinus, L., Chapuis, G. (2007). J. Appl. Cryst., **41,** 786–790.
Palatinus, L., Correa, C. A., Steciuk, G., Jacob, D., Roussel, P., Boullay, P., Klementova, M., Gemmi, M., Kopecek, J., Domeneghetti, M. C., Camara, F., Petricek, V. (2015b). Acta Crystallogr. B 71, 740-751 Palatinus, L., Petříček, V., Correa, C.A. (2015a). Acta Cryst., **A71**, 235-244.
Perez-Mato, J.M., Ribeiro, J.L., Petříček, V., Aroyo, M.I. (2012). J.Phys.: Condens. Matter, **24,** 163201. Petříček, V., Dušek, M. & Plášil, J. (2016a). Z. Kristallogr. **231**, 583-599.
Petříček, V., Dušek, M., Palatinus, L. (2014). Z. Kristallogr., **229,** 345–352.
Petříček, V., Eigner, V., Dušek, M., Čejchan, A. (2016b). Z. Kristallogr., **231,** 301–312. Petříček, V., Fuksa, J., Dušek, M. (2010). Acta Cryst., A**66**, 649–655.
Plášil, J., Kiefer, B., Ghazisaeed, S., Philippo, S. (2020). Acta Cryst., **B76**, 502–509.
Plášil, J., Petříček, V., Locock, A.J., Škoda., R., Burns, P.C. (2018). Z. Kristallogr., **233**, 223–232. Rohlíček, J., Skořepová, E. (2020). J. Appl. Cryst. **53**, 841-847.
Rohlíček, J., Skořepová, E., Babor, M., Čejka, J. (2016). J. Appl. Cryst. **49**, 2172-2183.
Saheli, S., Rezvani, A.R., Izadpanah, A., Dusek, M., Eigner, V. (2019). J. Saudi Chem. Soc., **23** (8), 1070-1079 Saheli, S., Rezvani, A.R., Malekzadeh, A., Dusek,

M., Eigner, V. (2018). Catal. Lett., **148** (11), 3557-3569 Sejkora, J., Škácha, P., Laufek, F., Plášil, J. (2017). Eur. J. Mineral., **29**, 663–672.
Šipr, O., Mankovsky, S., Ebert, H. (2019). Phys. Rev. B, **100**, 024435.
Šipr, O., Mankovsky, S., Polesya, S., Bornemann, S., Minár, J., Ebert, H. (2016a). Phys. Rev. B, **93**, 174409. Šipr, O., Minár, J., Ebert, H. (2016b). Phys. Rev. B, **94**, 144406.
Škácha, P., Plášil, J., Horák, V. (2019). Academia , pp. 1–688.
Skacha, P., Sejkora, J., Palatinus, L., Makovicky, E., Plasil, J., Macek, I., Golias, V. (2016). Mineralogical Magazine 80, 1115-1128
Slavík, P., Krupička, M., Eigner, V., Vrzal, L., Dvořáková, H., Lhoták, P. (2019). J. Org. Chem., **84** (7), 4229-4235 Steciuk, G., Ghazisaeed, S., Kiefer, B., Plášil, J. (2019). RSC Adv. **9**, 19657–19661.
Štejfa, V., Bazyleva, A., Fulem, M. Rohlíček, J., Skořepová, E., Růžička, K. & Blokhin, A.V. (2019). The Journal of Chemical Thermodynamics **131**, 524-543.
Tieger, E., Kiss, V., Pokol, G., Finta, Z., Dušek, M., Rohlíček, J., Skořepová, E., Brázda, P. (2016a). CrystEngComm **18**, 3819-3831.
Tieger, E., Kiss, V., Pokol, G., Finta, Z., Rohlíček, J., Skořepová, E., Dušek, M. (2016b). CrystEngComm **18**, 9260-9274.
Tlustý, M., Eigner, V., Babor, M., Kohout, M., Lhoták, P. (2019). RSC Adv., **9** (38), 22017-22030 Valach, F., Rohlíček, J., Lukeš, V., Kožíšek, J., Jorík, V. (2018). Inorganica Chimica Acta **479**, 106-112. Welch, M.D., Bindi, L., Petříček, V. & Plášil, J. (2016). Acta Cryst. **B72**, 822-827.
Wiedemann, D., Ludtke, T., Palatinus, L., Willinger, E., Willinger, MG., Muhlbauer, MJ., Lerch, M. (2018). Inorg. Chem. 57, 14435-14442
Zarei, L., Asadi, Z., Dusek, M., Eigner, V. (2019). J. Photoch. Photobio. A, **374**, 145-160
Zvoníček, V., Skořepová, E., Dušek, M., Babor, M., Žvátora, P., Šoóš, M. (2017). Crystal Growth & Design, **17**
(6), 3116-3127.
Zvoníček, V., Skořepová, E., Dušek, M., Žvátora, P., Šoóš, M. (2018). Crystal Growth & Design, **18** (3), 1315- 1326.

Research activity and characterization of the main scientific results

In 2013 our team was awarded the ambitious OP-PK project LABONIT, from EU Structural Fund. The project, was supported by a budget of about 46 million CZK, and enabled us to expand our experimental facilities, which was essential for our needs. The declared aim of the project was research in novel nitride-based structures for advanced semiconductor devices. In accordance with the project proposal, our first task was to build a modern laboratory complex enabling both, the growth and operative characterization of samples. During realization of the project, we have reorganized our team into five closely cooperating laboratories, namely, Laboratory of MOVPE Technology/LABONIT, Laboratory of Optical Spectroscopy/LABONIT, Laboratory of Luminescence, and Laboratory of Transport Phenomena complemented by the Research Group of Solid State Theory.

***Fig. 1**: MOVPE apparatus AIXTRON-CCS 3×2 for the growth of nitride-based semiconductor heterostructures. (Laboratory of MOVPE Technology/ LABONIT)*

The principal equipment placed in the newly reconstructed technological laboratory was an advanced research size apparatus from the renowned company AIXTRON, model CCS-3×2, for epitaxial growth of nitride-based structures by means of the MOVPE method (Fig. 1). In the revitalized basement room used as a laboratory for characterization of as-grown samples, a Raman and photoluminescence microspectrometer LabRAM HR Evolution– HORIBA (Fig. 2) was installed. Also, some specific properties of our structures were simultaneously studied in the Laboratory of Luminescence, where we were able to measure photoluminescence spectra at much lower excitation intensities and investigate resonant excitation in deeper layers of heterostructures. Optical measurements performed in both these laboratories were thus complementary to each other and essential for complete characterization of prepared heterostructures.

***Fig. 2**: Raman and photoluminescence microspectrometer LabRAM HR Evolution – HORIBA for characterization of semiconductor heterostructures. (Laboratory of Optical Spectroscopy/LABONIT)*

The transport properties of as-grown samples were systematically studied over a wide range of temperatures (0.3 – 700 K) by standard magnetotransport methods using conventional (0.9 T) and superconducting (SM8T – Oxford Instruments) magnets (Fig. 3). For the study of profiles of as-grown heterostructures various impedance and capacitance methods, including the mercury probe technique, were used. The crucial problem in characterization of samples by transport methods is the preparation of reliable and reproducible electrical contacts. To serve this purpose, a thin film vacuum deposition system Edwards-AUTO 500, also containing a special chamber for sample annealing in vacuum was utilised.

***Fig. 3**: Equipment for routine magnetotransport characterization of semiconductor structures. (Laboratory of Transport Phenomena)*

Installation of the facilities mentioned above was finished in the summer of 2015 and from this time onward all equipment was in full operation. Nevertheless, other improvements to the experimental facilities of our laboratories were carried out during 2015-2019. For example, in 2017 the Laboratory of Luminescence obtained a refurbished scanning electron microscope (Fig. 4), which enabled us to study cathodoluminescence spectra, being of special importance for characterization of scintillators.

***Fig. 4**: Refurbished scanning electron microscope Philips XL ESEM TMP with SEM/EDAX/cathodoluminescence facilities. (Laboratory of Luminescence).*

From the 2018 budget of the OPVV project Solid21 we purchased a Hydrogen Generator MicroPROGEL UHP-Rack19'' 5U for the easier supply of H_2 into the MOVPE apparatus. Finally, in 2019 we obtained a Probe Station Janis Research ST-500 (Fig. 5), which is very convenient for magnetotransport measurements of miniature samples (e. g. HEMTs) over a wide range of temperatures (5 – 500 K) and in a well-defined environment.

As mentioned above, in 2015 we completed our long-lasting extensive research into MOVPE grown Stranski-Krastanow InAs quantum dots embedded in GaAs-based heterostructures. Valuable results of this research were regularly published during the whole evaluated period. For example, noteworthy is the review [1] summarizing our results in this field. Among improvements launching our structures to the advanced level we should mention increased recombination rates by means of optimization of active layers surrounding [2-6] and introduction of GaAsSb capping of InAs QDs and of auxiliary layers with Sb concentration gradation. This enabled us to shift the emission wavelength as high as ~ 1.8 μm [3] and also to separate the confinements of electrons and holes [2, 5, 6]. Using this idea, a new type of solar cell structure with non-crossing trajectories of electrons and holes was developed (see patent [P1]).

***Fig. 5**: Probe Station Janis Research ST-500 for transport measurements of small samples in a defined atmosphere and over a wide range of temperatures (5 – 500K). (Laboratory of Transport Phenomena).*

Simultaneously with concluding activities related to QDs, project LABONIT started with two main topics, namely, MOVPE grown nitride-based fast scintillators and nitride-based high electron mobility transistors (HEMT) for high power applications. Both research directions use different unique properties of nitrides. Scintillators make use of high luminescence efficiency, fast luminescence response, which is due to the high exciton binding energy and good resistance of nitrides when exposed to ionizing radiation. High power and high frequency applications takes advantage of the wide band gap, high polarization field in heterostructures, high thermal conductivity and high temperature resistance of nitrides.

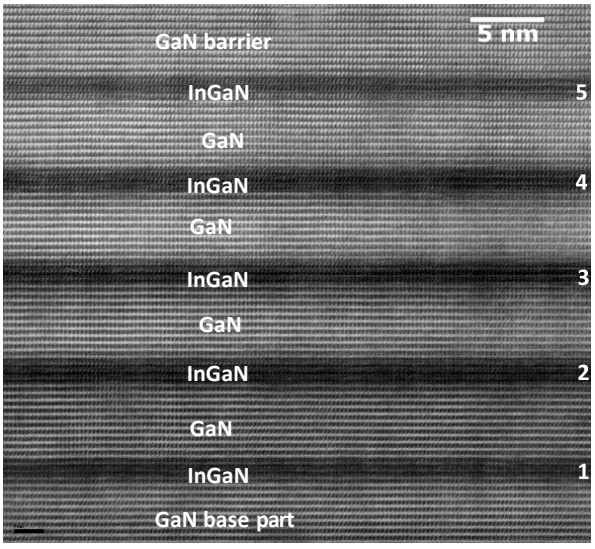

***Fig. 6**: HR TEM image of initial part of the scintillator structure with InGaN QWs surrounded by GaN barriers. Notice, separate atomic layers can be distinguished [9].*

A part of our scintillator structure based on InGaN/GaN multiple quantum well (QW), is shown in the HR TEM image with atomic resolution, see Fig. 6. As for the homogeneity of active layers, the progress of structure development is in brief demonstrated in Fig. 7. Scintillators need to be fast and have high intensity photoluminescence; in order to meet these requirements, it is advantageous to grow the high number of QWs absorbing a sufficient part of radiation penetrating the heterostructure [7]. We have found that such structures also reveal improved photoluminescence quality [7-10] with effective suppression of undesirable defect bands, e.g. yellow band. Moreover, a special optimization of the buffer layer for practical applications is required [11, 12]. Designing the scintillator, our team has opened a new research area; we have established records in the QW number in the active region (N = 70 - 100) [13] and prepared unique, highly sensitive devices

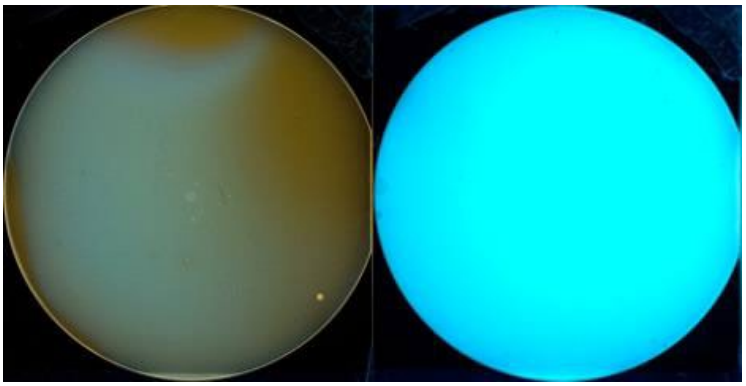

***Fig. 7**: Difference between luminescence of one of the first scintillator discs prepared at the beginning of the project LABONIT (left) and that grown after optimization of design and technology (right).*

with the fastest luminescence response well below ~1 ns [10]. As a result, our nitride-based structures belonged at the end of 2019 to **the best scintillators in the world**. Some of the inventions behind this progress are covered by our national and international patents the list of which is given below [P2–P5, P7]. An example of the design and technology improvements is depicted in Fig. 8, where cathodoluminescence (CL) spectrum of our fast and sensitive scintillator is presented in comparison with standard devices.

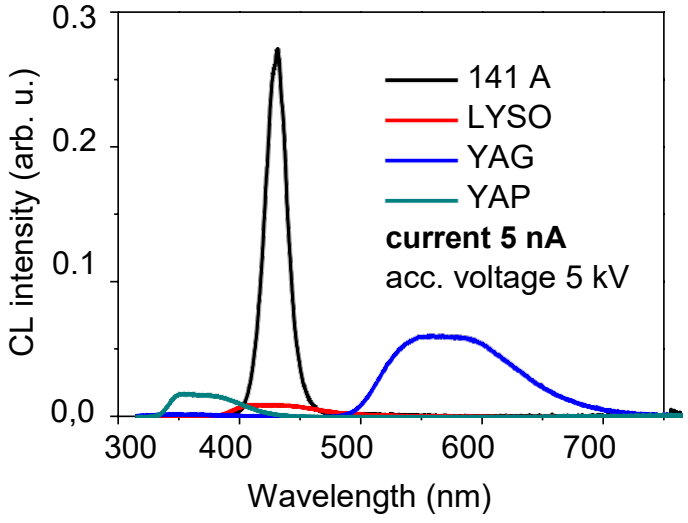

***Fig. 8**: CL of our newly developed fast scintillator (black line) showing appreciable increase of*

quantum efficiency in comparison with current fast scintillators (LYSO, YAP). Much slower YAG is shown for comparison. (All curves were measured with identical spectrograph setting.)

The actual performance of our devices was also verified in a practical application. One of our standard structures was shaped and replaced the original commercial scintillator in the chamber of a scanning electron microscope (Fig. 9). The cathodoluminescence signal revealed improved contrast and also the collection dynamics were faster than the commercial device. (cf. spectra in Fig. 8)

Fig. 9*: Light-guide flange of SEM chamber provided at the top with a fast nitride-based scintillator of our design and fabrication.*

We believe that, scintillator devices of similar construction may thus improve precision of positron emission tomography used in medicine or considerably increase the scanning rate of electron microscopes in inspection machines used in the electronic industry, etc.
The second item of LABONIT concerns the development of technology of high-power nitride-based HEMT structures intended for operation in extreme conditions. The aim is to prepare, on various foreign substrates, reliable HEMT structures with the special architecture of AlGaN barrier layers, which will take advantage of the high piezoelectric field at interfaces (see [P8]). At the end of 2019 first structures of such a type were under testing.
Our entrance into the area of nitride research, unique in the Czech Republic, attracted quite naturally attention of industry. The most intensive collaboration in recent years was thus established between our team and potential end-users of our research, Crytur, spol. s r.o. and On Semiconductor, both from the Czech Republic. The closeness of these collaborations may be demonstrated by the fact that our research is supported by joint TACR projects and that some of the validated patents are also common. Related to this we add a list of national and international patents validated during the evaluated period (see e.g. Fig. 10).


特 許 証
特許第６３８１８１５号
発明の名称 電離放射線のシンチレーション検出器
特許権者 チェコ共和国、１１０１、トゥルノフ ナ ルカーフ ２２８３
国籍 チェコ共和国
クライツール スボル、エス アール、オー、
発明者 ホスポドコーヴァ、アリス
プラチェク、カレル
フリチウス、エドゥアルド
その他別紙記載
登録番号 特願２０１７－５９８２４４
出願日 平成２８年 ２月 ８日
登録日 平成３０年 ８月１０日
この特許は、特許原簿に登録されたことを証する。
平成３０年 ８月１０日
特許庁長官
宗像直子

***Fig.10**: Copy of Japan patent No.6381815 (August 10, 2018) [P3].*

The main task of the Laboratory of Transport Phenomena is to provide immediate feedback for the Laboratory of MOVPE Technology/LABONIT and investigate the electronic properties of GaN-based systems by means of magnetotransport and magnetocapacitance methods. A typical example of such a result is depicted in Fig. 11. Besides this, the laboratory undertakes, in close cooperation with teams from FZU and other institutions, other research,
e.g. into transport properties of GaAs radiation detectors with unconventional metallic contacts [14-16], various aspects of the electron transport in diamond systems [17, 18], properties of ZnO thin films [19,20] and bulk and surface effects in materials for advanced solar cells [21].

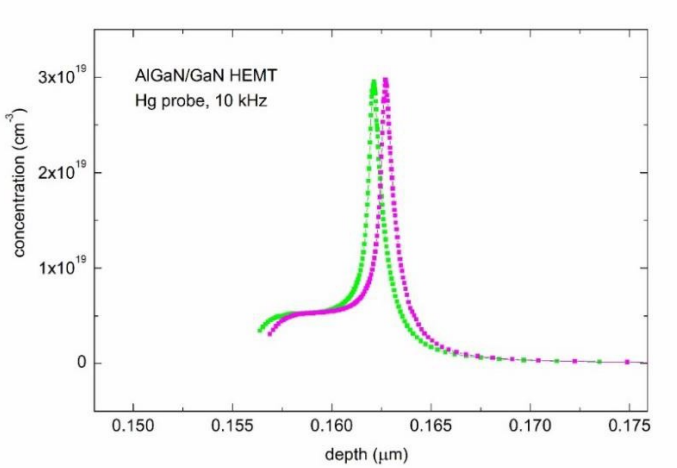

***Fig. 11**: Example of electron concentration profiles of AlGaN/GaN high-electron mobility transistor (HEMT) structure obtained by capacitance-voltage measurement using mercury probe. Green and violet curves were taken at different points of the sample.*

During the evaluation period colleagues from the Research Group of Solid-State Theory paid attention mainly to the fundamental problems of solid-state physics, such as is the connection between orbital moments and topological phase transformations in electronic structures [22] or the validity of fluctuation-dissipation theorems in non-equilibrium systems [23]. Our long-term studies related to the concept of temperature [24] and its relativistic transformation [25 developed into a contribution to the theory of the mathematical structures of physical quantities [26], which is a chapter of a book [27] edited and co-authored by members of our team (see Fig. 12). Additionally, our expertise in electrical transport enabled us to formulate an alternative theory of quantum diffusion-controlled transfer of signals via nervous fibres [28].

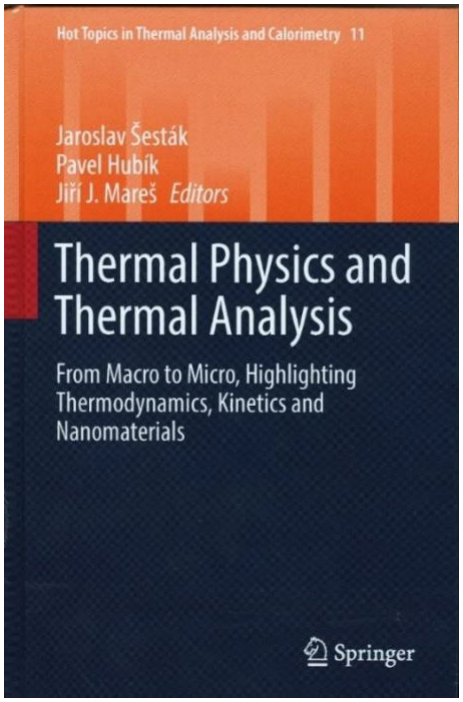

***Fig. 12**: Copy of a book [27], edited and co-authored by workers of our team.*

Research activity and characterisation of the main scientific results

Our research aimed to intentionally and purposefully influence the properties of new materials. The challenge to perform such research lies in understanding fundamental physical properties, namely magnetic, magnetocaloric, superconducting, thermal and electric ones. We thus prepared novel materials in diverse forms (bulk andnanocrystalline phases, nanocomposites, layered structures, thin layers and molecular compounds) and probed their properties at variable external parameters (temperature, pressure, magnetic field). The experimental results analysed with the support of the theoretical approach and DFT calculations are illustrated by the research topics highlighted below. We attempted to uncover the interconnection between the microscopic mechanism of magnetic order on one side and magnetic, electronic and thermal properties on the different characteristic length and time scales on the other.
As well as our ongoing interest in magnetic oxide systems, their assemblies and intermetallics, the research newly focused on magnetic functionalized nanomaterials suitable for medical and biological applications. Later we also embarked on the study of magnetic chalcogenides, aiming above all at their use in thermoelectric energy conversion. With respect to thermoelectric energy conversion, we note that our activities in applied research targeted the effective use of waste heat by means of thermoelectric generators (Fig.1). This last activity opened the door to the cooperation with industry and commercial sphere (ŠKODA auto, ZEVO Malešice).

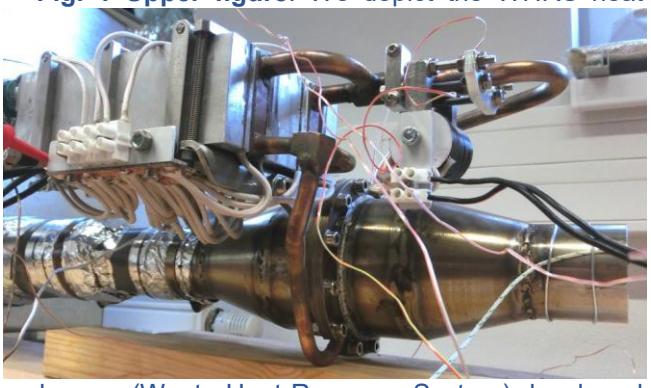

Fig. 1 Upper figure. We depict the WHRS heat exchanger (Waste Heat Recovery System) developed within the TAČR project in cooperation with the Škoda Auto a.s. and Sobriety s.r.o. The unit achieved an electrical output exceeding 100 W, leading to a reduction in fuel consumption when used in recuperation, which confirms the functionality and accuracy of our chosen WHRS concept.

Left figure-upper. Installed thermoelectric generator (TEG) in solid waste incineration plant ZEVO Malesice. The TEG (1) on flue gas conduct (2) with measuring and control unit (3).

Left figure-lower. Detail of thermoelectric generator constructed to recover the waste heat energy from the combustion gas after the depuration procedure.

We illustrate the work of the team by highlighting the following four most important topics:

(i) Magnetotransport properties, thermoelectric conversion and its utilization in devices

We continued our extensive study of perovskite manganites and cobaltites. The studies on the $La_{1-x}Sr_xMnO_3$ phases with x =0.35–0.55 in the form of bulk and nanogranular ceramics and 0-3 dim nanocomosites (with thin insulating layer around the metallic cores) revealed a coexistence of distinct low- and high-field magnetoconductance, related to the field-induced alignment of ferromagnetic (FM) granules, the spin canting in antiferromagnetic (AFM) matrix and/or temperature assisted tunnelling. The magnetoconductance of FM cores embedded in AFM and/or insulating (silica, TiO_2) matrix is illustrated in Fig. 2 [1].

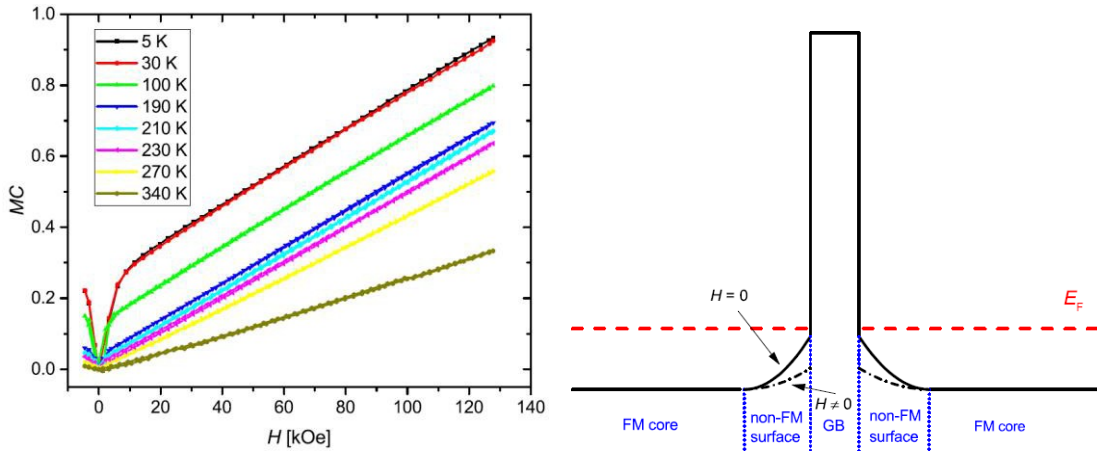

Fig. 2 Magnetotransport in nanogranular La,Sr-manganites. The magnetoconductance ratio of nanogranular $La_{0.55}Sr_{0.45}MnO_3$ densified by spark plasma sintering is shown in the left panel for different temperatures. The scheme in the right panel described the tunnelling junction between two FM manganite grains. The wavefunction of the metallic carrier that propagates from the grain core on the left is gradually attenuated in the ~1.5 nm thick surface region, which is structurally identical to the core but modified magnetically. Before the carrier enters the neighbouring grain, it traverses a tunnelling barrier formed by the grain boundary. Its actual width depends on the degree of grain intergrowth, eventually it can be intentionally increased by embedding manganite particles into an insulating matrix.

The impact of the substrate/thin layer mismatch on the metal–insulator transition associated with spin-state (SS) transition of Co ions in $(Pr_{1-y}Y_y)_{(1-x)}Ca_xCoO_3$ epitaxial films was probed by standard methods complemented with the X-ray absorption of near-edge structure (XANES) spectra [2]. The study of chemically stable high temperature thermoelectric misfit Bi- Sr-Co-O cobaltates demonstrated that the spark plasma sintering process yields ceramics with the value of Seebeck coefficient of 190 V/K at RT, which is among the highest reported for the polycrystalline Bi-222 material [3]. Due to the need for detailed knowledge of the relationship between the thermoelectric coefficient and the electronic structure of cobaltates, we also dealt with open-ended questions concerning the origin of the high value of the thermoelectric coefficient and its relationship with the spin entropy of charge carriers. Measurement of the dependence of the thermoelectric power (see Fig. 3) and specific heat on the magnetic field to the lowest temperatures in the misfit cobaltate $[Ca_2CoO_{3-t}]_{(0.62)}(CoO_2)$ showed that the contribution of spin entropy is unusually large and reaches up to 50% of the theoretical value of $k_B/|q_e|\ln 2 = 60\ \mu V/K$, which is not expected for carriers of Fermi liquid character [4].

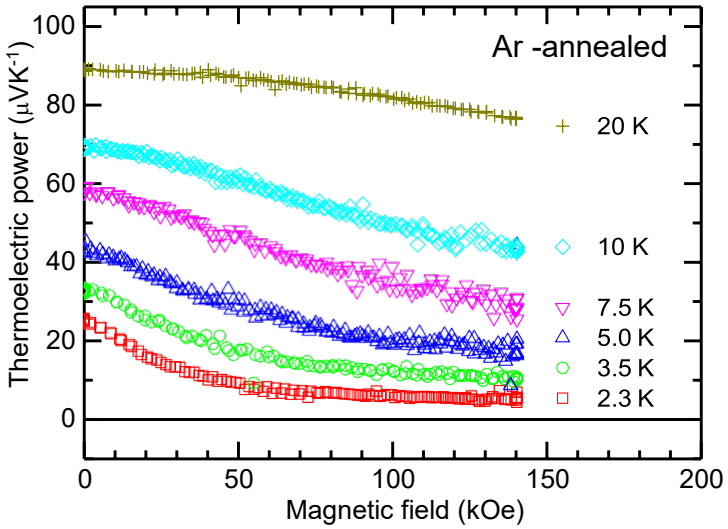

Fig. 3 The magnetic field dependence of the thermopower in the misfit cobaltate $[Ca_2CoO_{3-t}]_{(0.62)}(CoO_2)$. The strong depression at low temperatures demonstrates the role of spin entropy to the thermoelectric power.

Further, we have enriched the investigation of layered cobaltates of Na_xCoO_2 type demonstrating that Na^+ species can be replaced via ionic-exchange by La^{3+}, Pr^{3+} and Ca^{2+} ions, respectively, which leads to the $Re_{0.33}CoO_2$ phase with a 2-dimensional superstructure in the ab-plane [5].

Apart of chemically stable oxides, we started, in close cooperation with longstanding cooperating researchers from the Institute Jean Lamour (CNRS, Nancy, France), to uncover the thermoelectric properties of perspective chalcogenides: tetrahedrites, layered tin sulfides/selenides. In this respect we have revisited the thermal properties of single crystal SnSe [6] and studied in detail the tetrahedrite thermoelectric performance, where we succeeded to dope the tetrahedrite by Mg (s-block metal) and, most importantly, to confirm the robustness of the thermoelectric performances of tetrahedrites with respect to natural chemical fluctuations [7].

Our research in the field of thermoelectric energy conversion was extended by an experimental investigation into a phenomenon of the newly emerging field of spin caloritronics, namely the spin Seebeck effect (SSE). The SSE layered device, depicted in the Fig. 4b, was discovered in 2008 and refers to the conversion of a heat current into a spin current (in a magnetically ordered material) which is further converted into an electrical current by means of the inverse spin Hall effect (ISHE) in the conductive nonmagnetic metal with a large spin Hall angle. The SSE can thus be used as thermoelectric application where the mutually orthogonal orientation of the spin current $\vec{J}_S$, the magnetization $\vec{M}$ and the electric field $\vec{E}_{ISHE}$, (Fig. 4) is the crucial condition to achieve maximum energy gain in the composite device. We have developed and constructed the experimental SSE measurement apparatus (in collaboration with the Instituto de Nanociencia de Aragon, Universidad de Zaragoza) and focused the research on thin films of Y-type hexagonal ferrites $Ba_2(Zn,Co)_2Fe_{12}O_{22}$ for their high critical temperature and an easy plane of magnetization parallel to the film surface. Interestingly our results have proved that despite their complicated magnetic structure (limiting the mean free path of spin waves) Y-hexaferrites can be used as highly efficient spin sources down to low temperatures [8].

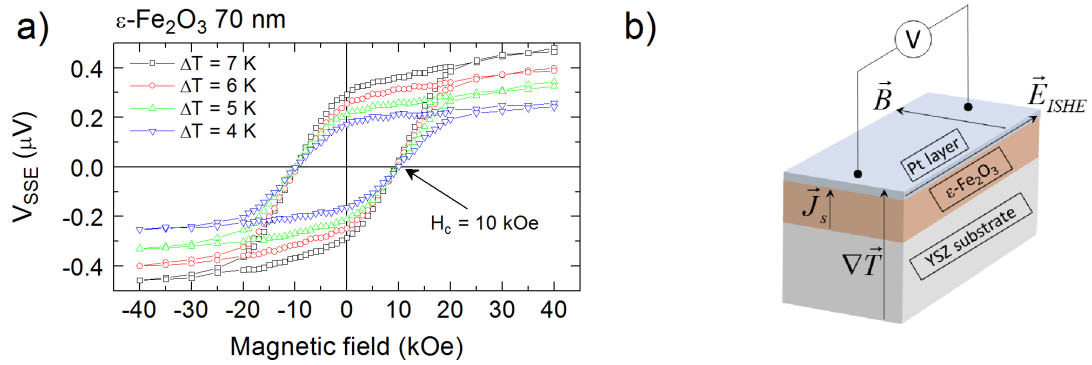

Fig. 4 (a) SSE for various temperature differences of ε-Fe_2O_3 70 nm film, (b) Schema of the longitudinal experimental configurations. Directions of spin current ($\vec{J}_S$), temperature gradient ($\vec{\nabla T}$), external magnetic field ($\vec{B}$), and electrical field resulting from inverse spin Hall effect ($\vec{E}_{ISHE}$), are shown.

We also succeeded in synthesizing thin films of ε-Fe_2O_3 phase, which is known to exhibit giant coercive field of ~2 T and therefore may be tentatively used for SSE device without an external magnetic field. The experiment (magnetization, the SSE signal - Fig. 4a) confirmed a coercive field ~1.1 T which is the highest value so far reported for ε-Fe_2O_3 thin films [9]. We finally note, considering the increasing importance of the thermoelectric metrology, that our team also participated in a round robin test on the measurement of the thermoelectric figure of merit, where various sources of errors and uncertainties were analysed by 8 European laboratories [10].

References

[1] O. Kaman, Z. Jirak, J. Hejtmanek, A. Ndayishimiye, M. Prakasam, G. Goglio, Tunneling magnetoresistance of hydrothermally sintered La1-xSrxMnO3- silica nanocomposites, Journal of Magnetism and Magnetic Materials, 479 (2019) 135-143. 10.1016/j.jmmm.2019.01.114.

[2] H. Fujishiro, Y. Noda, K. Akuzawa, T. Naito, A. Ito, T. Goto, M. Marysko, Z. Jirak, J. Hejtmanek, K. Nitta, Electrical resistivity anomaly, valence shift of Pr ion, and magnetic behavior in epitaxial (Pr(1-y)Yy) 1-xCa(x)CoO(3) thin films under compressive strain, JOURNAL OF APPLIED PHYSICS, **121**, (2017) 115104

[3] K. Rubesova, T. Hlasek, V. Jakes, S. Huber, J. Hejtmanek, D. Sedmidubsky, Effect of a powder compaction process on the thermoelectric properties of Bi2Sr2Co1.8Ox ceramics, JOURNAL OF THE EUROPEAN CERAMIC SOCIETY**, 35**,(2015) 525-531

[4] J. Hejtmanek, Z. Jirak, J. Sebek, Spin-entropy contribution to thermopower in the [Ca2CoO3-t](0.62)(CoO2) misfits, PHYSICAL REVIEW B, **92** (2015), 125106

[5] K. Knizek, Z. Jirak, J. Hejtmanek, P. Brazda, J. Bursik, M. Soroka, P. Beran, Structural study of layered cobaltate Lax/3CoO2 (x ~ 1) at temperatures up to 800 K, JOURNAL OF SOLID STATE CHEMISTRY**, 229**, (2015) 160-163

[6] D. Ibrahim, JB. Vaney, S. Sassi, C. Candolfi, V. Ohorodniichuk, P. Levinsky, C. Semprimoschnig, A. Dauscher, B. Lenoir, Reinvestigation of the thermal properties of single-crystalline SnSe, APPLIED PHYSICS LETTERS , **110**, (2017) 032103

[7] P. Levinsky, C. Candolfi, A. Dauscher, J. Tobola, J. Hejtmanek, B. Lenoir, Thermoelectric properties of the tetrahedrite-tennantite solid solutions Cu12Sb4-xAsxS13 and Cu10Co2Sb4-yAsyS13 (0 x, y 4), PHYSICAL CHEMISTRY CHEMICAL PHYSICS, **21** ,(2019) 4547-4555

[8] J. Hirschner, M. Maryško, J. Hejtmánek, R. Uhrecký, M. Soroka J. Buršík, A. Anadón, M. H. Aguirre, K. Knížek: Spin Seebeck effect in Y-type hexagonal ferrite thin films., Phys. Rev. B ,**96** (2017) 064428.

[9] K. Knížek, M. Pashchenko, P. Levinský, O. Kaman, J. Houdková, P. Jiříček, J. Hejtmánek, M. Soroka, J. Buršík: Spin Seebeck effect in epsilon-Fe_2O_3 thin layer with high coercive field, J. Appl. Phys., **124** (2018) 213904.

[10] E. Alleno, D. Berardan, C. Byl, C. Candolfi, R. Daou, R. Decourt, E. Guilmeau, S. Hebert, J. Hejtmanek, B. Lenoir, P. Masschelein, V. Ohorodnichuk, M. Pollet, S. Populoh, D. Ravot, O. Rouleau, M. Soulier: A round robin test of the uncertainty on the measurement of the thermoelectric dimensionless figure of merit of Co0.97Ni0.03Sb3, Rev. Sci. Instrum. , **86,** (2015) 011301

(i) Role of external pressure, magnetic field or the local chemical environment in the appearance of new magnetic states

Our effort was focused on studying the effects of external pressure, magnetic field or local chemical environment on the electronic structure of selected intermetallic compounds and in particular on the formation of novel magnetic states. Two basic types of materials have been investigated. The first ones were the compounds with rare earth elements (namely, Ce, Eu and Yb with variable valence induced by external pressure and field) that dominate in magnetic behaviour and in the appearance of new magnetic phases of these intermetallics. The second ones were materials exhibiting itinerant *f*- or *d*-electron magnetism that is very sensitive to the application of both the external pressure and the magnetic field. Newly, our study of the complex magnetic state of the Cantor high entropy alloy under high pressure and magnetic field provides a new and valuable contribution to the determination of their magnetic structure. The new magnetic phases and their transformations have been characterized by a comparative investigation of not only their magnetic properties, but, their electric and thermal transport, magnetocaloric, structural and magnetostriction properties.

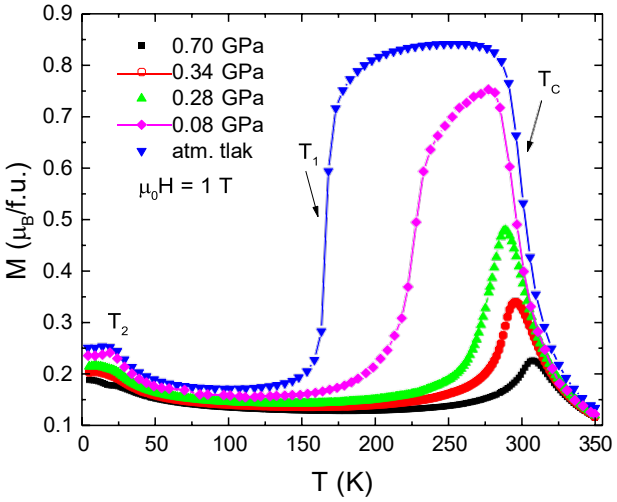

Fig. 5 The huge impact of hydrostatic pressure on the temperature dependence of magnetization in 1 T for $La_{0.6}Pr_{0.4}Mn_2Si_2$.

The results of our investigation are important not only for the improvement of the functionality of magnetic materials. They also challenge the basic understanding of magnetic interactions and electronic structure properties near criticality. Among others we can mention the effect of pressure on the properties of high entropy Cantor alloy [1], the effect of pressure, up to 6 GPa on magnetic and structural properties of Fe_5SiB_2 [2], complex magnetic and transport properties of the $Ni_{1.92}Mn_{1.56}Sn_{0.52}$ [3], experimental and theoretical study of $LuPd_2Si_2$ superconductor [4], and the study of magnetic, structural and magnetocaloric properties of $La_{0.6}Pr_{0.4}Mn_2Si_2$ under high pressures and magnetic field [5], see Fig. 5. The research has been extended in recent years to study the exotic states of materials on the border of long-range

magnetic ordering, peculiarities of their complicated phase diagrams and details of exciting phase transitions existing in the limit of zero temperature. Emergent quantum critical behaviour has been investigated in the case of a few carefully selected representatives from a group of ferromagnetic UTX compounds (U - actinides, T – transition metals, X – p-metals) [6]. Much attention has been devoted to searching for unconventional superconductivity in cerium-based heavy fermion systems driven by pressure as a tuning parameter [7]. Materials with complex magnetic phase diagrams, unusual anisotropy and lattice behaviour were the subject of the magnetoelastic study [8]. Our experiments on the fine pressure tuning of the photomagnetic behaviour of Fe-II Nb-IV cyano-bridged coordination polymers revealed the first known pressure driven spin-crossover photomagnet with attractive properties for potential applications [9].

References

[1] J.Kamarád, M.Friak, J. Kaštil, O.Schneeweiss, M. Šob, A. Dlouhý: Effect of high pressure on magnetic properties of CrMnFeCoNi high entropy alloy. Journal of Magnetism and Magnetic Materials, **487** (2019) 165333.

[2] J. Kaštil, R. Hirian, O. Isnard: Effect of pressure on the magnetic and structural properties of Fe5SiB2 compound. Intermetallics **110** (2019) 106484

[3] J. Kaštil, J.Kamarád, M. Míšek, J. Hejtmánek, Z. Arnold: Complex transport properties of the Ni1.92Mn1.56Sn0.52 Heusler alloy and its magnetic behavior. Journal of Magnetism and Magnetic Materials **466** (2018) 260-266.

[4] J. Kaštil, M.Diviš, K.Vlášková, P. Doležal, J. Fikáček, J.Prchal, M. Míšek, J.Kamarád, Z.Arnold: Experimental and first-principle study of LuPd2Si2 superconductor, Intermetallics **100** (2018) 171-174.

[5] J. Kaštil, Z. Arnold, O. Isnard, Y. Skourski, J. Kamarád, J.P. Itié: Study of magnetic, structural and magnetocaloric properties of La0.6Pr0.4Mn2Si2 under high pressures and magnetic field. Journal of Magnetism and Magnetic Materials, **424** (2017) 416–420.

[6] M. Míšek, J. Prokleška, J. Opletal, P. Proschek, J. Kaštil, J. Kamarád, V. Sechovský: Pressure-induced quantum phase transition in the itinerant ferromagnet UCoGa. AIP Advances **7** (2016) 055712.

[7] M. Kratochvílová, K. Uhlířová, J. Prchal, J. Prokleška, M. Míšek, V. Sechovský: Tuning the pressure-induced superconductivity in Pd-substituted CeRhIn5. Journal of Physics – Condensed Matter **27** (2015) 095602.

[8] M. Vališka, H. Saito, T. Yanagisawa, C. Tabata, H. Amitsuka, K. Uhlířová, J. Prokleška, P. Proschek, J. Valenta, M. Míšek: Magnetoelastic phenomena in antiferromagnetic uranium intermetallics: The UAu2Si2 case. Physical Review **B, 98**, (2018) 174439.

[9] D. Pinkowicz, M. Rams, M. Míšek, K.V. Kamenev, H. Tomkowiak, A. Katrusiak, B. Sieklucka: Enforcing Multifunctionality: A Pressure-Induced Spin-Crossover Photomagnet. Journal of the Amercian Chemical Society, **137,** (2015) 8795-8802.

(ii) Functionalized nanomaterials and their application in medicine and biological research

Our experimental background and extensive expertise in magnetic materials has enabled us to deal with magnetic nanomaterials on a complex basis including their synthesis, detailed structural studies and analysis of magnetic behaviour. Our research on this topic, drawing on more than a decade's worth of knowledge, has been devoted to three types of materials: (i) magnetic nanoparticles with narrow size distribution, (ii) complex core-shell particles with plasmonic components and organic functionalization, and (iii) nanostructured phases and nanocomposites. Our work has been motivated not only by the fundamental study of physical phenomena that occur on the nanoscale level but also by the development of novel tools for biological and medical applications, above all contrast agents for magnetic resonance

imaging (MRI) and magnetic particle imaging (MPI) and stimuli-responsive systems for the physically controlled release of drugs. For example, the effort to understand surface and finite size effects in nanocrystallites, which both influence the magnetic behaviour of fine particles, can be illustrated on $La_{1-x}Sr_xMnO_{3+\delta}$ nanoparticles from molten salt synthesis [1,2]. Furthermore, superspin glass transition was demonstrated on monodisperse Zn-doped magnetite particles [3]. Significant results were also achieved in the development of nanoparticles for bioapplications [4-6]. Specifically, gold nanoshells containing silica-coated Mn-Zn ferrite cores were synthesized and applied in surface-enhanced Raman spectroscopy, and their fluorescently functionalized derivatives were tested in vitro, see Fig. 6 [5].

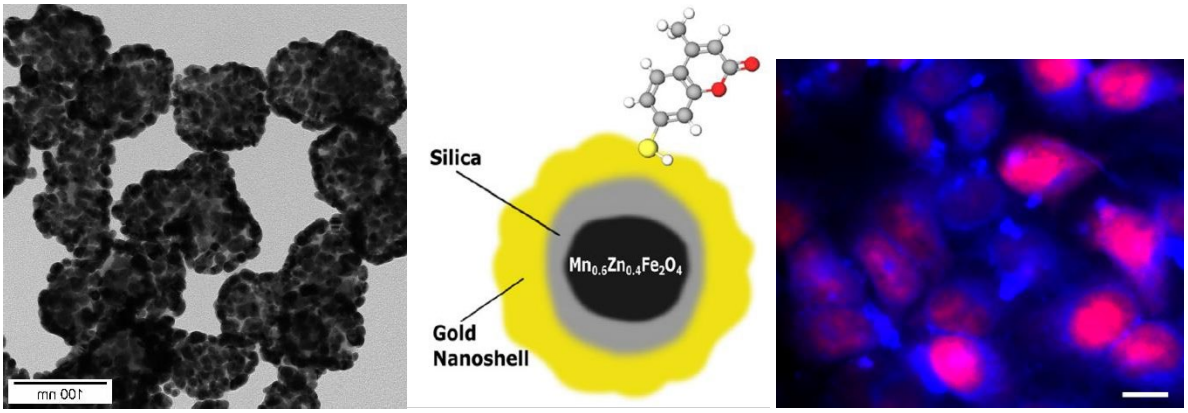

Fig. 6 Gold nanoshells with silica-coated $Mn_{0.6}Zn_{0.4}Fe_2O_4$ ferrite cores (transmission electron micrograph in the left panel) and their functionalization with 7-mercapto-4-methylcoumarin (see scheme in the central panel) as a fluorescent label for fluorescence microscopy of cells (labelling of A549 cells is demonstrated in the right panel, the blue signal is from the nanoshells whereas the red signal comes from nuclei stained with propidium iodide).

Moreover, these particles were employed for the construction of an advanced biosensor for prostate cancer diagnostics [6]. Our interest in the temperature and field dependences of the transverse relaxivity led to the design of novel contrast agents and explanation of the regime of transverse relaxation [7,8]. As regards the third group of nanomaterials, the successful preparation of nanostructured manganites and nanocomposites with the 0-3 connectivity (e.g. ferromagnetic and metallically conducting $La_{0.35}Sr_{0.65}MnO_3$ nanoparticles uniformly dispersed in an insulating titania or silica matrix) were used in magnetotransport studies, and the theory of grain-boundary tunnelling has been revisited [9-11].

References

[1] M. Kačenka, O. Kaman, Z. Jirák, M. Maryško, P. Veverka, M. Veverka, S. Vratislav, The magnetic and neutron diffraction studies of $La_{1-x}Sr_xMnO_3$ nanoparticles prepared via molten salt synthesis. J. Solid State Chem. **221** (2015) 364-372.

[2] N. M. Belozerova, S. E. Kichanov, Z. Jirák, D. P. Kozlenko, M. Kačenka, O. Kaman, E. V. Lukin, B. N. Savenko, High pressure effects on the crystal and magnetic structure of nanostructured manganites $La_{0.63}Sr_{0.37}MnO_3$ and $La_{0.72}Sr_{0.28}MnO_3$. J. Alloy. Compd**. 646** (2015) 998-1003.

[3] O. Kaman, T. Kořínková, Z. Jirák, M. Maryško, M. Veverka, The superspin glass transition in zinc ferrite nanoparticles. J. Appl. Phys. **117** (2015) 17C706.

[4] M. Kacenka, O. Kaman, S. Kikerlova, B. Pavlu, Z. Jirak, D. Jirak, V. Herynek, J. Cerny, F. Chaput, S. Laurent, I. Lukes, Fluorescent magnetic nanoparticles for cell labeling: Flux synthesis of manganite particles and novel functionalization of silica shell. J. Colloid Interf. Sci**. 447** (2015) 97-106.

[5] J. Koktan, K. Královec, R. Havelek, J. Kuličková, P. Řezanka, O. Kaman, Magnetic oxide particles with gold nanoshells: Synthesis, properties and cytotoxic effects. Colloids Surf. A Physicochem. Eng. Asp. **520** (2017) 922-932.
[6] T. Bertok, L. Lorencova, S. Hroncekova, V.. Gajdosova, E. Jane, M. Hires, P. Kasak, O. Kaman, R. Sokol, V. Bella, A. A. Eckstein, J. Mosnacek, A. Vikartovska, J. Tkac, Advanced impedimetric biosensor configuration and assay protocol for glycoprofiling of a prostate oncomarker using Au nanoshells with a magnetic core. Biosens. Bioelectron **131** (2019) 24-29.
[7] O. Kaman, V. Herynek, P. Veverka, L. Kubíčková, M. Pashchenko, J. Kuličková, Z. Jirák, Transverse Relaxivity of Nanoparticle Contrast Agents for MRI: Different Magnetic Cores and Coatings IEEE Trans. Magn**. 54** (2018) 1-5.
[8] L. Kubíčkova, P. Brázda, M. Veverka, O. Kaman, V. Herynek, M. Vosmanská, P. Dvořák, K. Bernášek, J. Kohout, Nanomagnets for ultra-high field MRI: Magnetic properties and transverse relaxivity of silica-coated epsilon-Fe2O3. J. Magn. Magn. Mater 480 (2019) 154-163.
[9] Z. Jirak, O. Kaman, K. Knizek, P. Levinsky, M. Misek, P. Veverka, J. Hejtmanek, High-field magnetoconductance in La-Sr manganites of FM and AFM ground states. J. Magn. Magn. Mater **456** (2018) 167-178.
[10] O. Kaman, Z. Jirak, J. Hejtmanek, A. Ndayishimiye, M. Prakasam, G. Goglio, Tunneling magnetoresistance of hydrothermally sintered La1-xSrxMnO3- silica nanocomposites. J. Magn. Magn. Mater **479** (2019) 135-143.
[11] A. Ndayishimiye, S. Buffiere, M. A. Dourges, A. Largeteau, M. Prakasam, S. Mornet, O. Kaman, J. Zdenek, J. Hejtmanek, G. Goglio, Design of 0-3 type nanocomposites using hydrothermal sintering, Scr. Mater. **148** (2018) 15-19.

(iii) Theory and spectroscopy of superconducting vortices

During the last five years, our activity was focused on two different fields: magnetic and optical properties of compounds containing rare-earth (RE) atoms [1-5] and the physics of magnetite, studied in cooperation with the research groups in the Faculty of Mathematics and Physics, Prague and in Academic Center of Materials and Nanotechnology, Krakow, Poland. [6-7]. In the first group of problems, we used the method developed by us during 2012-14 for the calculation of the RE crystal field. The method was applied not only to insulators but newly, also to intermetallic systems as demonstrated in Fig. 7 where good matching between calculated and experimentally measured magnetic moment for intermetallic $NdCuAl_3$ is shown. This method is now used independently by several groups thanks to the availability of programs and the detailed user guide (WWW pages of the WIEN2k group from the Technical University of Vienna).

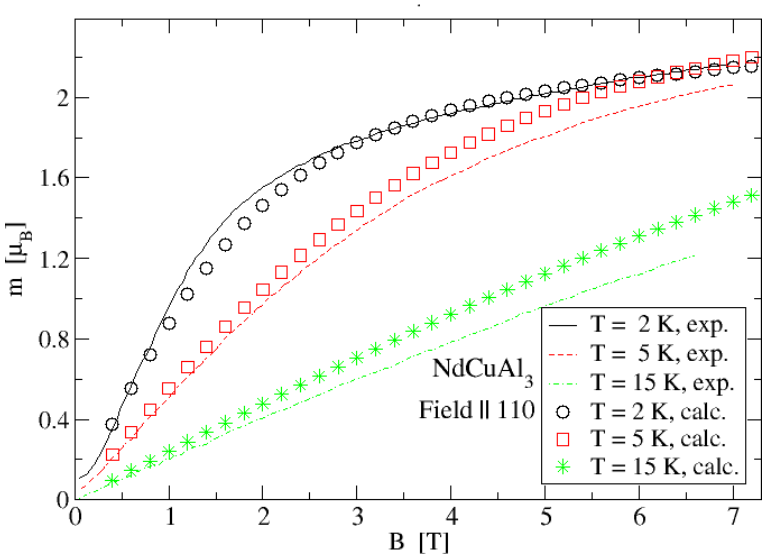

Fig. 7 The comparison of the experimentally determined (open symbols) and calculated (lines) magnetic moments in $NdCuAl_3$ intermetallic phase.

Outside the above groups of materials is the study of possible exciton magnetism in iridate perovskites [8]. To contribute to an increased activity of our department in thermoelectricity, we implemented recent versions of two program packages important for the study of this phenomenon: WIEN2k_19.1 and BoltzTraP2.

In the Far-Infrared Magnetospectroscopy Laboratory (FIRM lab), we continued with the study of high-frequency vortex dynamics in superconducting materials. The Abrikosov vortices in thin superconducting films can serve as qubits for fluxonics, or as carriers of elementary information in the next generation of logical devices. An understanding of vortex dynamics is essential for any high-tech application, especially knowledge of forces driving vortex motion and their effective inertial mass. Estimates of vortex mass, however, are particularly troublesome; its theoretical estimates span more than seven orders of magnitude, and only very few experimental data are available.

Our approach is analogical to the determination of effective electron mass. The standard model of the vortex dynamics shows that free vortices circulate with a frequency, known as the vortex cyclotron frequency. Due to a resonant enhancement, near this frequency circular dichroism should become observable. For this purpose, we designed a homemade broadband- tunable terahertz circular polarizer developed for magneto-optical measurements using the far-infrared/THz laser source in the range of 0.25–7.5 THz [9], which was successfully tested on a standard semiconducting GaAs sample, see Fig. 8. Later we successfully observed circular dichroism in an optimally doped YBaCuO thin film and determined its vortex effective mass [10].

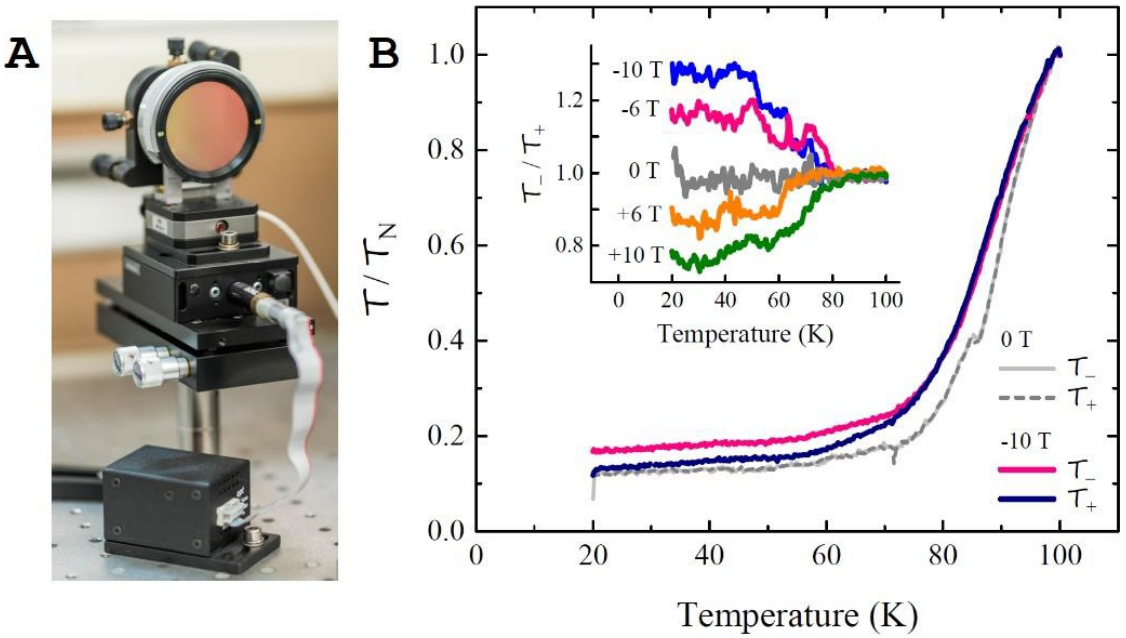

Fig. 8 (A) We constructed a broadband-tunable THz retarder capable of converting the linearly polarised state into right- or left-handed circularly polarised state (RHCP, LHCP respectively).
(B) Transmittance through the superconducting YBaCuO sample was measured for both circular polarisations (T_+ for RHCP, T_- for LHCP). While observed curves in zero magnetic field are essentially the same within experimental error, the dichroism is clearly visible in an applied magnetic field below 75 K. The inset shows the transmittance ratio T_+/T_- measured in several applied magnetic fields for wavelength 311 μm. These experimental data strongly suggests a finite vortex mass.

We also observed non-equilibrium destruction of superconductivity by a strong optical pulse in thin NbN films [11]. In cooperation with colleagues from Israel and Slovakia, we described and explained giant flux jumps observed in the hollow superconducting cylinder when a slowly increasing external magnetic field reached a threshold value [12].

References

[1] Z. Huesges, K. Kliemt, C. Krellner, R. Sarkar, H.-H. Klauß, C. Geibel, M. Rotter, P. Novák, J. Kuneš, O. Stockert: Analysis of the crystal electric field parameters of $YbNi_4P_2$. New J. Phys. **20** (2018) 073021.

[2] H. Tsuchiura, T. Yoshioka, P. Novák: Bridging atomistic magnetism and coercivity in Nd-Fe-B magnets. Scripta Mater. **154** (2018) 248.

[3] O. Kaman, J. Hejtmánek, Z. Jirák, K. Knížek, M. Maryško, P. Novák, S. Vratislav: Effects of Tb^{3+} dopants in the $La_{1-x}Sr_xMnO_3$ bulk and nanoparticle ferromagnets. J. Phys.-Condens. Mat. **28** (2016) 206001.

[4] K. Knížek, P. Novák, Z. Jirák, J. Hejtmánek, M. Maryško, J. Buršík, Magnetism and transport properties of layered rare-earth cobaltates $Ln_{0.3}CoO_2$. J. Appl. Phys. **117** (2015) 17B706.

[5] T. Yoshioka, H. Tsuchiura, P. Novák: Crystal field parameters with Wannier functions: application to $Nd_2Fe_{14}B$ systems. Mater. Res. Innov. **19** (2015) S34.

[6] R. Řezníček, V. Chlan, H. Štěpánková, P. Novák: Hyperfine field and electronic structure of magnetite below the Verwey transition. Phys. Rev. B **91** (2015) 125134.

[7] R. Řezníček, V. Chlan, H. Štěpánková, P. Novák, J. Zukrowski, A. Kozlowski, Z. Kakol, Z. Tarnawski and J. M. Honig: Understanding the Mössbauer spectrum of magnetite below the Verwey transition: Ab initio calculations, simulation, and experiment. Phys. Rev. B **96** (2017) 195124.

[8] K. Pajskr, P. Novák, V. Pokorný, J. Kolorenč, R. Arita, J. Kuneš: On the possibility of excitonic magnetism in Ir double perovskites. Phys. Rev. B **93** (2016) 035129.

[9] R. Tesař, M. Šindler, J. Koláček, and L. Skrbek, *Terahertz wire-grid circular polarizer tuned by lock-in detection method,* Rev. Sci. Instrum. **89,** (2018) 083114(1) - 083114(7).

[10] M. Šindler, R. Tesař, J. Koláček, and L. Skrbek, *Abrikosov vortex mass in high-Tc YBaCuO superconductor emerging from observed circular dichroism of far-infrared transmission,* http://arxiv.org/abs/1911.12050

[11] M. Šindler, C. Kadlec, P. Kužel, K. Ilin, M. Siegel, and H. Němec, *Departure from BCS response in photoexcited superconducting NbN films observed by terahertz spectroscopy,* Phys. Rev. B **97**, (2018) 054507(1) - 054507(5).

[12] M. I. Tsindlekht, V. M. Genkin , I. Felner, F. Zeides, N. Katz, Š. Gazi, Š. Chromik, J. Koláček, and M. Maryško, *Magnetic flux penetration into finite length thin-walled niobium cylinders,* Physica C **545** (2018) 10 - 13.

Research activity and characterization of the main scientific results

Chemical vapor deposited diamond and carbon materials

We are focused on the **science and technology** of diamond materials, in particular diamond nanoparticles (nanodiamonds) and thin films. We note that in the evaluated 2015-2019 period our **systematic joint cross-departmental activity** of two complementary research groups from the Laboratory of Diamond and Carbon Nanostructures (Dept. of Optical Materials) and the Laboratory of Nanomaterials and Functional Interfaces (Dept. of Thin films and Nanostructures) significantly contributed to achieved results. Our comprehensive, yet focused line of inter-disciplinary research **embraces technology, characterization, computing, and applications** of diamond nanoparticles and thin films. We have studied diamond growth and preparation of well-defined nanodiamonds down to the molecular scale as well as their structural and chemical modifications. We have developed specialized microscopic and spectroscopic characterization methods, studying fundamental physical phenomena related to electronic and optical properties, molecular and material interactions as well as biological effects. We have explored the application potential of these diamond materials **in biomedicine, tissue engineering, chemical sensors, water purification, photocatalysis, photovoltaics, photonics, and power electronics**.

Our activities were supported by national and international projects **in collaboration** with other Institutes of the Czech Academy of Sciences, CTU in Prague, Charles University, MUNI Brno, Slovak Academy of Sciences (SK), Uni Wien (AT), CEA Saclay (FR), Uni Basel (CH), AIST/NIMS (JP), KIST (KOR). They resulted in a rich publication output of more than 110 scientific articles in international journals and conference proceedings incl. 2 book chapters. **The selected research highlights** are summarized below in more detail.

Nanodiamonds (NDs) as a relatively novel type of carbon nanomaterial are gaining increasing interest worldwide in spintronics, quantum computing and biomedicine. They are available in large quantities, biocompatible, non-toxic and environmentally safe. We focused on fundamental physical and chemical properties of individual ND particles (size control, purity and surface chemistry in the range of a few nanometers) with prospective use of NDs for bio-chemical sensing, catalysis, and energy generation.

Here we highlight some of our top breakthrough results: (i) Surface chemistry of NDs was controllably modified on atomic and molecular levels; (ii) We reduced the mean size of NDs below 2 nm and we identified a transition from the diamond nanocrystal to a carbon nanocluster at around 1 nm; (iii) We obtained 2 nm in size hydrogenated NDs (H-NDs) demonstrating that the large variability of ND surface chemistry and corresponding zeta potential variations (positive to negative) is available down to a few nm. We used such H-NDs to grow ultrathin diamond films which enabled a full On-Off switching of Silicon-Vacancy (Si-V) photoluminescence as illustrated in **Fig. 1**.

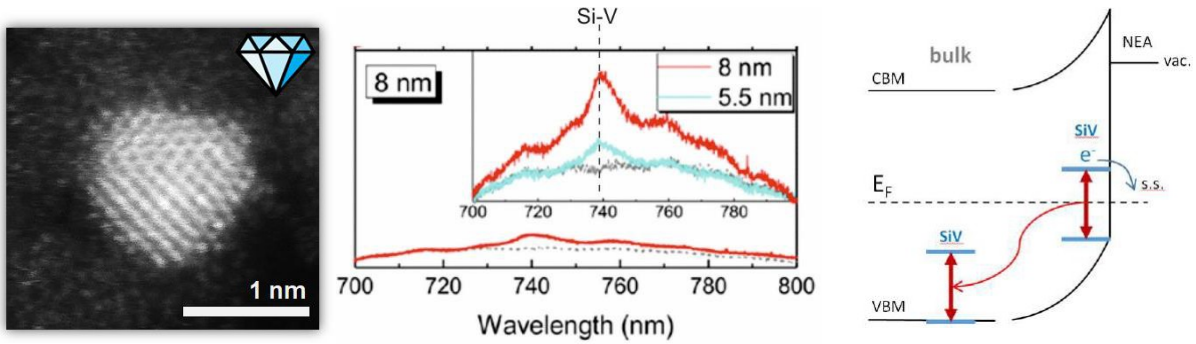

Fig. 1: STEM image of diamond nanoparticles used for nucleation on a Si substrate. PL spectra of Si-V centers in ultra-thin diamond film (8 and 5.5 nm) with controlled surface termination (grey – hydrogen terminated film, cyan/red – oxygen terminated film) and corresponding valence bandgap diagram.

The growth of diamond thin film consists of two steps, (i) nucleation/seeding (pre-growth

treatment of non-diamond substrates) and (ii) growth via microwave plasma chemical vapor deposition (MWCVD). **Various process parameters** (substrate surface chemistry, gas composition, pressure, power, etc.) were studied **to understand and apply CVD growth** for specific diamond structures and properties demanded by applications. Novel diamond-based **composite materials** (i.e. with polymers, organic dyes, TiO2, ZnO, Au, G/GO) have been developed, characterized and employed. Specifically, for soft and mechanically sensitive substrates, we have optimized a nucleation procedure based on **nanodiamonds in polymer composites** (PS, PLGA, PVA – microspheres, nanofibers, thin films), such as on carbon foams for gas sensors, supercapacitors, electrically active lab-on-chip devices. We have significantly improved the **standard nucleation** density from common 10^{10} cm^{-2} up to 10^{13} cm^{-2}. We made a breakthrough in fabrication methods of **porous diamond materials** by the direct bottom-up growth using linear antenna MWCVD on flat Si substrates, or templated substrates, **Fig. 2**.

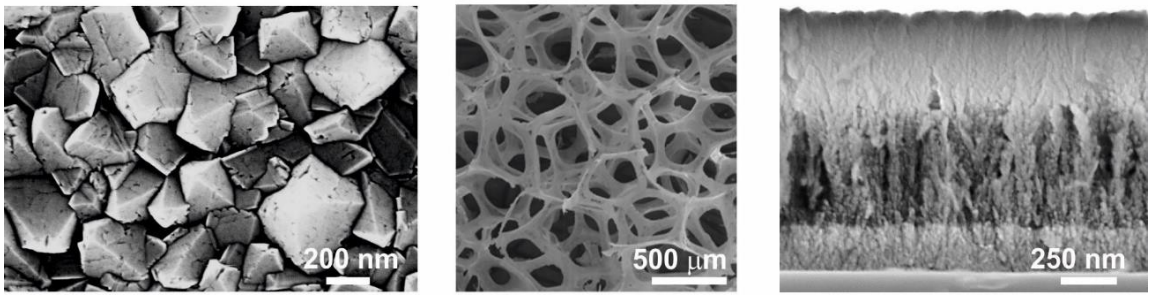

Fig. 2: Top-view SEM images of microcrystalline diamond and diamond-coated carbon foam. Cross-section SEM image of closed/ultra-porous/closed diamond heterostructure grown by bottom-up strategy.

Correlation of data from various characterization methods such as photoelectron, vibrational (Raman, IR) and optical spectroscopies (PL, PDS), electron microscopy (SEM, TEM, STEM), scanning probe microscopy (AFM, KPFM, Peakforce, etc.) has been systematically applied. We have also established a novel methodology using the **Kelvin probe force microscopy for understanding an electrical potential assumed by nanoparticles** on various substrate materials with different work functions. We have developed so-called AFM nanoshaving and AFM phase imaging **methodology for understanding the assembly and adhesion of organic molecules on diamond** thin films and nanoparticles. This research was significantly supported by developing **novel diamond-coated optical elements for IR vibrational spectroscopy.** We also prepared the reference sp^2/sp^3 hybridized carbon composites which were used as an application example(s) for Raman Imaging Scanning Electron Microscopy (RISE), a unique analytical tool developed by Tescan company (CZ).

Computation methods from atomic scale to multiphysics simulations were an inherent part of our research. Theoretical computations of polypyrrole PPy-ND interface using DFT revealed various structural arrangements, HOMO and LUMO spatial separation, and energy level alignment depending on the surface chemical groups on NDs. Polyfunctional NDs were shown as the most favorable for exciton dissociation and charge transport, **NDs acted as inorganic electron acceptors**. Multiphysics simulations (in Comsol) were employed to study the **gas flow and temperature distribution in plasma and thermal reactors** for understanding material growth, modification processes, and device structures such as a GaN-diamond interface. To describe the behavior of eukaryote cells on hydrogen- and oxygen-terminated diamond patterns, we have developed a general **stochastic mathematical model** (in Matlab) using only three fundamental parameters (cell movement, adhesion, and proliferation), explaining e.g. the **osteoblastic cell array formation**.

We explored fundamental physical phenomena as well as practical use of the developed diamond materials and interfaces. Thanks to their unique and adjustable semiconducting, optical, and surface chemical properties we have employed diamond as a promising **platform for electrical and optical sensing and actuation of chemical and biological effects. Fig. 3** reviews three representative examples.

The diamond solution-gated field effect transistors (SGFET) exhibited sensitivity to metabolic

activity and gate triggering-effect applicable for a label-free cell culture monitoring in real-time. Hybridization/denaturation of DNA molecules showed 15× higher sensitivity on diamond. [9] We have also explored diamond as an extraordinary material in optical sensors by hosting **different color centers** (including several together) such as nitrogen, silicon, erbium, etc. We have developed technologies for **making diamond photonic crystals** with chemical sensitivity.

Tissue engineering on chemically patterned nanocrystalline diamond (NCD) thin films and graphene showed that osteoblast cells adhere slower and migrate farther on H-NCD than O-NCD. On graphene, cell proliferation was promoted by hydrophobic graphene with a large number of nanoscale wrinkles independent of proteins. [11] **Antibacterial properties** of graphene oxides, H-/O-/F-terminated diamond films and H-/O-NDs were observed on *Escherichia coli*, *Bacillus subtilis, Proteus mirabilis*, showing prospects for the fight against bacterial resistance.

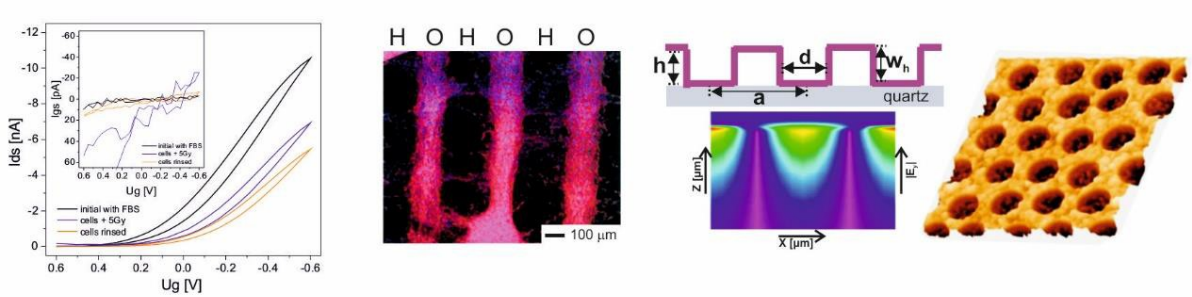

Fig. 3: (From left to right) (1)Transfer and gate current (inset) characteristics of a SG-FET at U_{DS} = -0.6 V measured in the HEPES medium with FBS (black curve), SAOS-2 cells irradiated by 5 Gy (blue curve) and after rinsing in deionized water (orange curve). (2) PL images of patterned neuron growth on O-/H-terminated diamond stripes. (3) Schematic cross-section of diamond photonic crystal and calculated amplitude of E_y electric field component of vertically extracted TE leaky mode. (4) AFM image of diamond PhC fabricated using microsphere lithography.

Fabrication of **diamond heterostructures** with other materials brings new features and facilitates state- of-the-art applications. For instance, the combination of p-type H-terminated diamond thin films and **n- type ZnO nanorods** exhibited higher sensitivity to NO2 as a gas sensor. To improve thermal management and reduce intrinsic stress of materials for power electronics, heterostructures of nanocrystalline diamond thin films with **AlGaN/GaN** have been prepared. With modern 2D materials, preferential horizontal or vertical growth of **MoS_2 layer(s)** on the nanocrystalline diamond surfaces was engineered by the initial Mo film thickness. Three major stages of diamond film catalytic transformation were determined from in-situ XPS during the thermal annealing of Ni on diamond resulting in **graphite- on-diamond** (GOD) heterostructures. Rapid thermal annealing studies revealed that diamond could form covalent bonds to graphitic planes via the Ni-mediated catalytic process, **Fig. 4**. We created a comprehensive model explaining the diamond transformation, covalent bonding, relaxation of uniaxial stress as well as the mechanism of electrical conductivity at the interface (see figure below), thereby paving the way for future graphene-on-diamond nanodevices.

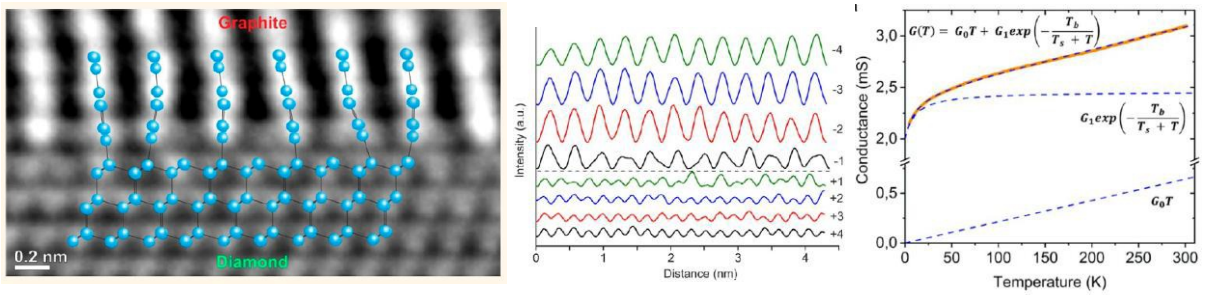

Fig. 4: Fourier-filtered HRTEM image of the graphite-diamond interface. Intensity profiles in the direction parallel to the diamond and graphite interface. Temperature dependent conductance of GOD sample.

Luminescent and Scintillating Materials – Preparation and characterization

We deal with preparation and characterization of a **variety of scintillator and phosphor materials**. While the former can find usage in several fields incl. high energy physics, medical imaging, security or industrial high-tech devices, the latter are intended mainly for the solid-state lighting. Amongst possible preparation methods, we mention a **modern micro-pulling-down technique for the oxide and halide single crystal materials** imported to our lab from Japan in 2015 and 2017, thanks to our long-lasting collaboration with Tohoku university, in the framework of the Praemium Academiae prize awarded to M. Nikl. Within long-running collaboration with laboratories at Charles University and Czech Technical University in Prague, we use the **liquid phase epitaxy to prepare single crystalline films** and **radiation techniques to prepare nanocrystals,** respectively. We also study **optical ceramics** in collaboration with the Shanghai Institute of Ceramics, CAS, where this technology has been developed. We use a **broad portfolio of characterization techniques** to measure the luminescence and scintillation spectra, decays, efficiency and light yield and radiation resistance of bulk, film, powder and composite materials. For **defect and trap characterization,** we use correlated thermoluminescence and electron paramagnetic resonance experiments. Within the 2015-2019 period, we published more than 180 original papers in impacted international periodicals incl. four invited review papers, four chapters in books and one book. We co-authored more than 100 contributions incl. more than 10 invited keynote or plenary talks at international conferences. Our core international collaborations include teams in Japan, China, Ukraine, Estonia and Italy. In large international consortia, we participated in four projects in EC FP7 and H2020 programs and one COST project. We are members of the Crystal Clear Collaboration coordinated from CERN.

We employed a highly systematic effort for the further development of **advanced garnet scintillators** using strategies of **electronic band structure and defect engineering**. In 2011, together with collaborators at the Tohoku university, we participated in the discovery of the cerium-doped multicomponent garnet scintillators (GGAG:Ce) which are currently the most efficient oxide scintillators. In 2014 we came with the **novel optimization concept based on Ce^{4+} stabilization** in garnets by stable divalent ion (Mg^{2+}, Ca^{2+}) codoping. The Ce^{4+} center provides another fast radiative recombination pathway in scintillation mechanism in garnets so that their timing characteristics are notably improved, which we have reported for bulk garnet crystals. Starting from 2015 we studied the effect of Mg codoping and host stoichiometry also for optical ceramics. Several papers were as well devoted to composition, tailoring and divalent ion codoping in epitaxial films the properties of which were tuned up to the same level as in the best bulk GGAG:Ce single crystals. Possible novel ways of electronic band structure engineering were also studied theoretically in collaboration with C. Stanek's group in Los Alamos. We have shown that such an optimization strategy cannot be used in case of the Pr^{3+} luminescence center in garnets due to the positioning of the 4f ground and $5d^1$ excited states in the host forbidden gap. Due to a large overlap of the charge transfer absorption of Pr^{4+} and fast $5d^1$-4f emission of Pr^{3+} remarkable re-absorption of the scintillation light occurs, and the light output is drastically diminished. The **application potential** of these Ce-doped garnet scintillators is very high in the **field of medical and industrial X-ray and gamma-ray imaging**, **high energy physics detectors** at accelerator rings and others. Especially bulk GGAG:Ce crystals became commercially available very soon after their discovery. Thus, we have **patented the derived material concepts in garnets and other material groups together with our Czech industrial partner CRYTUR** spol. s r.o. and extended the national patent to international PCT application and further to many countries (applications are pending) given the business territory of CRYTUR.

We emphasize the role of the **micropulling-down method in screening of the single crystal material composition, doping and codoping**. It allows preparation of single crystals of a few cm in length and a few mm in diameter within several hours and rapid, cost-effective composition screening and optimization, which accelerates the material research. The crystal is pulled in a downward direction through the capillary in the die at the bottom of the crucible, **Fig. 5**

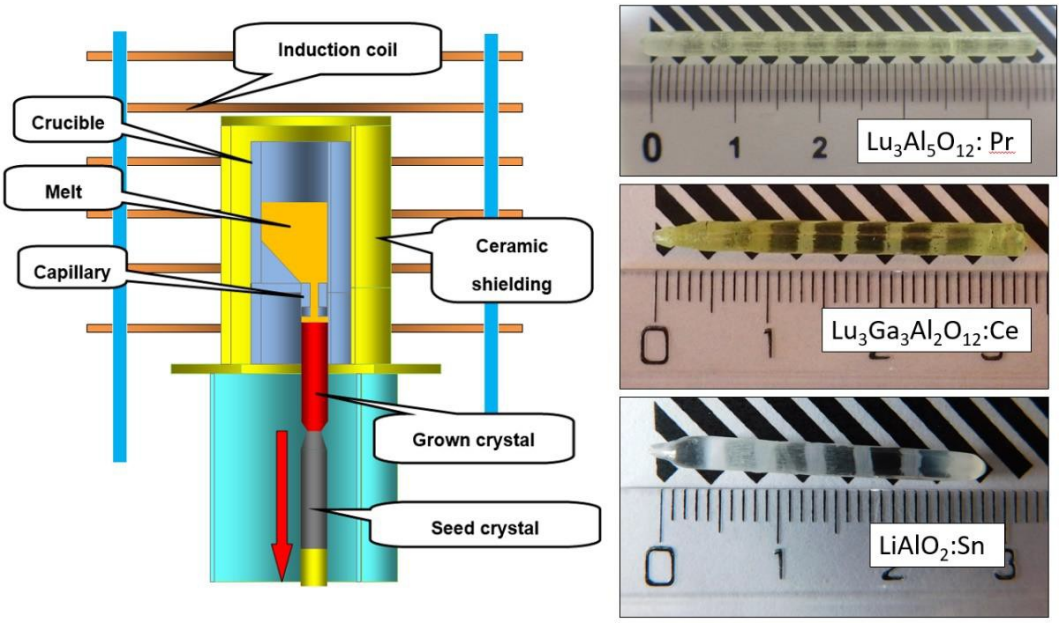

Fig. 5: Sketch of the micro-pulling-down growth chamber (left), examples of grown crystals (right).

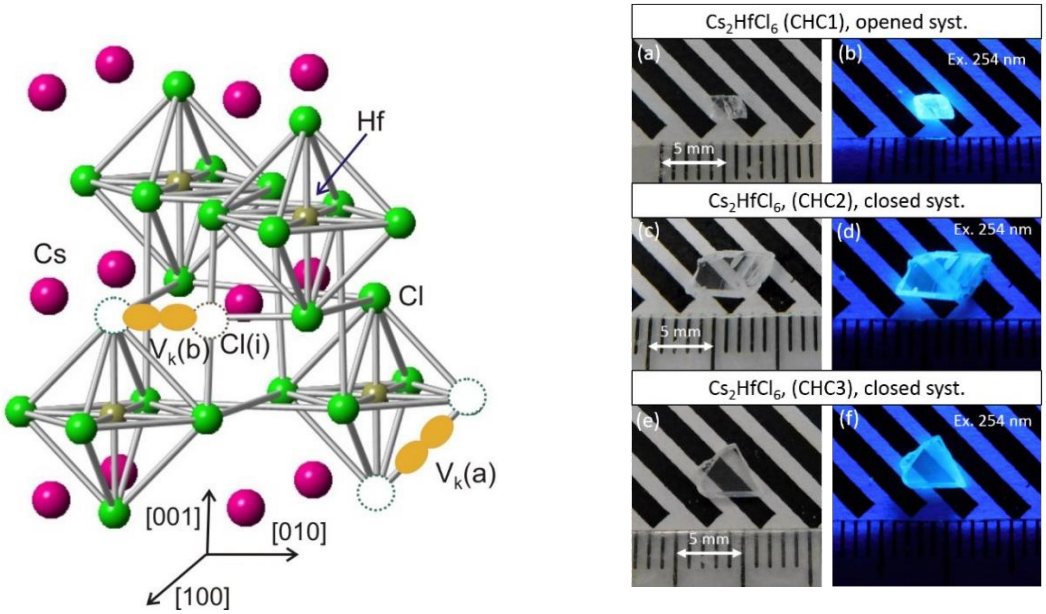

Fig. 6: Local structure of Cs_2HfCl_6 with V_k centers (left) and polished pieces of the grown crystals (right). The V_k(a) center is created by two Cl ions belonging to the same octahedron. The V_k(b) center is created by one Cl lattice ion and an interstitial Cl ion placed along [100] crystal directions.

As mentioned above, in 2017 the **halide micro-pulling-down apparatus was installed in our lab, the first of this kind in Europe**, for the growth of hygroscopic halides and other materials under a protective inert atmosphere (Ar, N2). Its removable growth chamber can be transported into a glove box, where all the preparatory work is carried out without exposing the crystal to the atmosphere. The apparatus can also be modified for so-called **micro-vertical Bridgman growth by modifying the hot-zone accordingly**. Single crystals of Cs2HfCl6 (CHC) were grown with this method, **Fig. 6**. CHC is a promising scintillator due to its low hygroscopicity, high

density, light output, and very good energy resolution. We have studied its complicated luminescence mechanism composed of three processes dominating at different temperatures. Furthermore, scintillation mechanism can be additionally complicated by the presence of charge traps, the electron or hole ones, which were studied in CHC crystals of different quality by means of **correlated electron paramagnetic resonance (EPR) and optical experiments.** EPR revealed formation of two configurations of V_k centers (Cl^{2-} molecular ion) at low temperatures. One of the V_k centers ($V_{k,a}$) is created by a hole self-trapping at two neighboring Cl ions, while at 70–80 K it is thermally disintegrated and reappears in another configuration formed by an interstitial Cl ion, see **Fig. 6**. The influence of (non) stoichiometry was further studied by EPR combined with thermally stimulated luminescence, which proved reduction of $V_{k,a}$ with improving stoichiometry.

Another more recent research interest of ours is focused on **nanomorphological scintillators** in the form of **nanopowders or nanocomposites**. We have been taking part in a concerted international effort (project COST FAST TD1401) to develop **superfast scintillators for fast timing.** Composite scintillation materials could provide the coincidence time resolution of a few tens of picoseconds critically required in the time-of-flight techniques, such as positron emission tomography medical imaging with the time-of-flight functionality (TOF-PET). For this purpose, we studied several ultrafast nanoscintillators, e.g. (Zn,Cd)O quantum dots incl. preparation of **core-shell structures** where the shell is constituted by thin amorphous SiO2. Finally, we also prepared bulk composite material where ZnO nanocrystals are embedded into the polystyrene host and which efficiently preserve the scintillation speed of ZnO (500 ps decay time) due to ultrafast energy transfer from the polystyrene host toward the ZnO nanophase. The novel **photochemical (radiation) method** used for manufacturing of ZnO and other oxide nanocrystals was presented in detail in an invited paper. Another studied direct-gap nanoscintillator is also gaining attention in other fields, such as photovoltaics, and is constituted by colloidal $CsPbBr_3$ nanoplatelets. Their emission wavelength can be tuned by the nanocrystal size due to the **quantum confinement effect,** therefore enabling smaller nanocrystals to emit blue light with fast sub-nanosecond decay, **Fig. 7**.

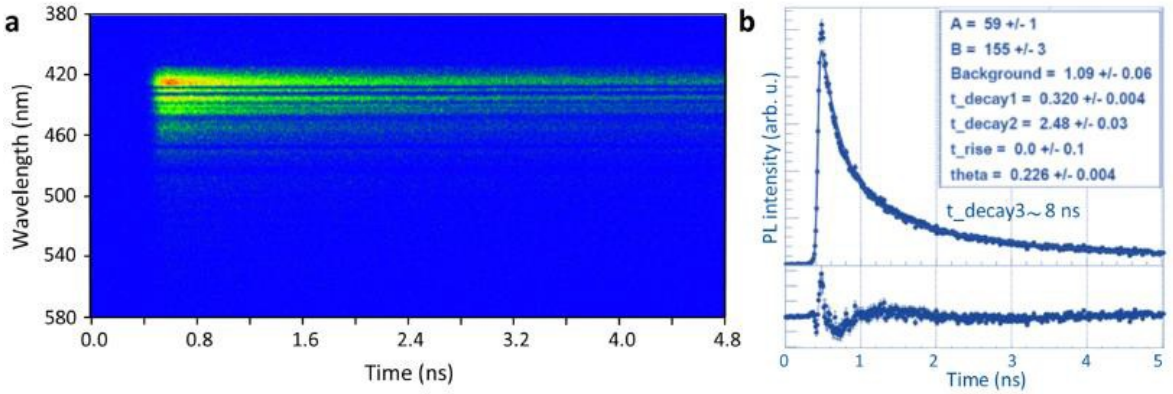

Fig. 7: Time resolved PL spectrum of the blue emission from the colloidal $CsPbBr_3$ nanoplatelets sample with maximum at 425 nm (a) and its decay curve (b).

One of the rapidly developing medical therapy method is the X-ray induced photodynamic therapy (PDTX). PDTX uses tumor-destroying agents based on **scintillating nanoparticles conjugated with photosensitizer molecules**. Upon irradiation, cytotoxic singlet oxygen is produced. We have studied the LuAG:Pr^{3+}-porphyrin based nanohybrid system as a **candidate for the future PDTX drugs**.

We also design, prepare and characterize **phosphors for solid state lighting**. The search for efficient color conversion phosphors for white light emitting diodes (w-LEDs) has sparked renewed interest in the photoluminescence behavior of mainly rare-earth doped materials. We have been investigating a very novel group of w-LED phosphors based on the Eu^{2+}-doped garnets and ternary ALnS2 sulfides (A
= Na,K,Rb; Ln = La,Gd,Lu,Y), and in selected cases further extended to multicomponent

sulfides, e.g. KxNa1-xLuS2. In the latter, the **photoluminescence spectra can cover a broad emission range** and be finely tuned by changing the K/Na ratio, see **Fig. 8**. Both near UV and blue excitations are efficient,
and a circadian light source can be constructed using these phosphors, which were also the subject of an application-minded project in a program of Technological Agency of CR.

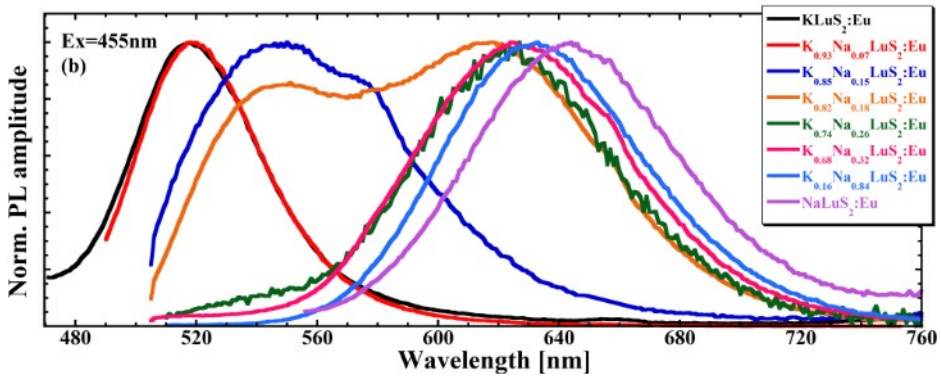

Fig. 8: Photoluminescence spectra of W-LEDs phosphors based on Eu^{2+}-doped $K_xNa_{1-x}LuS_2$ under 455 nm excitation.

We have also studied an interesting problem of stabilization of the Eu^{2+} emission center at the trivalent site of YAG in powder samples. Such material shows potential for “all-in-one” white light emission phosphor to constitute an innovative class of phosphors for the solid-state lighting. Therefore, we have also filed a national patent application (granted in 9/2020).

Theory of nucleation and phase transitions

Crystals are formed within the supersaturated or supercooled parent phase via nucleation and subsequent growth. These processes determine the resulting physical properties of the obtained product. However, understanding the molecular mechanisms, which occur during crystallization, remains a scientific challenge.
In cooperation with the University of Lyon and Interdisciplinary Center of Nanoscience in Marseille within the COST project CM1402 we studied crystallization of L-glutamic acid (Lglu) at three different scales: the liter scale in a 2 L stirred crystallizer, milliliter scale in a 4 mL stagnant cell, and microliter scale in microfluidic channels. In various experiments at different temperature and supersaturation conditions the metastable α or stable β polymorphs crystallized. Lglu obeyed the Ostwald rule of stages at low temperatures, therefore simulations were carried out at the temperature T = 5 ^{o}C. Kinetic equations describing the formation of polymorphs were solved numerically to determine basic characteristics of the phase transition process, i.e. the size distribution of nuclei, nucleation rate, and crystallization fractions of both polymorphs. We have shown that at the early stages of formation of polymorphs, the formation of α and β nuclei increased and reached a maximum – see **Fig. 9**. However, after less than 0.3 s, the number of nuclei of the stable polymorph decreased to negligible values. These simulations showed a fundamental result: a few stable clusters, which had nucleated, disappeared after 0.3 s.

We studied the dimensionless nucleation rate of clusters to explain how the stable clusters dissolution). The system obeyed the Ostwald rule of stages.

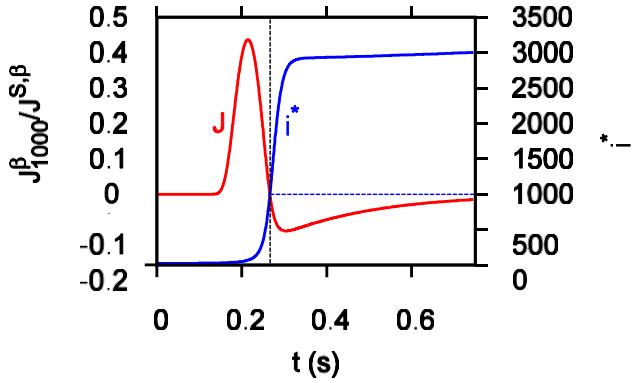

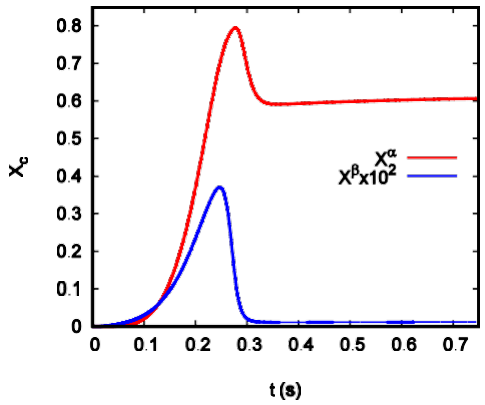

Fig. 9: Dimensionless nucleation rate J of polymorph β composed of 1000 molecules (red line) and the critical size i^* of nuclei (blue line) as a function of time (left).
Fig. 10: Time evolution of the crystallization fractions X_C of α (red line) and β (blue line) Lglu (right).

Application of magnetic resonance spectroscopies in the solid state

By means of magnetic resonance spectroscopies we investigate **processes of charge trapping** in optical, luminescence and scintillation materials, physics of their point defects, and physical properties of ferroelectric and multiferroic materials. Whenever possible, we correlate them with the optical experiments, which also include the above-mentioned garnet and sulfide materials. This enables a precious **understanding of the atomistic aspects of energy transfer and storage** in wide band gap optical materials. Experimental methods involve advanced electron paramagnetic resonance (EPR), solid-state nuclear magnetic resonance (NMR), electron-nuclear double resonance and electrically detected EPR.

Understanding of **electron and hole trapping in wide band-gap scintillation materials** and the nature of corresponding lattice defects is of crucial importance to optimize material performance close to its intrinsic limits. EPR allows not only to detect impurity ions or lattice defects in material but also to determine their local structure and interaction with the neighborhood. The trapping phenomena were studied in the Ce (Pr)-doped garnet scintillators, $Y_3Al_5O_{12}$ and $Lu_3Al_5O_{12}$. Due to host traps, their scintillation response is degraded by very slow components which deteriorate efficiency and timing characteristics. We found that holes created by ionizing radiation are dominantly self-trapped at regular oxygen ions forming O^- hole center (O^- small polaron) stable up to 100 K, **Fig. 11**. At higher temperatures, thermally liberated holes are retrapped at oxygen ions in the vicinity of an acceptor ion such as Mg^{2+} and AlY or AlLu antisite ions and are stable up to ≈ 150 K. Irradiation also creates an F^+ center, an electron trapped at the oxygen vacancy (V_O)**, Fig. 11**. The temperature behavior of the F^+-center electron in oxygen-deficient crystals is entirely similar to the behavior of the donor electron in a semiconductor. This is probably the first observation of a donor-like behavior of the F^+ center in wide band-gap insulating crystals.
We **clarified the processes of cation substitution in solid solutions - multicomponent garnet scintillators** which became a hot topic due to their enhanced performance achieved by the band gap and defect tailoring. Varying the ratio of constitutional cations in $(Lu,Y,Gd)_3(Ga,Al)_5O_{12}$ garnets, one cancontrol the short-range order of atoms in the crystal host, which affects the transport of electronic excitations to activators. Since the site occupation has not been well understood, we applied NMR as a unique tool to quantify the site occupancy over a full compositional range. Both experimental and theoretical (DFT calculations) results indicated non-uniform distribution of Al and Ga over the tetrahedral and octahedral sites in the garnet structure. The strong preference of Ga to occupy the tetrahedral sites at all Ga

concentrations, **Fig. 12**, is primarily driven by the involvement of Ga $3d^{10}$ electrons in interactions and due to the different nature of the chemical bonds formed by Al and Ga.

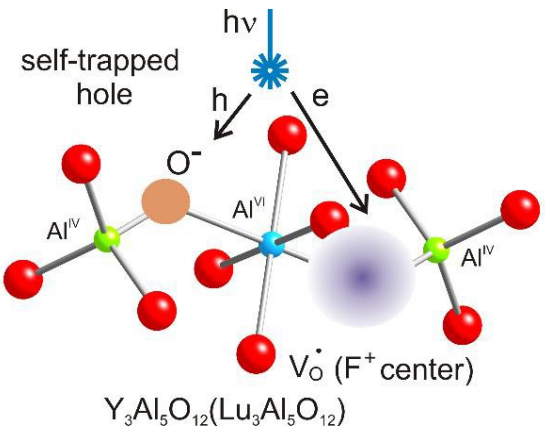

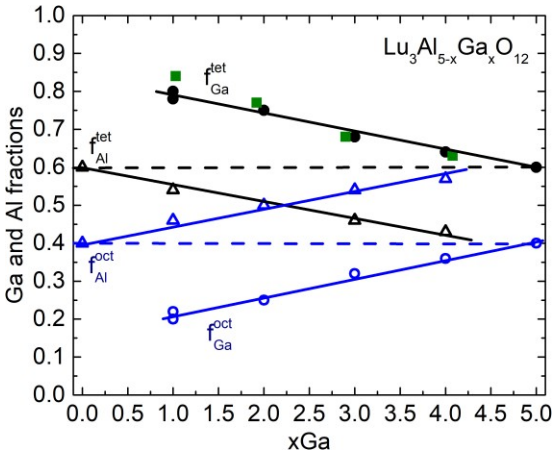

Fig. 11. Models of the self-trapped hole (O^- small polaron) and F^+ center in the garnet lattice(left).
Fig. 12: Fractional occupations of Ga and Al ions in $Lu_3Ga_xAl_{5-x}O_{12}$ mixed crystals as a function of the total Ga content. Dashed lines correspond to the random distribution of Al and Ga over tetrahedral and octahedral sites (right).

Another example of the critical importance of EPR experiment in understanding atomistic aspects in energy transfer processes and charge capture in a host lattice is demonstrated in our study of the electron and hole trapping in Eu- or Eu,Hf-doped LuPO4. Peculiarities of the emission center embedding are studied by EPR for the Ce^{3+} incorporation in heavy perovskite LuAlO3 LPE films.

Finally, we also investigated **multiferroic materials** with magnetoelectrical coupling. These materials are attractive for **spintronics and random-access memory applications and telecommunication**. Based on the systematic study of EPR, NMR and Mössbauer spectra, we explained the coexistence of the long-range ordered antiferromagnetic and spin-glass phases in Pb(Fe1/2Nb1/2)O3 -based multiferroics. The main physical mechanism of such coexistence is the interplay between chemical disorder and the anisotropy and frustration of exchange interactions between Fe^{3+} spins in the above multiferroics. The electric field of only 20-25 kV/cm is able to switch the antiferromagnetic domains in Pb(Fe1/2Nb1/2)O3 and align them with the ferroelectric ones even in ceramics offering the possibility of electric field control and switching antiferromagnetic domains off.

Materials for photovoltaics

The surface and size effects in zinc oxide nanostructures impose challenges for **energy conversion and sensing applications i.e. in solar cells, optoelectronic devices, gas sensors, or energy storage**. We have optimized hydrothermal synthesis of densely packed, perpendicularly oriented aligned ZnO nanocolumns on seeded glass substrates as well as hedgehog-like nanoparticles (NPs) dispersed in colloids, see **Fig. 13**. We have recently reported the paramagnetic resonance lines in the ZnO NPs and attributed the signals to the F+ center (electron captured in an oxygen vacancy). **ZnO nanorods perpendicularly oriented to the fused silica substrates** were directly grown under hydrothermal conditions with UV irradiation. The results showed a significant increase in the length of ZnO nanorods as well as an improvement in their uniformity and enhancement of the opto-electrical quality, **Fig. 14**. Plasma modification of surfaces by plasma processing provides another tool for tailoring of characteristics. We have developed a novel **inductively coupled plasma (ICP) reactor in a cooperation with the SVCS Process Innovation company** which enables strong enhancement of the exciton related sub-nanosecond UV photoluminescence.

Absorption spectra of recently emerged **photovoltaic materials, inorganic-organic hybrid perovskites,** have revealed a very sharp absorption edge and very low deep defect density. This has become one of the highly cited reasons for the success of this technology. More information, especially on the degradation processes, was obtained from subsequent studies by also combining photocurrent techniques. In collaboration with the Centre for Advanced Photovoltaics at the Faculty of Electrical Engineering of the Czech Technical University in Prague, we have recently developed a **solar cell with efficiency over 19%.** We explained reversible changes of solar cells based on the lead iodide residue decomposition likely leading to iodine interstitial defects. These defects appear as sub-bandgap absorption observed by photocurrent spectroscopy, namely Fourier Transform Photocurrent Spectroscopy, **Fig. 14**.

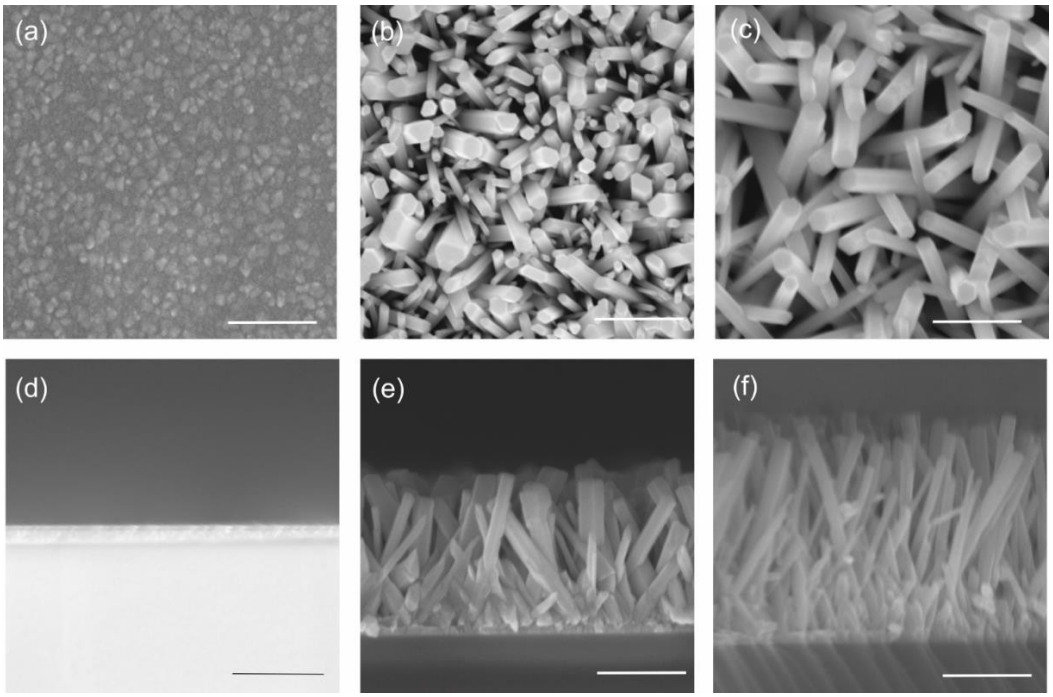

Fig. 13: Scanning electron micrographs of ZnO sputtered seeding layer in top view (a) and cross-section view (d) and ZnO nanorods growth with (b,e) and without UV irradiation (c,f) in the top and cross-sectional views. Scale bar: 500 nm

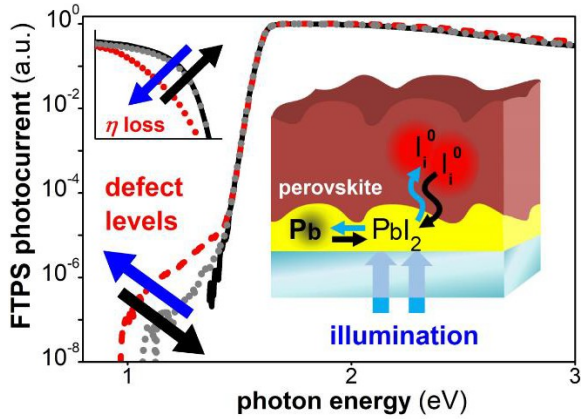

Fig. 14: Defect levels related to PbI_2 residue in the inorganic-organic hybrid perovskites identified by Fourier-Transform Photocurrent Spectroscopy.

Application of Photoelectron Spectroscopy in the Solid State

Activities of the Group of photoelectron spectroscopy were focused on **characterization of solid surfaces by photoelectron spectroscopy**. Investigated samples were prepared not only in FZU laboratories but also many off-site workplaces and foreign institutions. Obtained results were published in 29 papers. We have a very fruitful cooperation with colleagues from

the Institute of Physical Chemistry PAS in Warsaw where research was directed to investigation of **carbon modifications decorated by metal nanoparticles.** Such systems are promising **catalysts for fuel cells**.

GaN has attracted much attention due to its importance for photo-electronics. Non-destructive assessment of the polarity of GaN nanowire ensembles and electron band bending of GaN surfaces were investigated in the framework of a collaboration with North Carolina State University, USA and Paul-Drude-Institut für Festkörperelektronik, Berlin, Germany.
We have also focused on analysis of **buried heterointerfaces**. GaP is a promising material for III-V semiconductors integration to Si for multijunction solar cells. The GaP/Si heterointerface properties are the main theme of the bilateral project between our laboratory and the Photovoltaics Division at the Ilmenau University of Technology, Germany. Thin GaP/Si heterostructures were prepared by MOVPE. For the in-situ study of the heterointerface, we applied the gas cluster ion beam (GCIB) sputtering in combination with XPS and hard X-ray photoelectron spectroscopy at Spring-8 (Japan). The depth concentration profile of the GaP/Si sample is shown in **Fig. 15**. Core level analysis revealed a bonding configuration at the interface and the interface polarity. The valence band offset dependence on the GaP film thickness and preparation conditions have been investigated.

Diamond-like carbon (DLC) films are extensively studied materials due to their unique properties. They have widespread applications as **protective coatings** in areas such as optical windows, car parts, and biomedical systems. Hydrogen-free DLC films were prepared by a pulsed laser deposition under the medium energy Ar ion beam assisted growth. Carbon atom coordination has been determined nondestructively from the high-energy resolved C 1s photoelectron spectra, X-ray induced C KVV Auger electron spectra, and angular-resolved C 1s spectra aided by the maximum entropy method (MEM). Analysis of angular-resolved C 1s spectra by the MEM approach revealed the detailed shape of the depth dependences. The sp^2 coordination dominates at the top of the surfaces, it reaches a minimum below the surface and finally creates a wide maximum. The sp^3 coordination in-depth dependence shows a mirror-like behavior with respect to sp^2 and dominates at deeper layers, **Fig. 16**.

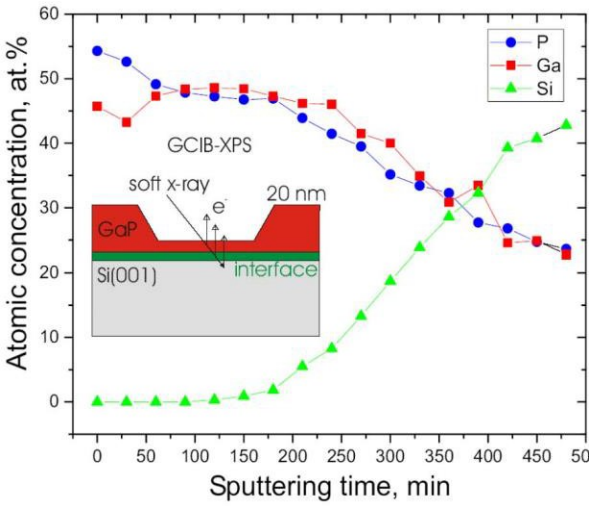

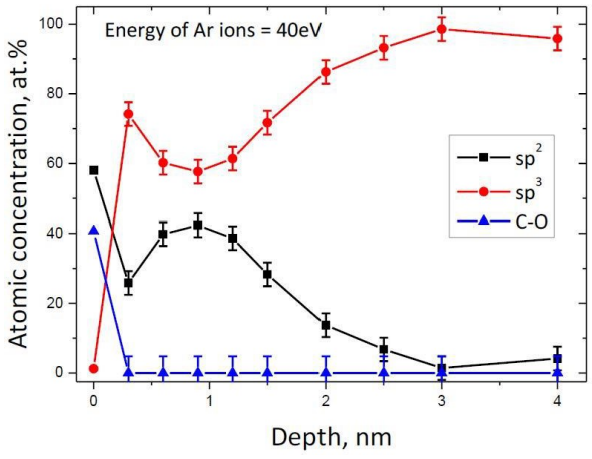

Fig. 15: Depth concentration profile of GaP/Si sample. Thickness of the GaP layer is 20 nm. The heterointerface is reached by sputtering using a gas cluster ion beam (GCIB). The energy of the cluster ions was 2.5 keV, the number of the atoms in the cluster was 1000, and the crater size was about 1.5 x 1.5 mm^2.(left)
Fig. 16: Reconstructed depth profiles of the C sp^3, C sp^2, and C-O carbon atom bonding states of DLC sample grown under 40 eV Ar ion beam energy with error bars to judge the reliability of the profiles. (right)

Research activity and characterisation of the main scientific results

The research activities of the team may be divided by main research topics to three topical subgroups that will be treated in detail as follows. The subgroups are not equal in manpower and there is substantial personal overlap among them.

Quantum and nonlinear optics

In the field of quantum and nonlinear optics, the topics mostly researched are related to detection and quantum processing of information, using the fields of photon pairs obtained by parametric down-conversion as the main tool.

In the area of quantum information processing, main effort has been exerted on design and construction of elements for manipulation of quantum states of single photons based on linear optics that can represent elements of future quantum communication networks. These include a general quantum gate that is optimal in the sense of maximizing the probability of success (Phys. Rev. Lett. 2015, 114, 153602), or a quantum router (Sci. Rep. 2018, 8, 13480) that can use a quantum-superposition state both as a routed and controlled quantum bit. Quantum gates have been used in the realm of quantum machine learning when the gate 'learns' to achieve the required transformation, in our case optimum cloning of quantum bits (Opt. Express 2019, 27, 32454). Some quantum machine learning algorithms rely on effective measurement of distance in the space of quantum states (Hilbert space) that can be interpreted as 'quantum rulers' (Phys. Rev. Lett. 2019, 123, 260501). Another building block of the future quantum internet has been realized in terms of the first execution of controlled quantum teleportation (Phys. Rev. Lett. 2019, 122, 170501) which can significantly increase the quantum data flow in multi-user networks and even across large distances. Our implementation of quantum teleportation uses tests and measures of entanglement at three-qubit quantum state (Phys. Rev. A 2019, 99, 042123).

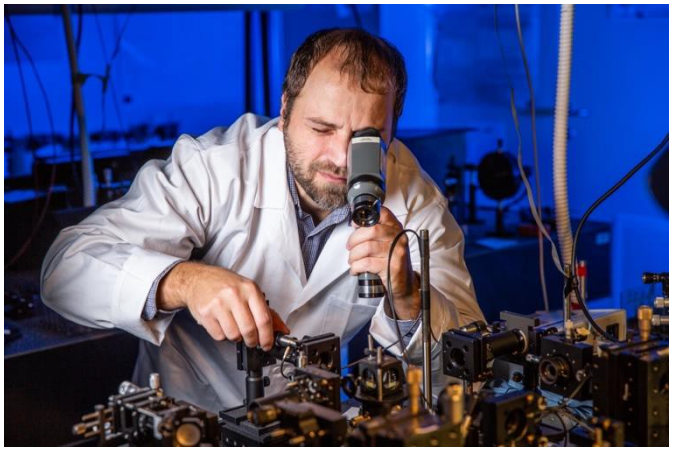

Figure 2: Member of the group of quantum and nonlinear optics A. Černoch in the laboratory of quantum information processing.

A lot of attention has been devoted to different methods of characterization of quantum states and quantification of their quantum correlations, non-classicality, and entanglement. An example of a robust entanglement witness is the collectability (Phys. Rev. A 2016, 94, 052334). A number of non-classicality criteria have been developed and experimentally tested (Opt. Express 2016, 24, 29496; Phys. Rev. A 2017, 96, 043845; Phys. Rev. A 2016, 94, 013807), some of which proved to be very useful for characterizing the robustness of non-classicality, evaluating non-classicality in higher orders of intensity moments (Phys. Rev. A 2017, 96, 033852; Sci. Rep. 2019, 9, 8961). Different tomography approaches have been compared and their efficiency examined (Sci. Rep. 2016, 6, 19610). Also, development of entanglement in time (quantum steering) has been explored (Sci. Rep. 2016, 6, 38076) including its possible impact on security of quantum cryptography (Phys. Rev. A 2016, 93, 062345). A peculiar application of quantum-entanglement-based security is presented in the experimental protocol

implementing quantum banknotes (npj Quantum Inf. 2017, 3, 7) including evaluation of its security limits and possible risks (Sci. Rep. 2019, 9, 16318).

We have also used detection and quantification of quantum entanglement in quantities other than photon numbers. We have shown, how a nonlinear entanglement witness can be used to diagnose quantum entanglement in an entanglement-swapping device (Phys. Rev. A 2017, 95, 030102). In another experiment we have demonstrated that nonlinear entanglement witnesses can be made particularly useful for entanglement detection in hyperentangled or multilevel states (Phys. Rev. A 2018, 98, 032307), where one can directly measure the witness on a single copy of a hyperentangled state instead of using several simultaneous copies of two-photon entangled states. Spatial quantum correlations in photon pairs have also been successfully used to suppress the noise in photon-number-resolved measurements (Phys. Rev. Appl. 2017, 8, 044018). The migration of coherence between composite quantum systems (entanglement) and their subsystems) has been demonstrated (Phys. Rev. A 2018, 97, 042305) and the conservation law for maximum accessible coherence has been revealed. Growing attention has been devoted to quantum correlations in strong beams (at classical intensities) in various nonlinear processes including transfer of quantum correlations through the nonlinear process (Sci. Rep. 2016, 6, 33802). In the case of stimulated down-conversion, an elegant experiment has been designed to show the transition from position correlations (in the near-field) to momentum correlations (in the far field) during propagation of the twin beams behind a nonlinear medium (Sci. Rep. 2015, 5, 14365). The nonlinear dynamics of the strong process when the pumping beam gets depleted with rich impact on quantum correlations has been solved in terms of the number of active mode triplets (Sci. Rep. 2016, 6, 22320).
The subgroup intensively cooperates with the groups from Adam Mickiewicz University, Poznań, Poland, University of Zielona Góra, Poland and University of Insubria, Como, Italy, including frequent staff visits, stays and student mobilities. In total, 34 publications in journals with impact factor have been published within the subgroup in 2015-2019.

Applied optics

This subgroup has dealt, for a long time, with advanced approaches and applications focused on various areas of applied and technical optics and optoelectronics. The main focus has been on proposals, analyses, designs and production of non-standard optical elements and systems (both imaging and non-imaging), e.g., optical systems of fluorescent detectors intended for particle physics research. Novel optical technologies using the subaperture method have been developed and employed. Related development has been performed in the area of optical layers and the methods of their analysis.

Figure 3: L. Nožka examines one of the mirror segments produced for the fluorescence telescope at the Pierre Auger Observatory.

The ability to manufacture low-scattering mirror surfaces of large dimensions created the basis for the participation of the group in building and operating the Pierre Auger Observatory (PAO) located in Argentina that continues and is being further developed (see, e.g., J. Instrum. 2018, 13, T05005, a study of long-time performance of PAO fluorescence detectors). With the participation of our subgroup, PAO achieved a number of significant results including the observation of large-scale anisotropy in the arrival directions of high-energy cosmic rays (Science 2017, 357, 1266) and contribution to the multi-messenger observations of a binary neutron star merger (Astrophys. J. Lett. 2017, 848, L12). The success of PAO resulted in involvement in the international collaboration CTA – Cherenkov Telescope Array – where the subgroup has contributed to the selection of final locations of the observatories (J. Instrum 2015, 10, P04012; Adv. Space Res. 2016, 57, 2559) using its all-sky cameras (also employed in PAO control system), and has developed measurement systems and methods for quality evaluation of production and service wear of mirror samples, supplied by different potential producers and intended for using in optical telescopes as detectors of cosmic rays. The subgroup also contributes to the development of electronic detectors for the observatory (Nucl. Instrum. Meth. A 2017, 845, 350; Eur. Phys. J. C 2017, 77, 47).
For a newly established collaboration FAST (Fluorescence detector Array of Single-pixel Telescopes) a prototype of a new generation of fluorescence detector has been designed and constructed (Astropart. Phys. 2016, 74, 64; J. Instrum. 2017, 12, T07001). Currently, four prototypes are in operation at the Telescope Array site (Delta, Utah, U.S.A.) and PAO (Malargüe, Argentina) offering new approaches to mutual calibration of both large cosmic-ray terrestrial facilities.

The subgroup contributes also to other tasks applicable in industry or academia (e.g., a device controlling, in real-time, colour markings of coil springs produced on the production line for the automotive industry, or delivery of specialized mirrors for the CERN LHCb experiment).
The involvement of the team in Pierre Auger and CTA collaborations resulted in contribution to 40 publications in Web-of-Science-registered journals (published with large [~500] author lists) and 7 papers with smaller teams. In these collaborations, the team closely cooperates with the Team 1 ("Astroparticle physics"). While our team focuses on tasks related to applied optics, optical systems and technologies, Team 1 concentrates on data processing and astro- particle physics. Both teams are involved in the daily operation of the Pierre Auger Observatory.

Measurement methods, layers and surfaces

This subgroup deals with a number of optomechanical methods of analysis of materials and processes.
In the area of optical non-contact measurement methods various techniques based on wave and statistical optics have been employed. Using white-light interferometry, the method of shape-from-focus has been modelled and implemented allowing for wide-field precise measurement of the shape of 3D objects based on search of local focus (Appl. Opt. 2015, 54, 9747). A high-speed white-light interferometry sensor based on Hilbert transform has been developed (Meas. Sci. Technol. 2015, 26, 085207) and patented (PV2015-348). A white-light 3D sensor without the need of any mechanical movement has been presented (Opt. Las. Eng. 2020, 124, 105800) where a fibre stretcher is used to change the optical path difference. Another method of 3D scanning of both polished and rough objects based on coherence scanning interferometry has also been improved to avoid the movement of measured objects using an electrically focus-tunable lens (Appl. Opt. 2019, 58, G91). Applications of electronic speckle pattern interferometry (ESPI) methods were studied, for instance an efficient evaluation of high-noise correlograms (Optik 2015, 126, 865), or new approaches for determination of mean speckle size (Measurement 2016, 88, 271). An optical non-contact method based on Fresnel diffraction has been suggested and tested for study of the biological activity of plants. An optical sensor is able to monitor the hydraulic surge propagating through a wounded plant (Plant Meth. 2018, 14, 38).
Another part of the subgroup was focused on the experimental analysis of mechanical and tribological properties at small scales using the state-of-the-art equipment and methods. Various types of thin films, coatings, micro-objects and surfaces of a wide range of bulks (composites, alloys, ceramics, glasses) have been examined using depth-sensing nanoindentation and nano/micro-scratch test, and correlated with advanced microscopy techniques (CLSM, AFM, SEM-FIB) and acoustic emission records that offer a large added value to traditional methods. Acoustic emissions are evaluated both in time- and frequency-domain and their benefits are evaluated in an overview paper (JOM 2019, 71, 3358). The method has been fully developed including necessary hardware and software and introduced into standard laboratory practice.

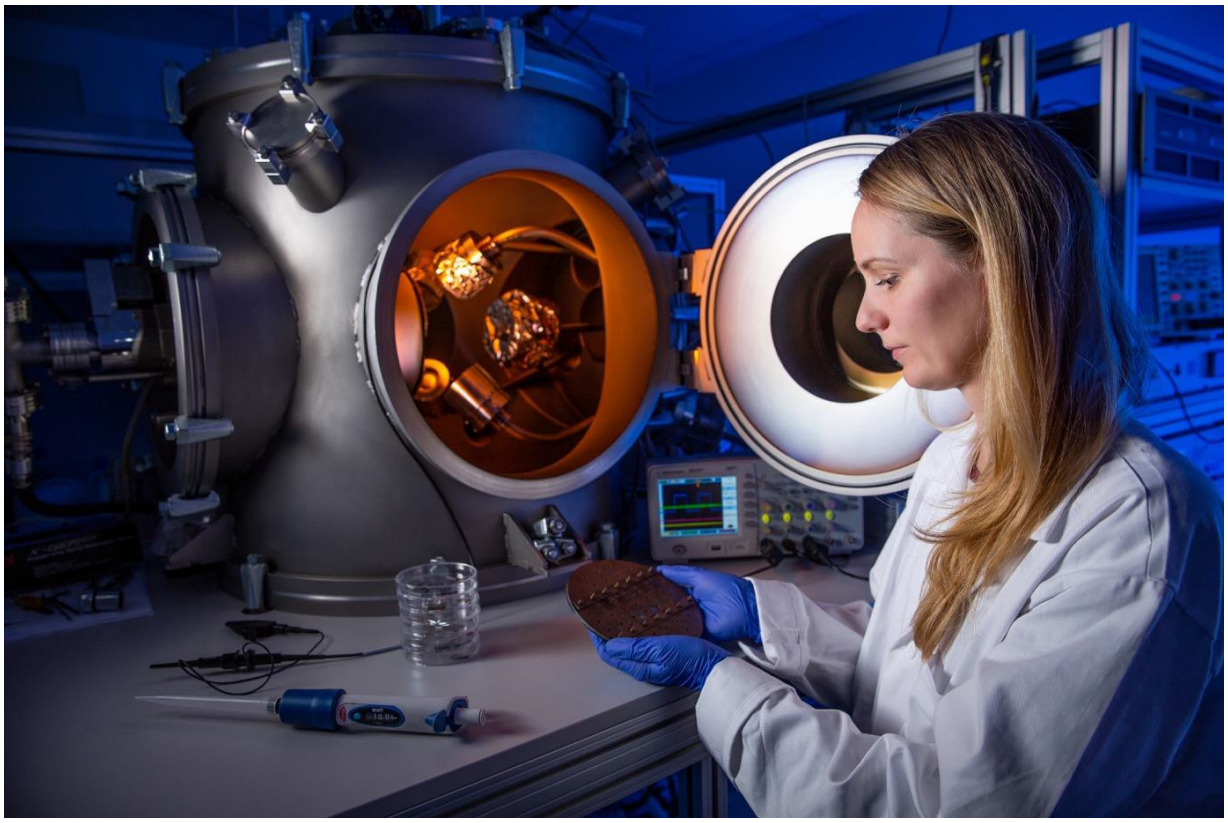

Figure 4: Cold plasma deposition system at the Joint Laboratory of Optics.

In particular, an in-depth study of the influence of deposition conditions on composition, structure, and thermal stability of SiC and SiCN layers has been performed. Incorporating nitrogen atoms into the SiC structure leads to improved resistance against the occurrence and propagation of cracks suppressing the intrinsic fragility of the ceramics (Sci. Rep. 2018, 8, 10428). Using the analysis of acoustic emissions recorded during local nano/micro-scratch testing and nanoindentation tests offers a deep insight into the mechanisms of mechanical failures of materials (Coatings 2018, 8, UNSP 196). These methods have also been used to study the mechanical stability of optical SiO_2 thin films deposited on glass (Chem. Pap. 2018, 72, 2143), or tests of adhesion/cohesion stability of composite thin layers based on diamond crystals embedded in a nanocrystalline SiC matrix (J. Alloy Compd. 2019, 800, 327). The research works dealing with thin films and coatings were mainly performed in cooperation with members of Teams 4, 6, 14, and 18 (our team supplied measurements and analyses of mechanical properties) and partly also in international cooperation with SŢSȩECAM Science and Technology Center, Gebze-Kocaeli, Turkey.

In the area of laser technologies, attention has been devoted to the interaction of intense laser pulses with metallic and glass materials with respect to applications in laser cutting, drilling, welding and marking (Adv. Mater. Sci. Eng. 2015, 584952). Investigation of interaction of ultrashort laser pulses with glass (Sci. Rep. 2016, 6, 39133) has been performed in cooperation with Team 20 resulting in a detailed description of the role of different ablation mechanisms (our team supplied the ultrafast laser techniques and optical part of the experiment, while the idea, analysis and substantial part of the laboratory work has been done by members of Team 20).

As a whole, the subgroup published 16 papers in journals with impact factor during 2015- 2019.

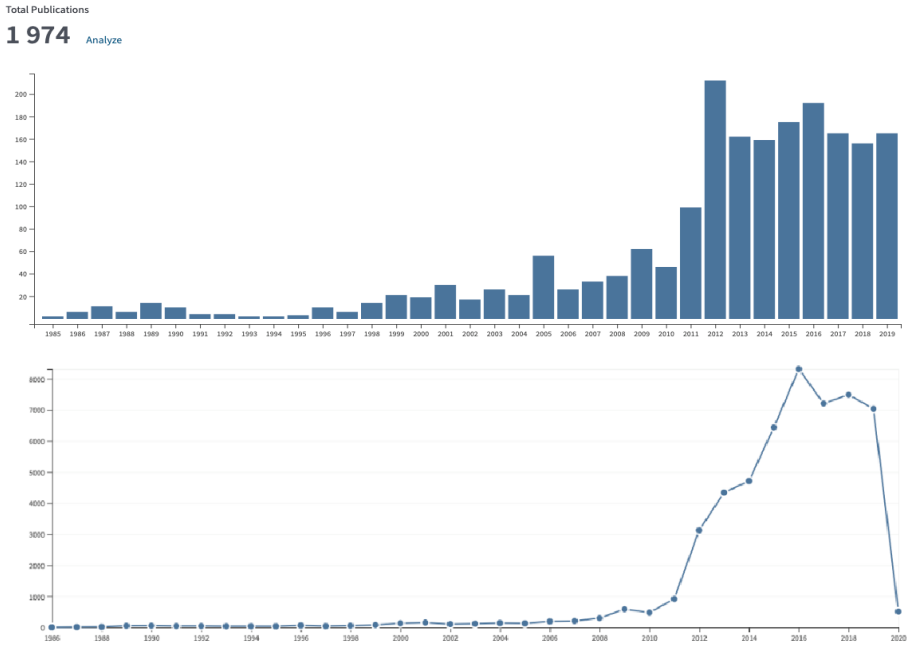

Figure 5: Total number of publications (top) and number of citations (bottom) of the Joint Laboratory Optics in the period 1995-2019 according to Clarivate Analytics Web of Science (to March 3, 2020). The total h-index of the Joint Laboratory of Optics is 101. These graphs include to output of the workplace as a whole, i.e. including its Palacký University part. The large increase in the number of publications in 2011-14 is partly caused by the participation in the CERN-ATLAS Collaboration that is realized mainly in the Palacký University part of the workplace. To document that the output of the workplace has solid growing trend regardless of this effect we show the Web of Science numbers without the large international collaborations in the next Figure.

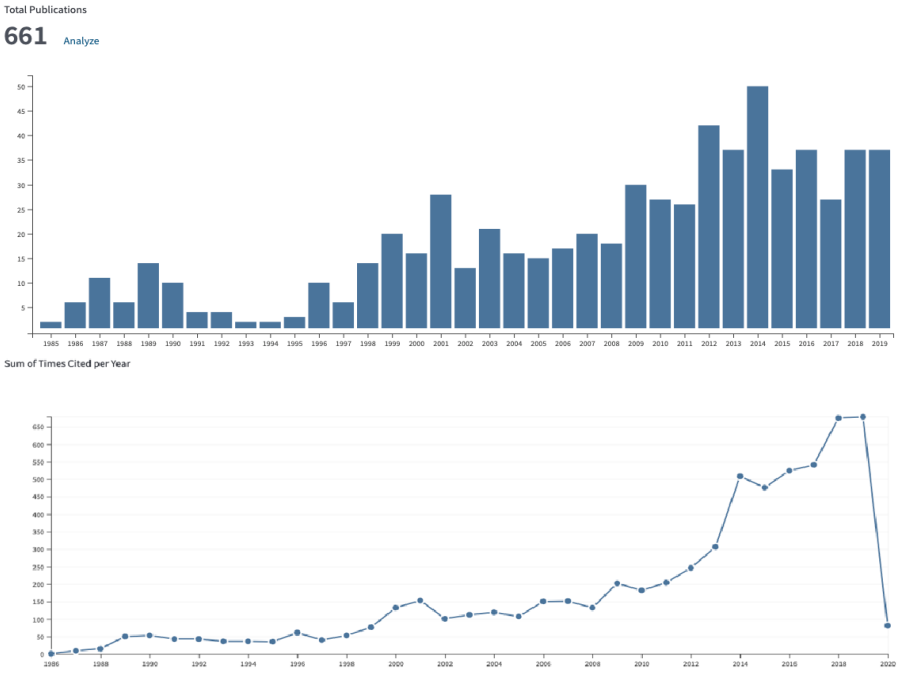

Figure 6: Number of publications (top) and number of citations (bottom) of the Joint Laboratory Optics in the period 1995-2019 according to Clarivate Analytics Web of Science (to March 3, 2020) excluding the output belonging to large international scientific collaborations (CERN-ATLAS, Pierre Auger Observatory). The plots include the output of both the Palacký University and the Institute of Physics parts of the workplace, nevertheless, to large majority of the results workers affiliating to both parts affiliated (h-index 36).

A number of grant projects have been solved in the evaluated period, a short list follows [title, code, provider (period), main (co-)investigator on behalf of the evaluated team]:

- Czech participation in the project AugerPrime at the Pierre Auger Observatory, LTT18004, Ministry of Education, Youth and Sports of the Czech Republic (2018-2022), M. Hrabovský.
- Development of Czech participation in CTA, LTT17006, Ministry of Education, Youth and Sports of the Czech Republic (2017-2021), M. Hrabovský.
- European support to the Czech participation in the building of CTA observatory, CZ.02.1.01/0.0/ 0.0/ 16_013/0001403, Ministry of Education, Youth and Sports of the Czech Republic (2017-2020), D. Mandát
- Precise optical 3D sensors with active optical elements, 17-05547S, Czech Science Foundation (2017-2019), P. Pavlíček
- Pierre Auger Observatory – participation of the Czech Republic, LM2015038, Ministry of Education, Youth and Sports of the Czech Republic (2016-2019), M. Hrabovský.
- Cherenkov Telescope Array – participation of the Czech Republic, LM2015046, Ministry of Education, Youth and Sports of the Czech Republic (2016-2019), M. Hrabovský.
- Statistical properties of intense paired fields, CNR-16-05, AS CR (2016-2018), J. Peřina.
- Scientific activities of the Czech Republic at the Pierre Auger Observatory, LG15014, Ministry of Education, Youth and Sports of the Czech Republic (2016-2017), M. Hrabovský
- Optical 3D sensors with high information efficiency, Czech Science Foundation (2013-2015), P. Pavlíček.
- Systems of acoustic emission for characterization of mechanical properties and stability of thin layer structures and functional surfaces, TA03010743, Technological Agency of the Czech Republic (2013-2016), M. Hrabovský.
- Suppression of quantum noise using entanglement of photon pairs, P205/12/0382,

Research activity and characterisation of the main scientific results

Plasma deposition of semiconducting oxide thin films for photoelectrochemical application.

In this basic research, our effort was focused on the research of plasmatic deposition of oxide semiconductor films for photoelectrochemical solar water splitting applications. Our team was oriented to research of plasma deposition by new configurations of reactive pulsed high-power impulse magnetron sputtering (HiPIMS)

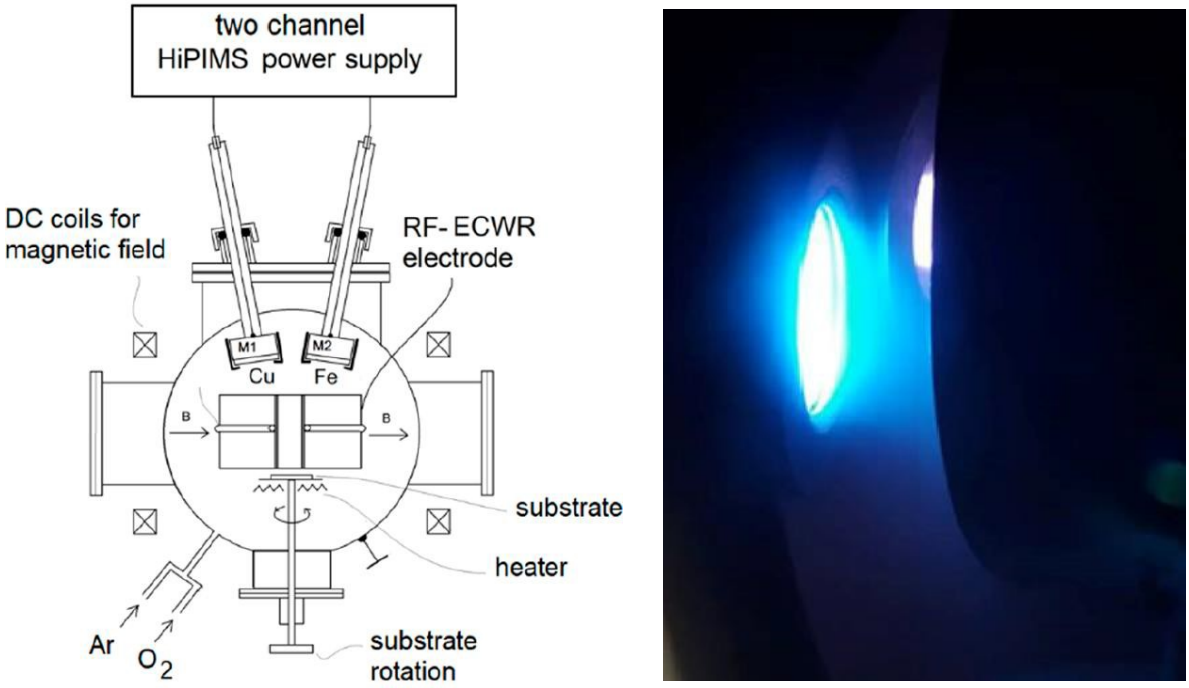

Fig. 1 *Experimental apparatus with two magnetrons and a radio frequency (RF) electron cyclotron wave resonance (ECWR) electrode for deposition of copper iron oxide thin films.*

and by hybrid reactive plasma systems combining reactive HiPIMS and midfrequency (MF) bipolar pulse sputtering. Another hybrid plasma deposition system employed a combination of reactive HiPIMS and inductively coupled plasma working with an electron cyclotron wave resonance ECWR (HiPIMS+ECWR). The general experimental set up of the HiPIMS+ECWR hybrid reactive plasma deposition system working with two magnetrons can be seen in Fig 1. Our team focused on the study of physical processes in the complex reactive plasma during the deposition process. This included plasma diagnostics carried out by several methods. Photoelectrochemical analysis of deposited

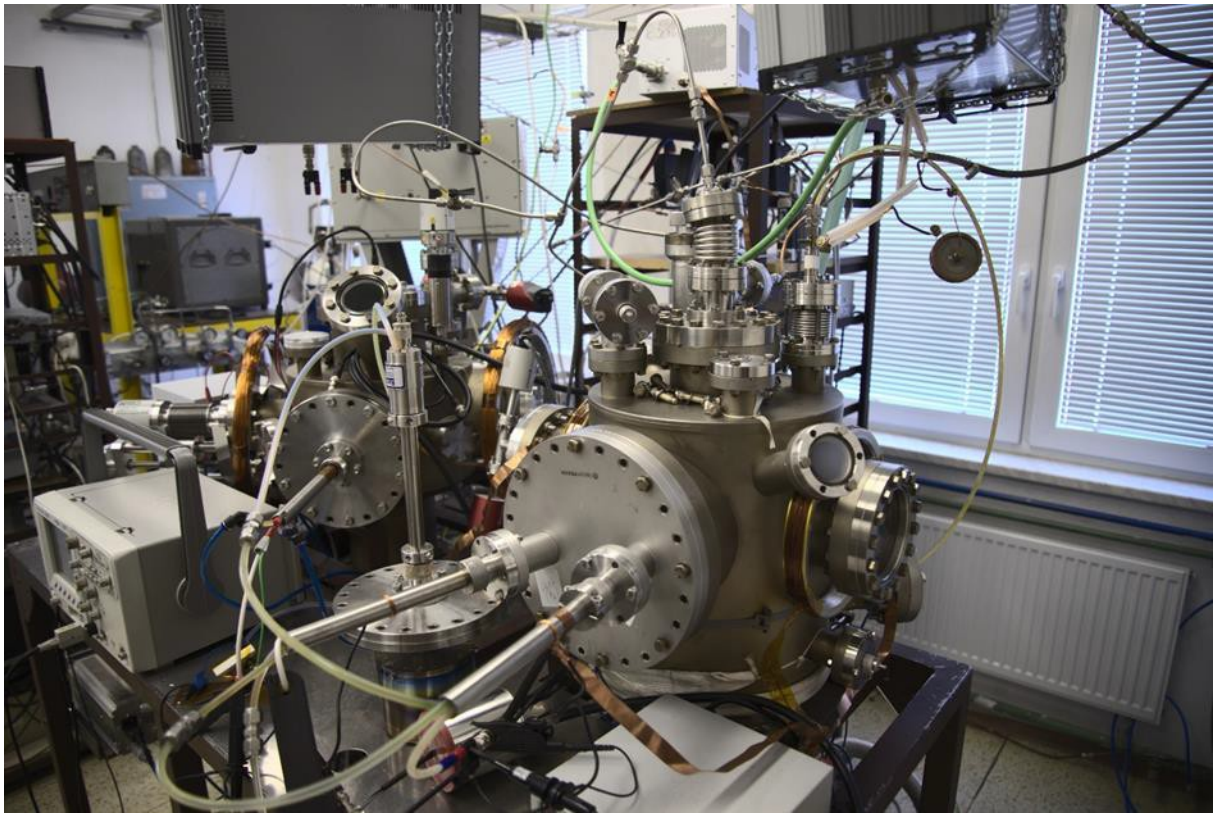

Fig. 2 *Photography of developed HiPIMS+ECWR plasma deposition system*

semiconductor thin films and correct interpretation of this data was carried out in cooperation with our scientific partners from different institutions. The main scientists responsible for photoelectrochemical measurements were professor dr. Josef Krýsa, dr. Martin Zlámal and dr. Neumann-Spallart from the Department of Inorganic Technology, University of Chemistry and Technology, Prague. The first group of investigated materials were semiconducting photoanode thin films based on hematite Fe_2O_3 [1, 2], monoclinic WO_3 [3] and TiO_2 [4,5] deposited by the reactive HiPIMS magnetron sputtering and by hybrid HiPIMS+MF or HiPIMS+ECWR on FTO glass at defined conditions in the pulsed plasma. These films exhibited a quite large photoelectrochemical response, good stability and adhesion. In order to extend this research, p-type photocathode films were also prepared. As a first p-type semiconductor, copper oxide films with different structures and ratios of Cu_2O to CuO were deposited by reactive HiPIMS in an $Ar+O_2$ gas mixture with a defined value of the ion flux on the substrate during the deposition process [6]. Photoelectrochemical response, in the cathodic region, and electrochemical stability were assessed and compared with other methods of depositing these types of films. Recently complex and more stable $CuFeO_2$ films with delafossite structure and p-type conductivity were deposited by reactive HiPIMS and HiPIMS+ECWR co-sputtering from two targets. This research was published in [7] and belongs rather into the next time period 2020-2024. The photography of developed HiPIMS+ECWR deposition system can be seen in Fig 2. Photography of n-type and p-type semiconducting oxide thin films deposited by reactive HiPIMS+ECWR on FTO glass can be seen on Fig 3.

Fig. 3 *Photography of deposited semiconductor thin films a) n-type photoanode Fe_2O_3 (2x left) and WO_3 (right) b) p- type photocathode $CuFeO_2$ with delafossite structure.*

Plasma diagnostics of low temperature plasma during the thin film deposition process

An important research activity in the team was investigation of new approaches in low temperature plasma diagnostics during the process of thin film growth. We aimed our investigation onto plasma behaviour within various technological applications, mainly in pulsed magnetron sputtering deposition. Our goal was to find relationships between plasma microscopic parameters and physical properties of deposited thin films. We developed new diagnostic techniques, which allowed the discharge to be examined in situations where known diagnostic techniques fail. Based on the outlined research strategy, a new diagnostic method of low temperature plasma was developed, which we called the modified Katsumata probe. We started from the concept of the Katsumata probe used to study ion temperature in fusion magnetic devices. By adding an external homogeneous magnetic field, of correct magnitude, to a standard Katsumata probe, we created a new probe, which allows measurement of the velocity distribution of ions in a low temperature plasma even without a strong magnetic field, such as in typical technological discharges. [8].
A new RF probe for the measurement of plasma parameters was developed by our team in cooperation with our scientific partners from the South Czech University, Faculty of Natural Sciences, Ceske Budejovice. This probe is supplied by an RF signal with a frequency well below the ion plasma frequency and can measure the ion flux on the substrate. When a new calculating algorithm for subtraction of capacitive current is applied, the ion plasma density and tail electron temperature can be calculated. This probe has a large benefit, as it is not sensitive to dielectric layer coatings on the probe surface, since it employs only the RF current on the probe. Results of use of this probe in reactive plasmas were published in [9].

Another important research goal was the study of velocity distribution functions of working gas ions and sputtered particles in a magnetron discharge. Here we used an energy resolved mass spectrometer (Hiden Analytical Ltd, UK). We focused our attention on the study of Ar, Ti, ArTi, O, O_2 ions and their possible dimers such as Ar_2 or Ti_2. The obtained velocity distribution functions of the various ions showed that the Ar^+ distribution consists of a low-energy and a high-energy part, while the Ti^+ distribution contained a predominantly high-energy part and the low-energy part of the distribution appears only with increasing working pressure. This shows the processes of formation of individual ions in the plasma and elementary processes taking place in the discharge. For example, the Ti_2^+ dimer is formed by ionizing the Ti_2 dimer in the plasma volume and the Ti_2^+ density decreases with increasing working pressure due to formation of Ti clusters [10]. We also applied a similar approach for measurement of ion velocity distributions in HiPIMS discharge. It has been shown that the argon and titanium ion velocity distributions exhibit similar shapes as in a standard magnetron discharge, i.e. the presence of a low-energy and high-energy part of the distribution. However, the velocity distribution can be well approximated by the so-called shifted bi-Maxwellian distribution. Such velocity distribution suggests that in the region of formation of ions an electric field of the opposite direction, which accelerates the ions towards the substrate, must exist. This supports the existence of the so-called potential hump, which has been observed by other authors based on plasma potential measurements [11]. We further developed plasma diagnostic techniques, which can be used easily during the technological process. An important technological parameter of the HiPIMS discharge is the degree of ionization of the sputtered particles. In our work, we focused on this topic by studying ionized fractions of deposited particles using our laboratory developed probe (so-called ion meter) and measured plasma parameters using a time-resolved Langmuir probe. Results have shown that by selecting a suitable model, the plasma parameters obtained from the Langmuir probe measurements can be used to determine the ionization fraction of the particles incident on the substrate. In this work, we investigated plasma parameters of various target materials, namely Ti, Al and C as can be seen in Fig 4. It has been shown that the peak of the ionized fraction of deposited particles exists for Ti material (78%) [12, 13]. We cooperated on this research with our scientific partner dr. Daniel Lundin from Université Paris-Sud, Orsay, France. Dr. Daniel Lundin focused on modelling of the processes in the plasma and our team designed and invented the experimental set up, carried out measurements and provided physical interpretation of experimental results.

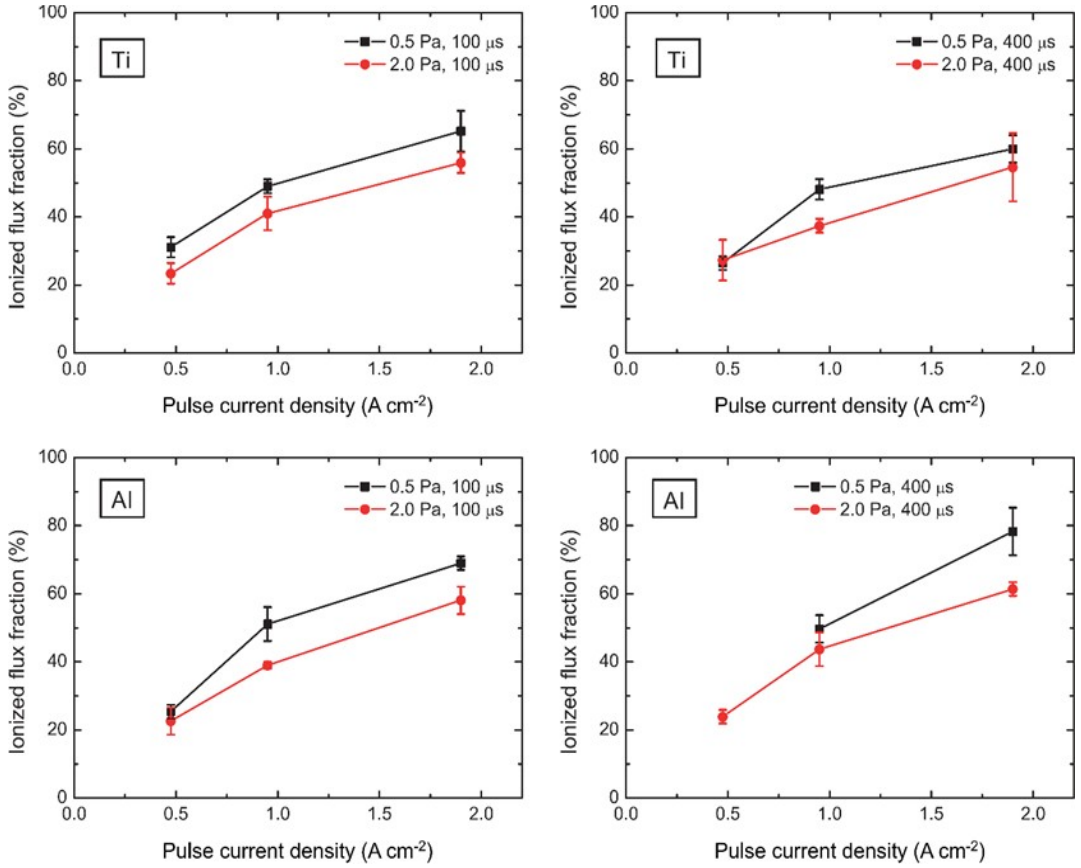

Fig. 4 *Ionized metal flux fraction of Ti (top) and Al (bottom) as a function of average HiPIMS pulse current density. The left column displays the case for 100 μs pulses and the right column the case of 400 μs pulses.*

Thin film Co_3O_4 catalyst

The next important research topic is the deposition of Co_3O_4 thin film catalysts and their characterization. We cooperated on this project with professor dr. František Kovanda from University of Chemistry and Technology, Prague and dr. Květa Jirátová from the Institute of Chemical Process Fundamentals CAS Prague. Our team was mainly focused on plasmatic depositions of these films and research of physical processes in the plasma during the deposition process. We have focused on the following tasks for these materials. The first task was to improve the properties of chemically prepared catalysts. The second task was to find out and describe the differences between catalysts prepared by high-power impulse magnetron sputtering (HiPIMS) and radio-frequency (RF) magnetron sputtering. The achieved key research results are summarized below.

The supported catalysts with Co_3O_4 coatings on stainless steel wire meshes were prepared by a combination of reactive magnetron sputtering and electrochemical deposition (ED). The cathodic reduction of cobalt nitrate in aqueous solution followed by heating of the deposited product resulted in Co_3O_4 catalyst with high activity in ethanol total oxidation. The coating of stainless steel meshes with Co_3O_4 thin films by RF magnetron sputtering or HiPIMS procedures led to an increase in adhesion of Co_3O_4 subsequently added by electrochemical

deposition, however the adhesion of deposited cobalt oxide was significantly further improved, when the obtained catalysts were coated with additional Co_3O_4 thin film by magnetron sputtering. RF-ED-RF catalysts prepared in such a manner showed the highest specific activity in ethanol total oxidation and the highest Co_3O_4 adhesion to the support. It was found that the catalytic activity of catalysts prepared by RF magnetron sputtering is higher than that of catalysts prepared using HiPIMS process. Activity of the supported catalysts was strongly affected by the presence of a porous cobalt oxide layer well accessible to the reactants, which was obtained after electrochemical deposition and subsequent heating. The ED catalyst with the highest Co_3O_4 loading showed the highest efficiency in total ethanol oxidation. Magnetron sputtering produced relatively compact Co_3O_4 coatings with lower catalytic activity, but these coatings were very important in order to obtain catalysts with good adhesion to the support. All supported catalysts with Co_3O_4 coatings on stainless steel meshes were more active in total oxidation of ethanol to CO_2 than pelletized commercial Co_3O_4, even though the cobalt oxide content in the bed of the supported catalysts was nearly 50 times lower. [14], [15].

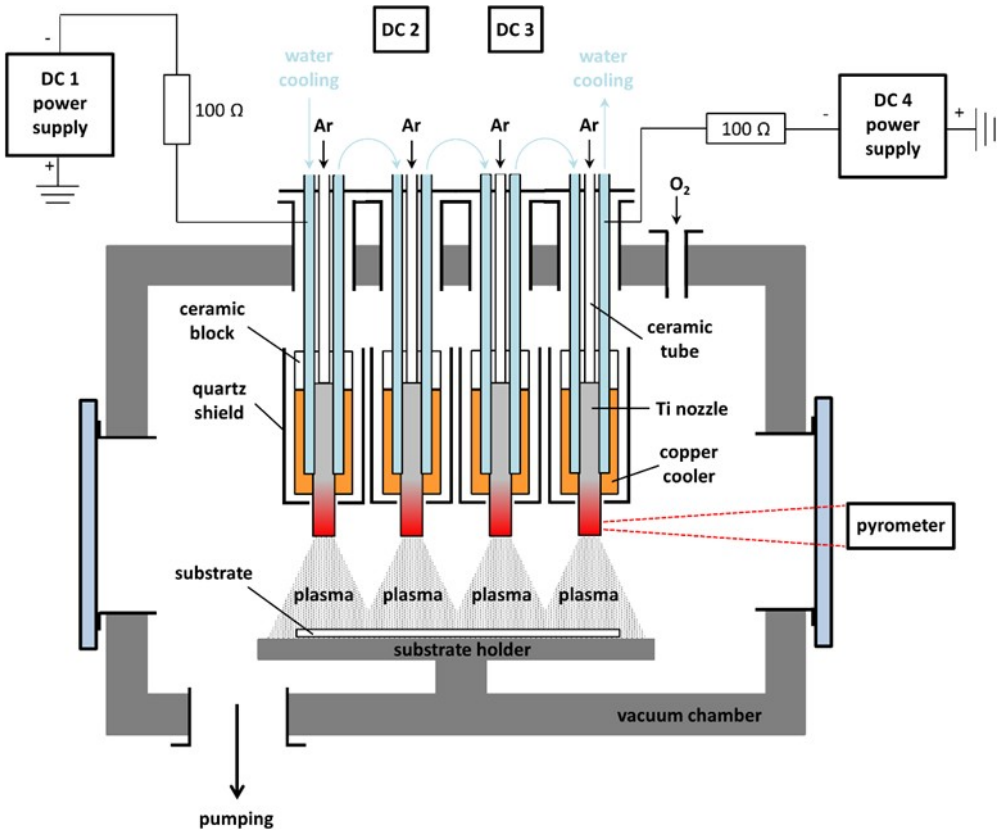

Fig. 5 *Schematic picture of a multi-jet deposition system using a hot hollow cathode for high-rate deposition of oxide films.*

High Rate Plasma Deposition of Thin Films on flat and 3D surfaces

Thin films of many different materials are in high demand for a wide range of industrial applications. Thanks to their diverse properties it is possible to create products with functional properties, which were previously impossible. In recent years, scientists have developed a wide range of technologies, that enable deposition of different thin films on different substrates.

However, for successful industrial applications, the developed technology must be able to produce coatings of the required quality, with high deposition rates and at an affordable price. A typical example of a desired but unavailable technology is high-rate sputtering of oxide layers such as titanium dioxide - TiO_2. Current technologies can deposit such films either slowly (and well) or quickly (and poorly). In the framework of our research, we managed to develop a new technology that combined both positive properties, i.e. speed and quality. This technology is based on the principle of hollow cathode discharge, which has been known for decades. A discharge is ignited inside the hollow metallic cathode causing the incident argon ions to eject atoms from the cathode surface, which are carried by the flowing gas towards the substrate. In contrast to classical reactive magnetron sputtering, in this case the cathode

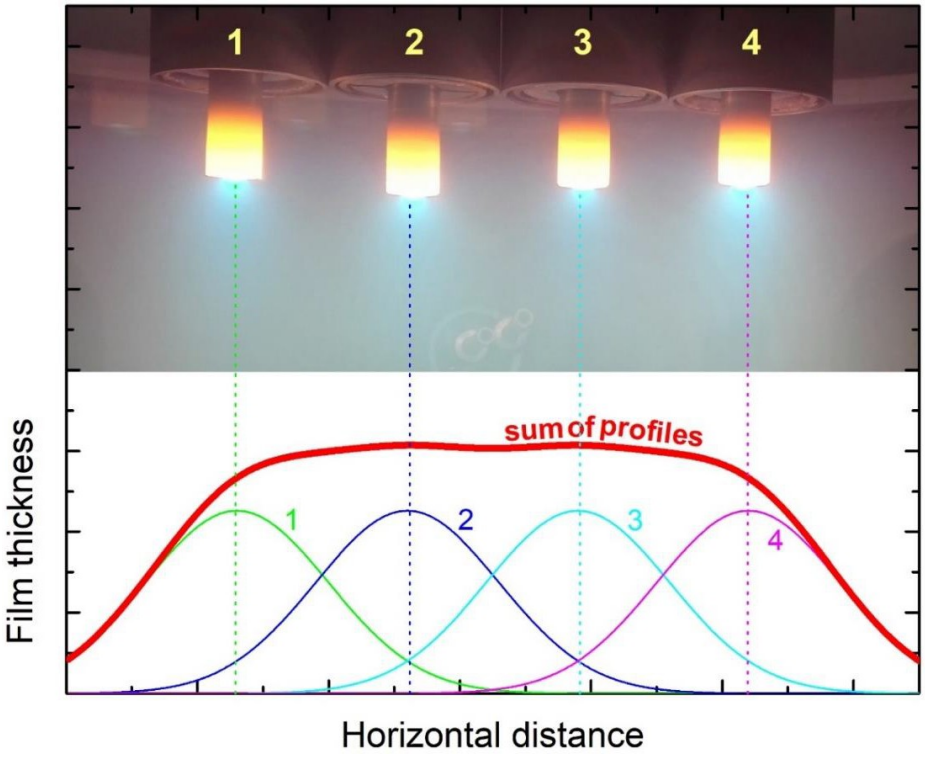

Fig. 6 *Photo of a burning discharge and hot titanium cathodes whose temperature can reach up to 1600 ° C. The bottom part of the figure shows the principle of homogenization of the film when sputtering is performed from several nozzles simultaneously.*

cannot be oxidized and thus the deposition rate cannot slow down, as oxygen is injected into the chamber by a different inlet than that used for argon. To achieve an even higher deposition rate, we placed a part of the hollow cathode outside the copper cooler. This causes an extreme increase in the temperature of the hollow cathode, which results in thermal evaporation of the individual atoms from its surface. By combining plasma sputtering with thermal evaporation, the deposition rate can be increased several times. The main disadvantage of this technology is the significant inhomogeneity of the deposited films caused by the geometry of the whole process. In order to be able to apply coatings to large areas, we have developed a multi-plasma-jet system with several parallel hollow cathodes, as shown in Figure 5. The homogeneity of deposited films is guaranteed by feedback control of the temperature of each nozzle (Fig 6). Since this system originated partly from business cooperation, we protected the

principle of regulation of homogeneity and the whole developed system by Czech and international patents [16]. At present, the developed system is mainly used for scientific purposes and for the preparation of thin or thick films of various difficult to obtain oxides. One of the possible applications was recently described in our last publication [17]. Several industrial partners have already expressed their interest in this technology. Currently we are discussing license conditions and partners intend on buying one prototype of this plasma source.

The hollow cathode plasma system with pulsed plasma excitation was used for coatings of inner surfaces of steel tubes within the scope of another project. The system of synchronized pulses was applied to the cathode to generate optimal ionized gas for reactive hollow cathode erosion and hard thin film deposition with good adhesion inside the steel tube. The system was patented [18] and is applied in industrial research in our team.

The schematic picture of the plasma deposition system for coatings of inner surfaces of steel tubes can be seen in Fig. 7. Synchronized pulsed current and voltage waveforms applied on the hollow cathode and the coated tube can be seen in Fig 8. These types of synchronized pulses allow stable operation of this plasma inside narrow metallic tubes and simultaneously enable defined ion bombardment of the coated surface and achieve improved adhesion and mechanical properties of deposited films. This system was tested on films of Cr and CrN deposited inside tubes.

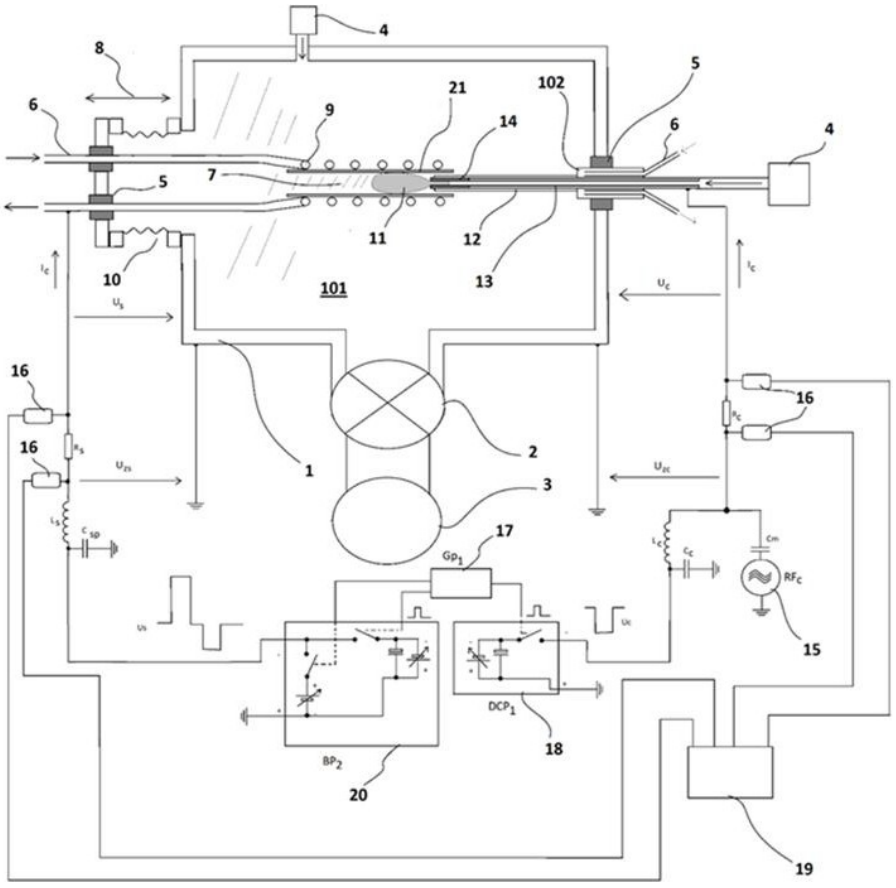

Fig. 7 *Plasma deposition system for coatings of inner walls of steel tubes.*

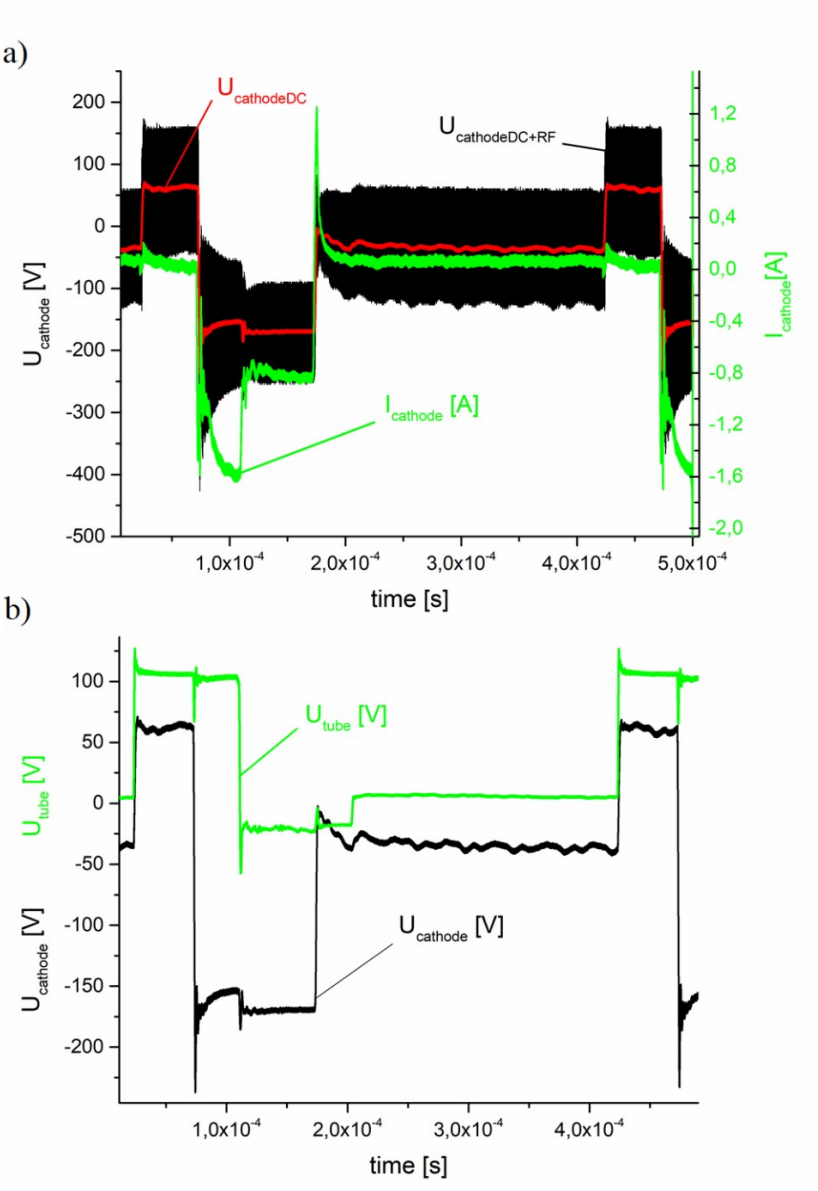

Fig 8 a) *Pulsed current and voltage waveforms on the hollow cathode* ***b)*** *pulsed voltage on the cathode and coated tube.*

References:

[1] J. Krýsa, A. Němečková, M. Zlámal, T. Kotrla, M. Baudys, Š. Kment, Z. Hubička, M. Neumann-Spallart, a-Fe2O3/TiO2 stratified photoanodes, Journal of Photochemistry and Photobiology A: Chemistry 366 (2018) 12–17.

[2] V. Straňák, Z. Hubička, M. Čada, R. Bogdanowicz, H. Wulff, C. A. Helm and R Hippler, Influence of reactive oxygen speciesduring deposition of iron oxide films by high power impulse magnetron sputtering ,J. Phys. D: Appl. Phys. 51 (2018) 095205.

[3] J. Olejníček, M. Brunclíková, Š. Kment, Z. Hubička, H. Kmentová, P. Kšírová, M. Čada, M. Zlámal, J. Krýsa, WO3 thin films prepared by sedimentation and plasma sputtering, Chemical Engineering Journal 318 (2017) 281–288.

[4] J. Krysa, M. Zlamal, S. Kment, M. Brunclikova, Z. Hubicka, TiO2 and Fe2O3 Films for Photoelectrochemical Water Splitting, Molecules 20 (2015) 1046-1058.
[5] Š. Kment, H. Krysová, Z. Hubička, H. Kmentová, L. Kavan, R. Zborila, Very thin thermally stable TiO2blocking layers with enhanced electron transferfor solar cells, Applied Materials Today 9 (2017) 122–129.
[6] Z. Hubička, M. Zlámal, M. Čada, Š. Kment, J. Krýsa, Photo-electrochemical stability of copper oxide photocathodes deposited by reactive high power impulse magnetron sputtering, Catalysis Today 328 (2019) 29–34.
[7] Z. Hubička, M. Zlámal, J. Olejníček, D. Tvarog, M. Čada, J. Krýsa, Semiconducting p-Type Copper Iron Oxide Thin Films Deposited by Hybrid Reactive-HiPIMS+ECWR and Reactive-HiPIMS Magnetron Plasma System, Coatings 10 (2020) 232.
[8] M. Čada, Z. Hubička, P. Adámek, J. Olejníček, Š. Kment, J. Adámek, J. Stöckel: A modified Katsumata probe-Ion sensitive probe for measurement in non-magnetized plasmas. Rev. Sci. Instrum. 86 (2015) 073510-7.
[9] P. Sezemský, V. Straňák, J. Kratochvíl, M. Čada, R. Hippler, M. Hrabovský, Z. Hubička Modified high frequency probe approach for diagnostics of highly reactive plasma, Plasma Sources Sci. Technol. 28 (2019) 115009(1) - 115009(10).
[10] R. Hippler, M. Cada, V. Stranak, Z. Hubicka, C.A.Helm: Pressure dependence of Ar2+, ArTi+, and Ti2+ dimer formation in a magnetron sputtering discharge. J. Phys. D: Appl. Phys. 50 (2017) 445205-8.
[11] R. Hippler, M. Cada, V. Stranak, C. A. Helm, Z. Hubicka: Pressure dependence of singly and doubly charged ion formation in a HiPIMS discharge. J. Appl. Phys. 125 (2019) 013301-7.
[12] D. Lundin, M. Čada, Z. Hubička: Ionization of sputtered Ti, Al, and C coupled with plasma characterization in HiPIMS. Plasma Sources Sci. Technol. 24 (2015) 035018-11.
[13] M. Čada, D. Lundin, Z. Hubička: Measurement and modeling of plasma parameters in reactive high-power impulse magnetron sputtering of Ti in Ar/O2 mixtures. J. Appl. Phys. 121 (2017) 171913-7.
[14] M. Dvořáková, R. Perekrestov, P. Kšírová, J. Balabánová, K. Jirátová, J. Maixner, P. Topka, J. Rathouský, M. Koštejn, M. Čada, Z. Hubička, F. Kovanda: Preparation of cobalt oxide catalysts on stainless steel wire mesh by combination of magnetron sputtering and electrochemical deposition, Catalysis Today 334 (2019) 13–23
[15] R. Perekrestov, A. Spesyvyi, J. Maixner, K. Mašek, O. Leiko, I. Khalakhan, J. Maňák, P. Kšírová, Z. Hubička, M. Čada: The comparative study of electrical, optical and catalytic properties of Co3O4 thin nanocrystalline films prepared by reactive high-power impulse and radio frequency magnetron sputtering, Thin Solid Films 686 (2019) 137427.
[16] J. Olejnicek, J. Smid, Z. Hubicka, P. Adamek, M. Cada, S. Kment (2018) A Method for Controlling the Deposition Rate of Thin Films in a Vacuum Multi-Nozzle Plasma System and a Device for Performing of the Method, int. p. number: WO 2018/059609 A8,
[17] J. Olejnicek, J. Smid, R. Perekrestov, P. Ksirova, J. Rathousky, M. Kohout, M. Dvorakova, S. Kment, K. Jurek, M. Cada, Z. Hubicka: Co_3O_4 thin films prepared by hollow cathode discharge, Surf. Coat. Technol. 366 (2019) 303-310.
[18] Z. Hubička, M. Čada, P. Kšírová, M. Klinger, Method of low-temperature plasma generation, method of an electrically conductive or ferromagnetic tube coating using pulsed plasma and corresponding devices WO2019210891A1.

Research activity and characterisation of the main scientific results

In the previous evaluation, the team announced the formation of an interdisciplinary research group with the aim of merging biology with physics. Recommendations from the previous evaluation clearly stated that the team should continue with our interesting and competitive research. The team developed an infrastructure of diverse physical methods, facilities and technologies. Despite the fact that the team started building a biological research foundation in the previous evaluation period, there was still a lack of biological laboratories and facilities at the start of this evaluation period. Therefore, during the current evaluation period the team has created two new biological laboratories that are integral to evolving the interdisciplinary network of the Department.

The main scientific achievements of our team during the evaluated period are presented below.

The Laboratory of Functional Biointerfaces

A new highly-interdisciplinary research program focusing on biointerface research was initiated by the FZU in 2018, followed by the formal establishment of the Laboratory of Functional Biointerfaces in 2019. This program addresses fascinating research phenomena concerning the behaviour of biomolecules and living cells at synthetic surfaces and thus bridges the gap between material science and biology. A specific research direction has been pursued to address one of the crucial issues in many fields, i.e., the nonspecific adsorption of biomolecules from biological fluids to synthetic surfaces. The main foreseen scientific achievement of this research program will be a new and fundamental insight into the molecular-level mechanisms of surface-mediated interactions at interfaces between materials and biological fluids, such as the cutting-edge exploration of molecular-level fouling mechanisms. Moreover, this knowledge will enable the design of new tailored artificial bioinspired materials and coatings exhibiting desired bioresponsive properties in native biological environments. Such functional materials have a potential to meet the critical requirements of many high-tech applications including bioanalytical methods for rapid detection of target analytes in

medical diagnostics, food safety, and security. Therefore, several observed research findings in the area of ultra-low fouling functional coatings have been applied in follow-up developments of biochip platforms in close collaboration with the industry. Namely, several industrial research projects focusing on development of new biochip technologies for food safety and security have been explored in close collaboration with potential end-users of developed biochip devices such as Police CR and several other government bodies.

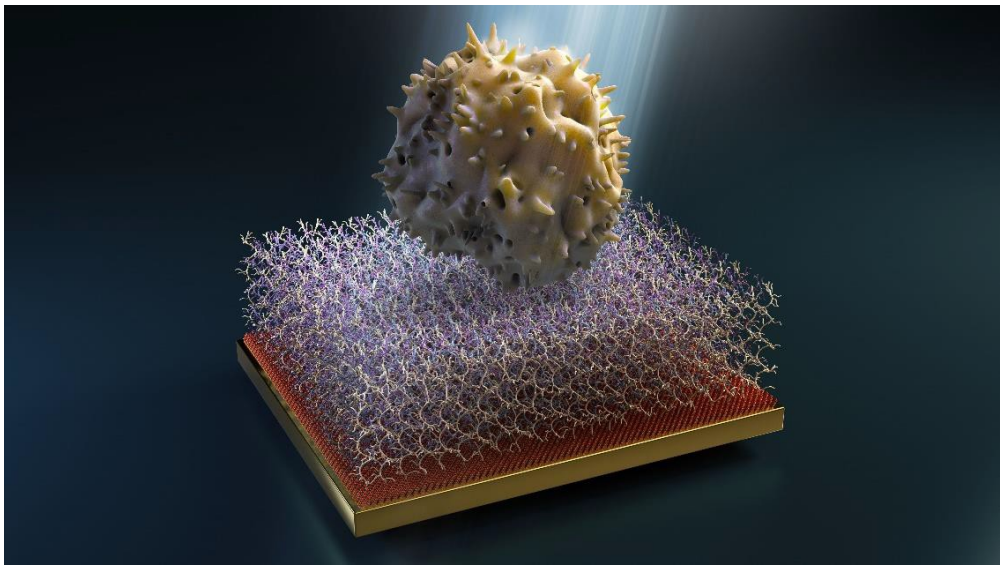

Figure 2. Ultra-low fouling coatings with tailored surface physico-chemical properties enable a stress-driven manipulation with living cells.

The research program of the Laboratory of Functional Biointerfaces will take advantage of well- established material science and a newly-established biological laboratory at FZU and will promote internal, national, and international collaborations. The research program has been supported by both Czech and European funds such as the prestigious Lumina Quaeruntur Award of the Czech Academy of Sciences or via the Operational Programme Prague – Growth Pole of the Czech Republic. Based on this financial support, as well as due to the high support of the FZU management, three laboratories have been built and equipped in 2019. These newly developed laboratories at FZU include the Laboratory of Polymer Synthesis for polymer coating preparation equipped with a unique custom-made polymerization apparatus, the Biochemical Lab and the Bio-Surface Characterization Lab equipped with a set of modern surface characterization facilities such as SPR, QCM, PM-IRRA spectroscopy or spectroscopic ellipsometer enabling precise characterization of samples in liquid environments. Although the research mission of the Laboratory of Functional Biointerfaces has been carried out for a relatively short time, the achievements of this research have been successfully presented at leading international conferences as well as recently published in a high-profile scientific journal [1].

The Laboratory of Biophysics

The Laboratory of Biophysics has been able to create a unique research environment, despite only existing since the end of 2016 (https://www.fzu.cz/novinky/nova-biofyzikalni-laborator-ve-fyzikalnim- ustavu-av-cr).
A growing number of studies has reported that external physical cues (e.g. mechanical forces, electromagnetic fields, nanomaterials, etc.) may have an impact on a broad range of cell behaviours and functions.
The ultimate goal of our laboratory is to gain insight in the understanding of how physical factors influence the processes that drive cell behaviour and functionality. Research of the laboratory is focused on the effects of materials, structures, interfaces, particles, and physical fields on biological systems as well as the development of new biotechnological concepts.

In the previous report we stated that the next five years we will explore in detail cellular responses and underlining mechanisms as well as their dependencies on the physical properties of magnetic nanomaterial, plasmas and different physical fields. We performed our research in accordance with the plan.

1. Effects of non-thermal plasmas on living cells.

Over the last decade, biochemical interactions between non-thermal plasmas (NTPs) and living objects have steadily gained increased attention due to recent developments in plasma medicine. Indeed, in light of the unprecedentedly rising problem of microbial antibiotic resistance, the bactericidal properties of plasma are under intensive study as an alternative approach to eradicate multidrug resistant strains. Already, the pilot clinical use of NTP devices has shown promising results in skin and wound decontamination of multidrug-resistant bacteria. The past decade has seen an explosion of scientific literature, investigating the bactericidal properties of NTPs.
Additionally, for decades it was believed that bacteria as unicellular organisms would not have a cellular suicide program (apoptosis). It was counterintuitive to our understanding of evolutionary processes and the driving forces of natural selection. We were the first group to show that non-thermal plasma triggers apoptosis-like cell death in bacteria (Figure 3) [2]. Overall, this study not only reveals underlying molecular mechanisms of plasma action on bacteria, but more importantly provides an additional insight into the evolution of apoptosis in prokaryotes [2].

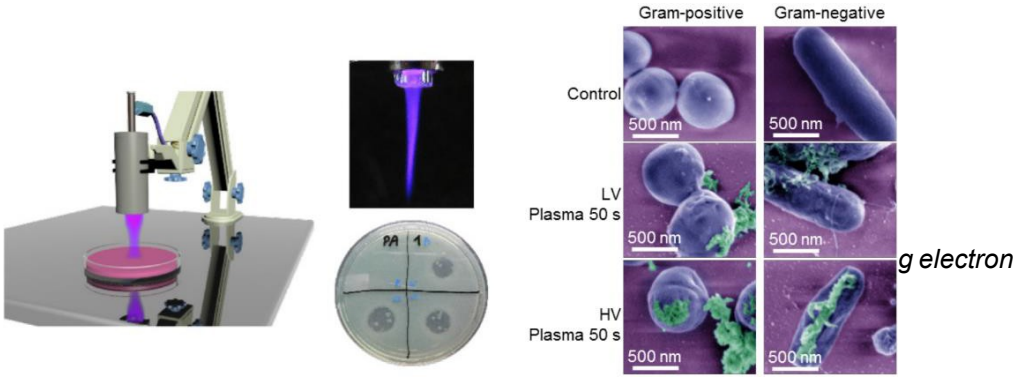

Figure 3. The scheme of the experimental setup and scanning electron microscopy (SEM) images of bacteria destroyed by plasma.

The explored possibilities of tuneable bacteria deactivation provide a basis for the development of advanced plasma-based therapies. To a great extent, our study opens new possibilities for controlled non-thermal plasma interactions with living systems [2]. Further, we analysed the effect of cold plasma on the healing of a full-thickness acute skin wound model in rats [3]. In summary, plasma treatment improved the healing efficacy of acute skin wounds without noticeable side effects and concomitant activation of pro-inflammatory signalling [3]. The obtained results highlight the favourability of plasma applications for wound therapy in clinics.

Moreover, we reported thorough time- and dose-dependent kinetics of reactive oxygen species (ROS) accumulation in cancer cells [4]. We revealed nuclear compartmentalization of the superoxide anion triggered by plasma. Plasma induced apoptotic death in Huh7 liver cancer cells via simultaneous downregulation of mutated p53, pSTAT1 and STAT1 [4]. Contrary, hydrogen peroxide treatment results in autophagic cell death. We disclosed detailed mechanisms of NTP-mediated alteration of redox signalling in liver cancer cells [4, 5].
In summary, we created a solid expertise on the biomedical application of plasmas [2-7].

2. Manipulating mitochondrial activity by laser irradiation.

Low-power laser irradiation of red light has been recognized as a promising tool across a vast variety of biomedical applications. However, deep understanding of the molecular mechanisms behind laser- induced cellular effects remains a significant challenge. We decoupled distinct cell death pathways targeted by laser irradiations of different powers (Figure 4). Firstly, we showed that high dose laser irradiation exhibited the highest levels of total reactive oxygen species production, leading to cyclophilin D-related necrosis via the mitochondrial permeability transition [8]. On the contrary, low dose laser irradiation resulted in the nuclear accumulation of superoxide and apoptosis execution [8].

Further, we expanded our research. We identified mitochondria as a sub-cellular "sensor" and "effector" of laser light non-specific interactions with cells [9]. We demonstrated that despite blue (398 nm) and red (650 nm) laser irradiation results in similar apoptotic death, cellular signalling and kinetic of biochemical responses are distinct. Based on our data, we concluded that blue laser irradiation inhibited cytochrome c oxidase activity in the electron transport chain of mitochondria [9]. In

contrast, red laser triggered excessive activation of cytochrome c oxidase. Moreover, we showed that Bcl-2 protein inhibited laser-induced toxicity by stabilizing mitochondria membrane potential. Thus, cells that either overexpress or have elevated levels of Bcl-2 are protected from laser-induced cytotoxicity [9].

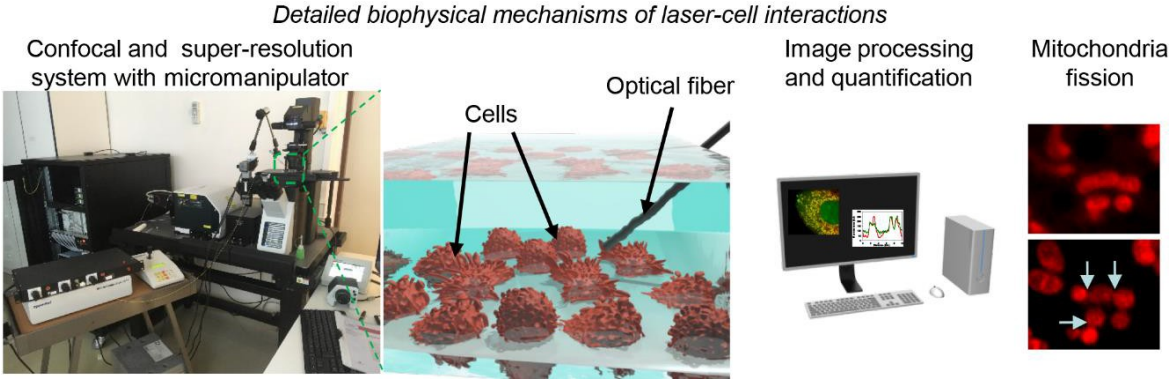

Figure 4. Scheme of the experimental setup and spinning disk super-resolution images of mitochondria fission initiated by laser irradiation.

Our findings offer a novel insight into laser-induced cellular responses, and reveal distinct cell death pathways triggered by laser irradiation.

3. Nano and microtechnologies in biomedicine.

Success of our other research lines together with a rapidly growing interest in biomedical nanotechnologies in biophysical research prompted us to expand our research line to broader studies of nano- and microtechnologies.

We analysed the molecular mechanisms of functionalized nanoparticle interaction with living cells. Specifically, we demonstrated that amino-functionalized polystyrene nanoparticles, but not amino- or hydroxyl-functionalized silica particles, trigger cell death in hepatocellular carcinoma Huh7 cells [10]. Importantly, biodegradability of nanoparticles plays a crucial role in the regulation of essential cellular processes. Thus, biodegradable silica nanoparticles having the same shape, size and surface functionalization showed opposite cellular effects in comparison with similar polystyrene nanoparticles. Importantly, we identified a major modulator of nanoparticle-induced cellular response – the mammalian target of rapamycin (mTOR) [11]. Proteins of the mTOR signalling axis are overexpressed or mutated in cancers. However, clinical inhibition of mTOR signalling as therapeutic strategy in oncology shows rather limited

progress. Nanoparticle-based mTOR targeted therapy proposes an attractive therapeutic option for various types of cancers [11].
Further, we designed a magnetic system that enhances magnetic cell labelling using pulsed magnetic fields [12]. The rate of uptake of superparamagnetic iron oxide nanoparticles (SPIONs) and transport across the cell membrane were enhanced upon application of a high intensity (7 T) short pulse width (~15 μs) magnetic field [12]. Next, we utilized this system for remote activation of apoptosis in liver cancer cells (Figure 5) [13]. The extent of cell death induced by LMP correlated with the accumulation of reactive oxygen species in cells [13].
LMP was achieved for estimated forces of 700 pN and higher. Furthermore, we validated our approach on a three-dimensional cellular culture model to be able to mimic in vivo conditions [13]. Overall, our results show that PMF treatment of SPION-loaded lysosomes can be utilized as a non-invasive tool to remotely induce apoptosis.

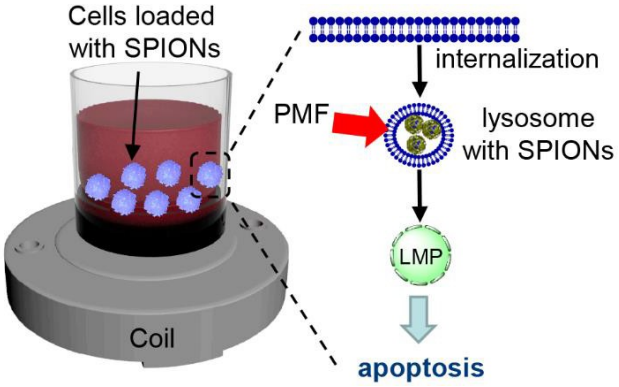

Figure 5. The concept of lysosomal membrane permeabilization by superparamagnetic iron oxide nanoparticles (SPIONs) in a pulsed magnetic field. Nanoparticles are taken up into endosomes and lysosomes due to receptor mediated endocytosis. When the pulsed magnetic field (PMF) is activated at this point, the clusters of nanoparticles exert mechanical forces that cause injury to the lysosomal membrane. This in turn causes leakage of the lysosomal contents into the cytoplasm, leading to a decrease in its pH and subsequent apoptosis.

The Laboratory of Pulsed Laser Deposition of Thin Films

The Laboratory of Pulsed Laser Deposition of Thin Films focuses on the development and application of advanced hybrid laser technology, combining in situ several excimer lasers, magnetron sputtering and ion bombardment. Additionally, the group is developing dual Pulsed Laser Deposition (PLD) utilizing two independent excimer laser sources and one solid state laser (Nd:YAG). Such a combination enables fabrication of coatings with better adhesion, higher density or novel composition and structure. In the framework of the developed systems, the lasers are also used for annealing thin layers of optical materials for waveguide applications, previously prepared by these hybrid technologies. The process enhances for example the luminescence of dopants and waveguiding quality. The laboratory has a special focus on doped layers, multilayers, super lattices, nanolayers, heterostructures, new biomaterials and nanocomposites. Besides this the laboratory has a very close cooperation with other groups of the evaluated team providing samples and participating in research of doped DLC layers (dopation with titanium, silver, chromium, germanium and calcium), hydroxyapatite (doped with silver), piezoelectric films for physical and biomedical applications, as well as perovskites and thermoelectric thin films [14-21].

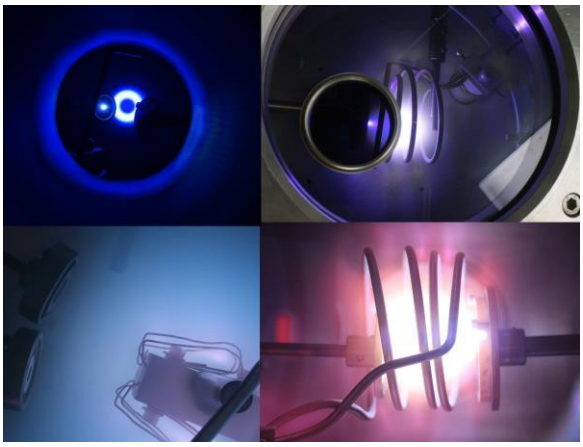

Figure 6. Visualization of the technology processes in the developed PLD-based systems.

Among the wide range of advanced coatings, it is worth mentioning the development of the complete technological process for deposition of gradient layers of hydrogen free diamond-like-carbon (DLC) doped with metals. The obtained gradient material exhibits extremely good adhesion to various metal substrates (such as implants) even for surfaces made by 3D printing or other additive technology. The combination of metal 3D printing and PLD is especially beneficial as both methods can be used to rapidly change parameters that influence the properties of the product and it is therefore possible to test a lot of different material properties. The results of this research were applied in 2019 in the pilot manufacturing project of moulding and casting together with the company BENEŠ a LÁT Inc. (BaL).

In the framework of close cooperation with the Institute of Physiology CAS, the laboratory developed new BaTiO3 based coatings that combine ferroelectric properties and biocompatibility that act as a bioactive material stimulating bone growth by surface charge generation and improves osseointegration [22]. Similarly, nickel-titan layers were fabricated and studied for their perspective memory-shape properties for biomedical applications.

The next interesting area of the laboratory research in recent years were thermoelectric materials. Advanced hybrid technology was used for deposition of ternary thermoelectric materials based on FeSbTe/YbCoSb. Additionally, multi-layered structures of these materials were successfully prepared for further research that is based on theoretical predictions claiming high efficiency of such materials.

The laboratory has strong cooperation with many Czech and foreign universities. One of the most fruitful cooperation is based on the agreement of joint sharing of the scientific devices of deposition laboratories with the Czech Technical University in Prague, Faculty of Biomedical Engineering. This long-term cooperation extends the research activities of both institutions and gives the possibility for the group members to participate in the education of bachelor, master and PhD students (supervising, lecturing etc.).

The Laboratory of Oxides

Epitaxial growth was implemented and investigated for thin films of ferroelectrics, paraelectric- magnetics, and rare-earth nickelates. The epitaxial effects on optical, polar, and charge-transport properties were explored in the films.

We achieved extraordinary optical behaviour using epitaxial growth of such ferroelectrics as $PbTiO_3$, $BaTiO_3$, $(Pb,Sr)TiO_3$, and $KNbO_3$ and related $NaNbO_3$ and $KTaO_3$ [14-20]. We identified interband optical transitions in the films that differ significantly from those in their bulk counterparts. Importantly for potential future technologies, we obtained noticeable enhancements of effective elasto- and electo-optic coefficients in the films. To bring these properties to fruition in integrated optics and photonics, clarification of their physical mechanisms is a necessity. Our experimental research is in progress and will continue.

We explored epitaxy for tailoring functional green films, when strict requirements are put to chemical composition because of environmental and sustainability issues as well as demand for applications in life sciences and medicine. We achieved efficient tuning of polarization and dielectric responses in films of environmentally friendly, biocompatible, and low-cost $BaTiO_3$. The gained in-plane polarization and polarization rotation under an applied electric field enabled excellent performance of bottom-to-top capacitors, akin to that of containing hazardous lead [23, 24]. Additionally, the dielectric permittivity significantly increased with ac field, enabling enhanced dynamic dielectric and piezoelectric performance. The work has raised much interest worldwide and entered the top 100 most read articles of Scientific Reports in 2019.

We investigated epitaxy as ensuring phase-pure perovskite films. Synergetic effects of film-substrate mismatch and chemical bonding in the film's material were detected in epitaxial perovskite films of $NaNbO_3$, $Sr(Ti,Mn)O_3$, and $BaTiO_3$. We succeeded in epitaxial stabilization of the unconventional $Sr(Ti,Mn)O_3$ perovskite, which belongs to a family of magnetoelectric multiferroic manganites by its cationic composition. We also found stabilization of strongly strained $BaTiO_3$ films using a controlled introduction of oxygen vacancies during the growth [25-27]. The studies involved detailed structural analysis, which was performed in cooperation with research partners (Aalto University and University of Oulu, Finland). Roles of the chemical bonding and oxygen vacancies in epitaxy and properties of the films are now being scrutinized.

We searched for basic abilities to epitaxially manipulate charge transport and magnetoelectric properties. We found polaronic electrical conduction, which evidences electron-phonon correlations in $Sr(Ti,Mn)O_3$ films. These correlations can lead to magneto-dielectric coupling in the absence of spin- phonon correlations. We also detected low-temperature magnetoresistance, not reported before, in epitaxial films of metal-insulator-transition (MIT) $NdNiO_3$. The behaviour is related to magnetically-induced splitting of in-gap states, through which hopping transport is realized. Studies of charge transport are ongoing in a broader variety of thin films [26, 28].

Since 2017, our experimental research is supported by theoretical investigations of ferroelectric epitaxial films, domains and flexoelectric phenomena therein, and potential energy harvesting with ferroelectric films. In particular, heat-electricity conversion using pyroelectric and flexoelectric effects was theoretically demonstrated. Fundamental understanding of domains and their behaviour under applied electric, elastic and thermal stimuli will be further pursued through combined theoretical and experimental efforts [29-32]. The work is ongoing in cooperation with the Swiss Federal Institute of Technology and Novosibirsk State University, Russia.

Centre for Digital Innovation B4I

Existing advanced technologies, patents and know-how makes the team an ideal partner for development of cutting-edge applications. Dialog with industrial partners resulted in numerous projects in contractual and applied research. The knowledge of the Department is therefore not only used in scientific literature, but also in hands-on projects that started due to demands from the industry and society. This bottom-up

approach creates innovative and pioneering research projects. This cooperation gave rise to the National Centre of Competence MATCA (www.matca.cz) - a robust applied research centre. The National Centre of Competence MATCA does not only consist of industrial partners, but also has research institutions involved. This ideal combination of fifteen academic and industrial partners supports the development of technologies of strategic importance - laser, plasma and additive technologies. As part of long-term research and development (https://matca.cz/about/dilci-projekty/), MATCA aims to cover the entire product life cycle - from smart design, through gentle production, repairs and restoration of functional properties to the disposal of hazardous waste. In addition to research, development and provision of services (https://matca.cz/sluzby/), the National Centre of Competence MATCA also focusses on the popularization and education of students and the professional public.

References

1. Visova, I., et al., *Modulation of living cell behavior with ultra-low fouling polymer brush interfaces.* Macromolecular Bioscience, 2020. **20**(3): p. e1900351.
2. Lunov, O., et al., *The interplay between biological and physical scenarios of bacterial death induced by non-thermal plasma.* Biomaterials, 2016. **82**: p. 71-83.
3. Kubinova, S., et al., *Non-thermal air plasma promotes the healing of acute skin wounds in rats.* Scientific Reports, 2017. **7**: p. 45183.
4. Smolkova, B., et al., *Non-thermal plasma, as a new physicochemical source, to induce redox imbalance and subsequent cell death in liver cancer cell lines.* Cellular Physiology and Biochemistry, 2019. **52**(1): p. 119-140.
5. Lunov, O., et al., *Chemically different non-thermal plasmas target distinct cell death pathways.* Scientific Reports, 2017. **7**: p. 600.
6. Lunov, O., et al., *Towards the understanding of non-thermal air plasma action: effects on bacteria and fibroblasts.* Rsc Advances, 2016. **6**(30): p. 25286-25292.
7. Lunov, O., *Plasma will.* British Journal of Dermatology, 2016. **174**(3): p. 486-487.
8. Lynnyk, A., et al., *Manipulating the mitochondria activity in human hepatic cell line Huh7 by low- power laser irradiation.* Biomedical Optics Express, 2018. **9**(3): p. 1283-1300.
9. Lunova, M., et al., *Light-induced modulation of the mitochondrial respiratory chain activity: possibilities and limitations.* Cellular and Molecular Life Sciences, 2019: p. https://doi.org/10.1007/s00018-019-03321-z.
10. Lunova, M., et al., *Nanoparticle core stability and surface functionalization drive the mTOR signaling pathway in hepatocellular cell lines.* Scientific Reports, 2017. **7**: p. 16049.
11. Lunova, M., et al., *Targeting the mTOR signaling pathway utilizing nanoparticles: A critical overview.* Cancers, 2019. **11**(1): p. 82.
12. Uzhytchak, M., et al., *The use of pulsed magnetic fields to increase the uptake of iron oxide nanoparticles by living cells.* Applied Physics Letters, 2017. **111**(24): p. 243703.
13. Lunov, O., et al., *Remote actuation of apoptosis in liver cancer cells via magneto-mechanical modulation of iron oxide nanoparticles.* Cancers, 2019. **11**(12): p. 1873.
14. Tyunina, M., et al., *Effect of epitaxy on interband transitions in ferroelectric KNbO3.* New Journal of Physics, 2015. **17**: p. 043048.
15. Tyunina, M., et al., *Interband transitions in epitaxial ferroelectric films of*

NaNbO3. Physical Review B, 2015. **92**(10): p. 104101.
16. Tyunina, M., et al., *Concurrent bandgap narrowing and polarization enhancement in epitaxial ferroelectric nanofilms.* Science and Technology of Advanced Materials, 2015. **16**(2): p. 026002.
17. Chernova, E., et al., *Strain-controlled optical absorption in epitaxial ferroelectric BaTiO3 films.* Applied Physics Letters, 2015. **106**(19): p. 192903.
18. Kocourek, T., et al., *Effects of doping and epitaxy on optical behavior of NaNbO3 films.* Applied Physics Letters, 2015. **107**(17): p. 172906.
19. Pacherova, O., et al., *Thermooptical evidence of carrier-stabilized ferroelectricity in ultrathin electrodeless films.* Scientific Reports, 2018. **8**: p. 8497.
20. Dejneka, A., et al., *Optical effects induced by epitaxial tension in lead titanate.* Applied Physics Letters, 2018. **112**(3): p. 031111.
21. Jelinek, M., et al., *Preliminary study of Ge-DLC nanocomposite biomaterials prepared by laser codeposition.* Nanomaterials, 2019. **9**(3): p. 451.
22. Jelinek, M., et al., *Laser-synthesized nanocrystalline, ferroelectric, bioactive BaTiO3/Pt/FS for bone implants.* Journal of Biomaterials Applications, 2018. **32**(10): p. 1464-1475.
23. Tyunina, M., et al., *Perovskite ferroelectric tuned by thermal strain.* Scientific Reports, 2019. **9**: p. 3677.
24. Tyunina, M. and M. Savinov, *Dynamic nonlinearity in epitaxial BaTiO3 films.* Physical Review B, 2016. **94**(5): p. 054109.
25. Yao, L., et al., *Chemical-bond effect on epitaxial strain in perovskite sodium niobate.* Physical Chemistry Chemical Physics, 2018. **20**(6): p. 4263-4268.
26. Savinov, M., et al., *Dielectric relaxation in epitaxial films of paraelectric-magnetic SrTiO3- SrMnO3 solid solution.* Applied Physics Letters, 2018. **112**(5): p. 052901.
27. Tyunina, M., D. Chvostova, and A. Dejneka, *Optical revelation of defects in epitaxial barium titanate films.* Physical Chemistry Chemical Physics, 2019. **21**(15): p. 7874-7878.
28. Stupakov, A., et al., *Negative magnetoresistance in epitaxial films of neodymium nickelate.* Physical Review B, 2019. **99**(8): p. 085111.
29. Maheux, E., et al., *A strategy for high specific power pyroelectric energy harvesting from a fluid source.* Applied Physics Letters, 2017. **111**(23): p. 233903.
30. Ahluwalia, R., P.V. Yudin, and A.S. Yurkov, *Order parameter boundary conditions for ferroics: Application to flexoelectricity.* Physica Status Solidi B-Basic Solid State Physics, 2018. **255**(3): p. 1700312.
31. Bednyakov, P.S., et al., *Physics and applications of charged domain walls.* Npj Computational Materials, 2018. **4**: p. 65.
32. Yurkov, A.S., A. Dejneka, and P.V. Yudin, *Flexoelectric polarization induced by inhomogeneous heating and implications for energy harvesting.* International Journal of Solids and Structures, 2019. **162**: p. 96-104.

Research activity and characterisation of the main scientific results

The main scientific results of the team have been achieved within the framework of synergetic cooperation of all PVD, NanoESCA and Functional materials analyses groups.

Hybrid deposition systems

In the field of thin film fabrication by Physical Vapour Deposition, we developed and constructed new technologies for different kinds of coatings and nanostructured thin film fabrication. Attention was focused on development of hybrid deposition techniques with auxiliary plasma discharges for optical, magnetic and organics films. In our research we do not want to use a single deposition technique, for example magnetron sputtering, for fabrication of some specific coatings. The scientific idea in our PVD laboratory is for particular physical and technological problems to find the best methods for fabrication of films and nanostructures with focus on their structural and functional (optical, luminescence electric) properties. This method is schematically shown in Fig.1. Attention is also paid to plasma characterisation by means of Langmuir probes, mass spectroscopy and optical emission spectroscopy, as well as, examination of its influence on film properties. Attention is paid to in-situ film monitoring by spectral ellipsometry and reflectometry, real time electrical and transmission measurements. Interesting results for the PVD community were obtained by investigation of contamination of sputtered films by oxygen from residual atmosphere performed by our team [1].

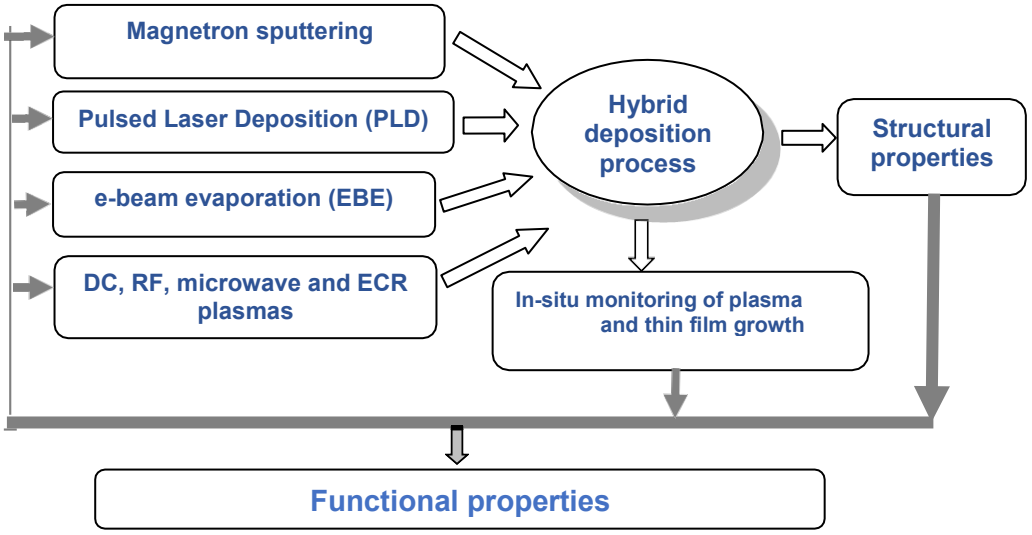

Fig. 1. *Scheme of advanced PVD systems for thin film and nanostructures fabrication*

An important result was achieved in the field of graphene layer preparation by microwave heating of SiC crystals [2]. Microwave heating is known for its exceptional efficiency and speed in processing and synthesis technologies. In this work, high quality epitaxial graphene sheets were synthesized by direct microwave annealing of 4H-SiC (0001) under vacuum at 1700 ° C for, less than 1 minute. The prepared graphene consists of 2 to 4 layers and covers a large part of the surface. This microwave technology, by its very nature, bypasses the need for heat transfer to the sample, since the sample itself is acts as a heater, thereby minimizing contamination and thermal load on the reactor [2].

Ultrathin metallic films

The growth of ultrathin metallic films has attracted significant research interest due to their optical and catalytic properties, which are strongly correlated to their nanostructure. Pulsed laser deposition is a competitive method for preparation of ultrathin coating. However, the control of the layer morphology in real-time is often limited and must be improved to exploit

the full benefit of the deposition. We proposed to exploit in-situ measurements of electrical properties during the deposition process for monitoring of the growing film's quality. The electrical parameters of thin films and their percolation threshold are determined from this measurement. In this study, we can monitor the formation of metallic nanostructures in real-time [3]. After mastering of the deposition technology and in situ thin film monitoring we performed fabrication of plasmonic structures. This research was carried out in collaboration with Institute de Optica, CSIC, Madrid, Spain (laser patterning experiments).

Thin film for optoelectronics and gas sensors

Research dealing with metal oxides for applications in optoelectronics and gas sensors has been carried out in cooperation with the University of Chemistry and Technology in Prague, Charles University in Prague and Institute Lumière Matière in Lyon, France. ZnO as a wide band gap semiconductor is, due to its properties, a very promising candidate for several applications not only in the fields mentioned above. Difficulties with p-type preparation still prevent the usage of the full potential of ZnO. We have performed complex investigation of point defects in ZnO to shed more light on their relation with ZnO properties toward possibilities of the growth of p-type ZnO. Defects in ZnO single crystals were compared with those in epitaxial and nanocrystalline ZnO thin films. Defect studies by positron annihilation spectroscopy were combined with electrical and optical measurements in order to find a link between predominant defect configurations and specific electrical and optical properties of ZnO samples [4]. Analyses enabled us to clarify the origin of green luminescence, which is the subject of long-term discussions in the literature. It was found that green luminescence in ZnO has multiple origins and consists of a band at 2.3 eV due to recombination of electrons in the conduction band by zinc vacancy acceptors coupled with hydrogen and a band at 2.47 eV related to oxygen vacancies. The interaction of hydrogen and nitrogen with point defects in ZnO and their influence on electrical and optical properties was investigated. Research was further extended to dopants such as rare-earths metals (Eu^{3+}, Sm^{3+}, Gd^{3+}, Ho^{3+}) [5]. Eu or Sm doped ZnO was shown as a promising candidate for chemical gas sensors based on luminescence response detection. The luminescence properties of Eu^{3+} doped oxide emitting layer can be significantly improved when deposited on porous alumina membranes as we demonstrated in the case of Y_2O_3:Eu^{3+} [6].

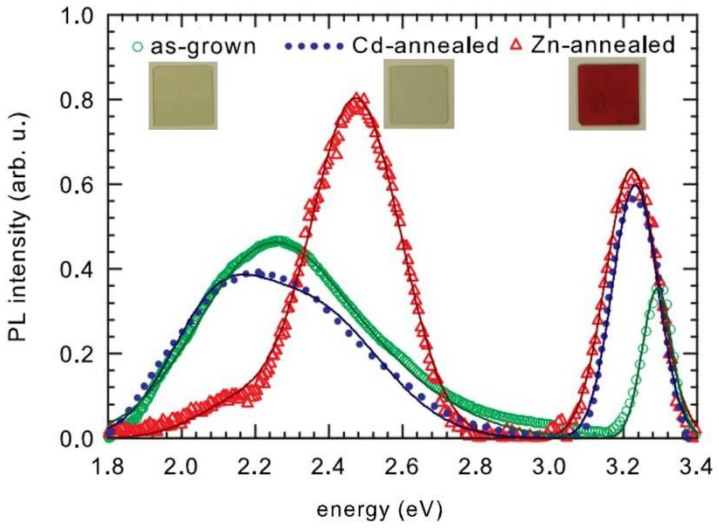

Fig. 2 *Photoluminescence spectra of ZnO crystals in the as-grown state and after annealing in Zn and Cd vapor under excitation at 325 nm. Embedded pictures are photographs of ZnO single crystals.*

Research of new types of highly sensitive gas sensors based on inorganic and organic materials was also carried out. Inorganic materials based on metal oxides, such as ZnO, SnO_2 and CuO_x, were fabricated by our team in the form of layers and nanostructures (nanodots, nanowires and nanosheets). The research revealed links between material morphology, surface chemistry and reactions with gaseous analytes, and sensory response. In-situ measurement by photoelectron spectroscopy was performed for characterization of the detection mechanism [7,8]. Polymerized ionic liquids or phthalocyanines were employed as organic materials, which have the potential for use in chemical conductivity sensors, sensor

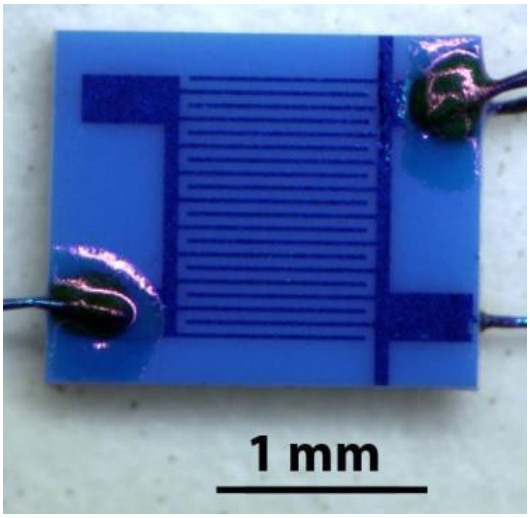

fields or plastic electronics. Our work [9] presents pioneering research into textile chemiresistors with sensitive layers based on two types of cationic polymerized ionic liquids. An advanced sensor substrate for detecting gaseous substances facilitating contacting, heating and controlling was invented. A novel type of gas sensor utilizing black metal layers in the sensor working with a quartz crystal monitor were developed. Equipment based on these materials could be used in the future to detect toxic gas leaks, to control air quality, and in food or medical applications. E. Marešová defended her Ph.D. thesis in cooperation with the University of Chemistry in Prague and Dublin University, Ireland in the field of polymeric ionic liquid.

Fig. 3. *Thin layer chemiresistor made on alumina ceramics with Pt electrodes.*

NanoESCA

The NanoESCA laboratory is equipped for detailed analysis of a wide scale of materials. AFM and STM are used for complex material surface characterization (surface topography, Youngs modulus, adhesion, dissipation, surface with atomic precision, and scanning tunnelling spectrum). NanoESCA as a unique device gives information on weakly bound states and the valence band structure in real space and the surface electronic band structure in k-space. Also, NanoESCA can give quantitative information on the chemical composition of a surface and quantitative maps of surface work function. With this excellent method, the team provides detailed specific analysis not only for cooperative FZU groups, but also for groups from other global institutions. Beside this activity, NanoESCA group members intensively developed these research topics: materials for energy applications – polycrystalline diamond layers against corrosion in nuclear reactors, materials thermoelectric and photovoltaic applications based on layered chalcogenide Bi_2Te_3, organic semiconductors, zirconium-based materials and its passivation layers with respect of Hydrogen and Oxygen. Recently, we have also focused on materials for bio applications - liposomes for modern vaccines and materials and methodologies for human oocytes cryopreservation.

Doped diamond layers for photovoltaic applications

Work was carried out in cooperation with Team 4, namely with Dr. P. Ashcheulov in the scope of his thesis (advisor. as.prof. I. Kratochvílová). Work was supported by project MATCON – EU FP7-PEOPLE-ITN-2008, PITN-GA-2009-238201, Marie Curie Initial Training Networks, Materials and Interfaces for Energy Conversion and Storage and done by PhD. Student P. Ashcheulov, in cooperation with company Solartech a.s. (Dr. A. Poruba). P. Ashcheulov defended his thesis “Nanocrystalline diamond thin films for solar and nuclear energy applications” at the Czech Technical University under the leadership of I. Kratochvílová in 2015 [10]. We also studied the dependence of boron-doped diamond layer thickness and boron content on optical and electrical properties of the solar cell complexes. This work was carried out in cooperation with A. Kovalenko (Brno University of Technology), whose advisor to his doctorate work was also I. Kratochvílová [11].

Polycrystalline diamond coating for protection of Zr cladding surface against corrosion in water cooled nuclear reactor.

During March 2011, at the Fukushima nuclear plant, Japan, the nuclear fuel's cladding, a zirconium alloy, reacted with boiling coolant water to form hydrogen gas, which then exploded, resulting in the biggest nuclear power related disaster since Chernobyl. Challenged by this event, research teams have made progress in developing fuel claddings, which are capable of

withstanding the high temperatures resulting from a Loss of Coolant Accident, such as occurred at Fukushima. The team found a new effective concept of Zr alloy nuclear fuel rod surface protection against degradation at both working and accident conditions by covering the outer surface of the nuclear fuel rod with a protective layer consisting of a polycrystalline diamond (PCD) layer. [12]. Carbon released from the PCD film enters the underlying Zr material and changes its properties, such that uptake of oxygen and hydrogen is significantly decreased. In the scope of a common project (Technology Agency of the CR, TA04020156) with Westinghouse, USA it was proved that the protective PCD layer reduced Zr nuclear fuel cladding oxidation at operating temperatures (by 30-50%), which prolongs the lifetime of the nuclear cladding and consequently enhances nuclear fuel burn-up [13]. The PCD layer also reduced Zr surface oxidation in hot steam at 900 °C by 20%, which prolongs the lifetime of the nuclear cladding at crucial accident conditions, Fig. 2.1. In 2016 US and European patents were applied and filed. In 2020 European patent EP 14789772.2 was awarded by the European Patent Office. Zirconium fuel elements coated with anti-corrosion PCD layers were selected by Westinghouse as a potential candidate for Accident Tolerant Fuels. Long-term testing of PCD protected Zr fuel elements filled with UO_2 pellets began in the active environment of research nuclear reactors in Norway and now in Belgium.
The team was also the first to prepare a double-layered coating consisting of an active and passive part as a protective element for Zr alloy surface against high-temperature oxidation in a hot water environment. Double-layer coatings reduce ZIRLO nuclear fuel tube oxidation by more than 88% compared to that of uncoated ZIRLO tubes treated for 4 days in 400 °C hot steam. For double layer protection of Zr alloy against oxidation a Czech patent was filed [14].
J. Škarohlíd defended his thesis “Advanced Coatings of Nuclear Fuel Cladding” at the Czech Technical University in 2018 under I. Kratochvilova’s leadership. The discovery of a new method for protection of nuclear materials by PCD coating was widely presented in the media (newspapers and TV) and highly appreciated by society (Scientists Help Safeguard Nuclear Reactors, Meterials Performance, 2015), for more details see information in section Publicity of the result in the media.

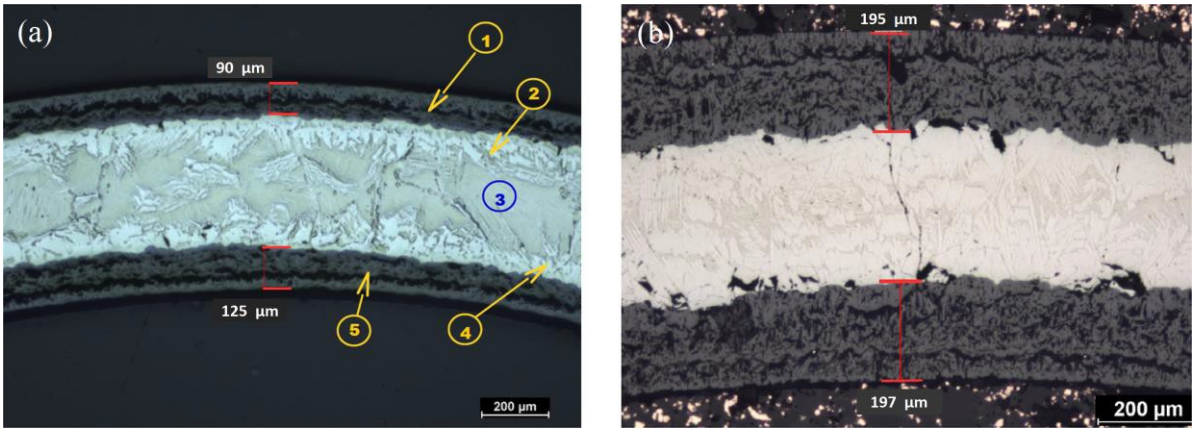

***Fig. 5**: Optical microscopy images of metallographic cross sections. (a) a 300 nm NCD-coated ZIRLO tube sample processed at 1000 °C in hot steam. (1) Outer-surface zirconium dioxide layer (2) Outer-surface oxygen-stabilized zirconium α phase (solid Zr-O solution). (3) Initial Zr β phase (metastable modified hexagonal close-packed structure). (4) Inner-surface oxygen-stabilized Zr α phase. (5) Inner-surface ZrO_2 layer [12].*

Materials for organic photovoltaic /heterojunctions solar cells.

Organic photovoltaics refers to the latest technologies in solar power generation, offering the perspectives of highly automated, low environmental impact production of highly customized products through printing technologies. Specifically, we investigated diketopyrrolopyrrole (DPP) derivatives as potential donor material for fullerene:DPP solar cells. We experimentally

verified the fullerene:DPP solar cell concept based on the coincidence of a smaller driving force for charge separation at the donor:acceptor interface and the crystallinity of studied DPP derivatives for preparing effective photovoltaic devices. Using a wide range of experimental methods, we determined the parameters of studied DPP materials with PC70BM in thin films. This work contributes to practical applications by verifying the concept of this organic solar cell design [15].

Topological insulators and 2D Materials

Due to their unique electronic, thermal and optical properties, two-dimensional (2D) and quasi-2D systems, as well as, their respective van-der-Waals crystals are currently the subject of intense research. Systems with large spin-orbit coupling are particularly interesting as they promote the formation of spin-polarized band structures, complex magnetic order, and topological phase transitions. The complexity of such systems bears potential for future applications, e.g. in the fields of spintronics, valleytronics, thermoelectrics, or solar cell technology.

Focus on material systems in recent years has been on Bi-chalcogenide topological insulators, iron-chalcogenides, and transition metal dichalcogenides (TMDCs). Research is typically carried out in an efficient combination of local SAFMAT material growth and analysis infrastructures (NanoESCA photoelectron emission spectroscopy, variable temperature scanning tunnelling microscopy (STM) by Omicron, low-temperature magneto-transport and magneto-optical Kerr effect setups) and frequent external synchrotron-based measurements, consisting mainly of highly-resolved angle-resolved photoemission and x-ray absorption spectroscopy.

The potential the local SAFMAT infrastructure for 2D research was proven in structural and electronic studies of CVD-grown graphene monolayers on Cu surfaces, where a facet-induced spatial modulation of Dirac state doping levels was resolved using local NanoESCA, STM, low-energy electron diffraction (LEED), atomic force microscopy (AFM), and Electron backscatter

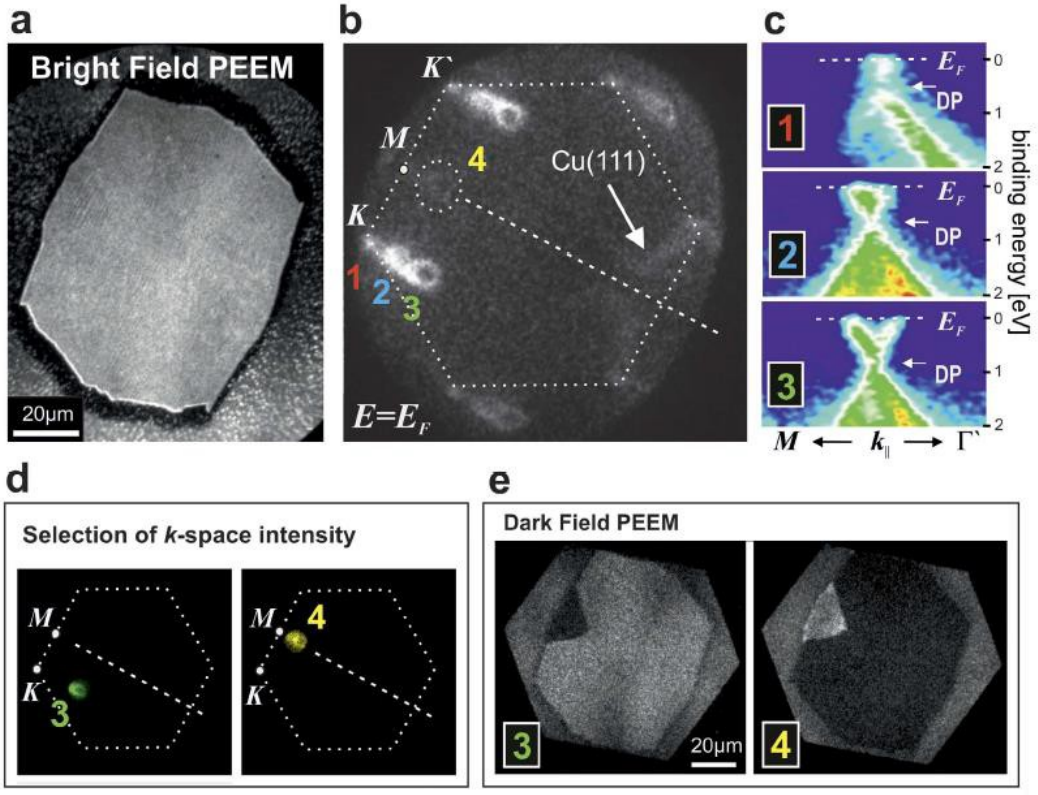

Fig.6 *Fermi level shifts of faceted graphene seen in the angle-resolved photoemission mode of NanoESCA [16]*

diffraction (EBSD) facilities [16]. Here, so-called *dark field* methods available via NanoESCA instrumentation were found to be particularly suitable for the study of 2D system properties and growth modes at the sub micrometre scale [see Fig.6].
This methodical expertise triggered studies on other 2D systems, such as functionalized graphene [17], and transition metal mono- (SnS and FeTe) and di-chalcogenides (WS_2, and MoS_2). Heavy elements, such as Tellurium or Tungsten, boost relativistic spin-orbit coupling effects in these systems and involve interesting fundamental physics, forming the basis for potential applications, e.g. in new and upcoming valleytronic concepts in optics. Also, in topological insulators fascinating properties emerge from large spin-orbit coupling effects, which generate an intimate relation of topology and time reversal symmetry. Studying time-reversal symmetry breaking effects by magnetic atoms in *$Bi_2(Te, Se)_3$ topological* insulators [see Fig.7] using surface states led to fundamental works in the field [18, 19, 20]. Moreover, entirely new families of topological non-trivial materials were tested for the case of Bi-doped GaAs [21], which is also a promising functional material system for light emitters, optical fibre detectors and solar cells.

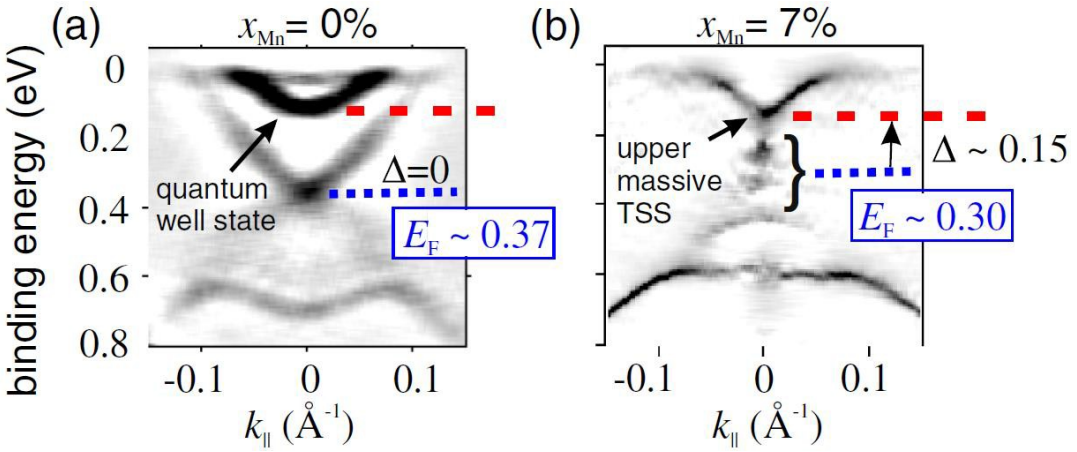

***Fig. 7** Mn-induced disruption of the Dirac-shaped topological surface state in Bi_2Se_3 [19]*

Heusler alloys

Ni_2MnGa Heusler alloys are studied intensively both from the applied and fundamental physics point of view. Angle-resolved photoemission spectroscopy (ARPES) is an important tool to study the electronic structure of solid-state materials, namely, functional materials, structures with reduced dimensions or quantum systems with confined geometries. Apart from splitting due to twinned microstructure and spectra smearing ascribed to magnetic and compositional disorder (present even in austenite), we observed additional effects, which became apparent by comparing with theoretical spectra. In the spectrum taken from twinned martensite there is an apparent hollow space in the vicinity of the Γ point, which is in contrast to the spectrum measured from a single domain and theoretical spectra, which exhibits non-negligible intensity in the central part. The illuminated surface consists of twinned ferroelastic domains with different crystallographic and magnetization orientations, i.e. there is a high concentration of magnetic domains walls and ferroelastic domain interfaces or twin planes. Furthermore, the magnetic domains branch on the surface and their structure mimics a quasi-fractal stage increasing the density of the boundaries close to the surface. Owing to Snell's law, electrons with a k-vector close to the Γ point are filtered out on these interfaces and do not contribute to measured spectra. In a single a-c domain this effect is negligible as there are no twin boundaries. Angle-resolved UPS measurement using PEEM microscopy combined with theoretical simulation of equi-energetic, which cuts through the first BZ, has been successfully applied to map out the electronic structure in off-stoichiometric $Ni_{49.7}Mn_{29.1}Ga_{21.2}$(100) single crystal Heusler alloy (Fig.8) and [22]. The most important result of our work is demonstration that the measured photoelectron spectra are a projection of three

separate electronic structures originating in a-a and two perpendicular a-c twinned ferroelastic variants, which results in the pseudo-splitting of bands at EF observed in the experiment [22]. Our work demonstrates that in a twinned low symmetry phase not only structure, but also microstructure must be considered in order to properly understand the electronic properties of such a material (Fig.8-right). This research was carried out in the cooperation of three teams from FZU supported by GAČR projects

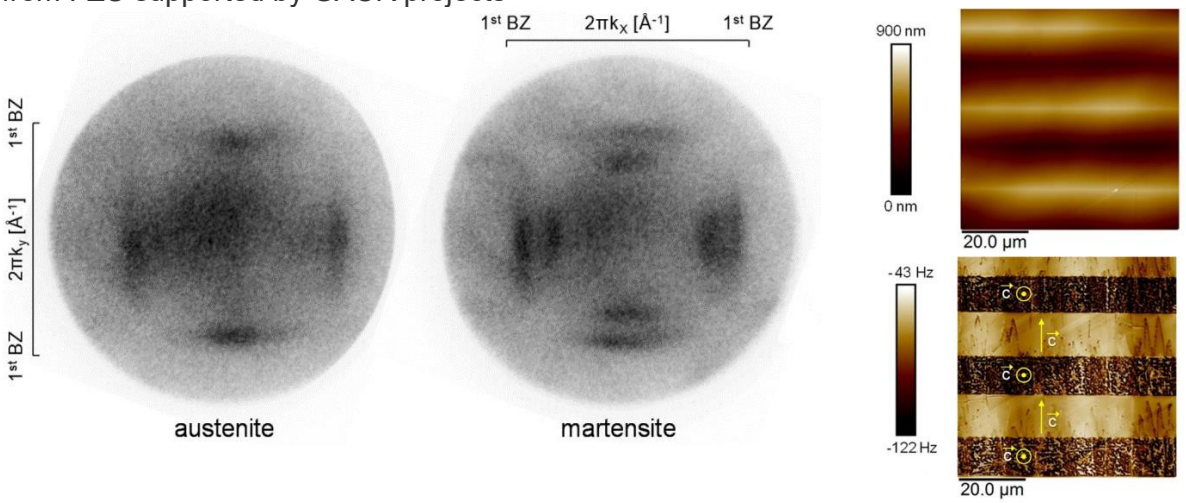

Fig. 8 *PEEM images of an equi-energetic cut at Fermi level of martensite and austenite and their difference. High intensity is dark. (left). AFM/MFM images (right) of the (001) surface of the Ni49.7Mn29.1Ga21.2(100) single crystal in the martensitic phase. The twinned microstructure of the ferroelastic domains is visible as surface relief in the topographic AFM image (right up). MFM image of the magnetic domains of the individual a-a and a-c ferroelastic domains (right down). The orientation of the c axis, identified as the easy direction of magnetization, is marked on the MFM image.*

Nanoparticles for bio applications

The team has participated in successful investigation of materials for recombinant vaccines and biocompatible drug carriers. Here, we focus on development of safe molecular adjuvants, biocompatible nanosystems for construction of recombinant vaccines, and nanofibre-based mucoadhesive films for non-invasive sublingual vaccination.
The FZU team carried out theoretical modelling of complexes (finding stable systems) and made selected analysis of the final construct. A technology for preparation of corpuscular immunogens was discovered and certified. Corpuscular immunogens involve liposomal carrier, (Fig. 9) molecular adjuvants and antigen structures [24]. Clinical evaluation of a liposomal recombinant vaccine against Lyme boreliosis combined with lipophilic derivatives of norAbuMDP/GMDP is under way in animals. Safety and induction of immune response has been demonstrated. Excellent research results were published in high impacted journals and successfully completed by filing a national patent application. The uniqueness of the vaccine is given by the fact that it operates on a wide variety of Borrelia, which are the main agents of the disease. Discovery of the new vaccine against Lyme borreliosis was widely presented in the media and highly appreciated by Czech society – Award of the Technological Agency of the CR 2015 "Synthetic multi-epitope vaccine against Lyme disease for veterinary applications", Czech Head 2018 nomination "Synthetic multi-epitope vaccine against Lyme disease for veterinary applications". European patent EP 15727869.8 Vaccine for prevention of

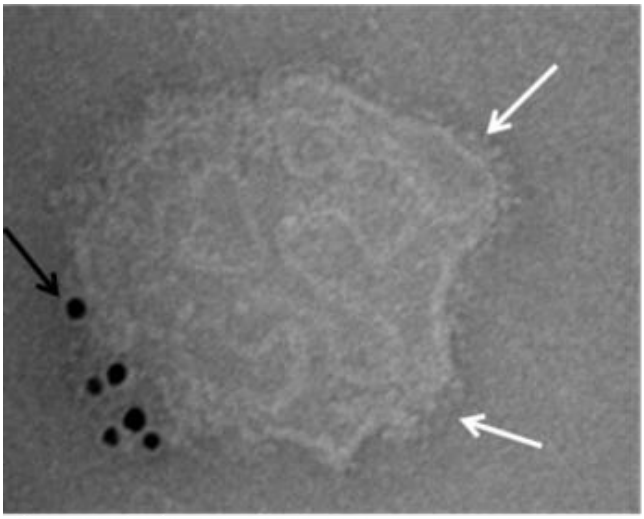

Lyme borreliosis has been awarded by European Patent Council. The patented preparation of multi-epitope vaccine against Lyme disease has been used by the Czech company Bioveta for the production for veterinary medicine (***BORRELYM***).
Currently, we are working on development of a recombinant vaccine against SARS-COVID-2 for non-invasive sublingual vaccination. Vaccines based on non-invasive sublingual application is a promising method to quickly develop a vaccine ready for entering phase I of clinical testing.

Fig. 9*: Proteoliposome shown by TEM. ROspC antigen molecules are indicated by a white arrow. The identity of the antigen is also confirmed by immunoaffinite labelling by colloidal gold particles (black arrow) [23].*

Cryobiology

Currently, cryopreservation of cells remains an unresolved task posing many challenges. By combining experimental and theoretical methods, the team systematically studied the way in which cryopreservation affect the constitution of ice as well as the state of cryopreserved cells. By correlating the physico-chemical properties of cryoprotectants with their effects on frozen/thawed oocytes, their nuclei and membranes (yet unaddressed questions), the team identified key attributes of cryoprotectants, which are responsible for their cryoprotective effect. The aim was to achieve a deeper understanding of the process of freezing and thawing of cells, as well as the mechanism of related cellular stress, particularly in the nucleus [24,25] Fig. 10.

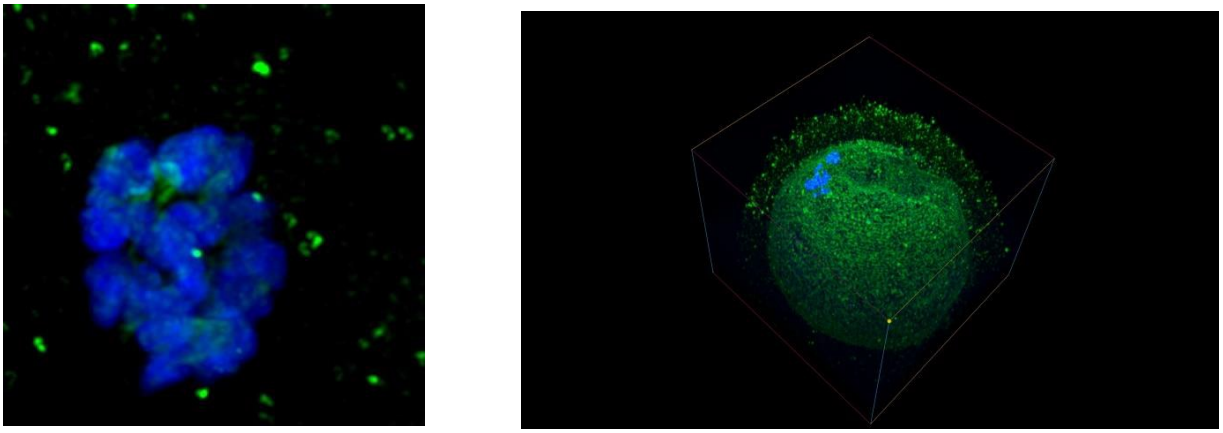

Fig. 10 *Chromosomes and meiotic spindles states of human oocyte (spatial pattern/organization) observed by confocal fluorescence microscopy.*

Part of the work was to determine the probability of oocyte vitrification success during IVF cycle using a clinically applicable method of clinical photographic records recognition. In cooperation with the Department of Cybernetics of the Czech Technical University in Prague, a neural network will be created to determine the probability of success (i.e. fertilization) of oocytes during IVF cycle. The ultimate application-oriented goal will be to design optimal methodologies for working with oocytes, so that the probability of their success in the IVF cycle is as high as possible.

M. Golan defended his Ph.D. work “Influence of freezing and thawing process on cryopreserved cells nuclei and surfaces. Functions and physico-chemical properties of cryoprotectants” under the leadership of I. Kratochvilova at the Faculty of Mathematics and Physics, Charles University in 2018, M. Golan was awarded the **Best poster at the Society for Low Temperature Biology Meeting**: “Complex description of cryopreserved cell nuclei defects by immunofluorescence microscopy: DNA lesions, chromatin decondensation, nuclei membrane ruptures”.

Structure defects in multifunctional materials.

EPR is suitable for investigation of the effect of the structure on functional properties of materials. A typical example of the use of this technique is investigation of structure defects in semiconductors and multifunctional materials (e.g. scintillators, ferroelectric and piezoelectric materials or ferroelectrics),

We focused in collaboration with Institute of Physics, Polish Academy of Science, Warsaw, on single crystals of rare-earth borates [26]. In these materials it is possible to produce an effective frequency conversion of laser radiation, which is much higher than the similar parameters of known media. Laser crystals of femtosecond duration were obtained on borate crystals doped with ytterbium ions. This involves a complex study of phase formations, magnetic and optical properties in multi-component borate melts with anion polymerizations, crystal growth and crystal “conditions–composition–structure–properties” relationships. The ability of crystals to contain a large concentration of impurity ions, combined with excellent physical and chemical properties, makes these borates a promising medium for solid-state lasers. Interest in small lasers pumped with LEDs in the green-blue spectral region supports the study of new solid-state laser systems based on nonlinear crystals. New data about the state of doping ions of Cr^{3+} in a single crystal of $YGa_3(BO_3)_4$ have been obtained when studying EPR spectra. It is demonstrated that the ions of Cr^{3+} substitute for the trivalent gallium ions. The obtained parameters of spin Hamiltonian of the Cr^{3+} ions in the $YGa_3(BO_3)_4$ single crystal have been analysed and compared with those in $TmAl_3(BO_3)_4$, $EuAl_3(BO_3)_4$, and $YAl_3(BO_3)_4$. The deviation of the Z-axis of the spectrum from the crystallographic axis C_3 is 2,5 °, 2 °, 0,7 ° and 1,7 ° in $TmAl_3(BO_3)_4$, $YAl_3(BO_3)_4$, $EuAl_3(BO_3)_4$ and $YGa_3(BO_3)_4$ respectively.

References

[1] P. Pokorný, J. Musil, P.Fitl, M. Novotný, J., Lančok, J. Bulíř, Contamination of magnetron sputtered metallic films by oxygen from residual atmosphere in deposition chamber; Plasma Processes and Polymers 12 (2015) 416-421
[2] S. Cichon, P. Macháč, L. Fekete, L. Lapcak, Direct microwave annealing of SiC substrate for rapid synthesis of quality epitaxial graphene, Carbon **98** (2016) 441
[3] N. Abdellaoui, A. Pereira, M. Novotný, J. Bulíř, P. Fitl, J. Lančok, B. Moine, A. Pillonnet, In situ monitoring of electrical resistance during deposition of Ag and Al thin films by pulsed laser deposition: Comparative study, Applied Surface Science **418** (2017) 517
[4] J. Cizek, J. Valenta, P. Hruska, O. Melikhova, I. Prochazka, M. Novotny, and J. Bulir, Origin of green luminescence in hydrothermally grown ZnO single crystals Appl Phys Lett, 2015. 106(25). (IF=3.411)
[5] M. Novotný, M. Vondráček, E. Marešová, P. Fitl, J. Bulíř, P. Pokorný, Š. Havlová, N. Abdellaoui, A. Pereira, P. Hubík, J. More-Chevalier, and J. Lančok, Optical and structural properties of ZnO:Eu thin films grown by pulsed laser depositionApplied Surface Science, 2019. 476: p. 271-275. (IF=5.155)
[6] N. Abdellaoui, A. Pereira, T. Kandri, E. Drouard, M. Novotny, B. Moine, and A. Pillonnet, J Mater Chem C, 2016. 4(39): p. 9212-9218. (IF=5.256)
[7] M. Vorokhta et. al Investigation of gas sensing mechanism of SnO2 based chemiresistor using near ambient pressure XPS, Surf Sci, 2018. 677: p. 284-290.

[8] P. Hozák et al. New Insight into the Gas-Sensing Properties of CuOx Nanowires by Near-Ambient Pressure XPS, Jpurnal of Physical Chemistry C 123 (2019) 29739
[9] E. Maresova, et. al.Textile chemiresistors with sensitive layers based on polymer ionic liquids: Applicability for detection of toxic gases and chemical warfare agents Sensor Actuat B-Chem, 2018. 266: p. 830-840.
[10] P. Ashcheulov et. al. Nanocrystalline Boron-Doped Diamond as a Corrosion Resistant Anode for Water Oxidation via Si Photoelectrodes, ACS Materials and Interfaces, 10, 29552- 29564
[11] A. Kovalenko, et. al. Diamond-based electrodes for organic photovoltaic devices, Solar Energy Materials and Solar Cells, 143 (2015) 73-79
[12] P. Ashcheulov, I. Kratochvílová et.al. *Thin polycrystalline diamond films protecting Zirconium alloys surfaces: from technology to layer analysis and application in nuclear facilities*, Applied Surface Science 359 (2015) 621-628
[13] Jan Škarohlíd, et. al. Nanocrystalline diamond protects Zr cladding surface against oxygen and hydrogen uptake: Nuclear fuel durability enhancement, *Scientific Reports* 7, Article number: 6469, 2017
[14] I. Kratochvílová et. al. Zr alloy protection against high-temperature oxidation: Coating by a doublelayered structure with active and passive functional properties, Corrosion Science 163 (2020) 108270(1)-108270(11).
[15] P. Heinrichová, et. Al. Diketopyrrolopyrrole Based Organic Solar Cells Functionality: the Role of Orbital Energy and Crystallinity, Journal of Physical Chemistry C 123 (2019) 11447-11463.
[16] M.Vondracek et. al. Nanofaceting as a stamp for periodic graphene charge carrier, Scientific Reports **6** (2016) 23663
[17] M. Wehrold et. al. pH sensitivity of interfacial electron transfer at a supported graphene monolayer, Nanoscale 11 (2019) 14742
[18] M. Vališka et. al. Topological insulator homojunctions including magnetic layers: The example of n-p type (n -QLs Bi2Se3/Mn-Bi2Se3) heterostructures, Appl. Phys. Lett. 108, (2016) 262402
[19] M. Vondracek et.al.. Nickel: The time-reversal symmetry conserving partner of iron on a chalcogenide topological insulator Phys. Rev. B **94** Rapid Comm., (2016) 161114(R)
[20] V.Tkac et al. Influence of an Anomalous Temperature Dependence of the Phase Coherence Length on the Conductivity of Magnetic Topological Insulator, Phys. Rev. Letters **123**, (2019) 036406,
[21] J. Honolka et. al. Electronic properties of GaAsBi(001) alloys at low Bi content, Phys. Rev. Materials **3** (2019) 044601
[22] O. Heczko et.al. Electronic structure in the twinned 10M martensite phase of the Ni.sub.49.7./sub.Mn.sub.29.1./sub.Ga.sub.21.2./sub. Heusler alloy: experiment and theory, Phys. Rev. B 98 (2018) 1-8
[23] P. Turánek et. al. Molecular adjuvants based on nonpyrogenic lipophilic derivatives of norAbuMDP/GMDP formulated in nanoliposomes: Stimulation of innate and adaptive immunity, Pharmaceutical Research 32 (2015) 1186-1199.
[24] M. Falk, I et. al. *Chromatin architecture changes and DNA replication fork collapse are critical features in cryopreserved cells that are differentially controlled by cryoprotectants*, Scientific Reports, 8/14694, 1-18
[25] I. Kratochvílová, et.al. Changes in Cryopreserved Cell Nuclei Serve as Indicators of Processes during Freezing and Thawing, Langmuir 35 (2019) 7496-7508.
[26] A.A. Prokhorov et. al. Optical and magnetic properties of the ground state of Cr3+ doping ions in REM3(BO3)(4) single crystals, Scientific Reports 9 (2019) 12787

Research activity and characterisation of the main scientific results

1 Interaction of intense high-LET radiation with matter, including characterization and application of focused XUV/x-ray laser beams

Interaction of extreme-ultraviolet radiation (XUV; 10 nm < λ < 100 nm), soft x-rays (SXR; 0.2 nm < λ < 30 nm) and x-rays (λ < 0.2 nm) with matter differs dramatically from that of the long-wavelength (i.e., UV-Vis-IR) radiation. The interaction of short-wavelength radiation occurs mostly due to the photo-effect in atoms of the irradiated material. Valence electrons play in general a minor role in the interaction. Thus an absorption coefficient depends on the elemental composition and density of the irradiated material. Contrary to long-wavelength radiation, there is a little influence of the fine chemical structure of the particular material chosen for an irradiation.
Similar effects can be caused by accelerated charged particles, e.g., electrons, protons and atomic ions. Finding similarities and differencies in an action of high-LET radiation of different kinds is a new area of research followed in the period 2015-2019 by our team.

1.1 Low and medium irradiance interaction conditions

Shining laser pulses of any wavelength and pulse duration onto a sample surface may induce phase transitions in the target material. We theoretically predicted that diamond, one of the hardest substances known on Earth, is surprisingly easy to convert into graphite irradiating it with extreme ultraviolet or x- ray free-electron laser (XFEL) femtosecond pulses (1 fs = 10^{-15} s). In a dedicated experiment confirming
our predictions, it was observed that such a structural change is remarkably quick – within ~ 150-200 fs irradiated atoms in diamond align themselves into the new structure of graphite, making it the fastest solid-solid phase transition observed so far [1] (illustrated in Fig.1). This is possible due to the process known as non-thermal phase transition, which is a result of the excitation of a large number of electrons, instead of the heating of atoms that triggers phase transitions we are accustomed to such as melting or boiling. In a non-thermal phase transition, excitation of electrons alters the interatomic potential, inducing new forces on atoms that guide them into a new phase [2].
Increasing XFEL pulse intensity leads to even more unusual effects. Diamond pumped with sufficient energy can turn into warm dense matter (WDM, an intermediate state between solids and plasma). Formation of WDM is extremely fast, yet is composed of a complex sequence of processes starting from electronic cascades, collapse of the electronic structure, followed by a collapse of the atomic one, as revealed by our dedicated modelling [3]. To study processes occurring in matter under such extreme conditions, a comprehensive model had been developed, which enabled us for the first time to address in such detail the interplay of the various physical mechanisms involved [4].
Diamond is not a unique example; other materials irradiated with femtosecond laser pulses may also experience non-thermal transition, as we demonstrated on examples of silicon [2] and group III-V semiconductors [5]. Both thermal and non-thermal effects can play a role in material damage, stirring a scientific controversy on their relative importance for decades. We used our model to untangle these effects and theoretically demonstrated that the two processes can be discerned, allowing us to propose a conceptual design of such an experiment at XFELs [6].
In more complex materials, other mechanisms start to play a role. We showed in a

combined experimental-theoretical study that a fullerene crystal (C60 molecules assembled into a periodic structure) can experience a molecular Coulomb explosion which repels individual C60 molecules from one another due to accumulated charge after electron emission from the XFEL-irradiated surface [7]. Intriguingly, the C60 molecules stayed intact, which indicated that selective manipulation of chemical bonds was achieved, cutting only the van der Waals bonds that kept fullerenes together, but not covalent bonds that glue atoms within a C60 molecule. This possibility was confirmed by modelling [7].
Apart from x-rays, charged particle impacts on matter cause nanoscale phase changes and damage. To study these, another multiscale model was developed in a collaborative effort. It enabled us to identify that the damage along an ion trajectory in matter does not coincide with the energy deposition profile, with the maximal damage located beyond the position of the maximal deposited dose [8] (shown in Fig.2). The revealed effect, potentially important for design of experiments and radiation therapies, is a result of different electronic spectra produced by ions with different energies, and material recovery after transient damage [9].

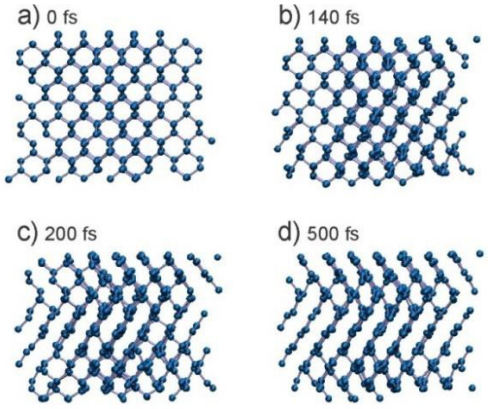

Figure 1 Calculated atomic snapshots in diamond irradiated with an XFEL pulse at a dose of 0.8 eV/atom. Reproduced from [1].

Although the major part of our interaction experiments is conducted with ultra-short XUV/x-ray pulses, we are also studying the interaction of short pulses. Recently, interesting results were obtained in CdTe irradiated by picosecond and nanosecond pulses delivered by plasma-based soft X-ray lasers [10].

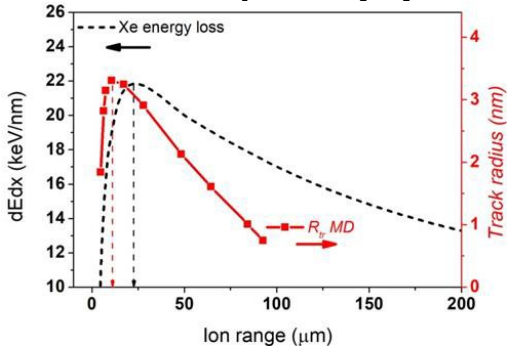

Figure 2 Track sizes and electronic energy losses of Xe ion vs. ion range in forsterite. Vertical arrows indicate the positions of maxima in the respective curves. Reproduced from [8].

2.1 High irradiance interaction conditions

We have continued to investigate ionization potential depression (IPD) [11] and optical properties [12] of solid density plasmas produced by a volumetric heating of various

targets by focused beams of short- wavelength lasers. In addition to this, we have studied collision rates in such plasmas [13,14]. Especially, the electron-ion collisional dynamics which is of fundamental importance in determining plasma transport properties, non-equilibrium plasma evolution, and electron damage in diffraction imaging applications using x-ray free-electron lasers (FELs). We contributed to the first experimental measurements of ultrafast electron impact collisional ionization dynamics using resonant core-hole spectroscopy in a solid-density magnesium plasma, created and diagnosed with the x-ray FEL, i.e., LCLS - *Linac Coherent Light Source* operated at SLAC in Menlo Park, CA, USA [14]**.**

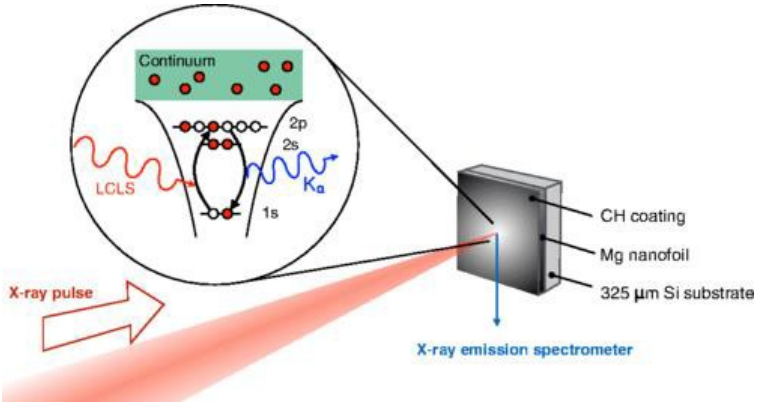

Figure 3 Layout of the interaction experiment making it possible to determine collisional frequency in dense plasmas produced at the LCLS facility. A 54-nm-thick Mg foil is irradiated by the focused x-ray laser pulse. The x-ray wavelength is tuned to the bound-bound resonance in a Mg^{7+} ion, resonantly driving a 1s→2p transition creating a core-hole excited state. The excited state can then decay through Auger recombination or Kα emission. Reproduced from [14].

As we see in numerous examples shown above and spread throughout the literature on the subject, it is difficult to provide a reliable theoretical description of IPD in warm dense matter. In our Department, Monte Carlo simulation code for calculating IPD in dense plasmas was developed [15]. The code was, in the beginning, designed for dense hydrogen plasmas and successfully compared with known results. Later it was extended for heavier elements and compared with results for aluminum at the state reached after irradiation with x-ray free-electron laser (LCLS). In collaboration with the Theory Division of CFEL (*Center for Free-Electron Research in Hamburg*) we optimized of the selection processes of photo- ionization and Auger cascades occurring in elemental metallic solids (Ti, Co, Au) after irradiation with a short-wavelength free-electron laser. This is a part of the joint project dealing with the kinetic Boltzmann modelling of highly internally ionized matter [16].

2 Characterizing, guiding and focusing the XUV/x-ray laser beams

In high-energy-density physics, it is important not only to approach an appropriate high-energy-density level but also to diagnose and characterize the system investigated under the unsteady conditions. Therefore systematic experimental and theoretical works dealing with an accurate and reliable characterization of focused laser beams are conducted in our Department to carry out the short- wavelength laser-matter interaction research properly. The detailed knowledge of transverse energy distribution within the beam profile turns out to be essential for interpretation of the quite nontrivial experimental results obtained at an enormous irradiance. Our recent work is therefore devoted to a detailed characterization of focused general laser beams [17,18].

Another key problem being solved at our Department is the damage to heavily loaded optical elements designed and used for guiding and focusing of XUV/x-ray laser beams. During the reported period, we determined damage thresholds of grazing incidence mirror carbonaceous coatings exposed to ultra- short X-ray pulses at SACLA facility in Hyogo, Japan [19]. In collaboration with industrial partners (ASML, Zeiss) and research teams (University of Twente, DESY, IFPAN, and so on) we tested resistance of a model mirror material (monocrystalline silicon) to multiple pulses delivered in MHz train [20]. These findings are important for the current and prospective development of compact high- repetition-rate XUV/SXR free-electron lasers. Such devices promise to bring the short-wavelength laser technology from large-scale facilities into the standard laboratory environment.

3 Investigating photons and charged particles emitted from laser-produced plasmas

3.1 High-energy photons

Advanced X-ray spectroscopic methods provide unique and critical data to study matter under extreme environmental conditions induced by high-intensity and high-energy lasers. Investigation of exotic x-ray emission from dense matter including transitions in hollow ions with multiple holes in inner electronic shells or complex satellite structure of resonance lines emitted from highly charged ions represent a very efficient tool for diagnosis of plasma- and laser-induced radiation fields, suprathermal electrons, and strong electromagnetic field effects [21,22].
Spectroscopic research activities pursued in a series of experiments at the Prague laser facility PALS concentrated on investigation of suprathermal electrons produced due to interaction of high-intensity laser beam (10^{15}-10^{16} W/cm^2) with solid targets [23]. This intensity regime is particularly interesting for development of alternate scenarios of inertial confinement fusion, namely the shock ignition scheme. Suprathermal electrons may significantly affect the deposition of laser energy into the fusion pellets, thus their detailed characterization is of paramount importance. The results achieved in several experimental campaigns provided information on conversion efficiency of the focused laser light into suprathermal electrons, contributed to measurements of their characteristic energy and spatial distribution, and showed their effects in context with creation of strong magnetic fields; selected publications are listed below [24-28]. Finally, the highly resolved spectral data were interpreted in terms of a delayed production of hot electrons with respect to the maximum of the interacting laser beam [29]. This research is being conducted in close collaboration with Université Bordeaux, Talence, France; Institute of Plasma Physics and Laser Microfusion, Warsaw, Poland; Ecole Polytechnique and Sorbonne Université, Paris, France; P.N. Lebedev Physical Institute of RAS and National Research Nuclear University MEPhI, Moscow, Russian Federation; and Czech Technical University in Prague.

3.2 Charged particles and low-energy photons (EMP)

The classification of laser-generated plasma is based inter alia on observation of the electrical polarity of the irradiated target [30]. Electrons, which have energy large enough to pass through the plasma potential barrier, escape the plasma and strike the walls of the interaction chamber. This macroscopic separation of electrons from plasma results in its positive polarization. This is transmitted to the irradiated target and its positive electrical charge is then neutralized by the return current flowing from the

grounded chamber through the target holder to the plasma. The magnitude and time development of this current depends on the number of electrons which escape the plasma and on the speed of the process. Thus, ultra-short target currents can reach extreme values of time derivative dj/dt of the current in the order of tera-amperes per second. The target holder becomes an antenna emitting a high-intensity electromagnetic pulse (EMP) which can be dangerous for laboratory electronic devices. Comparison of the dj/dt waveform with the intensity of the laser pulse IL(t) as well as j(t) with the laser energy EL(t) deposited on the target showed that plasma does not disappear at the end of laser-mass interaction (i.e. target and plasma). The plasma survives for many times longer than the duration of the laser pulse. During this second phase, the plasma is still a source of electrons, ions, and x-rays. Figure 4 shows two basic phases of laser-generated plasma, the ignition phase and the active phase.

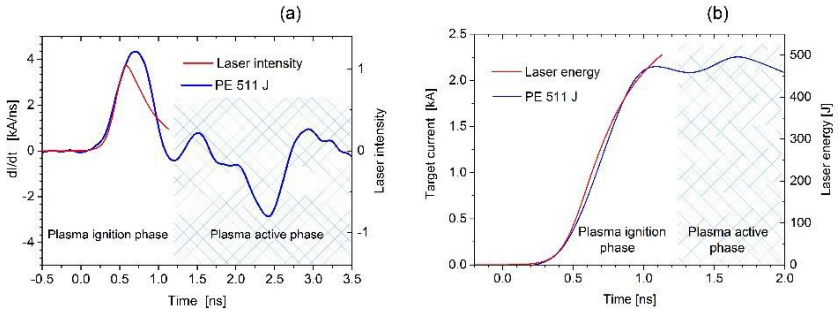

Figure 4 (a) Comparison of leading edges of signals of inductive target probe with normalized time-resolved laser intensity measured by streak camera, (b) and target current with laser energy deposited in a polyethylene target. The target current duration is ~70 ns. Reproduced from [30].

The target current, lasting at least several tens of nanoseconds, is the source of EMP, which can have devastating effects on laboratory electronics and can also totally disturb signals of detectors monitoring the plasma properties. The spectral characteristics of EMP are determined not only by the geometry of the transmitting antenna, i.e. the holder of the irradiated target, but also by the geometry of the interaction chamber, which acts as a resonator. The natural frequency of our chamber is about 260 MHz. Due to its complex shape and accessories housed in the chamber, the spectrum contains a series of resonant lines. The same applies to the target holder. Experiments have shown that the amplitude of the dj/dt frequencies in the 10-600 MHz range increases with the laser pulse energy, while the fluctuations in the 600-2000 MHz frequency amplitude obscure any possibility to observe the dependence on the laser parameters, see Figure 5.

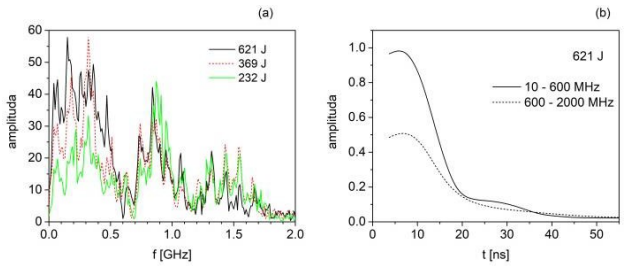

Figure 5 (a) Frequency spectra of inductive target probe signals UT(t) for laser energy of 232, 369, and 621 J focused onto a polyethylene target. **(b)** Time evolution of amplitudes of frequency bands from 10– 600 and from 600–2000 MHz. Reproduced from [30].

The EMP frequency spectrum then depends on the site of observation, whether the receiving antenna is inside or outside the interaction chamber. In both cases the measurement takes place in the near zone of the radiation source. The spectrum of

EMP measured outside the interaction chamber differs from that of the target current dj/dt also due to the arrangement and geometry of the chamber windows, which mainly affect the emission of frequencies up to 600 MHz, as shown in Figure 6.

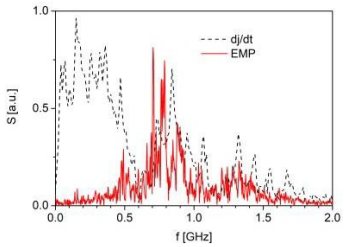

Figure 6 Comparison of the frequency spectrum of time derivative of target current with the EMP spectrum observed at 5 degrees. PE target was exposed to 621 J laser pulse. Reproduced from [30].

4 New techniques for probing fine structure of matter by x-rays

Researchers at the Department are also working on the determination of local atomic structures of crystalline materials with short-range chemical and/or displacement disorder by means of x-ray diffuse scattering including resonant x-ray diffuse scattering [31,32]. Three-dimensional arrangement of atoms at the sub-nanometer and nanometer scale is very important from the point of view of physical and chemical properties of materials and its importance is rapidly growing with the advance in nanotechnologies. This gives rise to fast development of fascinating imaging methods with atomic resolution in three dimensions, such as combined transmission electron microscopy and discrete tomography, coherent diffractive imaging, x-ray fluorescence holography etc. Obviously, each of these methods has its own specific limits and fields of applications. For example, electron tomography with atomic resolution requires a priori knowledge of a crystallographic structure, coherent diffractive imaging is limited to objects restricted to a confined region smaller than the beam size, and x-ray holograms provide information on only a few of the nearest neighbours of atoms of a selected element. For this reason we developed a novel method of multienergy anomalous x-ray diffuse scattering (MADS) which can be employed to the three-dimensional reconstruction of atomic arrangements around atoms of a selected element extending up to the distances of several nanometers. The method of MADS was applied successfully, for example, to the study of short-range chemical ordering in lead magnesium niobate [31] or to the study of atomic displacements in strontium titanate [32].

In spite of the fact that $PbMg_{1/3}Nb_{2/3}O_3$ (PMN) has been studied intensively as a model ferroelectric relaxor some questions on the local atomic structure and its relation to dielectric properties of this material still remain. Our work gives evidence for the sub-nanometric correlation length and isotropic nature of the Nb/Mg distribution in this relaxor system. These conclusions were drawn from the three- dimensional image of the average electron density distribution around the niobium ions (Figure 7 - right). The image was directly reconstructed from the measured distribution of the anomalous portion of scattered intensity in the reciprocal space (Figure 7 - left), involving both a discrete and continuous part (the Bragg reflections and diffuse scattering) of x-ray scattering. The diameter of the entire imaged region was about 10 nm but it could be even further increased by improvement of the momentum space resolution of the experiment. These results are very interesting for understanding the physics of PMN and related relaxor ferroelectrics, but this example also nicely demonstrates that this direct method can be indeed used for three-dimensional imaging of short-range chemical ordering in many other areas of condensed matter physics and material

science research.

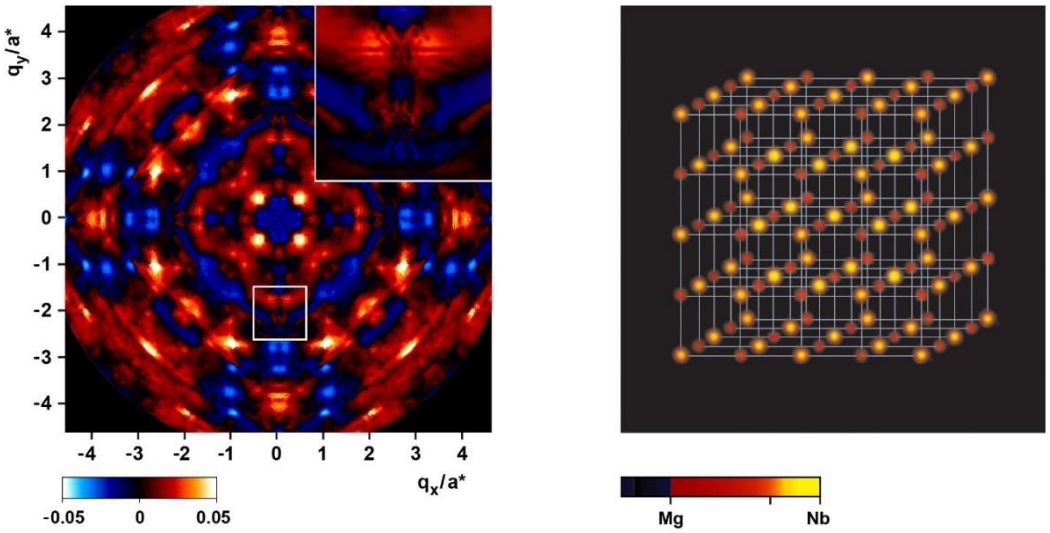

Figure 7 (Left): The anomalous portion of x-ray diffuse scattering obtained as difference between the data taken at the photon energies of 18.500 and 18.971 keV (b). (Right): The real-space image of the average surroundings of niobium ions. The coordinate system is related to the reference niobium ion at r = (0,0,0). For clarity, lead and oxygen ions are suppressed. Reproduced from [31].

In the case of SrTiO3 (STO), two different models of cation displacement comply with the single-energy diffuse scattering patterns, because single-energy diffuse scattering provides only ambiguous information on the directions of displacement of the Sr^{2+} and Ti^{4+} cations and their mutual correlations. However, the use of two photon energies, the first just below the absorption edge and the second far from the K absorption edge of strontium, determines unambiguously that the Sr^{2+} cations are moved from their ideal positions in the [100] direction and the Ti^{4+} cations are shifted in {111} directions.

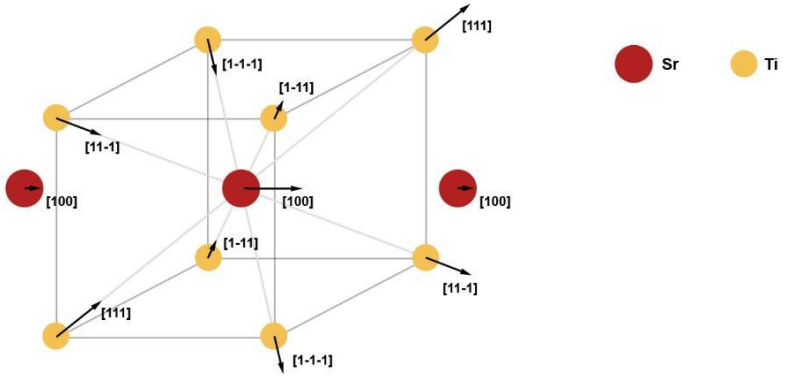

Figure 8 The model of cation displacement in a single crystal of strontium titanate. Reproduced from [32].

5 Interactions of laser radiation with atoms and molecules

The AMO team of the Theory Group of our Department performed research focused on finding ways of detecting fingerprints of exceptional points (EPs) in laser driven atoms. EPs represent singularities in the parameter space of non-Hermitian Hamiltonians, where their presence is associated with a qualitative change of a system. We are motivated by the fact that experimental evidence for such effects has been gathered from optical devices, however, experiments showing effects of EPs in atomic physics has not been done yet. The first experiment we proposed is related to a change

between oscillatory and monotonous behaviour of an atomic transition, if irradiated with Gaussian chirped pulses. It is well known that atomic transitions oscillate with the Rabi cycle. If a pulse is used, the oscillations also occur, but they occur with integer multipliers of pi of the pulse area, which is also known and used. On the other hand, it is also known that if the pulse is chirped and a sufficiently large chirp is used, a transition occurs and no oscillations are present. This is known as the adiabatic rapid passage. We showed and proved that there is a sharp transition between the two behaviours for a certain value of the chirp, which is associated with a coalescence of EPs, which are found in an artificial complex plane of time. This effect is possibly measurable in any transition between two bound states. However, we thought that it is more interesting to measure the same effect in transitions between a bound state and an autoionizing resonance of an atom, such as in the 1s2p → 2p2p transition of the helium atom, because, unlike in bound to bound transitions, there is a *physical* EP in the driven atoms, if the laser is tuned near such a resonance. We showed theoretically that the anticipated effect exists in these transitions and it useful to detect experimentally the position of the physical EP. The theory has been published on ArXiv [33], while an improved report will be resubmitted to a peer reviewed journal soon. We also made preparations for an experimental measurement of the atomic EPs based on the studied effect in the laser facilities associated with PALS. Next, we collaborated with the group of Nimrod Moiseyev (Technion, Haifa) to propose another effect of an EP in atoms, which is based on a modification of Fano profiles where two resonances of an atom (e.g. 2s2p and 2p2p in the helium atom) are brought to a non-Hermitian degeneracy (EP) using a coupling by a pump continuous wave (cw; a nanosecond pulse can work here as cw) radiation. The EP can cause either suppression or an enhancement of the associated resonance peak in the XUV absorption spectrum. The theoretical work has been published [34] and a discussion on possible experimental realizations on the current associated laser facilities to PALS took place. We further plan to investigate an impact of EP on high-order harmonic generation (HHG). As the first step we worked out a non-Hermitian theory to calculate the HHG spectra in an atom, where more than one Floquet resonance is involved due to a non-adiabatic coupling [35]. Earlier, we also participated on some improvements of numerical non-Hermitian methods for atoms and molecules [36].
The spontaneous emission (SE) is usually studied in the field of quantum dissipation theory. In recent work [37], members of the theory group looked at this from the perspective of nonhermitian quantum mechanics, interpreting the SE as a Feschbach type resonance. It has been shown that this approach is feasible and it is possible to calculate decay rate using the complex scaling method. As an illustration, the standard Golden Rule formula for decay rate is revealed from the complex scaled nonhermitian perturbation theory.

To provide a unique way to mimic the chemical effects of high-energy-density events in planetary atmospheres (cometary impact, lightning) and related environments, single ≤1 kJ pulses from a high- power laser PALS have been focused into homogeneous and heterogeneous molecular systems to create large amounts of dense, chemically active plasma that closely matches their natural energy- density and plasma-volume in a fully-controlled laboratory environment. Recently, we obtained interesting results in formaldehyde vapours [38]. Another research stream simulates meteor flight and meteoritic impact by laboratory plasmas created at the PALS facility [39]. In these studies, our Department is responsible for the laser plasma generation and revealing its characteristics by advanced plasma diagnostic techniques. Colleagues from the chemical institutions participating in these experiments are dealing with the chemical analysis of laser-plasma exposed samples.

In the laboratory of chemical lasers, a novel plasma-chemical gas-flow laser concept was found [40]. Unexpected strong mid-ultraviolet (UV) emission has been observed from the merger of two low- pressure supersonic gas-flows previously leaving two radiofrequency (RF) discharges, one containing Ar, He, O2 and traces of NO, the other He and plasma-chemically produced C2F4. Analysis of the spectral emission data shows that the main energy carriers are He, C2F4 (or CF2) and NO. Plasma-chemical excitation and energy transfer amongst the main energy carriers result in a spectrum dominated by a vibronic structure, covering the spectral range 190-300 nm, which is assigned to the spontaneous emission from excited NO. The strongest line located at 236.2 nm is due to the NO($A^2\Sigma^+$, 0–1) transition. The experimental conditions exclude any direct excitation of NO by the RF discharge itself. The observed phenomenon has potential as a plasma-chemical gas-flow laser emitting in the mid-UV spectral region.

References

1. F. Tavella, H. Höppner, V. Tkachenko, N. Medvedev, F. Capotondi, T. Golz, Y. Kai, M. Manfredda,
   E. Pedersoli, M.J. Prandolini, N. Stojanovic, T. Tanikawa, U. Teubner, S. Toleikis, B. Ziaja: Soft x- ray induced femtosecond solid-to-solid phase transition, *High Energy Density Physics* **24**, 22 (2017).
2. N. Medvedev, Z. Li, B. Ziaja: Thermal and nonthermal melting of silicon under femtosecond x-ray irradiation, *Phys. Rev.* B. **91**, 054113 (2015).
3. N. Medvedev, B. Ziaja: Multistep transition of diamond to warm dense matter state revealed by femtosecond X-ray diffraction, *Sci. Rep.* **8**, 5284 (2018).
4. N. Medvedev, V. Tkachenko, V. Lipp, Z. Li, B. Ziaja: Various damage mechanisms in carbon and silicon materials under femtosecond X-ray irradiation, *4open* **1**, 3 (2018).
5. N. Medvedev, Z. Fang, C. Xia, Z. Li: Thermal and nonthermal melting of III-V compound semiconductors, *Phys. Rev. B* **99**, 144101 (2019).
6. N. Medvedev, M. Kopecky, J. Chalupsky, L. Juha: Femtosecond x-ray diffraction can discern nonthermal from thermal melting, *Phys. Rev. B* **99**, 100303 (2019).
7. M. Toufarová, V. Hájková, J. Chalupský, T. Burian, J. Vacík, V. Vorlíček, L. Vyšín, J. Gaudin, N. Medvedev, B. Ziaja, M. Nagasono, M. Yabashi, R. Sobierajski, J. Krzywinski, H. Sinn, M. Störmer, K. Koláček, K. Tiedtke, S. Toleikis, L. Juha: Contrasting behavior of covalent and molecular carbon allotropes exposed to extreme ultraviolet and soft x-ray free-electron laser radiation, *Phys. Rev. B* **96**, 214101 (2017).
8. R. A. Rymzhanov, S. A. Gorbunov, N. Medvedev, A. E. Volkov: Damage along swift heavy ion trajectory, *Nucl. Instrum. Meth. Phys. Res. B* **440**, 25 (2019).
9. R. A. Rymzhanov, N. A. Medvedev, J. H. O'Connell, A. Janse van Vuuren, V. A. Skuratov, A. E. Volkov: Recrystallization as the governing mechanism of ion track formation, *Sci. Rep.* **9**, 3837 (2019).
10. V. Vozda, T. Burian, J. Chalupský, V. Dědič, V. Hájková, P. Hlídek, L. Juha, M. Kozlová, M. Krůs, J. Kunc, M. Rejhon, L. Vyšín, P. Mojzeš, J. J. Rocca, J. Franc: Micro-Raman mapping of surface changes induced by XUV laser radiation in cadmium telluride, *J. Alloys Comp.* **763**, 662 (2018).
11. O. Ciricosta, S. M. Vinko, B. Barbrel, D. S. Rackstraw, T. R. Preston, T. Burian, J. Chalupsky, B. I. Cho, H. K. Chung, G. L. Dakovski, K. Engelhorn, V. Hajkova, P. Heimann, M. Holmes, L. Juha, J. Krzywinski, R. W. Lee, S. Toleikis, J. J. Turner, U. Zastrau, J. S. Wark: Measurements of continuum lowering in solid-density plasmas created from elements and compounds, *Nature Commun.* **7**, 11713 (2016).
12. D. S. Rackstraw, O. Ciricosta, S. M. Vinko, B. Barbrel, T. Burian, J. Chalupský, B.

I. Cho, H.-K. Chung, G. L. Dakovski, K. Engelhorn, V. Hájková, P. Heimann, M. Holmes, L. Juha, J. Krzywinski, R. W. Lee, S. Toleikis, J. J. Turner, U. Zastrau, J. S. Wark: Saturable absorption of an x-ray free- electron-laser heated solid-density aluminium plasma, *Phys. Rev. Lett.* **114**, 015003 (2015).

13. S. M. Vinko, O. Ciricosta, T. R. Preston, D. S. Rackstraw, C. R. D. Brown, T. Burian, J. Chalupský, B. I. Cho, H.-K. Chung, K. Engelhorn, R. W. Falcone, R. Fiokovinini, V. Hájková, P. A. Heimann, L. Juha, H. J. Lee, R. W. Lee, M. Messerschmidt, B. Nagler, W. Schlotter, J. J. Turner, L. Vysin, U. Zastrau, J. S. Wark: Investigation of femtosecond collisional ionization rates in a solid-density aluminium plasma, *Nature Commun.* **6**, 6397 (2015).
14. Q. Y. van den Berg, E. V. Fernandez-Tello, T. Burian, J. Chalupský, H.-K Chung, O. Ciricosta, G. L. Dakovski, V. Hájková, P. Hollebon, L. Juha, J. Krzywinski, R.W. Lee, M. P. Minitti, T. R. Preston, A.G. de la Varga, V. Vozda, U. Zastrau, J. S. Wark, P. Velarde, S. M. Vinko: Clocking femtosecond collisional dynamics via resonant X-ray spectroscopy, *Phys. Rev. Lett.* **120**, 055002 (2018).
15. M. Stransky: Monte Carlo simulations of ionization potential depression in dense plasmas. *Phys. Plasmas* **23**, 012708 (2016).
16. B. Ziaja V. Saxena, S. K. Son, N. Medvedev, B. Barbrel, B. Woloncewicz M. Stransky: Kinetic Boltzmann approach adapted for modeling highly ionized matter created by x-ray irradiation of a solid. *Phys. Rev. E* **93**, 053210 (2016).
17. J. Krzywinski, A. Andrejczuk, R. M. Bionta, T. Burian, J. Chalupský, M. Jurek, M. Kirm, V. Nagirnyi, R. Sobierajski, K. Tiedtke, S. Vielhauer, L. Juha: Saturation of a Ce:Y3Al5O12 scintillator response to ultra-short pulses of extreme ultraviolet, soft x-ray and x-ray laser radiation, *Opt. Mat. Express* **7**, 665 (2017).
18. J. Chalupský, P. Boháček, T. Burian, V. Hájková, S. P. Hau-Riege, P. A. Heimann, L. Juha, M. Messerschmidt, S. P. Moeller, B. Nagler, M. Rowen, W. F. Schlotter, M. L. Swiggers, J. J. Turner, J. Krzywinski: Imprinting a focused X-ray laser beam to measure its full spatial characteristics, *Phys. Rev. Appl.* **4**, 014004 (2015).
19. A. Aquila, R. Sobierajski, C. Ozkan, V. Hájková, T. Burian, J. Chalupský, L. Juha, M. Stormer, S. Bajt, M. T. Klepka, P. Dluzewski, K. Morawiec, H. Ohashi, T. Koyama, K. Tono, Y. Inubushi, M. Yabashi, H. Sinn, T. Tschentscher, A. P. Mancuso, J. Gaudin: Fluence thresholds for grazing incidence hard x-ray mirrors, *Appl. Phys. Lett.* **106**, 241905 (2015).
20. R. Sobierajski, I. Jacyna, P. Dluzewski, M. T. Klepka, D. Klinger, J. B. Pelka, T. Burian, V. Hajkova, L. Juha, K. Saksl, V. Vozda, I. Makhotkin, E. Louis, B. Faatz, K. Tiedtke, S. Toleikis, H. Enkisch, M. Hermann, S. Strobel, R. A. Loch, J. Chalupsky: Role of heat accumulation in the multi-shot damage of silicon irradiated with femtosecond XUV pulses at a 1 MHz repetition rate, *Opt. Express* **24**, 15468 (2016).
21. F.B. Rosmej, R. Dachicourt, B. Deschaud, D. Khaghani, M. Dozières, M. Šmíd, O. Renner: Exotic x-ray emission from dense plasmas, *J. Phys. B: At. Mol. Opt. Phys.* **48**, 224005 (2015).
22. O. Renner, F.B. Rosmej: Challenges of x-ray spectroscopy in investigations of matter under extreme conditions, *Matter Radiat. Extremes* **4**, 024201 (2019).
23. O. Renner, M. Šmíd, D. Batani, L. Antonelli: Suprathermal electron production in laser-irradiated Cu targets characterized by combined methods of x-ray imaging and spectroscopy, *Plasma Phys. Control. Fusion* **58**, 075007 (2016).
24. T. Pisarczyk, S. Yu. Gus'kov, R. Dudzak, T. Chodukowski, J. Dostal, N. N. Demchenko, Ph. Korneev, Z. Kalinowska, M. Kalal, O. Renner, M. Smid, S. Borodziuk, E. Krousky, J. Ullschmied, J. Hrebicek, T. Medrik, J. Golasowski, M. Pfeifer, J. Skala, and P. Pisarczyk: Space-time resolved measurements of spontaneous magnetic fields in laser-produced plasma, *Phys. Plasmas* **22**, 102706 (2015).

25. G. Cristoforetti, A. Colaïtis, L. Antonelli, S. Atzeni, F. Baffigi, D. Batani, F. Barbato, G. Boutoux, R. Dudzak, P. Koester, E. Krousky, L. Labate, Ph. Nicolaï, O. Renner, M. Skoric, V. Tikhonchuk and L. A. Gizzi: Experimental observation of parametric instabilities at laser intensities relevant for shock ignition, *EPL-Europhys. Lett.* **117**, 35001 (2017).
26. G. Cristoforetti, L. Antonelli, S. Atzeni, F. Baffigi, F. Barbato, D. Batani, G. Boutoux, A. Colaitis, J. Dostal, R. Dudzak, L. Juha, P. Koester, A. Marocchino, D. Mancelli, Ph. Nicolai, O. Renner, J. J. Santos, A. Schiavi, M. M. Skoric, M. Smid, P. Straka, and L. A. Gizzi: Measurements of parametric instabilities at laser intensities relevant to strong shock generation, *Phys. Plasmas* 25, 012702 (2018).
27. T. Pisarczyk, S. Y. Gus'kov, A. Zaras-Szydłowska, R. Dudzak, O. Renner, T. Chodukowski, J. Dostal, Z. Rusiniak, T. Burian, N. Borisenko, M. Rosinski, M. Krupka, P. Parys, D. Klir, J. Cikhardt, K. Rezac, J. Krasa, Y.-J. Rhee, P. Kubes, S. Singh, S. Borodziuk, M. Krus, L. Juha, K. Jungwirth, J. Hrebicek, T. Medrik, J. Golasowski, M. Pfeifer, J. Skala, P. Pisarczyk, Ph. Korneev: Magnetized plasma implosion in a snail target driven by a moderate intensity laser pulse, *Sci. Rep.* **8**, 17895 (2018).
28. D. Batani, L. Antonelli, F. Barbato, G. Boutoux, A. Colaïtis, J.-L. Feugeas, G. Folpini, D. Mancelli, Ph. Nicolai, J. Santos, J. Trela, V. Tikhonchuk, J. Badziak, T. Chodukowski, K. Jakubowska, Z. Kalinowska, T. Pisarczyk, M. Rosinski, M. Sawicka, F. Baffigi, G. Cristoforetti, F. D'Amato, P. Koester, L.A. Gizzi, S. Viciani, S. Atzeni, A. Schiavi, M. Skoric, S. Gus'kov, J. Honrubia, J. Limpouch, Klimo, J. Skala, Y.J. Gu, E. Krousky, O. Renner, M. Smid, S. Weber, R. Dudzak, M. Krus,J. Ullschmied: Progress in understanding the role of hot electrons for the shock ignition approach to inertial confinement fusion, *Nucl. Fusion* **59**, 032012 (2019).
29. M. Šmíd, O. Renner, A. Colaitis, V.T. Tikhonchuk, T. Schlegel, F. B. Rosmej: Characterization of suprathermal electrons inside a laser accelerated plasma via highly-resolved Kα-emission. *Nature Commun.* **10**, 4212 (2019).
30. J. Krása, M. De Marco, J. Cikhardt, M. Pfeifer, A. Velyhan, D. Klír, K. Řezáč, J. Limpouch, E. Krouský, J. Dostál, J. Ullschmied, R. Dudžák: Spectral and temporal characteristics of target current and electromagnetic pulse induced by nanosecond laser ablation, *Plasma Phys. Control. Fusion* 59, 065007 (2017).
31. M. Kopecký, J. Kub, J. Fábry, J. Hlinka: Nanometer-range atomic order directly recovered from resonant diffuse scattering. Phys. Rev. B 93, 054202 (2016).
32. M. Kopecký, J. Fábry, J. Kub: Modelling of cation displacements in SrTiO3 by means of multi-energy anomalous X-ray diffuse scattering, *J. Appl. Cryst.* **49**, 1016 (2016).
33. P. R. Kaprálová-Žďánská, M. Šindelka, N. Moiseyev: Topological-like phenomenon when encircling an exceptional point. arXiv:1903.10383 [quant-ph]
34. A. Pick, P. R. Kaprálová-Žďánská, N. Moiseyev, Ab-initio theory of photoionization via resonances, *J. Chem. Phys.* **150**, 204111 (2019).
35. P. R. Kaprálová-Žďánská, High-order harmonic generation spectrum from two coupled Floquet resonances – a non-Hermitian formulation, *Mol. Phys.* **117**, 2138 (2019).
36. A. Landau, I. Haritan, P. R. Kaprálová-Žďánská, and N. Moiseyev, Atomic and molecular complex resonances from real eigenvalues using standard (hermitian) electronic structure calculations. *J. Phys. Chem. A* **120**, 3098 (2016).
37. M. Šindelka, D. Šimsa: Spontaneous emission from nonhermitian perspective: complex scaling of the photon coordinates, *Mol. Phys.* **117**, 1989 (2019).
38. M. Ferus, F. Pietrucci, A. M. Saitta, O. Ivanek, A. Knizek, P. Kubelík, M. Krus, L. Juha, R. Dudzak, J. Dostál, A. Pastorek, L. Petera, J. Hrncirova , H. Saeidfirozeh, V. Shestivská, J. Sponer, J. E. Sponer, P. Rimmer, S. Civis, G. Cassone: Prebiotic synthesis initiated in formaldehyde by laser plasma simulating high-velocity impacts,

Astron. Astrophys. **626**, A52 (2019).
39. M. Ferus, P. Kubelík, L. Petera, L. Lenža, J. Koukal, A. Křivková, A. Knížek, H. Saeidfirozeh, A. Pastorek, T. Kalvoda , L. Juha, R. Dudzak, S. Civiš, E. Chatzitheodoridis, M. Krůs: Main meteor spectral features studied using terawatt-class high power laser, *Astron. Astrophys.* 630, A127 (2019).
40. J. Schmiedberger, W. Fuss, L. Juha: Strong sensitized ultraviolet luminescence from He–C2F4–NO flowing plasma afterglow: a route to short-wavelength gas-flow lasers? *Plasma Chem. Plasma Process.* **39**, 1115 (2019).

Research activity and characterisation of the main scientific results

1. 'Bivoj' - the first kilowatt average power 100 J-level diode pumped solid-state laser

The HiLASE 100J/10 Hz laser system ('Bivoj') has been developed by a joint effort of British and Czech teams at the Central Laser Facility (CLF) in the UK. Construction of the laser began in April 2013 and was completed in October 2015. After shipment from CLF to HiLASE, the Bivoj laser was re- commissioned by a multi-disciplinary team including surveyors, electricians, mechanical, vacuum and control system engineers, and laser scientists. This involved 17 separate visits to HiLASE by 15 team members from CLF, and a total of ~140 working days. The Bivoj laser was successfully commissioned (Fig. 2) at HiLASE in December 2016, representing **the world's first** kW average power, high-energy, nanosecond pulsed diode pumped solid-state laser (Optica **4**, 438 (2017)).

Fig. 2: The Bivoj super laser at HiLASE.

The Bivoj laser is based on master oscillator power amplifier architecture incorporating multiple amplification stages. A front end provides temporally (2-10 ns) and spatially (21.5 mm square flat-top) shaped seed pulses with energies in excess of 100 mJ at 1029.5 nm. These pulses are amplified up to 10 J in a cryogenic pre-amplifier. The square output beam from the pre-amplifier is then expanded to a width of 75 mm before a final cryo-amplifier boosts the pulse energy to the 100 J-level at 10 Hz (Fig. 3). Both cryo-amplifiers are based on a multi-slab design, using Yb:YAG ceramic as their gain media, cooled by a high velocity stream of helium gas at cryogenic temperature, and employ a multi-pass architecture to extract the stored energy from the separate 940 nm pump diode sources.

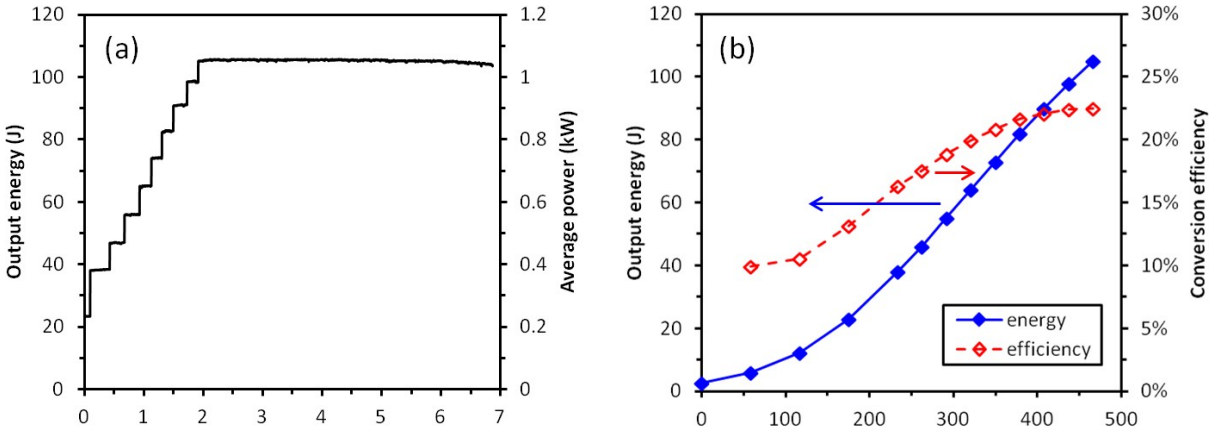

Fig. 3: Bivoj laser performance.

In order to satisfy a variety of different users from industrial and scientific communities, the laser system layout has been modified to allow a fast switch between operation of the 100 J and the 10 J laser amplifiers. The Bivoj laser system has proven to be very robust. For example, it has successfully provided more than 25 million laser pulses resulting in reliable, stable and high-energy laser operation during the period from August 2017 to July 2018. These laser shots have, for example, been extensively used for internal tests and for experimental campaigns in the areas of Laser Shock Peening (LSP), Laser Induced Damage studies and laser-generated ions. Due to increasing interest from industrial and scientific communities, in 2018 HiLASE began launching regular calls for access to the Bivoj laser on an annual basis.

In order to broaden the spectrum of novel industrial and scientific applications, HiLASE and the teams from the UK Research and Innovation (UKRI) Science and Technology Facilities Council (STFC) have worked together and demonstrated high energy second (SHG) and third harmonic generation (THG) at 515 nm and 343 nm, respectively. Over an extended period of 110 minutes, the conversion efficiency remained stable with a SHG energy stability of 0.8% rms. We have also successfully demonstrated high energy THG at 343 nm with a nonlinear LBO crystal on the Bivoj laser system as a sum frequency of fundamental and second harmonic frequencies. Over an extended period of 60 minutes, the conversion efficiency remained stable with a THG energy stability of 2% rms. Several materials have a significantly greater absorption at 515 nm or 343 nm laser radiation and this will allow users of the HiLASE facility to efficiently process non-ferrous metals, such as copper or aluminium alloys. In addition, these wavelengths are weakly absorbed by water, and thus new experiments under water could be conducted for specific industrial applications.

2. Characterization of magneto-optical materials

We have developed a novel measurement method for determining the Verdet constant in magneto- optical (MO) materials. The HiLASE team in collaboration with NIFS (Japan) jointly designed the concept and the experimental setup. This new method proved to be very useful in characterizing the MO properties of TGG crystals and ceramics. Our original setup provides an accurate measurement of the Verdet constant of the material as a function of wavelength and temperature. Such measurements are crucial for characterization of MO materials in high-power Faraday devices, and for the extensive study of material properties, including comparison with theoretical models. An original fitting function has been proposed, and contains the individual contributions of four distinct physical phenomena responsible for the overall Faraday rotation. It is worth mentioning that several other groups worldwide currently use our measurement setup, data analysis, and the Verdet constant data fitting procedure.

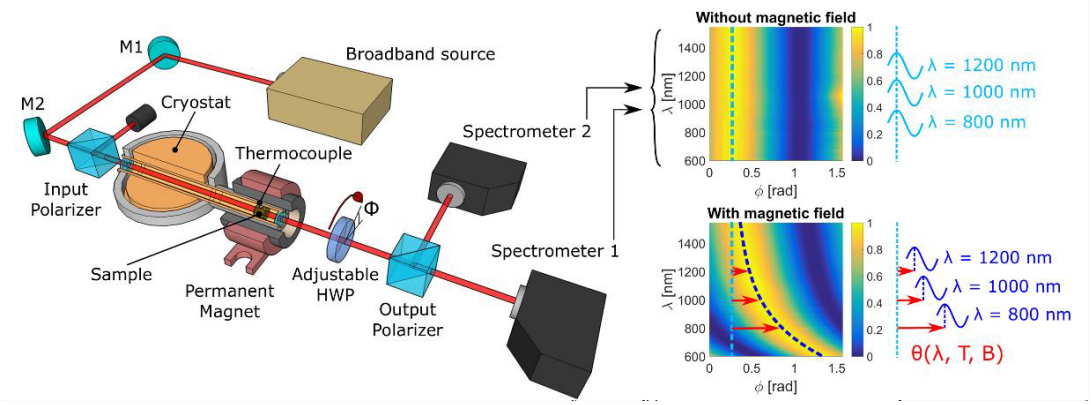

Fig. 4: Experimental setup for the measurement of the Verdet constant in magneto-optical materials (left) and example of data processing for a fixed temperature of the sample (right).

Our experimental setup has been systematically used to characterize the properties of many different magneto-optical materials, including holmium sesquioxide (Ho_2O_3) and dysprosium sesquioxide (Dy_2O_3) transparent ceramics, cerium fluoride (CeF_3) and potassium terbium fluoride KTb_3F_{10} (KTF) crystals. The results have been published in scientific journals, such as Optics Express, Optical Materials Express and High Power Laser Science and Engineering.

3. Development of compact cryogenic and microchip laser systems

Transparent ceramics, a relatively new candidate in the field of solid-state lasers, have gained significant attention for the development of high-energy and high-intensity class lasers. We have experimentally evaluated the dependence of the laser performance on the high-power laser diodes as the pumping sources, the use of Yb^{3+} as dopant ion and cryogenic cooling of the ceramics gain media. Yb^{3+} based solid-state gain media demand cryogenic cooling for operating lasers with higher efficiency. Yb: YAG is widely used as gain medium due to its excellent thermal and spectroscopic properties. However, at cryogenic temperature the emission bandwidth of Yb:YAG decreases tremendously, limiting the generation of short pulses. In order to mitigate this issue, laser host materials with broad emission bandwidths are necessary. Our team studied spectroscopic and lasing characteristics of a novel Yb- doped $Y_3Ga_2Al_3O_{12}$ (Yb:YGAG) transparent ceramic gain material at cryogenic temperatures. Our results show that the emission bandwidth is as much as three times larger than Yb:YAG at cryogenic temperatures, which makes this material very promising for short pulse generation at high average powers. We have also studied the laser characteristics of Yb:Lu_2O_3 transparent ceramics at cryogenic temperatures. Two different pump diodes, which match two of the absorption bands of Yb:Lu_2O_3 have been employed. A wavelength stabilized narrow band pump diode was found to perform significantly better with an output power four times better than that of conventional broadband pump diodes. The results of this study give crucial insights into the role of pump wavelength and gain media temperature at continuous wave and Q-switched operation. We have also reported efficient continuous-wave and pulsed laser operation of Yb:Y_2O_3 transparent ceramic at cryogenic temperatures.

We have investigated the effect of Gd^{3+} and Ga^{3+} on Yb:YAG emission at cryogenic temperatures by preparing ceramic pellets using solid state reaction methods with different Gd^{3+} and Ga^{3+} content. The emission spectrum measured at 100K for Yb:YAG ceramic samples admixed with different concentration of Ga is shown in Fig. 5. The inset shows the spectra for sample with y=0.4 at 100 K and 300 K.

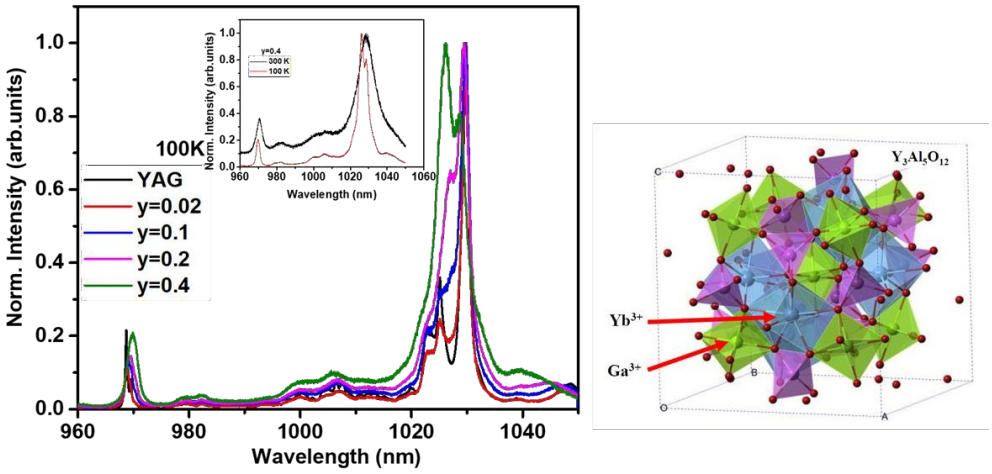

Fig. 5: Emission spectrum of a lab-made Yb:YAG ceramic samples measured at 100 K admixed with different concentrations of Ga^{3+}.

Efficient, compact and scalable microchip lasers have attracted considerable attention due to their low cost and easy alignment. In particular, we have investigated spectroscopic and laser characteristics of several microchip lasers, including Yb:LuGG, Yb:YGG, Yb:CNGG, Yb: CLNGG, Yb:CNGS, Yb: CALGO, Yb:CALYO, and Er:KLuW.

The mid-infrared region of the electromagnetic spectrum (2-20 μm) has long attracted much scientific and technological interest, due to the fact that virtually all molecules have their rotational-vibrational absorption lines in this wavelength range. For this reason, the mid-IR is often referred to as the “molecular fingerprint” region. Therefore, we have extended the study of solid-state cryogenic lasers to the mid-infrared and have obtained excellent performance of cryogenic spectroscopic and laser characteristics in thulium-doped yttrium oxide (Tm:Y2O3) materials. At room temperature, a power scaling concept maintaining the high efficiency of compact of diode-pumped Tm:Lu2O3 and Tm:Sc2O3 lasers was investigated utilizing the plano-plano laser cavity geometry. In collaboration with the University of Jena (Germany), our team members have performed detailed measurements of laser cross sections of thulium doped yttrium-aluminum-garnet (Tm:YAG) and yttrium-aluminum-perovskite (Tm:YAP) at temperatures ranging from 80 K to 300 K, and estimated fluorescence lifetimes using the pinhole method. This data provide useful information for the design and optimization of next generation laser systems around 2 μm.

We have also achieved successful operation of a compact high-energy pulsed laser based on a novel unstable cavity design. This concept is based on the inscription of a tailored gain media profile generated by a spatially top hat shaped longitudinal pump beam into the gain medium. A maximum energy of 285 mJ at 10 Hz repetition rate was obtained with a rectangular beam profile in pulse operation. A prototype cavity based on the same design was able to generate energies of more than 1.2 J at 10 Hz with a pulse duration of 12 ns. A patent related to this laser cavity technology was awarded in

September 2019. Potential utilisation of high-energy unstable resonators include industrial applications (laser shock peening, advanced 3-D printing), scientific applications (generation of x-rays for biology and medicine), and technological applications such as energetic pumps for ultrashort Ti:sapphire lasers, optical parametric amplifiers, or high-energy 2-micron sources. Results have been published in scientific journals such as Optics Express, Journal of Luminescence, IEEE Journal of Selected Topics in Quantum Electronics, Ceramics International, Optical Materials Express, Optics Letters, Applied Physics B and High Power Laser Science and Engineering.

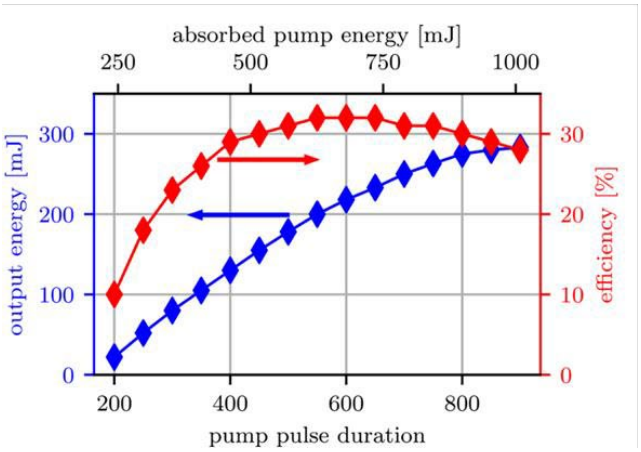

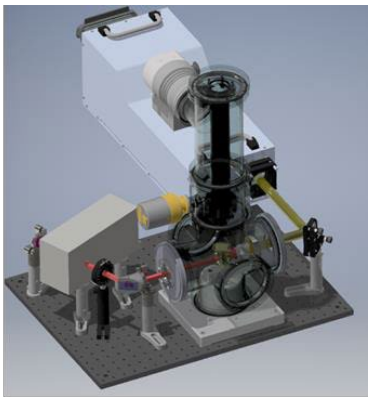

Fig.6: Output energy (blue curve) and efficiency (red curve) as a function of the pump pulse duration in the cryogenically-cooled unstable resonator (patent pending).

4. The Perla thin-disk laser platform

HiLASE has been strategically focusing on in-house development of ultrashort pulse diode-pumped compact lasers based on active media in the shape of a very thin disk since its establishing in 2011. We have created an international development team consisting of scientists, mechanical designers, and electrical engineers. Following requests of industrial partners, construction of three thin disk lasers systems called Perla A, B, and C (acronym for PERfect LAser) was proposed. The first laboratory prototype was commissioned in 2014 delivering 100 W average power. In 2015, a second stage regenerative amplifier based on a new design utilizing a 6.5 m long ring cavity was commissioned. This upgrade represented a major milestone for HiLASE, as we reached an average power > 400 W in a 100 kHz train of picosecond pulses. After several improvements the system generated 550 W with perfect beam shape close to the diffraction limit (Fig. 7). Despite the extremely long cavity of the system, the footprint of Perla C – 500 remains small for such a powerful picosecond laser.

Perla C integrates several unique, in-house developed solutions, for example a very compact pulse compressor made of a piece of glass inscribed with a Bragg grating inside, so called Chirped Volume Bragg Grating compressor. Another example is a HiLASE patented mount for large size, water cooled BBO Pockels cells for regenerative amplifier control. We had to solve complex engineering problems including special optomechanical mounts preventing deformation by fixing screws with integrated water cooling, residual absorption and laser induced damage threshold of optical coatings. In 2016, the Technical Readiness Level (TRL) of Perla C reached 4.

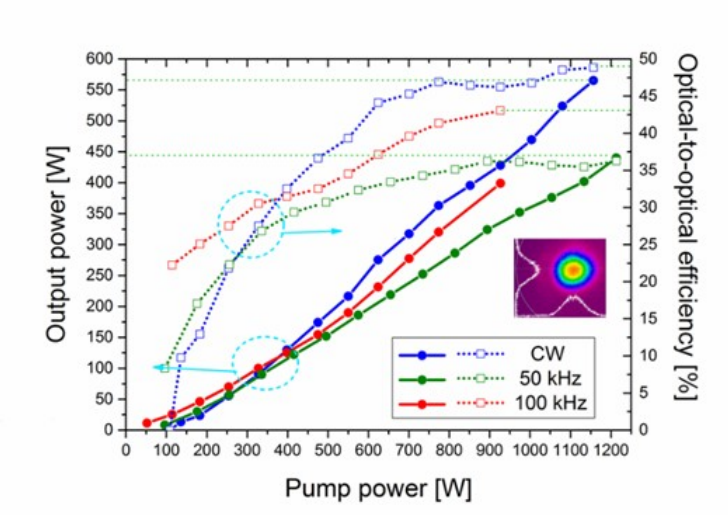

Fig. 7: Output power and optical efficiency of the Perla C laser under different operating conditions.

Extensive plans for adoption of the Perla C into several internal research project along with requests from industrial companies compelled us to develop a laser with TRL > 6 and transform Perla to a customized commercial device. The „commercial“ version of the Perla C – 100 platform (average power 100 W) was completed in 2019 (Fig. 8). The birth of this laser was preceded by engineering of in-house components optimized for our system, whilst not colliding with any existing intellectual property rights (Fig. 9). We have focused on development of a very stable fibre oscillator and a fully fibre-based seed laser delivering femtosecond pulses at the microjoule energy level. We have prototyped our own thin disk module. Due to the extreme conditions in the sub-mm active medium caused by high thermal load, high thermal gradients, and mechanical stress, a strong and homogeneous bond between the gain medium and a heatsink with high thermal conductivity had to be developed. We have systematically tested several different approaches including special epoxy gluing and atomic diffusion bonding.

Fig. 8: TRL 6 prototype of the commercial Perla C - 100 laser; 1W fibre-base prototype of a femtosecond front-end (left bottom); GoPico oscillator prototype (right, bottom).

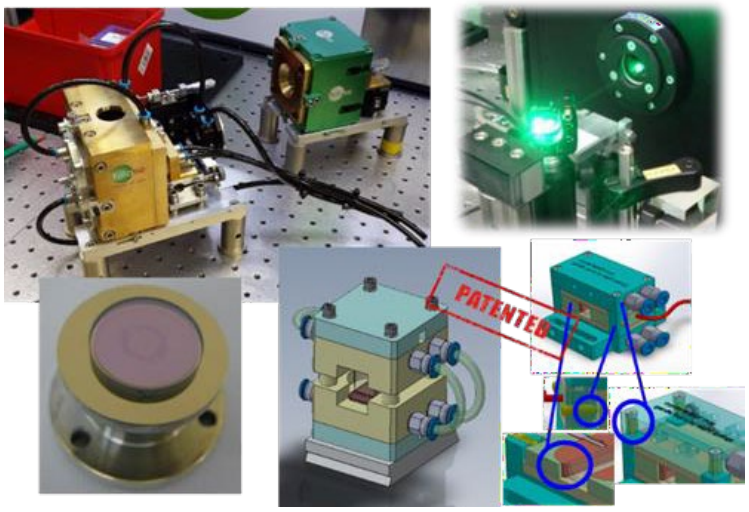

Fig. 9: In-house developed core technologies for the TRL 6 Perla C commercial prototype.

Although the Perla platform is a very powerful tool, some materials hardly interact with near infrared photons at 1030 nm. Thus, for welding of copper, for example, second harmonic frequency (green), is desirable, whilst for processing of glass and ceramics, deep ultraviolet (DUV) wavelengths are beneficial. High power DUV radiation at 257 nm and 206 nm was generated as the 4^{th} and 5^{th} harmonic frequencies from the fundamental wavelength of 1030 nm of the diode pumped high-power Yb:YAG thin disk laser Perla at a repetition rate of 77-100 kHz. The pulse duration is typically 1.5 ps. The application potential of such high-energy DUV pulses covers science (spectroscopy, photoelectron generation), medicine and mainly industry (efficient material processing, lithography). We used two CLBO crystals as convertors into DUV radiation. The 4^{th} harmonic was generated by frequency quadrupling of the fundamental beam and the 5^{th} harmonic as sum frequency 1w+4w. The 1 W output power of the 5^{th} harmonic ranks among the highest ever attained for picosecond pulses (Fig. 10).

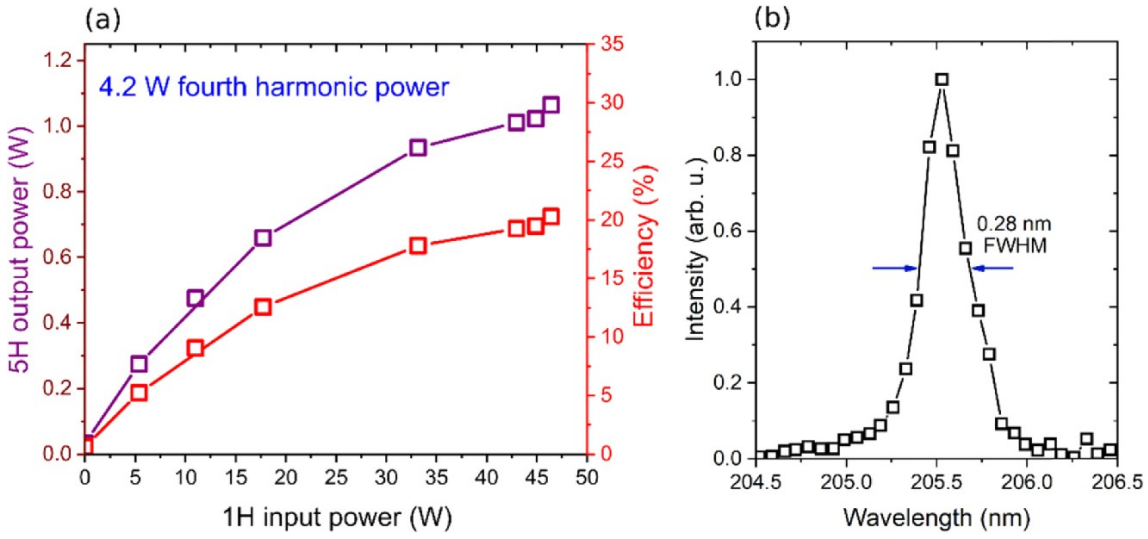

Fig. 10. (a) 5H-output power dependence on the 1H-input power at the 4H-input power being constant 4.2 W. (b) Spectrum of the fifth harmonic.

We have also developed a high-average-power picosecond mid-IR source. In 2018, we commissioned an optical parametric generator followed by tuneable picosecond

optical parametric amplifier covering the spectral range from 1.6 to 3.2 μm. This simple and power scalable mid-IR source is an excellent tool for processing organic materials, spectroscopy, biomedical applications, etc.

1.5 Industrial laser technologies

We launched our LSP program in 2016, shortly after commissioning the Bivoj laser system. LSP utilizes high energy nanosecond laser pulses to create deep compressive residual stresses in treated material surfaces, which increases hardness, prevents stress corrosion cracking and leads to significant prolonging of fatigue lifetime of critical industrial parts susceptible to fatigue failure. A protective enclosure has been built around the treatment area (Fig. 11) and full automation of the process has been achieved. The movement of the sample carrying robotic arm is integrated with the laser operation, thus ensuring high processing speed without any loss of precision. The LSP laboratory is equipped with an in-house X-ray diffractometer and hole drilling machine for post treatment residual stress analysis. Over the past three years, samples of distinct shapes and made of various materials have been treated. We have successfully applied LSP technique on various materials: aluminium, steel alloys, polycrystalline or monocrystalline copper, titanium, cobalt-chrome and magnesium alloys (Fig. 12). Initially, samples were mostly flat, while recently more complex shapes, such as tube segments, 3D printed structures and multiple cutting, drilling and forging tools have been modelled and treated by LSP. For example, we have managed to double the wear resistance of problematic forging tools, and increase the high cycle fatigue lifetime of stainless steels used in nuclear industry more than ten times.

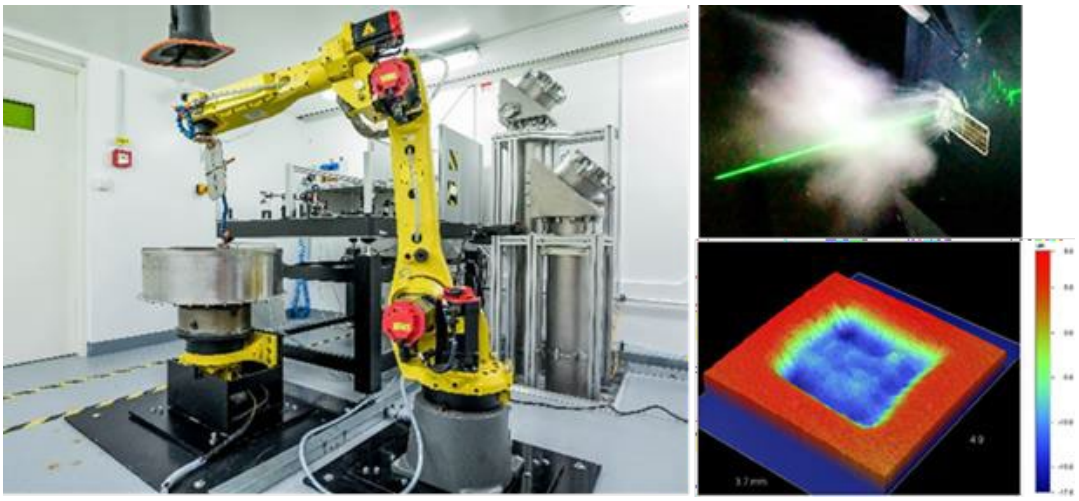

Fig. 11: LSP station with robotic arm carrying samples (left). Laser pulse impact captured on camera (top right) and resulted footprint in the material (bottom right).

Fig. 12: Examples of materials treated by LSP. Copper for microstructure investigation (top left); aluminium for marine applications (bottom left); cobalt-chrome bending as a result of one-sided compressive stresses (top right); magnesium for bio implants (bottom right).

The main focus of our Laser Micro Machining group has moved from development of new engraving and marking techniques for metals and plastics using nanosecond laser sources to smart processing of more complex materials with our picosecond Perla lasers. Thanks to its unique parameters, it is now possible to process glass, ceramics and/or composite materials with high precision in the nm-range (Fig. 13). We have been developing and fabricating functional surfaces with potential for aircraft (anti-ice, drag reduction surfaces), automotive (self-cleaning, superhydrophobic, friction reduction) and marine (anti-corrosion) industries, and health care (anti-bacteria, cell growth). In 2019, new methods for multi- beam and interference processing for rapid, large-scale functionalization have been successfully developed and tested in order to reach processing rates of more than 1 m^2/min with a structure resolution in a sub-μm range. Special diffractive optical elements (DOE) including programmable multi-beam spatial light modulators coupled with a galvo scanning head have been tested. In cooperation with an industrial partner, 784 holes were drilled in thin metal foil at the same time, thus significantly improving the fabrication time. A prototype interference processing station was completed in 2019 and successfully tested by drilling 10 000 micro-holes simultaneously into carbon fibre reinforced plastic (CFRP) sheet.

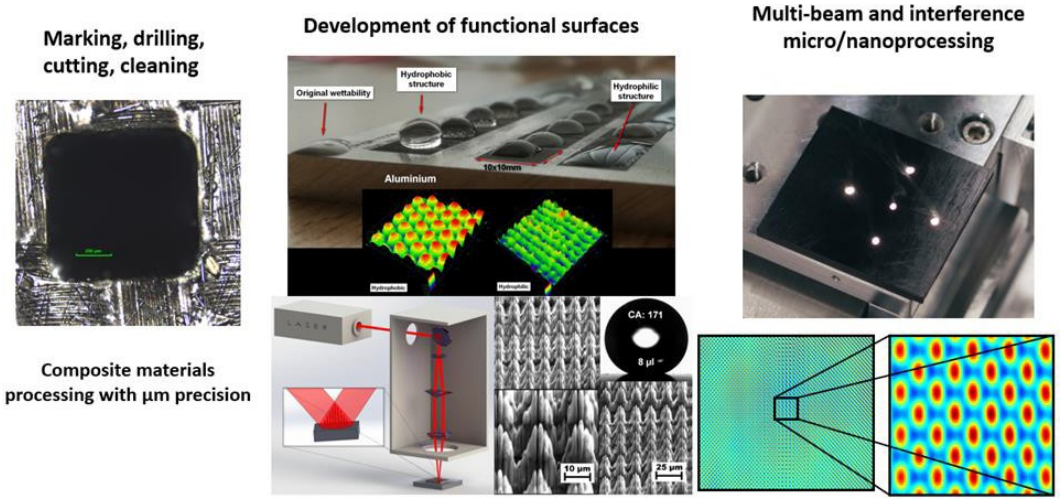

Fig.13: Examples of laser micro processing technologies at HiLASE.

A Laser Induced Damage Threshold experimental station has been developed over the period 2013- 2015. Since 2016, the station is ready for commercial cooperation and provides industrial-like measurements. We have been offering state-of-the-art testing of optical materials and components on resistance to laser irradiation under controlled conditions to companies. Different LIDT procedures are available, based on ISO standard 21254 series or customized according to specific needs. The LIDT station can accommodate various types of samples (Fig. 14), independent on shape and size up to 100x100x100 mm^3 and weight up to 2 kg.

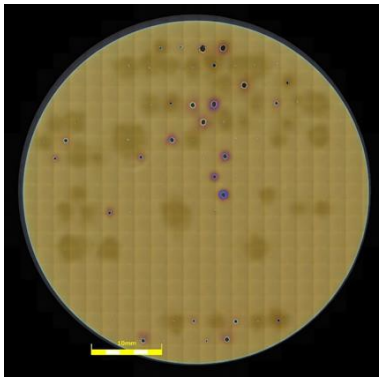

Fig. 14: Example of Ag coated mirror after LIDT test.

1.6 Laser applications in Science

HiLASE offers the unique possibility of utilizing laser beams of different wavelengths and pulse durations as well as their various combinations. This opens an unprecedented window of opportunity for developing novel laser applications for science, industry and bio-medicine. In 2016, project BIATRI was launched with the aim of exploring the evolution of different materials by ultrashort-pulse lasers, both newly-built at HiLASE and available in the market, in principally new regimes of irradiation, in particular when combining two or three laser beams of different wavelengths. BIATRI integrates experiments with the most sophisticated theoretical approaches for achieving fundamental understanding of material behaviour under laser light exposure, designing new materials and tuning their functional properties for innovative applications. To realize this project and contribute to further development of HiLASE, a new Scientific Laser Application laboratory has been designed and constructed. The laboratory (Fig. 15) consists of three experimental stations providing high-intensity laser pulses over a wide spectral range from UV to mid-IR, a high-vacuum chamber for laser synthesis of nanoscale materials, state-of-the-art diagnostics of the laser-induced processes, and advanced material characterization tools.

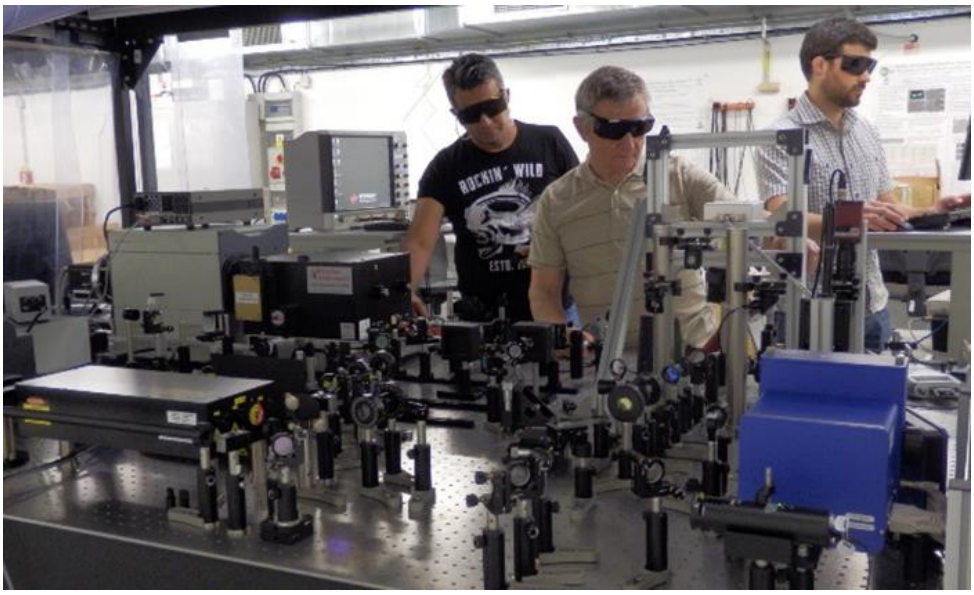

Fig. 15: The laboratory for Scientific Laser Applications during experiments on laser nanostructuring of surfaces of metals and semiconductors.

Breakthrough research has been performed on laser micro-/nanostructuring of metal surfaces, which are of high demand for applications such as photovoltaics, optoelectronics, creation of water-repellent and bio-compatible surfaces, and security marking. Based on a plasmonic theory, developed in our team, highly-periodic structures of subwavelength periodicity were produced at high throughput on surfaces of a number of metals (Fig. 16) in collaboration with the University of Modena and Reggio Emilia in Italy (Sci. Rep. **7**, 8485 (2017)). Predictions were also made on the conditions when such perfect structures can be fabricated on surfaces of any metals. This new achievement in the unprecedented level of control over the laser-induced periodic structure formation makes this laser- writing technology flexible, robust and, hence, highly competitive for advanced industrial applications based on surface nanostructuring. Our method and system of ultrafast laser writing of highly-regular periodic structures is a subject of an international patent application, PCT/CZ2017/050027.

Another novel laser-based technology developed at HiLASE in collaboration with Edinburgh University (UK) is blister-based-laser-induced forward-transfer (BB LIFT). This method enables clean desorption and transfer of nano- and micro-sized particles into the gas phase or onto receiver substrates without exposing the particles to the laser radiation or to any chemical treatment, which could damage intrinsic electronic and optical properties of the materials (Fig. 17). The BB-LIFT technique is highly suitable for depositing functional nanomaterials from the substrates on which they have been grown in a controlled fashion onto a substrate for device fabrication.

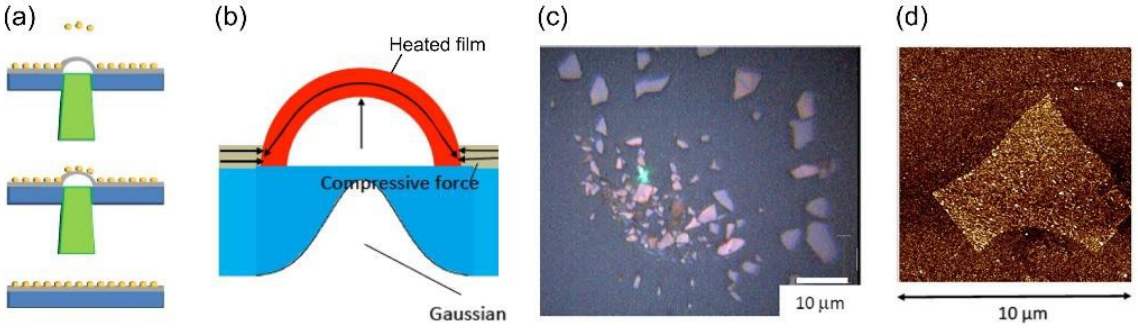

Fig. 17: (a) Schematics of BB LIFT: nano/microparticles are positioned on a thin metal film deposited on a glass substrate; the film is irradiated by a pulsed laser through the glass; as a result, the film bulges and particles are transferred on a receiver to a desired position. (b) Scheme of metal film bulging. High resolution optical microscope image of fullerene crystallites (c) and AFM image of a MoS_2 crystal (d) transferred by BB-LIFT to a substrate without inducing any damage.

Considerable effort has been made for gaining insights into damage mechanisms of bandgap transparent materials by ultrafast laser irradiation. A new effect of accumulation of laser energy during propagation of ultrashort laser pulses in air, due to formation of metastable states of excited air molecules, was observed for the first time using optical transmission measurements.

A very promising direction is also engineering of contamination-free nanomaterials with unique properties, which cannot be achieved using conventional physical and chemical synthesis. We have shown that laser-synthesized silicon nanoparticles with defect labels can be employed as contrast agents for optical bio imaging. Further plans include exploring new exotic states of matter, which have never been observed before in laboratories and which can yield new polymorphs with unique properties.

Research activity and characterization of the main scientific results

In case of ELI Beamlines there are a number of distinct research activities (Research Programs, RP1- RP6) which are based on the development and use of short pulse (femtosecond) high peak-power lasers (RP1). The diversity of orientation of the experimental RPs allows us to cover different scientific fields and provides a variety of opportunities for broad user communities. In addition to the research programs, two teams of excellence have been established lead by internationally recognized scientists to further foster flagship areas of research – the ELIBIO and HiFI projects.

Research Program 1: Lasers Generating High Repetition Rate Ultra-Short Multi-PW Peak Power Pulses

This ELI team developed a significant part of unique laser technology which is now integrated into the four main laser systems, L1 to L4.

L1-ALLEGRA high-power kHz laser

The L1-ALLEGRA is designed by the RP1 team to generate <15 fs pulses with an energy of 100 mJ per pulse at 1 kHz rep rate; the system output is readily upgradable to 200 mJ. The RP1 team used the concept of a laser based entirely on amplification of frequency chirped picosecond pulses in an optical parametric chirped pulse amplification (OPCPA) chain pumped by precisely synchronized picosecond pulses, generated by state-of-the-art thin-disk-based Yb:YAG laser amplifiers. This OPCPA setup for short-pulse amplification allows generation of pulses at very high (kHz) repetition rate, and amplification of a large spectral bandwidth. This makes it possible in principle for L1- ALLEGRA to deliver average power exceeding 100 W in ultrashort <15 fs pulses to the experimental teams RP2 and RP4.

The OPCPA chain of L1-ALLEGRA consists of seven amplifiers based on BBO and LBO crystals. The OPCPA amplifiers are pumped by pulses lasting only a few picoseconds which results in temporally very clean amplified pulses, with the absence of any prepulses. The L1-ALLEGRA developed by the RP1 team is the largest laser system currently using the technique of OPCPA ps amplification.

The L1-ALLEGRA is currently operates with an energy level output of about 30 mJ at the designed rep rate of 1 kHz for user experiments in the E1 experimental hall of ELI-Beamlines. In parallel with experiments the high-energy end of the laser chain it is expected to achieve >100 mJ performance in 2020.

L2 DUHA high-repetition laser system

The L2 DUHA beamline was also largely developed by the RP1 team. It is designed to provide >100 TW peak power at 20 Hz repetition rate readily upgradable to 50 Hz. The pump laser section of the L2 chain will be an upgraded Yb:YAG multi-slab, cryogenically cooled, 10 J laser amplifier originally developed by the STFC Rutherford Appleton Laboratory in 2014. The short-pulse amplification chain will be based on nanosecond OPCPA, delivering >3 J in pulses with a duration of <30 fs.

Several new technologies for L2-DUHA were developed by the RP1 team in cooperation with the industry, including the advanced Brayton cycle cryogenic gas engine for cooling of the Nd:YAG gain medium of the pump laser to temperatures of about -130° C, and technology for producing large homogeneous laser YAG crystals for the gain medium.

The L2 DUHA system will also include a small amplification chain for generation of ~5 mJ mid-IR pulses at 2.2 microns, with repetition rate of 2 kHz. The pulses will be generated from the L2-DUHA front end using so-called spectral super-continuum. This spectral super-continuum (extending approximately from 500 to 900 nm) is generated in bulk YAG driven by a thin disk picosecond laser. As the supercontinuum serves as seed for both the high energy OPCPA at 900 nm and to pump a crystal to generate the 2.2 μm wavelength, the main pulse and the mid-IT pulses are perfectly synchronized in time. This will allow the RP1 team femtosecond level synchronization between the final amplified 900 nm pulse and the mid-IR pulse at the experimental target.

The RP1 team is now working on building the short-pulse part of the L2-DUHA system, including the OPCPA amplification chain, developments of the pulse stretcher and the pulse compressor are underway. The system is planned to be completed by the RP1 team in 2021 and it should serve users from 2022.

L3-HAPLS PW 10 Hz laser system

The system L3-HAPLS (High repetition-rate Advanced Petawatt Laser System) was developed, built and tested between September 2013 and March 2017 in Lawrence Livermore National Laboratory (LLNL) with essential contribution of the RP1 team. The developments done by the RP1 team included the pulse compressor, the short pulse diagnostic system, and part of the L3-HAPLS control system. The purpose of the L3-HAPLS project was to supply cutting-edge laser technology for the ELI-Beamlines facility. The L3-HAPLS system is designed to deliver PW pulses with energy of at least 30 J and durations <30 fs, at a repetition rate of 10 Hz. It is the first all diode-pumped, high-energy femtosecond PW laser system in the world.

The commissioning of the system to >15 J uncompressed pulse energy, 28 fs compressed pulse duration and 3.3 Hz repetition rate was completed in November 2016 by the joint team of LLNL and RP1 for ELI Beamlines. At the same time, the Power Amplifier Diagnostic package (PAD), developed by the RP1 team, was successfully integrated with the laser system. In June 2017, the laser was shipped to the ELI-Beamlines facility. Following this the RP1 team installed and re-commissioned the system to parameters demonstrated at LLNL, along with installation and commissioning of the PW pulse compressor (built in cooperation with Czech industry). Operational testing and commissioning of the full L3-HAPLS system was successfully finished by the RP1 team in June 2018.

Since late 2018 L3-HAPLS has been used successfully by the RP1 team to deliver high-peak power laser pulses into the first experimental station TERESA (Testbed for high Repetition-rate Sources of Accelerated particles), operated by the RP3 team, to drive laser-matter interaction with solid and gas targets, to generate accelerated high-energy proton and electron beams. L3-HAPLS is now also used by the RP1 and RP3 teams for commissioning of the ELI Multidisciplinary Applications of laser-Ion Acceleration (ELIMAIA) endstation. The system will become the workhorse of the ELI-Beamlines facility, and in the upcoming months it will be used for acceleration of ions in the ELIMAIA station, for laser matter interaction experiments in the platform for plasma physics in the E3 experimental hall, and also to drive the Laser-driven Undulator X-ray source (LUX) beamline in the E5 experimental hall.

L4-ATON 10 PW kJ laser system with augmented repetition rate

The L4-ATON laser beamline is developed in cooperation between the RP1 team and the consortium National Energetics (USA) – EKSPLA (Lithuania). The system will deliver pulses with energy of 1.5 kJ, lasting about 150 fs and will thus generate peak power of 10 PW. L4-ATON will be the highest energy, highest peak intensity laser source of the ELI-Beamlines facility. It takes a different approach toward reaching 10 PW than other systems under development around the world - unlike Ti:sapphire or OPCPA-based systems which are designed to have output pulse durations of 30-40 fs, the designed laser pulse duration of L4-ATON is <150 fs with pulse energy of 1.5 kJ. L4-ATON will thus provide pulses with the highest energy amongst the 10 PW systems currently under construction.

The L4-ATON laser system is based on a combination of OPCPA and mixed Nd:glass amplification techniques. The OPCPA preamplifier laser chain generates 5 J broadband pulses, which are subsequently boosted in energy to >1.5 kJ in two high-energy amplifiers consisting of a mixture of Nd- doped phosphate and silicate glass supporting the required spectral bandwidth of ~15 nm needed for generation of pulses compressible to <150 fs. The L4-ATON architecture also uses an innovative technology of liquid cooling of the Nd:glass laser slabs, which makes it possible for the RP1 team to achieve a shot rate of 1/min, unprecedented in the in the field of kJ-class lasers.

The L4-ATON laser chain was implemented by the RP1 team into the ELI-Beamlines facility between September and December 2018, and by June 2018 all main performance parameters of the laser chain were demonstrated by the RP1 team, namely an output energy >1.5 kJ, capability of sustained operation at 1 shot/minute, and compressibility of output pulses to <150 fs. At present, the 10 PW vacuum compressor for compressing the full aperture, full energy output, pulses is installed. The compressor uses four large low-dispersion diffraction gratings with size 850x700 mm, manufactured by Lawrence Livermore National Laboratory. The compressor is a very large optical/mechanical/ electronic infrastructure and will be commissioned by the RP1 team in 2021.

Figure 1: ELI Beamlines Lasers

<u>Research Program 2:</u> Radiation Physics and Electron Acceleration

The objective of the Research program is the development and operation of stable and reliable laser- driven sources of high energy electrons and hard electromagnetic radiation, for applications and for fundamental science. The program includes the laser wakefield acceleration of ultra-relativistic electron beams with energies reaching tens of GeV. Their collision with multi-petawatt laser radiation will provide the conditions for entering as yet unexplored regimes allowing studies in fundamental science including studies of high-power gamma-ray flash generation in the radiation friction dominated laser plasma, nonlinear quantum electrodynamics of relativistic plasmas, and probing the nonlinear vacuum texture.

Another important application of laser accelerated electrons is in the construction and operation of the laser-driven compact X-Ray Free Electron Laser (X-FEL) for generation of coherent electromagnetic radiation in the range from XUV to hard X-Rays.

The sources of incoherent X-rays based on the interaction of ultrashort laser pulses with matter will be in routine use at the ELI Beamlines facility. The sources that are being implemented include, in particular, high-order harmonic generation, advanced plasma X-ray sources (K-alpha radiation) and sources based on relativistic electron beams accelerated by laser such as betatron radiation and inverse Compton scattering. Key benefits of those X-ray sources are in providing photon beams of high photon energy, extremely high spectral brightness, ultra-short pulse duration, and in the ability of internal X-ray pulse synchronization to infrared and visible laser pulses or electron bunches for advanced pump-probe experiments. The Research program consists of the following groups:

X-ray Sources

1) High-order harmonics generated in noble gases, where we have been studying the scaling of XUV beam characteristics with laser parameters [1-3], which helped in the design and implementation of the HHG Beamline [4] in the experimental hall E1 of the ELI Beamlines facility.

2) Plasma-based X-ray lasers where the RP2 team focused on development of new types of sources [5,6], as well as on characterization of the properties of generated radiation with the stress on temporal coherence [7,8]. The RP2 team also used the source for various diagnostic applications [9-12].

3) Plasma betatron, which employs relativistic interaction of intense laser pulse with underdense plasma to accelerate electrons to relativistic velocities and generates broadband X-ray radiation by oscillation of those electrons during acceleration [13-16]. The RP2 team also developed a unique method for characterization of gas jets with largely improved sensitivity [17].

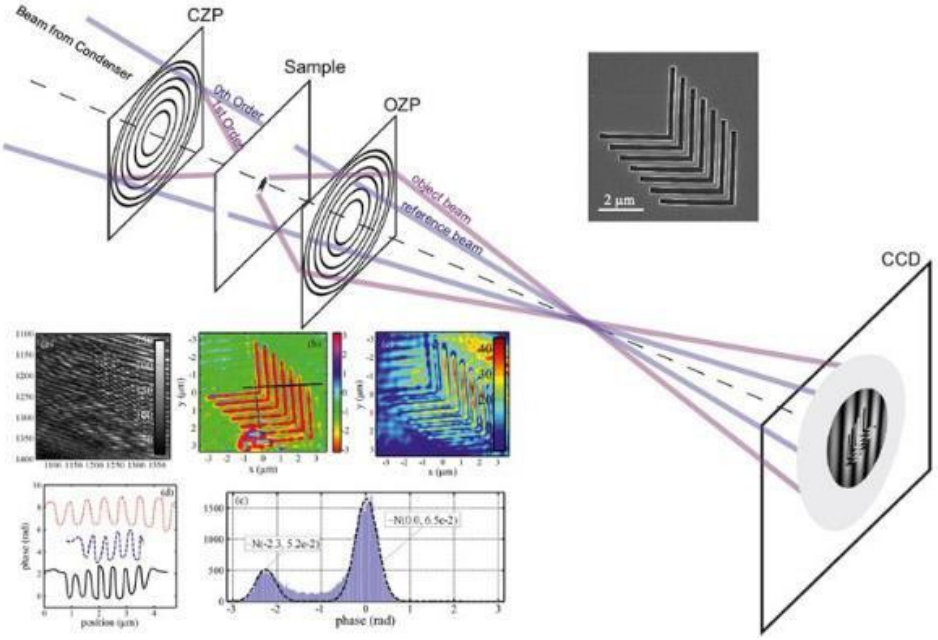

Figure 2: Digital holographic microscopy at 46.9 nm with two zone plates employing table-top capillary discharge XUV laser [12].

Selected Publications

[1] V. E. Nefedova, M. Albrecht, M. Kozlova, and J. Nejdl. J. El. Spectr. **220** (2017), 9.
[2] V. E. Nefedova, M. F. Ciappina, J. Nejdl et al. Appl. Phys. Lett. **113** (2018), 191101.
[3] V. E. Nefedova, M. F. Ciappina, J. Nejdl et al. Phys. Rev. A **98** (2018), 033414.
[4] O. Hort, M. Albrecht, J. Nejdl et al. Opt. Exp. **27** (2019), 8871.
[5] A. Depresseux, E. Oliva, S. Sebban et al. Nature Photonics **9** (2015), 817.
[6] A. Depresseux, E. Oliva, S. Sebban et al. Phys. Rev. Lett. **115** (2015), 083901.
[7] A. Le Marec, L. Meng, A. Klisnick et al. Phys. Rev. A **92** (2015), 033852.
[8] M. Albrecht, M. Kozlová, and J. Nejdl. Opt. Lett. **43** (2018), 4586.
[9] M. Krůs, M. Kozlová, J. Nejdl, and B. Rus. J. Instr. **13** (2018), C01004.
[10] R. L. Singh, J. Nejdl, et al. HEDP **23** (2017), 20.
[11] U. Chaulagain, C. Stehlé, J. Larour et al. HEDP **17A** (2015), 106–113.
[12] J. Nejdl, I. D. Howlett, C. S. Menoni et al. IEEE Phot. Jour. **7** (2015), 6900108.
[13] K. Bohacek, M. Kozlova, J. Nejdl et al. NIMA **883**,
p.24 (2018). [14] V. Horny, J. Nejdl et al. **24**, 063107
(2017).
[15] V. Horny, D. Maslarova et al. Plas. Phys. Contr. Fus. **60** (2018), 064009.
[16] A. Döpp, B. Mahieu, K. Ta Phuoc et al. Light-Sci. App. **6** (2017), e17086.
[17] J. Nejdl, J. Vančura, K. Boháček, et al. Rev. Sci. Instr. **90** (2019), 065107.

ELI-ELBA - ELectron Beam Accelerator for fundamental science and applications The ELI-ELBA's scientific goals are oriented in two main directions. In the long-term, using the configuration of multi-petawatt laser interaction with low density plasma targets the project aims to achieve high energy and high quality electron beams for use in fundamental science studies. The opposite configuration

of a moderate power laser pulse irradiating relatively high density plasma targets allows the team to conduct experiments in the high repetition rate regime enabling various applications of the laser accelerated electrons.

For its electron acceleration technique, ELI-ELBA experiments are based on Laser Wakefield Acceleration (LWFA), which is, at the state of the art, capable of producing very energetic (GeV) ultra- short (fs) electron beams by its extremely high accelerating gradients (>100 MeV/mm). The main principles of LWFA are illustrated in Fig. 3, where the intense laser driver excites plasma waves used to accelerate the electrons.

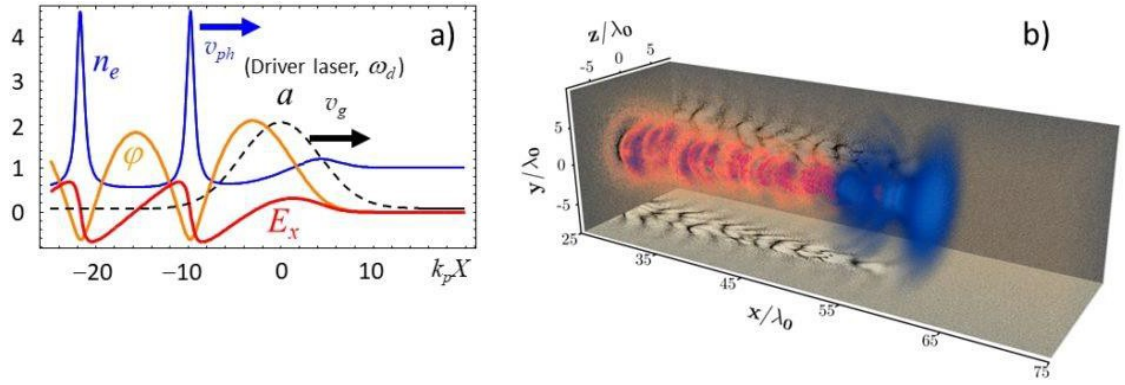

Figure 3(a): 1D wake wave: electric field, electrostatic potential, and electron density behind the laser pulse; (b) 3D wake wave (yellow-red) excited by ultra-short pulse laser (blue) in the near critical plasma density targets. In the (x,y) and (x,z) planes

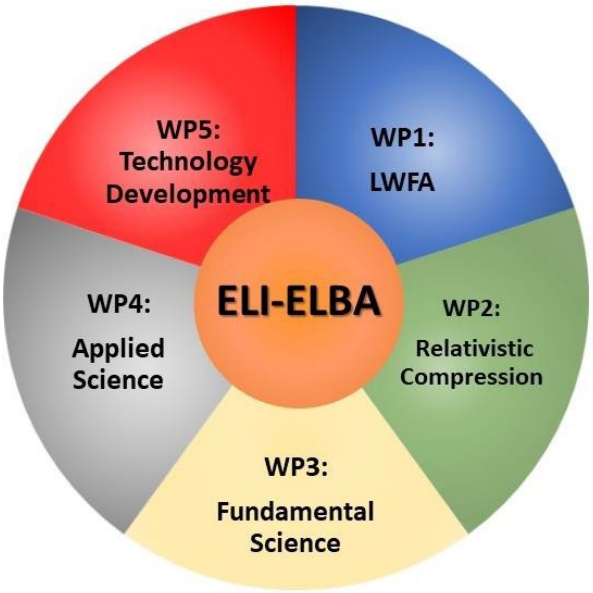

Figure 4: ELI-ELBA scientific activities overview

The scientific work being conducted by the ELI-ELBA team can be schematically summarized by the diagram shown in Figure 4, where the ELI-ELBA scientific activity is divided into five connected work packages.
The first work package, WP1, corresponds to the advancement of the state of the art of LWFA by using the unique ELI-Beamlines laser systems and technology.

LUIS Beamline

The goal of this research activity is development of compact laser-driven undulator-based photon radiation for users, aiming at both the incoherent and coherent regimes. Successful realization of this program by the RP2 team will open the way to a new generation coherent X-ray sources with sub- femtosecond photon bunches, using a OPCPA high repetition rate laser. Such a novel laser system (L2 DUHA laser) is now

being built at ELI Beamlines by the RP1 team. In the frame of the international collaboration between ELI Beamlines and University of Hamburg (Hamburg, Germany), the LUX setup (Laser-driven Undulator X-ray source) has been developed [1] in Hamburg (at Deutsches Elektronen-Synchrotron DESY campus), making it possible to move from a single-short demonstration experiment towards stable and controllable “laser wakefield” accelerator operation (Figure 5 and 6).

Figure 5: LUX experimental beamline (ELI Beamlines and University of Hamburg), assembled and commissioned at DESY in the frame of the ELI-BL and HH collaboration.

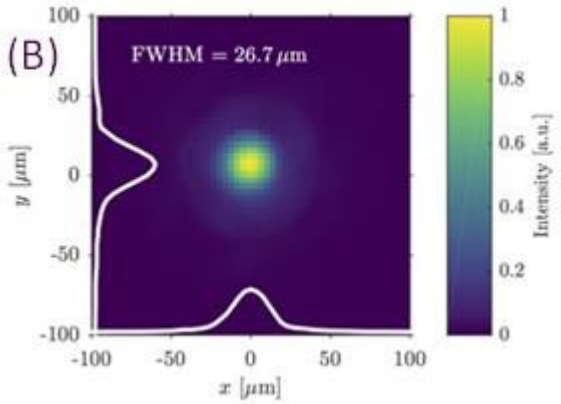

Figure 6: Measured focal spot size of the laser near the capillary

As the result of the ELI BL/UHH collaboration the stable operation of the whole setup, including the 200 TW laser, the laser beam transport, the electron beam transport and the photon beam transport has been achieved. Several RP2 team scientists worked on this task at UHH and continuous operation of the LUX setup with the repetition rate of 5 Hz over 24 hours has been demonstrated with a stable electron beam acceleration of up to 450 MeV and generation of spontaneous undulator radiation with the wavelength well below 9 nm. These joint experimental achievements are the result of the UHH/ELI BL collaboration activity. Main components of the LUX beamline have been produced and delivered to ELI Beamlines during 2019. These components were installed by the RP2 team in the ELI Beamlines E5 experimental hall as part of the LUIS setup (Figure 7).

Figure 7: Installation of the LUX components (ELI BL/UHH collaboration) in the E5 experimental hall of ELI Beamlines.

The conceptual design of the laser-driven free electron laser (LD-FEL) has been finalized by the RP2 team in collaboration with University of Hamburg (Figure LUIS-3). As the first step in the realization of such a setup at ELI- Beamlines, the laser-driven ‘demo’-FEL has been designed, which allows us to develop the whole setup step-by-step starting from the basic ‘incoherent’ photon radiation setup. The laser-driven ‘demo’-FEL requires a stable electron beam with energy around 400 MeV [2,3,4], accelerated in the discharge capillary with a length of

r

round 20 mm. The aim of this setup is to improve the electron beam parameters required for the FEL operation in long 'dedicated' undulator in parallel with the user-oriented operation. In frame of the LUIS development at ELI-Beamlines, both schemes tested continuous gas flow as well as the discharge regime in the Sapphire capillary. It will be used by the RP2 team to provide stable laser-driven acceleration of the electron beam.

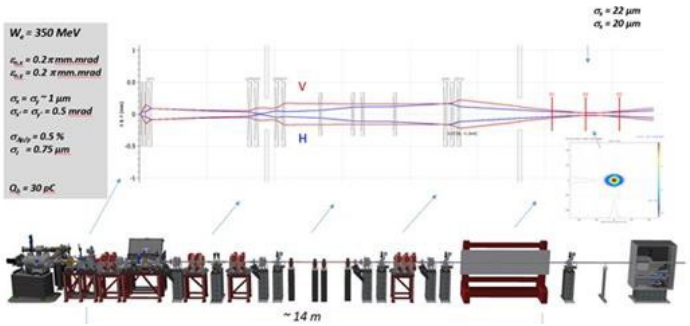

Figure 8: Conceptual design of the 'demo'-FEL electron beam transport including the 2.5m FEL-undulator.

The electron beam diagnostics and the plasma discharge developments are required to characterize the properties of the LWFA electron beam and the plasma parameters. The coherent transition radiation (CTR) technique allows us to perform the measurements of the parameters of the electron beam with the 'fsec'-bunch length. The setup for such measurement has been developed (Figure 8) by the RP2 team at ELI-Beamlines [5] and tested at INFN (Frascati, Italy).

Selected publications

[1] N.Delbos, C.Werle , I.Dornmair et al. NIM A 909 (2018) 318-322.
[2] A.Molodozhentsev, G.Korn, L.Prybil & A.R.Maier. Proc. 60th ICFA-FLS18 workshop, 62- 67, Shanghai, China, March 2018.[3] K.Kruchinin, A.Molodozhentsev, T.Green et al. Proc. of the SPIE19 International Conference, Prague, CZ, March 2019 and the HEDS19 International Symposium, Yokohama, Japan, March 2019.
[4] A.Molodozhentsev, K.Kruchinin, L.Pribyl. Proc. of International Conference IPAC18, Vancouver, Canada.
[5] K.Kruchinin, D.Kocon, A.Molodozhnetsev, L.Pribyl. Proc. of International Conference IPAC18, Vancouver, Canada.
[6] J.Hawke, K.Kruchinin, A.Molodozhentsev et al. 3rd European Conf. on Plasma Diagnostics, May 2019, Lisbon, Portugal.

Research Program 3: Ion Acceleration by Lasers

The main objective of the Department is to develop and operate laser-plasma based secondary sources of particles (protons/ions/neutrons) with energies approaching the GeV-level. The research team primarily focus on improving the stability and quality of the generated beams in terms of intensity, emittance and energy spectrum. Special effort is devoted to exploring multidisciplinary applications requiring pulsed, quasi-monochromatic proton/ion beams with unprecedented dose rate (up to giga-gray per second) in the energy range of 60-250 MeV, which are of high interest for potential use in medicine (hadron therapy), plasma and materials science (proton and neutron radiography), cultural heritage (PIXE and DPAA), and nuclear physics (ultraclean nuclear fusion and transmutation).

Selected scientific research outputs achieved by the RP3 team scientists during the evaluated period are represented by two publications in journals with high impact

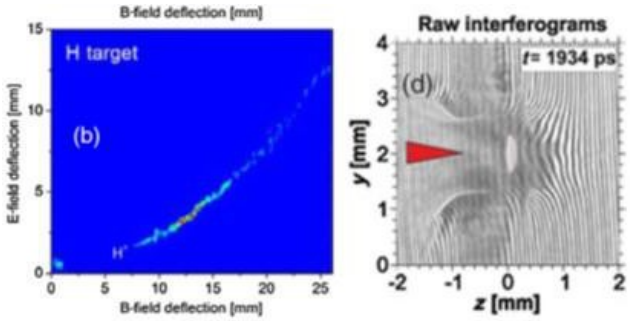

factor dedicated to laser-driven proton acceleration from cryogenic solid hydrogen targets and Proton Boron Capture Therapy (PBCT) with a potential strong impact in enhancing proton therapy biological effectiveness in cancer treatment (also covered by an EPO patent application). In [1] The world's first experimental test of a cryogenic targetry delivering system, made of a very thin solid hydrogen ribbon as a source of fast protons, produced by high-power lasers is reported. Pure streams of accelerated protons are key for both cancer therapies and experiments in condensed-matter physics. However, targets that are irradiated with high-power lasers often yield proton streams contaminated with carbon and other ions. The original idea driving these experiments is to produce a syringe with a virtual piston to push solid H2 through a nozzle to create a ribbon with a width of 1 mm and a thickness that can be modulated between 20 and 100 μm. In the RP3 team the linearly polarized nanosecond laser is focused on the H2 ribbon in vacuum conditions at cryogenic temperatures (10 K). RP3 scientists recovered a collimated stream of protons with energies in the MeV range, that is free of any contaminants. Using another laser as a probe beam, they examine the expansion of the hydrogen plasma at 3 billion kelvin a few nanoseconds before and after the arrival of the laser pulse. RP3 scientists show that the population of protons we recover is 3 times larger than number of protons derived from a CH_2 target. Additionally, they measure a laser-proton acceleration efficiency 2 to 3x higher than that of previous experiments.

[1] D. Margarone et al. Phys. Rev. X 6 (2016) 041030

The RP3 team has been first to report experimental proof of proton boron capture therapy to enhance proton therapy effectiveness [2]. This article reports on the use of proton-boron nuclear fusion to enhance proton therapy effectiveness in cancer cells. The killing rate of various tumour cells has been demonstrated experimentally. The experimental technique named PBCT (Proton Boron Capture Therapy) uses molecules containing 11B nuclei potentially administered on a deep-seated tumour and then bombarded with a proton beam typically used in hadron therapy. As a consequence of the interaction of one proton with one 11B nucleus, three alpha-particles with low energy (around 4 MeV) are generated and ultimately stopped inside the tumour, thus releasing their entire energy in a single cancer cell. The macroscopic effect is enhanced biological damage compared to the initial effect already caused by the incoming protons. This result of the RP3 team is of high scientific and clinical interest since it may enable the widening and improvement of current hadron therapy procedures, which would have a significant societal impact. The innovative PBCT capability would enhance radiobiological effectiveness of proton therapy keeping its unique ballistic properties, thus paving the way towards treatment of radioresistant tumours, such as glioma or pancreatic tumours.

[2] G.A.P. Cirrone, L. Manti, D. Margarone. Nat. Sci. Rep. 8 (2018) 1141

[3] L. Giuffrida, D. Margarone, G. Korn, P. Cirrone, A. Picciotto: "device and method for imaging and enhanced proton-therapy treatment using nuclear reactions„ EP20160178280 20160706 (2018)

<u>Research Program 4:</u> Applications in Molecular, Biomedical and Material science

The Research Program for applications in molecular, biomedical, and materials sciences (RP4) develops and runs experimental stations using secondary light sources driven by the 1 kHz L1 ALLEGRA laser as well as available support lasers. The RP4 team mainly develops scientific end stations for time-resolved photon science applications in the THz-to-hard X-ray range with a focus on dynamics in the femtosecond-to-microsecond time scales. These stations are:

Figure 10: The E1 experimental hall in August 2019. The hall is equipped with a beam transport system that allows the high intensity pulses from the L1 ALLEGRA laser, and the complementary support lasers, to be transported in high vacuum. To the left in the figure are located the HHG source with corresponding VUV science end stations (MAC and ELIps). Centrally, in the blue radiation shielding hutch, are the laser driven Plasma X-ray source and associated experimental stations for X- ray science. On the right is the optical spectroscopy cluster inside the black laser safety enclosure.

1) MAC: A multi-purpose end station for atomic, molecular, and optical (AMO) sciences and coherent diffractive imaging (CDI)
2) ELIps: A materials science platform based on time-resolved spectroscopic ellipsometry in the optical range and VUV magneto-optical ellipsometry
3) TREX: A modular station for hard X- ray sciences covering applications in diffraction, spectroscopy, pulse radiolysis and imaging
4) Advanced optical spectroscopy capabilities in the MIR-to-DUV range, including a setup for stimulated Raman scattering, transient optical absorption, IR (1D and 2D) spectroscopy and pulse- shaping and coherent control.

The period between 2015 and 2019 has been dominated by installation works and preparations for scientific work, both in-house and in user operations. The RP4 team has been scientifically very active on the ELI/HiLASE site since late 2016. Operations in the E1 experimental hall (fig. 1) have been increasing in intensity since the installation of the first support laser in early 2018. The first beam from the L1 ALLEGRA laser was sent to E1 in September 2018 and first user- assisted commissioning experiments using the L1 ALLEGRA laser took place in June 2019.

During 2018 the scientific instruments in the E1 experimental hall became increasingly available for early experiments and scientists from the RP4 team spent a total of about 1200 hours of experimental time together with external collaborators. In early 2019 the RP4 team published the first open call for user assisted commissioning and early experiments. This resulted in the scheduling of 20 experiments with external users from 10 countries. The scientific work through the commissioning phase (including work with early users) has resulted in the first publications based on experimental results obtained at the ELI Beamlines facility [1 to 4]. RP4 researchers are also active in research at other facilities and labs. This work has resulted in a number of high profile publications and a total of more than 35 papers published in peer-reviewed journals.

[1] E. Klimešová, O. Kulyk, Y. Gu et al. Scientific Reports 9 8851 (2019)
[2] S. Espinoza, G. Neuber, Ch. D. Brooks et al. Applied Surface Science 421 378-382 (2017).
[3] O. Hort, M. Albrecht, V. E. Nefedova et al. Optics Express 2 8871-8883 (2019).
[4] S. Espinoza, S. Richter, M. Rebarz et al. Applied Physics Letters 115 052105 (2019)

Research Program 5: Plasma and High Energy Density physics

Suprathermal electron effects in laser produced plasmas: The RP5 team is working on, and making progress in high-intensity laser systems, development of advanced theoretical models, and diagnostic tools explaining phenomena accompanying laser-matter interaction at extreme conditions. This is very important for laboratory astrophysics, high-energy-density physics and applied research benefiting from strong electric and magnetic fields generating energetic particle fluxes and intense radiation sources [1]. RP5 team scientists participated in a series of experiments [2-6] and contributed to development of the so-called shock ignition scheme where fuel is ignited from a central hot spot heated by a strong spherically convergent shock. Parametric plasma instabilities (such as stimulated Raman scattering or two-plasmon decay) couple a significant fraction of the laser energy to hot electrons, the role of which is ambiguous: The RP5 team studied the environmental conditions in plasmas generated at intensities around 10^{16} W/cm^2 using a diagnostic complex including optical interferometry, x-ray spectroscopy and imaging, laser backscattering, ion detectors, shock chronometry and crater analysis [2]. This research project is being performed in collaboration with Université Bordeaux, Talence, France, Institute of Plasma Physics and Laser Microfusion, Warsaw, Poland, Ecole Polytechnique and Sorbonne Université, Paris, France, P.N. Lebedev Physical Institute of RAS and National Research Nuclear University MEPhI, Moscow, Russian Federation, and Czech Technical University in Prague.

[1] O. Renner, F. B. Rosmej. Matter Radiat. Extremes 4 (2019) 024201.
[2] O. Renner, M. Šmíd, D. Batani, L. Antonelli. Plasma Phys. Control. Fusion 58 (2016) 075007.
[3] G. Cristoforetti, A. Colaïtis, L. Antonelli et al. EPL-Europhys. Lett. 117 (2017) 35001.
[4] T. Pisarczyk, S. Yu Gus'kov, A. Zaras-Szydłowska et al. Sci. Rep. 8 (2018) 17895.
[5] D. Batani, L. Antonelli, F. Barbato et al. Nucl. Fusion 59 (2019) 032012.
[6] M. Šmíd, O. Renner, A. Colaitis et al. Nat. Commun. (2019), (accepted for publication).

Plasma amplification of coherent light: The RP5 team is pushing for ever higher laser intensities to study the interaction of coherent light (laser) with matter in extreme conditions, and to develop sophisticated sources of particles and radiation for applications in material science, bio-medical science and for studying fundamental phenomena in physics. These experiments use optical elements with a limited damage threshold due to ionization of the atoms. Therefore the optical elements need to increase in size, these are difficult to produce and will be expensive. A possible solution explored by the RP5 team is the use of a fully ionized plasma to manipulate light. The energy uptake by the seed correspondingly increases the intensity of that pulse. The fundamental advantage of a plasma is the fact that it is already "destroyed" and can therefore handle enormous fluencies.
Plasmas can therefore serve as optical elements for the next generation of high-power lasers. This research project has been ongoing for more than a decade in collaboration with Ecole Polytechnique and Sorbonne University in Paris, France.

[1] L. Lancia, A. Giribono, L. Vassura et al. Phys. Rev. Lett. 116 (2016) 075001.
[2] M. Chiaramello, F. Amiranoff, C. Riconda, S. Weber. Phys. Rev. Lett. 117 (2016) 235003.
[3] F. Amiranoff, C. Riconda, M. Chiaramello et al. Phys. Plasmas 25 (2018) 013114.
[4] J.-R. Marques, L. Lancia,1, T. Gangolf et al. Phys. Rev. X 9 (2019) 021008.

Research Program 6: High Field Physics Ultra-high intensity laser-matter interaction

The RP6 team investigates interaction of laser pulses with ultra-high intensity, beyond 1020 W/cm2, which leads to the generation of extremely energetic particles and gamma-photons as well as producing new unexpected physical effects. Using kinetic simulations and analytic modelling the RP6 group tries to obtain a detailed understanding of novel physics effects as well as to learn how to optimize new generations of secondary sources of particles and radiation. These predictive simulation activities are also for the preparation of future experiments which will be performed with the 10 PW laser of ELI-Beamlines. Due to extremely high light intensities, the motion of the particles becomes relativistic and even quantum effects need to be accounted for. In principle well-known effects such as pair creation based on the Breit-Wheeler process and radiation-reaction effects can be studied for the first time in great detail with such high-intensity lasers. Due to the highly nonlinear physics taking place during the interaction process one needs to perform computationally very demanding multi- dimensional kinetic simulations in order to understand the details. In particular the group is looking into new configurations of laser-plasma interaction at ultra-high intensities to investigate extreme phenomena and determine possible measurable signatures of the processes of interest. The research performed is based on a strong collaboration with Czech Technical University in Prague, Instituto Superior Technico in Lisbon, Portugal and MEPhI in Moscow, Russia.

[1] M. Jirka, O. Klimo, M. Vranic et al. Sci. Rep. 7 (2017) 15302.
[2] Y-J. Gu, S. Weber. Opt. Express 26 (2018) 19932.
[3] E. Gelfer, N. Elkina, A. Fedotov. Sci. Rep. 8 (2018) 6478.
[4] M. Vranic, O. Klimo, G. Korn, S. Weber. Sci. Rep. 8 (2018) 4702.
[5] Y-J. Gu, O. Klimo, S. V. Bulanov, S. Weber. Comm. Phys. 1 (2018) 93.

Attosecond nanophysics, combined with nanoscale physics, has experienced a considerable rise in recent years both experimentally and theoretically. Its foundation rests on the sub-cycle manipulation and sampling of the coupled electron and near-field dynamics at the nanoscale. The RP6 team not only addresses questions of strong fundamental interest in strong-field light-matter interactions at the nanoscale, but also explores a considerable number of applications in ultrafast, petahertz-scale electronics, and ultrafast metrology for microscopy or nanoscopy. While conventional semiconductor- based optoelectronic devices are operated based on light intensity, lightwave-based petahertz electronics describe the manipulation of charge carrier dynamics by the electromagnetic field of light owing to the precisely controlled carrier-envelope phase (CEP) in few-cycle laser pulses at few and sub-femtosecond time scales. The driven ultrafast electronic dynamics, induced by intense few-cycle pulses, could occur at time scales of 10–1000 Attoseconds (1 as=10^{-18} s). For instance, Attosecond light pulses can be created in gases as a result of the highly nonlinear high-harmonic generation (HHG) process, where electron photoionization of gas atoms is restricted to a time window much shorter than a half-cycle of the oscillation of the driving laser light field, typically on the order of sub- 100 as for optical frequencies. A close collaboration with German and Korean experimental groups, as well as with Spanish theoretical ones, has been established.

[1] M. F. Ciappina, et al. Rep. Prog. Phys. 80 (2017) 054401.
[2] E. Osika, et al. Phys. Rev. X 7 (2017) 021017.
[3] Y. W. Kim, et al. ACS Photonics 6 (2019) 851-857
[4] S. Han, et al. Nat. Commun. 10 (2019) 3272.
[5] K. Amini, et al. Rep. Prog. Phys. (in press) (2019).

In order to further enhance the scientific excellence of the facility two projects devoted to flagship areas of ELI Beamlines have been established: HiFI and ELIBIO. Two internationally renowned scientists have been appointed to establish and lead the teams, respectively: Sergey Bulanov – leading scientist in high energy and high intensity interactions, and Janos Hajdu – leading scientist in molecular biophysics. Both groups aim to support the scientific community in their respective fields. They will receive 9 million euros over the next 4 years from the Support to Excellent Research Teams Program of the Czech government.

HiFI Project: High Field Initiative project - “Excellence Research Team

The HiFI team provides the leading program in the high field science. The HiFI scientists emphasize synergy between theory and experiments and include a strong theoretical group to develop new ideas for experiments, along with conducting extensive computer simulations. The HiFI team advances our knowledge of laser charged particle acceleration as well as high energy photon generation. It focuses on studying novel regimes when radiation friction and quantum electrodynamics processes, such as electron-positron pair creation and vacuum polarization, become significant.
The major project investigated by the HiFI scientific team is “**High Energy Charged Particle Acceleration**”. Within the framework of scientific collaboration between ELI Beamlines, LBNL-USA, and KIAM (Russia) the theoretical studies and MHD computer simulations of the capillary discharge plasma channels for the high intensity laser pulse guiding and the active lensing of electron/ion beams has resulted in obtaining the world’s highest energy of 8 GeV electrons accelerated by the Laser Wakefield Acceleration mechanism [1-3].

[1] G. A. Bagdasarov, P. V. Sasorov, V. A. Gasilov et al. Phys. Plasmas 24 (2017) 083109.
[2] G. A. Bagdasarov, N. A. Bobrova, A. S. Boldarev et al. Phys. Plasmas 24 (2017) 123120.
[3] A. J. Gonsalves, K. Nakamura, J. Daniels et al. Phys. Rev. Lett. 122 (2019) 084801.

The HiFI team formulated novel methods to downsize the systems emitting hard photon flashes: “**High Brightness Hard Photon Flash Generation**”. The regimes of dominant radiation reaction will provide the conditions for realization of a new powerful source of high brightness gamma-rays. This completely changes the electromagnetic wave-matter interaction. Using quantum electrodynamic particle-in-cell simulations, the HiFI scientists found conditions for the gamma flare generation in the interaction of high power Petawatt-class laser pulse with tailored targets having extended preplasma corona and with localized electromagnetic field. They demonstrated generation of an energetic flare of gamma-photons with energies in the GeV range and total flare energy being on kilojoule level with an efficient conversion of the laser energy to gamma radiation. They discussed how target engineering and laser pulse parameters influence gamma-flare generation efficiency. This type of experimental setup for a laser-based gamma source would be feasible for the upcoming high-power

laser facilities [1-4]. It also shows the major contribution of the HiFI team to other RP teams of ELI Beamlines and illustrates cross-team collaboration.

Another major result of the HiFI scientists is description of Burst Intensification by Singularity Emitting Radiation (BISER). Singularities in multistream flows of emitting media cause constructive interference of emitted travelling waves, forming extremely localized sources of bright coherent emission. Here we, for the first time, demonstrate this extreme localization of BISER by direct observation of nanoscale coherent x-ray sources in a laser plasma. The energy emitted into the spectral range from 60 to 100 eV is up to ~100 nJ, corresponding to ~10^{10} photons. Simulations of the HiFI team reveal that these sources emit trains of Attosecond x-ray pulses. These findings establish a new class of bright laboratory sources of electromagnetic radiation.

Another method of generation of coherent X-ray radiation is based on the reflection of coherent laser light by a relativistically moving mirror (flying mirror). Due to the double Doppler Effect, the reflected pulses are upshifted in frequency and compressed in time. Such mirrors are formed when an intense short laser pulse excites a strongly nonlinear plasma wave in tenuous plasma.

[1] K. V. Lezhnin, P. V. Sasorov, G. Korn, and S. V. Bulanov. Phys. Plasmas 25 (2018) 123105.
[2] J. Vyskocil, O. Klimo, S. Weber. Plasma Phys. Control. Fusion 60 (2018) 54013.
[3] Y.-J. Gu and S. Weber. Optics Express 26 (2018) 19932.
[4] Y.-J. Gu, O. Klimo, S. V. Bulanov, S. Weber. Communications Physics 1 (2018) 93.

ELIBIO Project: Future Biology with High-Power Lasers

The ELIBIO team explores new frontiers in light and optics to create breakthrough science in biology, chemistry and physics. The new Interdisciplinary Centre of Excellence at ELI Beamlines is formed for the support of life science research, together with BIOCEV (the joint biomedicine and biotechnology centre of the Czech Academy of Sciences and Charles University), and will be available for use by foreign partners, for example the European XFEL in Hamburg and the LCLS at Stanford. An essential goal of the project is to understand photon-material interactions in extremely intense X-ray fields where new physics can be expected. The experiments will explore fundamental questions in the physics of photoemission and electron dynamics in the relativistic regime with X-rays. The new knowledge in studies on structure, function and dynamics in cells, organelles, and biomolecules will be used to perform experiments that have been impossible thus far. We will develop new methods and technologies to enable such measurements and answer key questions in health and disease.

The research team of ELIBIO is formed at the interface between two complementary research centres, ELI Beamlines oriented to photon physics and BIOCEV oriented to biomedical and biotechnological research. The project team is headed by Prof. Janos Hajdu making strategic decisions as for the research direction and scope of experimental work. Prof. Hajdu has a rich scientific career. He worked as a professor of photon science at Stanford University in the USA, a professor of molecular biophysics at the University of Uppsala in Sweden and as advisor to the director of the European XFEL in Germany.